Science

7 September 2012 | $10

AAAS

CONTENTS continued >>

page 1162

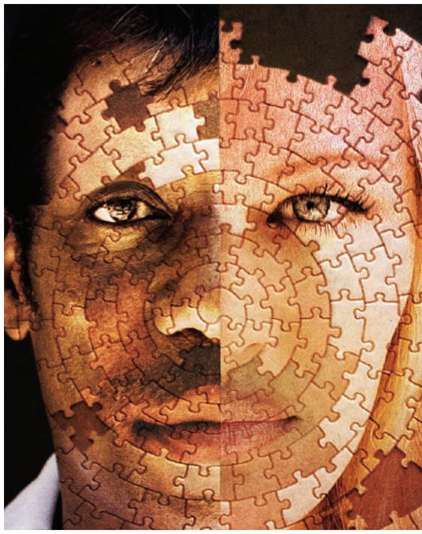

page 1174

COVER

Artist's conception of the complex network of relationships between disease and the human genome. Hundreds of diseases and traits (represented by colored dots) have been mapped to specific chromosomal positions in the genome. Most disease-associated genetic variants fall outside of protein-coding genes, instead affecting the genome's regulatory circuitry by modifying the DNA "switches" (some of which are depicted here as gray triangles, many others not shown) that control gene activity. See page 1190.

Image: Rachael Ludwig and John Stamatoyannopoulos

DEPARTMENTS

CONTENTS continued >>

page 1175

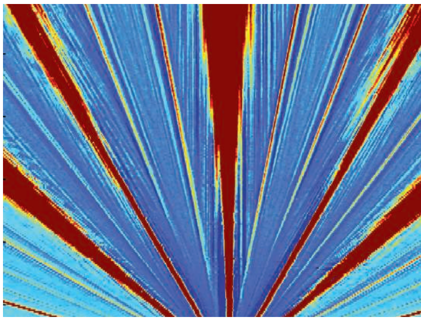

page 1196

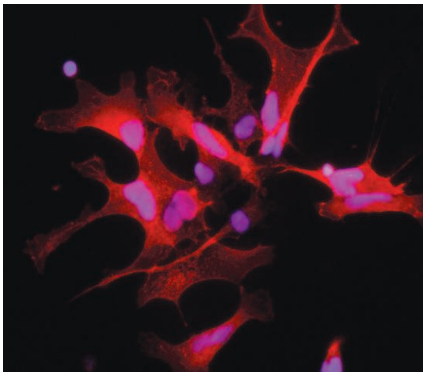

page 1231

*SCIENCE*ONLINE

*SCIENCE*XPRESS

www.sciencexpress.org

Systematic Localization of Common Disease-Associated Variation in Regulatory DNA
M. T. Maurano et al.
Genetic variants that have been associated with diseases are concentrated in regulatory regions of the genome.
10.1126/science.1222794

A GPS for Navigating DNA
E. Schadt and R. Chang
10.1126/science.1227739

Evidence of Abundant Purifying Selection in Humans for Recently Acquired Regulatory Functions
L. D. Ward and M. Kellis
Diversity in human-specific regions of the genome has been reduced by functional constraints.
10.1126/science.1225057
>> *News story p. 1159*

Wnt5a Potentiates TGF-β Signaling to Promote Colonic Crypt Regeneration After Tissue Injury
H. Miyoshi et al.
Repair of the intestinal epithelium requires both cell proliferation and replacement of crypt stem cells.
10.1126/science.1223821

Mutations in *BCKD-kinase* Lead to a Potentially Treatable Form of Autism with Epilepsy
G. Novarino et al.
When the balance of branched-chain amino acids transported into the brain goes awry, neurological deficits can ensue.
10.1126/science.1224631
>> *Science Podcast*

Relaxation and Prethermalization in an Isolated Quantum System
M. Gring et al.
Two halves of a split ultracold gas of rubidium atoms retain memory of the initial state for an extended time.
10.1126/science.1224953

TECHNICAL**COMMENTS**

Comment on "Orthographic Processing in Baboons (*Papio papio*)"
W. Bains
Full text at www.sciencemag.org/cgi/content/full/337/6099/1173-b

Response to Comment on "Orthographic Processing in Baboons (*Papio papio*)"
J. Grainger et al.
Full text at www.sciencemag.org/cgi/content/full/337/6099/1173-c

*SCIENCE*NOW

www.sciencenow.org
Highlights From Our Daily News Coverage

Microbe-Free Beaches, Thanks to Dogs
Canine patrols can cut down on harmful bacteria from seagull poop.
http://scim.ag/Harmful-Bacteria

Drinking Too Much? Blame Your Glass
A new study finds that the shape of beer glasses affects how fast we drink.
http://scim.ag/Beer-Glasses

Genome Brings Ancient Girl to Life
A Denisovan child sheds light on the evolution of humans and Neandertals.
http://scim.ag/Ancient_Girl

*SCIENCE*SIGNALING

www.sciencesignaling.org
The Signal Transduction Knowledge Environment
4 September issue: http://scim.ag/ss090412

RESEARCH ARTICLE: FAM123A Binds to Microtubules and Inhibits the Guanine Nucleotide Exchange Factor ARHGEF2 to Decrease Actomyosin Contractility
P. F. Siesser et al.
Unlike related proteins, FAM123A interacts with microtubule-associated proteins and alters microtubule dynamics.

RESEARCH ARTICLE: Guanylyl Cyclases A and B Are Asymmetric Dimers That Are Allosterically Regulated by ATP Binding to the Catalytic Domain
J. W. Robinson and L. R. Potter

PERSPECTIVE: Allosteric Regulation of Nucleotidyl Cyclases—An Emerging Pharmacological Target
R. Seifert and K. Y. Beste
An ATP-binding allosteric site could be pharmacologically targeted to alter the activity of membrane guanylyl cyclases.

*SCIENCE*TRANSLATIONAL MEDICINE

www.sciencetranslationalmedicine.org
Integrating Medicine and Science
5 September issue: http://scim.ag/stm090512

RESEARCH ARTICLE: Structural Basis for Benzothiazinone-Mediated Killing of *Mycobacterium tuberculosis*
J. Neres et al.

FOCUS: Bridging the Gap Between a TB Drug and Its Target
G. M. Cook and A. Heikal
The crystal structure of the mycobacterial DprE1 reveals how the TB drug benzothiazinone BTZ043 blocks this microbial enzyme target.

RESEARCH ARTICLE: Disruption of the Sleep-Wake Cycle and Diurnal Fluctuation of Amyloid-β in Mice with Alzheimer's Disease Pathology
J. H. Roh et al.

FOCUS: The Nexus of Aβ, Aging, and Sleep
J. R. Gerstner et al.
Decreased sleep and attenuation of circadian fluctuations in Aβ reflect amyloid-associated pathology in Alzheimer's disease.

RESEARCH ARTICLE: An Intravaginal Ring That Releases the NNRTI MIV-150 Reduces SHIV Transmission in Macaques
R. Singer et al.
An intravaginal ring loaded with the NNRTI MIV-150 prevents transmission of the HIV/SIV chimera SHIV-RT in macaques.

FOCUS: Regulatory Science Innovation—A Rate-Limiting Step in Translation
N. S. Sung and J. Burris
Sustained funding for academic regulatory science will drive innovation and implementation, forge a viable career path, and build an educated workforce.

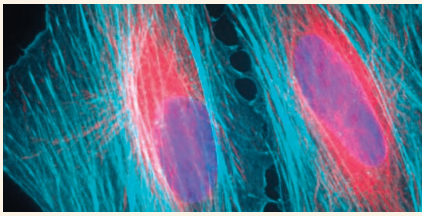

SCIENCE**SIGNALING**
The actomyosin cytoskeleton.

*SCIENCE*CAREERS

www.sciencecareers.org/career_magazine
Free Career Resources for Scientists

You Need a Game Plan
J. A. Hobin et al.
Introducing myIDP, the first comprehensive, online tool to help you choose and pursue a science career.
http://scim.ag/myIDPGamePlan
>> *Editorial p. 1149*

Taken for Granted: Rethinking the Ph.D.
B. L. Benderly
Overlong and insufficiently focused on available careers, traditional Ph.D. programs clearly need reform: What changes make sense?
http://scim.ag/TGF_Rethinking

*SCIENCE*PODCAST

www.sciencemag.org/multimedia/podcast
Free Weekly Show
On the 7 September *Science* Podcast: disease and regulatory DNA, treatable autism, reverse brain drain, and more.

SCIENCE (ISSN 0036-8075) is published weekly on Friday, except the last week in December, by the American Association for the Advancement of Science, 1200 New York Avenue, NW, Washington, DC 20005. Periodicals Mail postage (publication No. 484460) paid at Washington, DC, and additional mailing offices. Copyright © 2012 by the American Association for the Advancement of Science. The title SCIENCE is a registered trademark of the AAAS. Domestic individual membership and subscription (51 issues): $149 ($74 allocated to subscription). Domestic institutional subscription (51 issues): $990; Foreign postage extra: Mexico, Caribbean (surface mail) $55; other countries (air assist delivery) $85. First class, airmail, student, and emeritus rates on request. Canadian rates with GST available upon request, GST #1254 88122. Publications Mail Agreement Number 1069624. **Printed in the U.S.A.**

Change of address: Allow 4 weeks, giving old and new addresses and 8-digit account number. **Postmaster:** Send change of address to AAAS, P.O. Box 96178, Washington, DC 20090–6178. **Single-copy sales:** $10.00 current issue, $15.00 back issue prepaid includes surface postage; bulk rates on request. **Authorization to photocopy** material for internal or personal use under circumstances not falling within the fair use provisions of the Copyright Act is granted by AAAS to libraries and other users registered with the Copyright Clearance Center (CCC) Transactional Reporting Service, provided that $30.00 per article is paid directly to CCC, 222 Rosewood Drive, Danvers, MA 01923. The identification code for *Science* is 0036-8075. *Science* is indexed in the *Reader's Guide to Periodical Literature* and in several specialized indexes.

AAAS
ADVANCING SCIENCE, SERVING SOCIETY

CREDIT: PRISCILA SIESSER/DEPARTMENT OF CELL AND DEVELOPMENTAL BIOLOGY, UNIVERSITY OF NORTH CAROLINA AT CHAPEL HILL SCHOOL OF MEDICINE

EDITED BY CAROLINE ASH

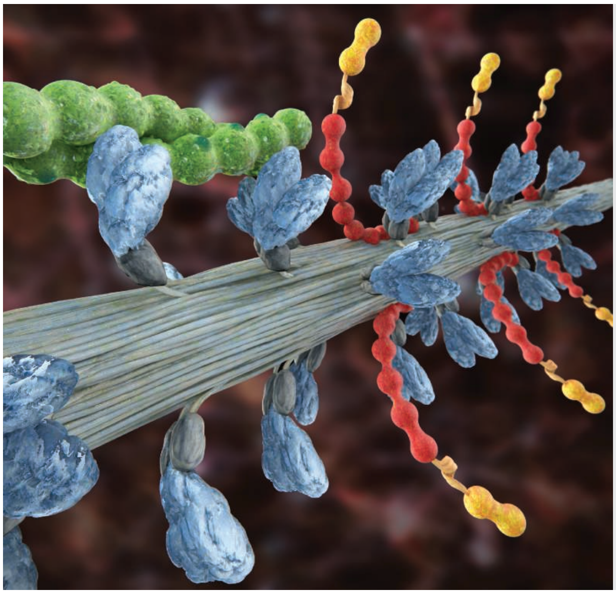

<< Understanding a Broken Heart

Cardiac myosin-binding protein C (cMyBP-C) is a thick filament–associated sarcomeric protein that modulates cardiac contractility in a phosphorylation-dependent manner; mutations in the *MYBC3* gene are the leading cause of hypertrophic cardiomyopathy. **Previs *et al.*** (p. 1215, published online 23 August; see the Perspective by **Burghardt and Ajtai**) have isolated native myosin thick filaments from transgenic mouse hearts, which retained the spatial distribution of cMyBP-C in the thick filament. Imaging of a single actin filament being propelled along the thick filament showed that the N-terminal 29-kD domain of cMyBP-C slows actomyosin motion in parts of the thick filament corresponding to the C-zones in which the thick filaments are cross-bridged. This effect on actomyosin contractility was tuned by graded phosphorylation of four serines adjacent to the 29-kD domain. The findings may explain the appearance of a cMyBP-C fragment in the serum of patients with cardiac ischemia and why cMyBP-C haploinsufficiency associated with cardiomyopathy patients might trigger a hypertrophic response.

Sensing Cell Size

How cells sense and control the size of their constituent parts is poorly understood, but an understanding is vital for interpreting normal cell function. **Chan and Marshall** (p. 1186) discuss how cells can sense and regulate the size of their internal structures or organelles. For example, bacterial flagellae act as their own tape measures. In eukaryote cells, reporter molecules may monitor cell and telomere length, and in molecular scaffolds, conformational changes and occupancy times measure organelle size. Indirect size selection may arise from a loss of function with growth or scaling problems with processes like intracellular transport. Now, advances in imaging offer glimpses into the mechanisms of cell sizing and the consequences if this process goes wrong.

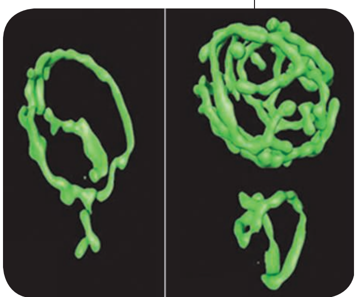

Predictions of Genetic Disease

Many genome-wide association studies (GWAS) have identified loci and variants associated with disease, but the ability to predict disease on the basis of these genetic variants remains small. **Maurano *et al.*** (p. 1190; see the Perspective by **Schadt and Chang**; see the cover) characterize the location of GWAS variants in the genome with respect to their proximity to regulatory DNA [marked by deoxyribonuclease I (DNase I) hypersensitive sites] by tissue type, disease, and enrichments in physiologically relevant transcription factor binding sites and networks. They found many noncoding disease associations in regulatory DNA, indicating tissue and developmental-specific regulatory roles for many common genetic variants and thus enabling links to be made between gene regulation and adult-onset disease.

Skipping the Odds

When confined to a plane and placed in a magnetic field at low temperatures, electrons are separated by energy into the so-called Landau levels; adding an extra electron after a Landau level that has been filled is costly. In some systems, electron-electron interactions cause the appearance of sublevels, in a phenomenon known as the fractional quantum Hall effect (FQHE). This effect has been observed in graphene, but the number of levels that had been resolved was limited. **Feldman *et al.*** (p. 1196) directly measured the change in the chemical potential caused by varying electron density, which is controlled by gate voltage. Once the FQH states were identified, the Landau levels with odd-numerator fractional fillings were found to be missing between filling factors 1 and 2, because of the broken and preserved symmetries of graphene. These observations help to explain how the FQHE in graphene is different from that observed in conventional semiconductors, and the technique will also allow local measurements to be made; hence, monitoring of spatial variations in sample behavior is possible.

Enols in the Atmosphere?

Keto/enol tautomerization (HC–C=O C=C–OH) plays a central role in the chemistry of carbonyl compounds in a solution in which solvent and catalytic acids or bases can facilitate the proton transfer from C to O and back again. In contrast, analyses of atmospheric chemistry tend to exclude enol structure, on the assumption that tautomerization does not proceed regularly in gas phase. **Andrews *et al.*** (p. 1203, published online 16 August) used isotopic labeling to probe the photoisomerization pathway of gaseous acetaldehyde in the lab and discovered evidence for an enol. Subsequent modeling indicates that photogenerated enols could build up sufficiently in the troposphere to account for previously puzzling observations of organic acids in the atmosphere.

Pinning Down Nuclear Shells

The nuclei of heavy atoms are destabilized by proton repulsions, and, conversely, the quantum-mechanical shell effects help to stabilize them. There are theoretical models for predicting the masses of yet-to-be-discovered superheavy elements, based on such shell effects, and these models can be tested by studying the shells of known actinide nuclei. The problem is that current mass values determined from studying radioactive decay products have

CREDITS (TOP TO BOTTOM): ROBERT W. MCGREGOR/WWW.MCGREGORFINEART.COM; MARSHALL *ET AL.*

Published by AAAS

substantial errors. **Minaya Ramirez *et al.*** (p. 1207, published online 9 August; see the Perspective by **Bollen**) were able to collect a sufficient number of nuclei of lawrencium and nobelium isotopes in an ion trap to determine their masses directly by mass spectroscopy. These results will be helpful in predicting the heaviest possible element.

Nighttime Sources

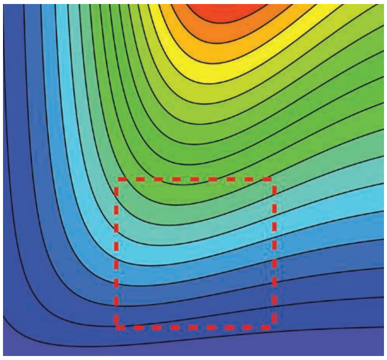

Organic aerosols account for about half of the total mass of small (submicrometer) particles in the troposphere, and most of them are believed to form through the oxidation of volatile molecules, rather than being emitted directly from specific sources. These particles have important roles in many atmospheric processes, and therefore a better understanding of their complex composition and chemistry is desirable. **Rollins *et al.*** (p. 1210) report on measurements of particulate organic nitrates, an important class of organic aerosols that form at night. However, they also found that high concentrations of organic molecules can suppress the growth of organic nitrate particles. These observations should help improve efforts to reduce organic aerosol pollution.

Responding to Light and Heat

The protein rhodopsin is sensitive to dim light, but its sensitivity is limited by signals caused by the noise of thermal activation. The basis of this relationship, known as the Barlow correlation, has long been debated. A recent study suggested that thermal activation involves a canonical isomerization reaction. **Gozem *et al.*** (p. 1225) confirm that isomerization is the rate-limiting step controlling thermal noise, and they provide a molecular understanding of the Barlow correlation. They use quantum mechanics coupled with molecular mechanics to show that the transition state mediating thermal activation has the same electronic structure as the photochemical excited state.

Toxic Neighborhood

Bacterial populations are often considered to be driven by gene-centric, selfish dynamics. Superficially, antibiotic production fits this picture as individuals can gain most benefit by inhibiting or killing close relatives with high niche overlap. Contrary to that notion, **Cordero *et al.*** (p. 1228; see the Perspective by **Morlon**) show that bacteria in the wild form social units in which antibiotic production and resistance leads to cooperation within, and antagonism between, populations. A combination of high-throughput interaction screening, molecular genetics, and genomics revealed that antibiotics are produced by only a few members of each population, while all other members are resistant. In the past, lack of knowledge of the ecological structure of microbial populations has led to interpretations of antibiotic production and resistance as being largely driven by short-lived, cyclic invasions of populations by antibiotic-producing resistant bacteria. This work shows that structured, socially cohesive bacterial populations exist in the wild and form organizational patterns similar to those of animal and plant populations.

Oncogenic TACC-tics

Human cancers exhibit many types of genomic rearrangements—including some that juxtapose sequences from two unrelated genes—thereby creating fusion proteins with oncogenic activity. Functional analysis of these fusion genes can provide mechanistic insights into tumorigenesis and potentially lead to effective drugs, as famously illustrated by the *BCR-ABL* gene in chronic myelogenous leukemia. **Singh *et al.*** (p. 1231, published online 26 July) identify and characterize a fusion gene present in 3% of human glioblastomas, a deadly brain cancer. In the resultant fusion protein, the tyrosine kinase region of the fibroblast growth factor receptor (FGFR) is joined to a domain from a transforming acidic coiled-coil (TACC) protein. The TACC-FGFR protein is oncogenic, shows unregulated kinase activity, localizes to the mitotic spindle, and disrupts chromosome segregation. In mice, FGFR inhibitors slowed the growth of tumors driven by the TACC-FGFR gene, suggesting that a subset of glioblastoma patients may benefit from these types of drugs.

CREDIT: ROLLINS *ET AL.*

Jim Austin is Editor of *Science* Careers.

Bruce Alberts is Editor-in-Chief of *Science*.

Planning Career Paths for Ph.D.s

THERE WAS A TIME NOT SO LONG AGO WHEN NEW SCIENCE PH.D.S IN THE UNITED STATES WERE expected to pursue a career path in academia. But today, most graduates end up working outside academia, not only in industry but also in careers such as science policy, communications, knowledge brokering, and patent law.* Partly this is a result of how bleak the academic job market is, but there is also a rising awareness of career options that Ph.D. scientists haven't trained for directly—but for which they have useful knowledge, skills, and experience. Still, "there is a huge disconnect between how we currently train scientists and the actual employment opportunities available for them,"† and an urgent need for dramatic improvements in training programs to help close the gap. One critical step that could help to drive change would be to require Ph.D. students and postdoctoral scientists to follow an individual development plan (IDP).

In 2002, the U.S. Federation of American Societies for Experimental Biology (FASEB) recommended that every postdoctoral researcher put together an IDP in consultation with an adviser. Since then, several academic institutions have begun to require IDPs for postdocs. And in June, the U.S. National Institutes of Health (NIH) Biomedical Research Workforce Working Group recommended that the NIH require IDPs for the approximately 32,000 postdoctoral researchers they support. Other funding agencies, public and private, are moving in a similar direction.

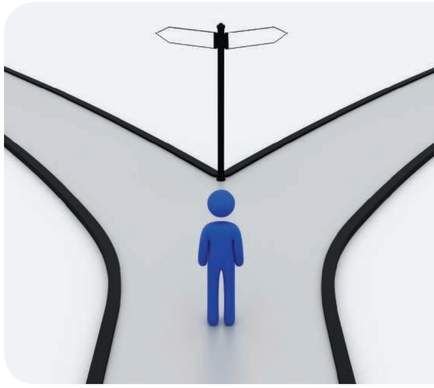

IDPs have long been used by government agencies and the private sector to achieve specific goals for the employee and the organization. The aim is to ensure that employees have an explicit tool to help them understand their own abilities and aspirations, determine career possibilities, and set (usually short-term) goals. In science, graduate students and new Ph.D. scientists can use an IDP to identify and navigate an effective career path.

A free Web application for this purpose, called myIDP, has become available this week.‡ It is designed to guide early-career scientists through a confidential, rigorous process of introspection to create a customized career plan. Guided by expert knowledge from a panel of science-focused career advisers, each trainee's self-assessment is used to rank a set of career trajectories. After the user has identified a long-term career goal, myIDP walks her or him through the process of setting short-term goals durected toward accumulating new skills and experiences important for that career choice. After each step, the user updates the plan, documenting efforts and progress. The user can opt to receive monthly e-mail reminders from myIDP to stay focused on goals and update progress and plans. Very importantly, the plan can be altered as skills develop, interests change, and career objectives are reconsidered.

Although surveys reveal the IDP process to be useful, trainees report a need for additional resources to help them identify a long-term career path and complete an IDP. Thus, myIDP will be most effective when it is embedded in larger career-development efforts. For example, universities could incorporate IDPs into their graduate curricula to help students discuss, plan, prepare for, and achieve their long-term career goals. The participation of faculty mentors is essential because trainees need a safe, supportive atmosphere in which to openly discuss their career plans and interests.

By turning introspection into a structured exercise, the use of IDPs allows trainees to translate a vague source of anxiety into a working plan, applying their well-developed analytical skills to the critical problem of building their own lives and careers.

– Jim Austin and Bruce Alberts

10.1126/science.1226552

*National Science Foundation, Science and Engineering Indicators 2012, Table 3-20 (www.nsf.gov/statistics/seind12/c3/tt03-20.htm). †M. Rosenberg, *ASBMB Today*, August 2012 (www.asbmb.org/asbmbtoday/asbmbtoday_article.aspx?id=17458). ‡http://myidp.sciencecareers.org.

EDITED BY GILBERT CHIN AND JAKE YESTON

CHEMISTRY

Cage Match

What does water look like? Many think of waves and ripples, and various shades of color, reflected from whatever materials contain and constrain the liquid, disrupting an otherwise perfect clarity. Chemists want to know about the structure—how individual H_2O molecules orient relative to one another and thereby lend water its range of remarkable properties. In this context, the hexamer (six molecules) has special significance: It's the smallest, and therefore most easily analyzed, three-dimensional assembly. Yet even this simplified sub-structure has been the subject of decades-long debate regarding which of three possible arrangements is the most stable. Only very recently were all three successfully observed in the same experiment (see Pérez *et al*., Reports, 18 May 2012, p. 897). This gave the so-called cage a slight edge over the prism, though results depended on the inert carrier gas used for spectral characterization. Wang *et al*. have now performed high-level theoretical calculations that give the prism the very slightest edge but suggest that the cage has nearly the same energy at the lowest temperature and soon overtakes the prism upon warming, on account of its greater entropy. Eventually, a book shape with the greatest entropy is predicted to overtake them both, closing the book, perhaps, on the whole question. —JSY

J. Am. Chem. Soc. **134**, 11116 (2012).

ATMOSPHERIC SCIENCE

Constraints from Above

Atmospheric aerosols exert their largest influence on climate through the indirect effects that they have on clouds. These indirect effects, which influence cloud formation, lifetimes, and radiative properties, contribute the largest uncertainty in estimates of the radiative forcing of past and future climate change. Measuring the magnitude of the aerosol indirect effect is difficult, though, in large part due to the competing effects of meteorological variables such as temperature, pressure, relative humidity, and convection. Wang *et al.* use results from a collection of global climate models to suggest a way in which one component of the aerosol indirect effect, liquid water path, might be better determined by satellite observations of clouds. Their analysis indicates that the liquid water path response to aerosol perturbation is significantly smaller than calculated by most models and that aerosols seem to have a substantially smaller impact on shortwave cloud radiative forcing over the oceans than current global climate models suggest. Though much more work is needed to quantify satellite-derived estimates of cloud properties and the aerosol indirect effect, this research reveals another piece of a complex mosaic of cause and effect. — HJS

Geophys. Res. Lett. **39**, L15709 (2012).

ECONOMICS

The Long Shadow of Genetic Capital

Comparative analyses of human genomes have contributed to a spatiotemporal narrative that begins in East Africa and extends to the other continents. These historical traces reveal a decrease in genetic diversity as migratory distance from Addis Ababa increases. Ashraf and Galor present the hypothesis that genetic diversity has exerted a long-lasting effect on economic development—which is quantified as population density in the precolonial era and as per-capita income for contemporary nations—beyond the influences of geography, institutions, and culture. They posit that intermediate levels of heterozygosity allow for a productive balance between the social costs of high diversity and the creative benefits of higher variance in cognitive skills. They show that the optimal level of diversity was approximately 0.68 in 1500 CE, and that this increased to 0.72 (which is pretty much where the United States sits) in the year 2000, with the most homogeneous country, Bolivia, placed at 0.63 and the most diverse country, Ethiopia, at 0.77. Just how large an effect are we talking about? They estimate that genetic diversity accounts of 16% of the cross-country dispersion in per-capita income; put in another way, shifting the diversity of the United States higher or lower by one percentage point would decrease per-capita income by 1.9%. — GJC

Am. Econ. Rev., in press (2012); http://ideas.repec.org/p/bro/econwp/2010-7.html.

MOLECULAR BIOLOGY

Untangling Linked DNA

To access the information stored in the genome during replication, repair, and recombination, the two strands of DNA must be unwound and sometimes cut and rejoined. Such synthesis and repair work can result in DNA strands becoming catenated, or topologically linked to one another, and topoisomerase enzymes have evolved to deal with such problems. Cejka *et al.* show that a topoisomerase complex in yeast, consisting of topoisomerase III (Top3), the helicase Sgs1, and Rmi1, works hand in hand with the single-stranded (ss)DNA binding protein RPA

CREDITS (TOP TO BOTTOM): ISTOCKPHOTO; ISTOCKPHOTO

to unlink catenated and hemicatenated dsDNA rings, arising from late or partially replicated DNA intermediates, double holliday junctions, and so forth. They show that Sgs1 acts to unwind the dsDNA and that RPA captures the ssDNA to provide a substrate for Top3, which prefers single strands. Sgs1 delivers Top3 to the ssDNA, where it first cuts a DNA strand, forming a gap, and then passes intact ssDNA strands through the gap to unlink the DNA. Rmi1 stimulates strand passage by stabilizing the Top3 reaction intermediate, thereby lengthening the time for strand passage to occur. — GR

Mol. Cell **47**, 10.1016/j.molcel.2012.06.032 (2012).

BIOCHEMISTRY

Screening Entry

Nuclear pore complexes are gateways between the cytoplasm and the nucleus, and they contain multiple copies of nucleoporins (Nups). Inert objects larger than 5 nm cannot pass, yet nuclear transport receptors (NTRs) facilitate the translocation of cargo up to 40 nm in diameter. Phenylalanine-glycine repeat–containing Nups (FG-Nups) bind NTRs during facilitated translocation, but how binding increases permeability and how FG-Nups keep out the nonbinders are unclear.

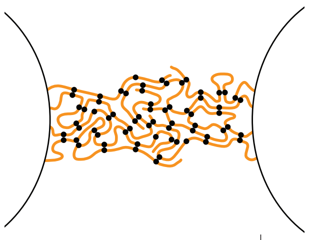

In a "reduction of dimensionality" model, the FG domains (black dots) form a surface that NTRs slide over to traverse the NPC. In two other models, the FG domains do bar passive transport: The virtual gate model relies on a brush-like behavior of noninteracting FG domains that repel inert material, whereas the selective phase model claims that the barrier is formed by a sieve-like hydrogel of interacting FG domains. Hülsmann *et al.* reconstituted nuclear pores and found that the FG-Nup Nup98 is essential both for active transport and maintenance of a passive barrier. The FG domain of Nup98 formed a hydrogel in vitro; this domain was required for the formation of a permeability barrier in reconstituted NPCs and could not be complemented by a noncohesive FG domain.

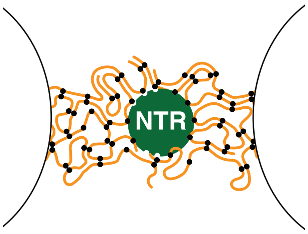

CREDIT: HÜLSMANN ET AL., CELL 150, 738 (2012)

These data support the selective phase model in which the meshwork formed by interacting domains excludes inert molecules, but NTRs bind to the FG domains and disrupt the mesh in order to transport their cargoes. — VV

Cell **150**, 738 (2012).

APPLIED PHYSICS

Flexible and Fast

High-speed communications are essential in many prospective applications of flexible electronics. However, organic polymers, amorphous silicon, and oxide-based thin-film transistors have limited carrier mobilities for high-frequency operation. Lee *et al.* demonstrate a fully bendable, all-graphene modulator circuit that can encode a carrier signal with quaternary (four-wave) digital information. The ambipolarity and the nonlinearity in a graphene transistor were exploited in two types of modulation scheme, one that can convey digital data as shifts in amplitude (quaternary amplitude-shift keying) and the other as shifts in phase (quadrature phase-shift keying). These schemes were realized with just one or two all-graphene transistors, respectively, and could greatly reduce circuit complexity relative to conventional digital modulators. The devices are also highly transparent (~95% transmittance) because all components (the channel, interconnects, load resistor, and contact and gate electrodes) were fabricated from graphene films. — PDS

Nat. Commun. **3**, 10.1038/ncomms2021 (2012).

GENETICS

Geography and Genetic Destiny

Humans are the most cosmopolitan species across the globe, because they are found on every continent and have established populations in almost every climatic zone. In order to evaluate the impact of local geography on human genetic diversity, Wang *et al.* looked at genome-wide Single-nucleotide polymorphism data across 100 populations. The authors evaluated the data at the continent and sub-continental levels and found that worldwide populations cluster with their respective local geography. This correlation was stronger in East Asia, in spite of the barriers presented by the Himalayas, relative to other well-studied populations, such as Europe. Thus, human demography was shaped by how topology affected human dispersal and migrations, and a greater understanding of these relationships may provide the tools to allow us to trace back the original peopling of the globe. — LMZ

PLoS Genet. **8**, e1002886 (2012).

Published by AAAS

AROUND THE WORLD

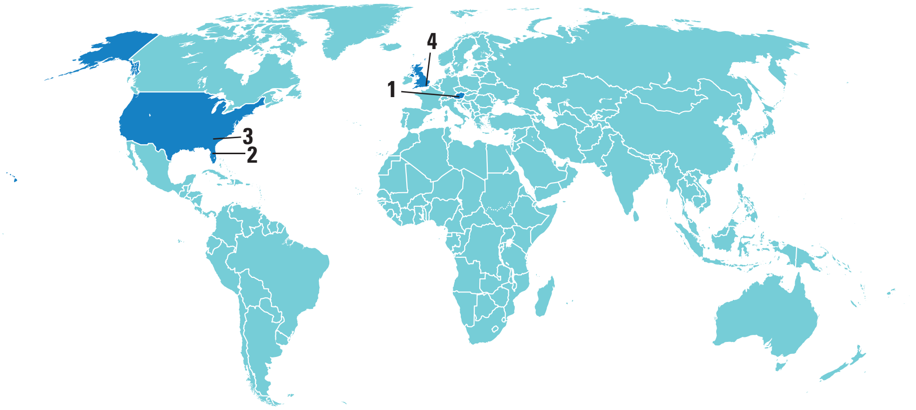

Vienna 1

Iran Accelerating Nuclear Program, Report Warns

Iran is continuing to expand its capacity to build a nuclear weapon and resist international oversight of its atomic program according to a 30 August report from the International Atomic Energy Agency (IAEA). Nuclear engineers have more than doubled the number of centrifuges capable of refining uranium at a fortified underground facility known as Fordow, and have accelerated production of highly enriched nuclear fuel, IAEA concludes. Iran now appears to be producing at least 10 kilograms of 20%-enriched uranium per month and has stockpiled at least 189 kilograms, enough to dramatically reduce the time it would take to produce the 90%-enriched material typically used in weapons. And production could accelerate rapidly if Iran activates its large number of newly installed centrifuges. The report says the number of installed centrifuges at Fordow nearly doubled to 2140 from 1064 in May, adding to the more than 9000 centrifuges already operating at another facility.

Tampa, Florida 2

Neuroscience In, Climate Change Out, In GOP Platform

More neuroscience research and a modernized nuclear arsenal are among the science priorities presented in the 2012 Republican Party Platform, approved 28 August at the GOP's national convention in Tampa, Florida. Other topics, such as sending humans into space and climate change, appear to have faded from the GOP agenda.

The 2012 GOP platform resembles its 2008 edition in supporting federal funding for biomedical research and opposing human embryonic stem cell studies. But it gives a new nod for more neuroscience research.

The GOP is vaguer than it was in 2008 about whether it would revive efforts to return humans to the moon. However, it lauds NASA's "spectacular results" over the

past few decades and warns against falling behind other countries in space research.

The largest shift is evident on climate change: While the 2008 platform spent nearly two pages on "addressing climate change responsibly" and "reducing demand for fossil fuels," the topics are barely mentioned this year. The GOP gives qualified support for a market-based approach to developing alternative energy sources, but the greater emphasis is on domestic oil, gas, and coal development. **http://scim.ag/GOPscience**

Atlanta 3

Drug-Resistant TB on the Rise

A large international study has confirmed the rise of so-called extensively drug-resistant (XDR) tuberculosis (TB) strains seen previously in national surveillance data. For the study, published online by *The Lancet* last week, sputum samples from 1278 patients from eight countries already resistant to two first-line antibiotics were shipped to the U.S. Centers for Disease Control and Prevention in Atlanta and tested for resistance against a panel of 11 TB drugs. Overall, almost 44% were resistant to a second-line drug as well, and almost 7% of the isolates were XDR, meaning that second-line drugs from two different groups failed.

Data from different TB studies are hard

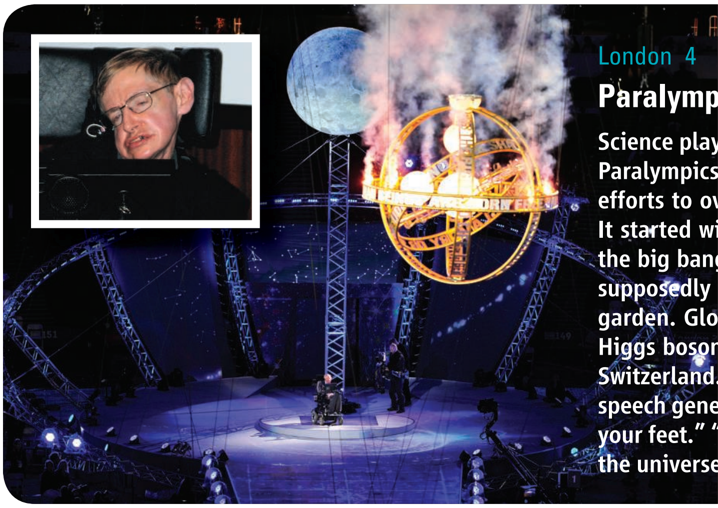

London 4

Paralympics' Praise for Science

Science played an unusually large role in the opening ceremony for London's Paralympics on 28 August. Titled Enlightenment, the show likened athletes' efforts to overcome obstacles to scientists' quest to expand our knowledge. It started with a sphere (pictured) setting off an explosion that represented the big bang and featured giant floating apples to honor Isaac Newton, who supposedly had a key insight about gravity after he saw an apple fall in his garden. Glowing, swirling umbrellas celebrated the recent discovery of the Higgs boson at the European particle physics laboratory CERN near Geneva, Switzerland. Physicist and narrator Stephen Hawking (*inset*)—using his iconic speech generator—urged onlookers to "[l]ook up at the stars and not down at your feet." "Try to make sense of what you see, and wonder about what makes the universe exist," he said. "Be curious."

CREDITS (TOP TO BOTTOM): AP PHOTO/JAE C. HONG; GLYN KIRK/AFP/GETTYIMAGES; (INSET) WIKIMEDIA COMMONS

Published by AAAS

BY THE NUMBERS

323,000 Number of deaths that could result from a magnitude-9.1 earthquake and subsequent 34-meter-high tsunami originating along the Nankai Trough off Japan's Pacific Coast between Tokyo and Osaka, according to a study by the government's Central Disaster Prevention Council.

1100+ Number of brain scans from subjects with autism and matched controls released last week by the Autism Brain Imaging Data Exchange consortium as part of an open science effort called the International Neuroimaging Data-Sharing Initiative.

to compare because they often use different patient populations, says Sven Hoffner of the Swedish Institute for Communicable Disease Control in Solna, "but these are among the highest figures ever reported." XDR rates varied widely however, from 0.8% in the Philippines to 15.2% in South Korea, reflecting different treatment regimens.

NEWSMAKERS

Richard Levin to Step Down As Yale President

It's a cliché to say that a long-serving university president has changed the landscape of the institution. But in the case of economist **Richard Levin**, who last week announced he would be stepping down next year after 19 years at the helm of Yale University, it's also true. Some 70% of the space on campus has been partially or comprehensively renovated since he took office in 1993, including a massive expansion of Yale's Science Hill.

Levin, 65, came to Yale in 1970 as a graduate student in economics and never left New Haven, Connecticut. During his remarkably long presidential tenure—twice the average of his Ivy League colleagues—Levin is also credited with improving contentious labor relations on campus, strengthening ties with city officials, and helping increase the school's endowment sevenfold, to $19 billion, despite two economic downturns. He plans to return to the faculty after taking a sabbatical to write a book on higher education and economics.


Levin

NOTED

>The free online server **arXiv**—on which scientists post their work before publication—**will receive up to $350,000 a year for 5 years** from the Simons Foundation, according to a 28 August announcement. Cornell University Library, which maintains and operates the repository, says that arXiv provided nearly 50 million free downloads and received more than 76,000 submissions in 2011, mainly research from physics, mathematics, statistics, and computer science.

Random Sample

No-Nonsense Views Of Edward Lear

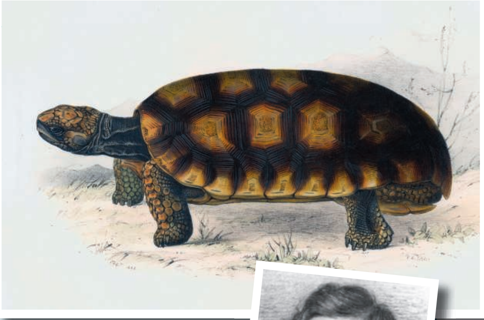

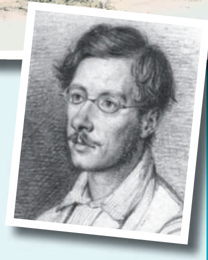

"The Owl and the Pussy-cat went to sea/In a beautiful pea green boat." So begins the famous poem by Edward Lear, the 19th century British artist and author. Best known for his nonsense literature, Lear was also a groundbreaking zoological illustrator. In honor of the bicentenary of his birth, London's Royal Society has opened an exhibition of rare books, drawings, and lithographs of his work entitled *Edward Lear and the Scientists*.

Lear came from a prosperous family that fell on hard times. He began selling his drawings while still a teenager, including pictures of diseased specimens for doctors. By drawing some of the inhabitants of the new London Zoo—particularly parrots—he made his name as an animal illustrator. Lear spent much of the early 1830s at the Earl of Derby's private menagerie at Knowsley Hall near Liverpool. The centerpiece of the Royal Society exhibition is a folio illustrated by Lear, *Gleanings from the Menagerie and Aviary at Knowsley Hall*, published in 1846. Lear provided illustrations, including the yellow-footed tortoise (above), for the work of 10 members of the Royal Society during the 1830s.

FINDINGS

Weighing Individual Molecules

Vibrating like a guitar string, a nanometer-sized beam of silicon can weigh individual molecules, opening the way to a new type of mass spectrometry.

When a molecule sticks to the beam, the added mass lowers the frequency of vibration, in principle revealing the molecule's mass. However, the frequency shift also depends on where on the beam the molecule lands: A lighter molecule landing in the middle could produce the same frequency shift as a heavier one landing closer to one end. To avoid this ambiguity, Michael Roukes, a physicist at the California Institute of Technology in Pasadena, and colleagues shake a beam at two frequencies simultaneously. That's possible because a beam can vibrate in various patterns of motion, or modes, each with its own frequency. An alighting molecule lowers the frequencies of two modes by different amounts, and the two frequency shifts reveal both the molecule's position and its mass, the team reported on 26 August in *Nature Nanotechnology*.

"How applicable this will be to generalized mass spectroscopy, time will tell," says John Kasianowicz, a biophysicist at the National Institute of Standards and Technology in Gaithersburg, Maryland, who was not involved in the work. "But I think this is a major advance." **http://scim.ag/mol_scale**

Science LIVE

Join us on **Thursday, 13 September, at 3 p.m. EDT** for a live chat on **intelligence and culture in Neandertals**. **http://scim.ag/science-live**

CREDITS (TOP TO BOTTOM): EDWARD LEAR/THE ROYAL SOCIETY; (INSET) WILHELM MARSTRAND; WORLD ECONOMIC FORUM (WWW.WEFORUM.ORG)/PHOTO BY NORBERT SCHILLER

ASTRONOMY

World-Class Observatory Rising on 'Roof of the World'

China mountain high. Shiquanhe Observatory on Tibet's Ngari Plateau may be Asia's answer to Mauna Kea.

BEIJING—Asian astronomers have long yearned for a premier mountaintop observatory—their own Mauna Kea, the Hawaiian volcano crowned with superb telescopes. After a 2-decade-long search, their hopes are about to be realized. Astronomers have identified a summit on the Ngari Plateau in southwestern Tibet Autonomous Region, near the border with Kashmir, as the likely site for an international observatory. At 5100 meters above sea level, Shiquanhe Observatory would be the highest permanent astronomical perch on Earth's surface.

Preliminary weather and atmospheric data suggest that Ngari would rival high-altitude facilities at Mauna Kea, the Atacama Desert in Chile, and in the Canary Islands. "It's comparable to the best sites in the world," says Cui Xiangqun, an astronomer at the Nanjing Institute of Astronomical Optics and Technology. But Shiquanhe is not quite ready for prime time. The critical testing phase begins this year, when researchers start collecting continuous environmental data and make observations with a small optical telescope. In the meantime, Chinese astronomers are drafting plans for a pair of megafacilities at Shiquanhe: their own version of Europe's Extremely Large Telescope (ELT) and a supersized edition of the Large Sky Area Multi-Object Fiber Spectroscopic Telescope (LAMOST) near Beijing that's about to launch a sky survey.

Scientists in the region are champing at the bit. "At that altitude, we can expect very good astronomy," Norio Kaifu, president of the International Astronomical Union, told *Science* here at IAU's general assembly last week. "I'm pleased that we finally seem to have found a place for an Asian observatory."

Ngari's expected anointment as the pinnacle of Asian astronomy follows a grueling selection process. The search began in 1993, when astronomer Liu Caipin of Purple Mountain Observatory in Nanjing led a survey team to western China's Qinghai Province, on the northern reaches of the Qinghai-Tibetan Plateau. Data were discouraging, so in 2000 they moved to Tingri in southern Tibet, a staging area for climbers setting out for Mount Everest. There they also met with disappointment. After nearly a decade, the team from China, Japan, South Korea, and Taiwan had little to show for their efforts. "I almost abandoned hope," says Kaifu, who is also an astronomer at the National Astronomical Observatory of Japan.

The surveyors cast a wider net and, by August 2005, they had winnowed the candidates to the eastern Pamir Mountains of Xinjiang Uyghur Autonomous Region and Tibet's Ngari Plateau. They put identical meteorological stations at each site, with four key variables in mind: cloud coverage, wind speed, water vapor, and seeing—a telescope's ability to focus starlight. Work at Ngari is not for the faint of heart. Until a couple of years ago, to reach the area, researchers had to drive more than a day on atrocious roads across a largely uninhabited moonscape while combating altitude sickness. "Sometimes on the way we'd have to change a tire four or five times," says site survey leader Yao Yongqiang, who is based here at National Astronomical Observatories of the Chinese Academy of Sciences. "We worried that our car would turn over or we'd break down and freeze to death."

Their tribulations were worth it. By 2007, it was clear that Ngari was superior. The next step was to pinpoint the astronomical sweet spot on a swath of the plateau a couple of hundred kilometers long. The survey team hit a speed bump in March 2008, when riots in Lhasa, Tibet's capital, prompted the government to lock down the region for months. Things got back on track late that year, and working conditions have improved considerably ever since. In 2010, Shiquanhe, the capital of Ngari, opened an airport, eliminating the harrowing trek. Then, last year scientists finished installing solar panels for a stable electrical supply, a satellite dish for communications, and two domes, one of which is now home to a 25-centimeter optical telescope for site testing.

The preliminary verdict on Ngari is mixed. On the bright side, the Ngari Plateau is bone-dry: The team so far has recorded about 1 millimeter of precipitation a year, less than half the amount Mauna Kea gets and a bit more than Chile. Ngari's air transparency is "pretty good," Kaifu says. And according to Yao, the site is not as windy as researchers initially feared. But light pollution from Shiquanhe, 25 kilometers to the north, might pose a problem. Ngari is often cloudy during the summer monsoon season, Kaifu says, so the number of nights there in which the heavens are "fully observable" is fewer than at Mauna Kea.

Those qualms aside, there's no doubt that Ngari would be a formidable location for astronomy, especially in the infrared and submillimeter wavelengths. Absorption of those photons increases sharply as the atmosphere

The site is right? One of Shiquanhe's two domes (*right*) now shelters a 25-centimeter optical telescope. Liu Liyong of China's National Astronomical Observatories prepares for survey work last November.

CREDITS: YAO YONGQIANG

Published by AAAS

thickens nearer Earth's surface. Kaifu estimates that telescopes at Ngari would capture about 30% more photons in the middle infrared band than do telescopes on Mauna Kea, which sits 4200 meters above sea level. "This is a huge difference," he says.

Next spring, researchers will gather in China to discuss which kinds of medium-sized telescopes, with mirrors up to 2 meters in diameter, would work best in Tibet. Taiwan intends to ship a 50-centimeter optical telescope to Ngari within 2 years, while Japan plans to install a 60-centimeter optical and infrared telescope there next year that could be used to observe gamma ray bursts and supernovae. Down the road, Kaifu says, Japan may wish to put a 3-meter segmented mirror telescope at Ngari.

Thinking even bigger, China aspires to erect two massive telescopes at Ngari. One is a 20- to 30-meter optical and near-infrared telescope similar to ELT, which Europe plans to build in the next decade in Chile. China has designated an ELT as a priority in the next 5-year plan that starts in 2016, Cui says. The best place to build an ELT in China, she says, is Ngari: "The roof of the roof of the world."

The other aim is scaling up LAMOST, an innovative instrument now known as Guo Shoujing Telescope that uses thousands of optical fibers to feed starlight into spectrographs for analysis (*Science*, 4 April 2008, p. 34). At the IAU meeting, China announced that LAMOST's commissioning data are now publicly available and that a formal sky survey will commence next month. More quietly, China has begun discussions with international partners on duplicating Beijing's LAMOST in Chile, says Zhao Yongheng, a vice director at LAMOST. He says that the plan for Ngari is far grander: doubling or tripling the size of LAMOST's 6-meter primary mirror.

Major decisions on how to instrument Ngari should wait until after 2 or 3 years of continuous data from the site are in hand, Kaifu says. "And we need some real astronomical observations," he says. One lingering issue for Kaifu and others is site access, as the Chinese government periodically closes Tibet to foreigners. Chinese astronomers understand that concern and are discussing the problem with authorities. "It will be an international observatory," Cui assures. And for Asian astronomers, it will be a long-awaited dream come true. **–RICHARD STONE**

With reporting by Zhang Dongdong.

PARTICLE PHYSICS

Fermilab Looks Abroad for Help With Neutrino Experiment

U.S. particle physicists hope that a smaller price tag and foreign support will enable the Department of Energy (DOE) to fund a flagship experiment in the next decade.

Five months ago, DOE officials balked at the then–$1.9 billion price tag for the proposed Long-Baseline Neutrino Experiment (LBNE) and asked Fermi National Accelerator Laboratory (Fermilab) in Batavia, Illinois, if it could be built in cheaper stages (*Science*, 30 March, p. 1553). Last week, lab officials presented a plan for a first stage that would cost only $789 million. But they said another $135 million would be needed for the scaled-down LBNE to approach the scientific potential of the original design.

"We are all pleased with the work that has been done to come up with a better approach that is not nearly as expensive as the first proposal," says William Brinkman, director of DOE's Office of Science, after viewing the lab's presentation to the federal High Energy Physics Advisory Panel in Rockville, Maryland. "We are considering how to fit it into our budget." With DOE's $792 million annual budget for particle physics likely to remain flat, LBNE could move forward only as construction winds down on other experiments (see table).

Neutrinos come in three types that morph into one another as the particles zip along. As originally designed, LBNE would make definitive measurements of such neutrino oscillations. It would look for evidence that neutrinos and antineutrinos oscillate differently, a phenomenon called CP violation that could help explain why the universe contains so much more matter than antimatter.

Name	Purpose	Cost	Status
NOvA	Long-baseline neutrino oscillation studies	$278 million	To be completed in 2015
MicroBooNE	Short-baseline neutrino oscillations	$20 million	To be completed in 2015
g-2	Measure magnetic moment of the muon	$41 million	Awaiting approval
Mu2e	Search for muons changing into electrons	$208 million–$287 million	Awaiting approval

Making room. Fermilab officials would like to begin building LBNE once construction ends on several smaller projects.

SOURCES: DOE FY13 CONGRESSIONAL BUDGET REQUEST; THE NEW (G-2) EXPERIMENT (PROPOSAL); MU2E CONCEPTUAL DESIGN REPORT

The original plan called for placing an enormous particle detector 1480 meters deep in the abandoned Homestake gold mine in Lead, South Dakota. It would catch neutrinos fired from a new beamline at Fermilab. A smaller "near detector" would sample the beam as it left Fermilab. The underground location would shield the main detector from cosmic rays, enabling it to look for signs that protons decay and to spot neutrinos from supernovae.

The new plan calls for no near detector and a main detector one-third of the original size on the surface at Homestake, reported Young-Kee Kim, Fermilab's deputy director and chair of the LBNE Reconfiguration Steering Committee. The surface location precludes significant science, but Fermilab officials hope international partners will help to build the detector underground.

The Indian government already collaborates with Fermilab and is weighing a contribution to LNBE, says Brajesh Choudhary of the University of Delhi.

Europe may also chip in. Since 2006, physicists have been shooting neutrinos from the European particle physics laboratory, CERN, in Switzerland, to a pair of detectors in Italy's subterranean Gran Sasso National Laboratory. CERN physicists have plans for a larger and more costly experiment like LBNE. But CERN also operates the world's largest atom smasher, the Large Hadron Collider, and has little money for a major new project.

"The idea that, with a contribution from Europe, [the LBNE detector] could go underground and be competitive with other proposals, I'm sure it will attract interest in Europe," says Sergio Bertolucci, CERN's research director. But the United States must first commit to the project, he says. **–ADRIAN CHO**

Published by AAAS

CARDIOVASCULAR DISEASE

Massive Trials to Test Inflammation Hypothesis

It's not often that eminent scientists enlist 24,000 volunteers and tens of millions of dollars to put their credibility on the line, but that's exactly what cardiologist Paul Ridker is doing. More than 20 years ago, early in his career at Harvard Medical School's Brigham and Women's Hospital in Boston, he began nurturing the idea that inflammation is deeply intertwined with cardiovascular disease. Ridker has never been able to prove that the body's inflammatory response causes heart attacks—or that blocking it can save lives. But he has built his case bit by bit. Now, his theory is being put to the test in a pair of massive clinical trials, both of which he's heading. One was launched last year by Novartis, and the other was announced last month by the U.S. National Heart, Lung, and Blood Institute (NHLBI).

"The question has always arisen, is inflammation simply a marker for risk, or is it a target for therapy?" says Steven Nissen, chair of cardiovascular medicine at the Cleveland Clinic in Ohio. With a pair of trials now focused on his thesis, Ridker has "two shots on goal," Nissen says, and if one or both succeed he will have identified the first new class of antiatherosclerosis drugs since 1987, when statins were introduced.

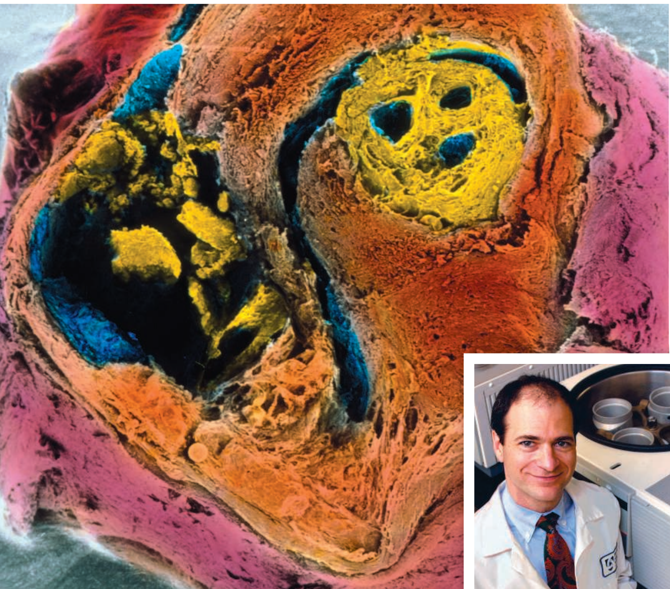

Grand test. Cardiologist Paul Ridker (*inset*) is leading two studies to see whether blocking inflammation can treat atherosclerosis.

NHLBI's study aims to sign up 7000 volunteers to test methotrexate, now used to treat rheumatoid arthritis and, at much higher doses, certain cancers. The Novartis trial is recruiting 17,000 others, about three-quarters of whom will inject different doses of a monoclonal antibody approved for an extremely rare class of inflammatory diseases. Both trials will treat patients for up to 4 years. Novartis has not revealed the cost of its trial, but NHLBI is budgeting nearly $80 million.

"This is testing a whole new paradigm, a whole new approach, towards treating atherosclerosis," because anti-inflammatory drugs are not now a therapy of choice, says Michael Lauer, director of the Division of Cardiovascular Sciences at NHLBI. Ridker's trial went through five rounds of review before being approved.

Ridker is well known among cardiologists for his work on C-reactive protein (CRP), a protein in blood that rises along with inflammation. High levels of CRP, he found, correlate tightly with an increased risk of heart attacks and strokes. In 1997, Ridker published a paper about apparently healthy men taking a low dose of aspirin, which both inhibits blood clots and is an anti-inflammatory. Those with the highest CRP levels who took asprin had the best shot at avoiding heart attacks. After that, "[we] jumped fast through dozens and dozens of papers," he says; in 2008—the same year he proposed the methotrexate trial to NHLBI—he published the JUPITER trial, which was similar to the aspirin study but looked at the effects of cholesterol drugs.

JUPITER recruited nearly 18,000 people with high CRP levels and normal cholesterol. Half took the statin Crestor that lowers both LDL cholesterol and CRP. The drug reduced heart attacks and strokes by 50% and deaths by 20% (*Science*, 14 November 2008, p. 1039).

In both the aspirin and Crestor studies, Ridker tried to tease out whether the benefits of the drugs came from targeting inflammation, or from their anticlotting or anticholesterol effects. But he couldn't get a definitive answer. Crestor may have helped not because it lowered CRP but because it pushed cholesterol down in people with supposedly normal levels. The results were only "indirect suggestions" about inflammation's role, Ridker admits.

"Half the world said Paul is wrong, and the other half said Paul is right," says John Kastelein, a vascular medicine specialist at the Academic Medical Center in Amsterdam. Ridker has some recent findings on his side. Among them is a paper published in *The Lancet* in March by a worldwide genetics consortium. The group found that people with a gene variant that blunted interleukin-6 signaling, and thereby reduced systemic inflammation, had a somewhat lower risk of heart disease. "I find that one of the most important pieces of information in the last 10 years" coming from human data, says Kastelein, who, like Ridker, is a member of the consortium. (Kastelein is also involved in the Novartis trial.)

Still, many believe that the Ridker trials are a long shot. Some see a stronger scientific rationale for testing the Novartis therapy, canakinumab, because it specifically targets interleukin-1 and interleukin-6, both of which have been linked to heart disease. Methotrexate targets inflammation much more broadly. On the other hand, canakinumab has been injected by only a few thousand people, which makes unexpected side effects more likely, whereas millions have taken methotrexate since it was introduced for cancer therapy about 40 years ago. It's also a cheap generic, which captured NHLBI's attention. Even so, the drug is foreign to cardiologists. One who spoke to *Science* said his colleagues "thought I was joking" when he asked if they could imagine giving it to patients.

Ridker hopes to boost his chance of success by enrolling only patients with systemic inflammation into the trials—either by screening for high CRP, or for type 2 diabetes or metabolic disease, which also correlate with inflammation. Participants must also have had a prior heart attack. About one-third of those who've had a heart attack also have systemic inflammation. The results from these two trials will be "the endgame for 20, 25 years' worth of inflammation biology," Ridker says. And now the waiting begins.

–JENNIFER COUZIN-FRANKEL

CREDITS: P. M. MOTTA, G. MACCHIARELLI, S. A. NOTTOLA/PHOTO RESEARCHERS INC.; BRIGHAM AND WOMEN'S HOSPITAL (INSET)

GENOMICS

ENCODE Project Writes Eulogy For Junk DNA

When researchers first sequenced the human genome, they were astonished by how few traditional genes encoding proteins were scattered along those 3 billion DNA bases. Instead of the expected 100,000 or more genes, the initial analyses found about 35,000 and that number has since been whittled down to about 21,000. In between were megabases of "junk," or so it seemed.

This week, 30 research papers, including six in *Nature* and additional papers published by *Science*, sound the death knell for the idea that our DNA is mostly littered with useless bases. A decadelong project, the Encyclopedia of DNA Elements (ENCODE), has found that 80% of the human genome serves some purpose, biochemically speaking. "I don't think anyone would have anticipated even close to the amount of sequence that ENCODE has uncovered that looks like it has functional importance," says John A. Stamatoyannopoulos, an ENCODE researcher at the University of Washington, Seattle.

Beyond defining proteins, the DNA bases highlighted by ENCODE specify landing spots for proteins that influence gene activity, strands of RNA with myriad roles, or simply places where chemical modifications serve to silence stretches of our chromosomes. These results are going "to change the way a lot of [genomics] concepts are written about and presented in textbooks," Stamatoyannopoulos predicts.

The insights provided by ENCODE into how our DNA works are already clarifying genetic risk factors for a variety of diseases and offering a better understanding of gene regulation and function. "It's a treasure trove of information," says Manolis Kellis, a computational biologist at Massachusetts Institute of Technology (MIT) in Cambridge who analyzed data from the project.

The ENCODE effort has revealed that a gene's regulation is far more complex than previously thought, being influenced by multiple stretches of regulatory DNA located both near and far from the gene itself and by strands of RNA not translated into proteins, so-called noncoding RNA. "What we found is how beautifully complex the biology really is," says Jason Lieb, an ENCODE researcher at the University of North Carolina, Chapel Hill.

Throughout the 1990s, various researchers called the idea of junk DNA into question. With the human genome in hand, the National Human Genome Research Institute (NHGRI) in Bethesda, Maryland, decided it wanted to find out once and for all how much of the genome was a wasteland with no functional purpose. In 2003, it funded a pilot ENCODE, in which 35 research teams analyzed 44 regions of the genome—30 million bases in all, about 1% of the total genome. In 2007, the pilot project's results revealed that much of this DNA sequence was active in some way. The work called into serious question our gene-centric view of the genome, finding extensive RNA-generating activity beyond traditional gene boundaries (*Science*, 15 June 2007, p. 1556). But the question remained whether the rest of the genome was like this 1%. "We want to know what all the bases are doing," says Yale University bioinformatician Mark Gerstein.

Teams at 32 institutions worldwide have now carried out scores of tests, generating 1640 data sets. While the pilot phase tests depended on computer chip–like devices called microarrays to analyze DNA samples, the expanded phase benefited from the arrival of new sequencing technology, which made it cost-effective to directly read the DNA bases. Taken together, the tests present "a greater idea of what the landscape of the genome looks like," says NHGRI's Elise Feingold.

Because the parts of the genome used could differ among various kinds of cells, ENCODE needed to look at DNA function in multiple types of cells and tissues. At first the goal was to study intensively three types of cells. They included GM12878, the immature white blood cell line used in the 1000 Genomes Project, a large-scale effort to catalog genetic variation across humans; a leukemia cell line called K562; and an approved human embryonic stem cell line, H1-hESC.

As ENCODE was ramping up, new sequencing technology brought the cost of sequencing down enough to make it feasible to test extensively even more cell types. ENCODE added a liver cancer cell line, HepG2; the laboratory workhorse cancer cell line, HeLa S3; and human umbilical cord tissue to the mix. Another 140 cell types were studied to a much lesser degree.

In these cells, ENCODE researchers closely examined which DNA bases are transcribed into RNA and then whether those strands of RNA are subsequently translated into proteins, verifying predicted protein-coding genes and more precisely locating each gene's beginning, end, and coding regions. The latest protein-coding gene count is 20,687, with hints of about 50 more, the consortium reports in *Nature*. Those genes account for about 3% of the human genome, less if one counts only their coding regions. Another 11,224 DNA stretches are classified as pseudogenes, "dead" genes now known to be active in some cell types or individuals.

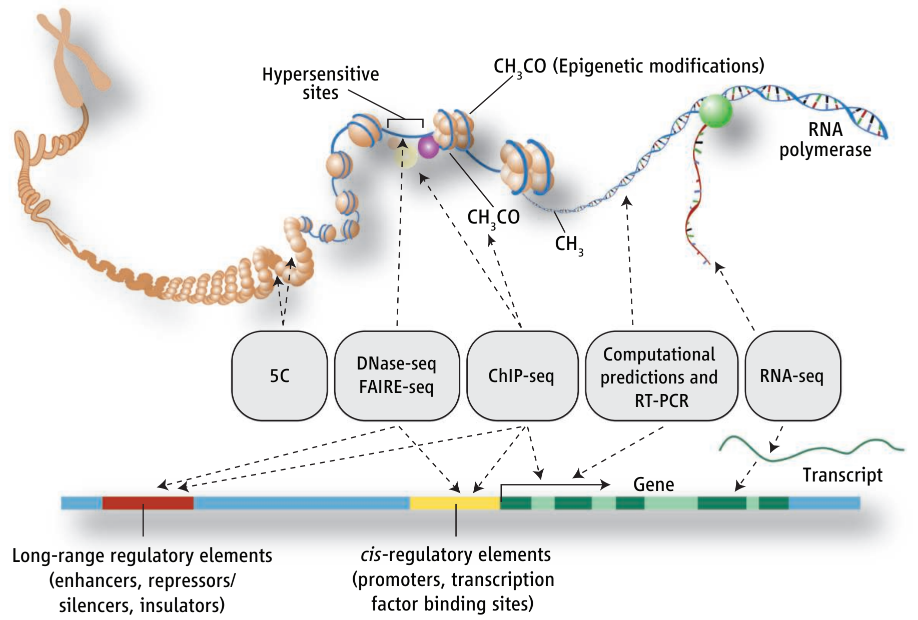

Zooming in. A diagram of DNA in ever-greater detail shows how ENCODE's various tests (gray boxes) translate DNA's features into functional elements along a chromosome.

CREDIT: ADAPTED FROM THE ENCODE PROJECT CONSORTIUM, *PLOS BIOLOGY* 9, 4 (APRIL 2011)

ENCODE drives home, however, that there are many "genes" out there in which DNA codes for RNA, not a protein, as the end product. The big surprise of the pilot project was that 93% of the bases studied were transcribed into RNA; in the full genome, 76% is transcribed. ENCODE defined 8800 small RNA molecules and 9600 long noncoding RNA molecules, each of which is at least 200 bases long. Thomas Gingeras of Cold Spring Harbor Laboratory in New York has found that various ones home in on different cell compartments, as if they have fixed addresses where they operate. Some go to the nucleus, some to the nucleolus, and some to the cytoplasm, for example. "So there's quite a lot of sophistication in how RNA works," says Ewan Birney of the European Bioinformatics Institute in Hinxton, U.K., one of the key leaders of ENCODE (see p. 1162).

As a result of ENCODE, Gingeras and others argue that the fundamental unit of the genome and the basic unit of heredity should be the transcript—the piece of RNA decoded from DNA—and not the gene. "The project has played an important role in changing our concept of the gene," Stamatoyannopoulos says.

Another way to test for functionality of DNA is to evaluate whether specific base sequences are conserved between species, or among individuals in a species. Previous studies have shown that 5% of the human genome is conserved across mammals, even though ENCODE studies implied that much more of the genome is functional. So MIT's Lucas Ward and Kellis compared functional regions newly identified by ENCODE among multiple humans, sampling from the 1000 Genomes Project. Some DNA sequences not conserved between humans and other mammals were nonetheless very much preserved across multiple people, indicating that an additional 4% of the genome is newly under selection in the human lineage, they report in a paper published online by *Science* (http://scim.ag/WardKellis). Two such regions were near genes for nerve growth and the development of cone cells in the eye, which underlie distinguishing traits in humans. On the flip side, they also found that some supposedly conserved regions of the human genome, as highlighted by the comparison with 29 mammals, actually varied among humans, suggesting these regions were no longer functional.

Beyond transcription, DNA's bases function in gene regulation through their interactions with transcription factors and other proteins. ENCODE carried out several tests to map where those proteins bind along the genome (*Science*, 25 May 2007, p. 1120). Two, DNase-seq and FAIRE-seq, gave an overview of the genome, identifying where the protein-DNA complex chromatin unwinds and a protein can hook up with the DNA, and were applied to multiple cell types. ENCODE's DNase-seq found 2.89 million such sites in 125 cell types. Stamatoyannopoulos and his colleagues describe their more extensive DNase-seq studies in *Science* (p. 1190): His team examined 349 types of cells, including 233 60- to 160-day-old fetal tissue samples. Each type of cell had about 200,000 accessible locations, and there seemed to be at least 3.9 million regions where transcription factors can bind in the genome. Across all cell types, about 42% of the genome can be accessible, he and his colleagues report. In many cases, the assays were able to pinpoint the specific bases involved in binding.

Last year, Stamatoyannopoulos showed that these newly discovered functional regions sometimes overlap with specific DNA bases linked to higher or lower risks of various diseases, suggesting that the regulation of genes might be at the heart of these risk variations (*Science*, 27 May 2011, p. 1031). The work demonstrated how researchers could use ENCODE data to come up with new hypotheses about the link between genetics and a particular disorder. (The ENCODE analysis found that 12% of these bases, or SNPs, colocate with transcription factor binding sites and 34% are in open chromatin defined by the DNase-seq tests.) Now, in their new work published in *Science*, Stamatoyannopoulos's lab has linked those regulatory regions to their specific target genes, homing in on the risk-enhancing ones. In addition, the group finds it can predict the cell type involved in a given disease. For example, the analysis fingered two types of T cells as pathogenic in Crohn's disease, both of which are involved in this inflammatory bowel disorder. "We are informing disease studies in a way that would be very hard to do otherwise," Birney says.

> ***"We are informing disease studies in a way that would be very hard to do otherwise."***
>
> **—EWAN BIRNEY, EUROPEAN BIOINFORMATICS INSTITUTE**

Another test, called ChIP-seq, uses an antibody to home in on a particular DNA-binding protein and helps pinpoint the locations along the genome where that protein works. To date, ENCODE has examined about 100 of the 1500 or so transcription factors and about 20 other DNA binding proteins, including those involved in modifying the chromatin-associated proteins called histones. The binding sites found through ChIP-seq coincided with the sites mapped through FAIRE-seq and DNAse-seq. Overall, 8% of the genome falls within a transcription factor binding site, a percentage that is expected to double once more transcription factors have been tested.

ENCODE By the Numbers

147 cell types studied

80% functional portion of human genome

20,687 protein-coding genes

18,400 RNA genes

1640 data sets

30 papers published this week

442 researchers

$288 million funding for pilot, technology, model organism, and current project

Yale's Gerstein used these results to figure out all the interactions among the transcription factors studied and came up with a network view of how these regulatory proteins work. These transcription factors formed a three-layer hierarchy, with the ones at the top having the broadest effects and the ones in the middle working together to coregulate a common target gene, he and his colleagues report in *Nature*.

Using a technique called 5C, other researchers looked for places where DNA from distant regions of a chromosome, or even different chromosomes, interacted. It found that an average of 3.9 distal stretches of DNA linked up with the beginning of each gene. "Regulation is a 3D puzzle that has to be put together," Gingeras says. "That's what ENCODE is putting out on the table."

To date, NHGRI has put $288 million toward ENCODE, including the pilot project, technology development, and ENCODE efforts for the mouse, nematode, and fruit fly. All together, more than 400 papers have been published by ENCODE researchers. Another 110 or more studies have used ENCODE data, says NHGRI molecular biologist Michael Pazin. Molecular biologist Mathieu Lupien of the University of Toronto in Canada authored one of those papers, a study looking at epigenetics and cancer. "ENCODE data were fundamental" to the work, he says. "The cost is definitely worth every single dollar."

–ELIZABETH PENNISI

Published by AAAS

Global Research Universities

IT'S NOT A FLUKE THAT THE UNITED States is home to most of the leading research universities in the world. But it's also not a given.

Many countries have paid close attention to what it took for the United States to climb to the top of the global academic research ladder in the past half-century. Some have now translated those lessons into national strategies that they hope will lift them up the ladder. What will it take for them to reach the top rungs?

Over the next several months, *Science* will examine the key ingredients needed to create and maintain what we have labeled global research universities. Indeed, ranking these universities has become a cottage industry. Although there is little consensus on what metrics to use, most scientists carry around in their heads their own list of top schools, compiled on the basis of anecdotal evidence, reputation, and personal preferences.

The first story in the series explores the role of mobility by focusing on the increasing flow of talent into East Asia, in particular Hong Kong and Singapore. Subsequent stories will look at other important factors that shape an institution's ability to become a global research powerhouse.

More than bragging rights are at stake in this race to the top. A world-class university system is a powerful engine for economic development, and research is the fuel powering that engine.

Flocking to Asia For a Shot at Greatness

Academics from around the world are taking jobs in Hong Kong, Singapore, and elsewhere in East Asia, lured by generous budgets and a welcome sign for foreigners

HONG KONG AND SINGAPORE—Ambitious academics have always been a mobile lot. But Stephanie Wehner has taken mobility to a new level. And her career choices reflect a fundamental shift in where some of the best science is being done around the world.

The 35-year-old quantum information scientist completed her undergraduate degree in her native Germany, earned a master's degree from the University of Amsterdam and a Ph.D. from the Centrum Wiskunde & Informatica in Amsterdam, and did a postdoc at the California Institute of Technology (Caltech) in Pasadena. Then she asked herself: "Where would it be scientifically interesting for me to go?" The answer took her further west, across the international dateline, in fact, to the Centre for Quantum Technologies at the National University of Singapore (NUS).

Online
sciencemag.org
Podcast interview with author Dennis Normile (http://scim.ag/pod_6099).

The center, established in December 2007, is already recognized as one of the world's top institutes for quantum studies. "It is unique" in combining computer science and physics, theory, and experiments, says Wehner, who joined its ranks in July 2010. The institute's generous funding from the government—$126 million over 10 years—means there is money for postdocs and state-of-the-art equipment for experimentalists. It also allows Wehner to concentrate on her research without having to apply for grants. A reduced teaching load of only one course a semester is another bonus. With those advantages, it's no accident that the center's 150 researchers hail from 33 countries.

Such diversity has long been the norm at the top U.S. research universities. For several decades after World War II, top academic talent gravitated to the United States. Researchers were attracted by generous and rising funding and a continually improving infrastructure, the result of broad societal support for higher education and a political consensus that investment in research reaped economic and social dividends.

Foreign-born scientists still come to the United States, but that faith in the benefits of vibrant universities is arguably stronger now in Asia. "Many Asian governments see educa-

CREDIT (LEFT TO RIGHT): ISTOCKPHOTO.COM; D. NORMILE/*SCIENCE*

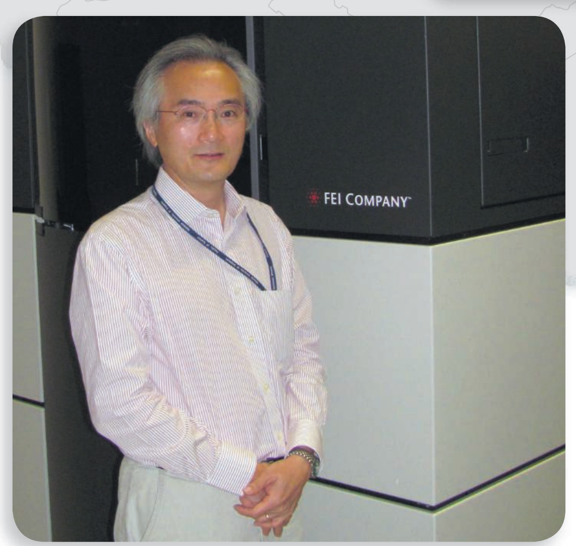

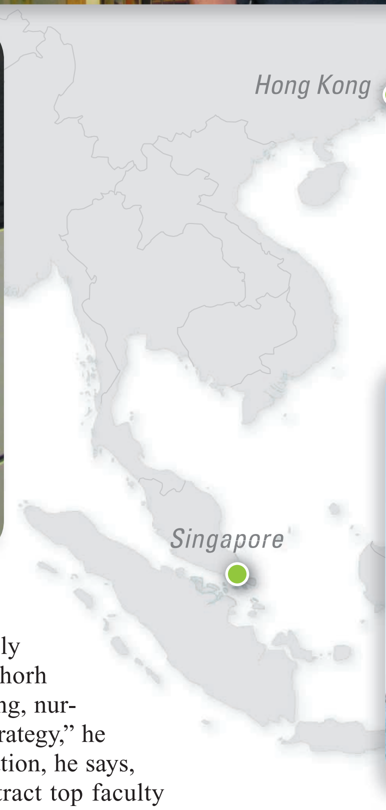

On the move. (*Clockwise from right*) Geologist Kerry Sieh, electrical engineer Khaled Ben Letaief, marine biologist Leszek Karczmarski, and biologist Paul Matsudaira followed job opportunities to Hong Kong and Singapore. (*Opposite page*) Stephanie Wehner, a quantum information scientist, was excited by the work going on at the National University of Singapore's Center for Quantum Technologies.

tion as a very critical way of societal and economic advancement, so they are investing very heavily in their universities," says NUS President Tan Chorh Chuan. To achieve academic excellence, "attracting, nurturing, and retaining top talent is the most vital strategy," he adds. With the region's rising investment in education, he says, "conditions are right for Asian universities to attract top faculty from the rest of the world."

Although its impact on academic mobility is hard to quantify, the great recession that has staggered Western economies appears to have given Asia an edge. "People on my science advisory board say this is a good time to hire Americans because there are no jobs and funding is looking dreadful," says geologist Kerry Sieh. In 2009, the former tenured professor at Caltech became founding director of the Earth Observatory of Singapore, another one of the city's five centers of excellence, based at Nanyang Technological University. Most of the center's 54 researchers were lured from positions overseas. The Hong Kong University of Science and Technology (HKUST) has made worldwide recruiting a firm policy. "We are filling all positions—faculty, deans, vice-presidents, and presidents—through open international searches," says Khaled Ben Letaief, the school's dean of engineering.

Hong Kong and Singapore schools aren't alone in recruiting globally. The National Research Foundation of Korea has committed $728 million for a 5-year World Class University Project that has attracted 321 foreign academics, most on full-time appointments. Three years ago, Japan's Ministry of Education began a program to internationalize both the faculty and the students at its universities, although budget constraints have crimped the effort. And Taiwan's Ministry of Education has an Aim for the Top University Project that supports overseas recruitment.

China has employed a variety of schemes in the past decade to lure back scientists who went overseas for advanced degrees or jobs. These include the Ministry of Education's Changjiang Scholars Program and the Chinese Academy of Sciences' 100 Talents Program. Last fall, it broadened that search by launching a program aimed at hiring 1000 nonethnic Chinese scientists, engineers, and entrepreneurs over 10 years.

Universities are tapping into these schemes, but in most countries they are starting from a low level of internationalization. The Korea Advanced Institute of Science and Technology in Daejeon has used the government support to more than double—to 49—the number of nonethnic Koreans holding tenure-track positions since 2007. The University of Tokyo is aiming to boost the percentage of non-Japanese

CREDITS (CLOCKWISE FROM TOP): D. NORMILE/SCIENCE (2); SZE WING YIU; D. NORMILE/SCIENCE

permanent and fixed-term staff members from 7% to at least 10% by 2020. (Only 2.4% of its current full-time faculty is nonnative.) And National Taiwan University is aiming to recruit 20 foreign full-time faculty members each year for the foreseeable future to bolster their presence, now at 7%.

Leading the way

But universities in Hong Kong and Singapore have a long head start. NUS boasts that more than 50% of its full-time academics are foreign-born and represent more than 70 countries. At the University of Hong Kong (HKU), 40% of the professoriate comes from beyond the city and mainland China. More than 80% of the full-time faculty at HKUST earned Ph.D.s at top American and European universities, and more than 20% are of non-Chinese ethnicity.

Those schools are setting the pace in internationalization thanks in part to their colonial legacies. One big advantage is the use of English. To teach students in the local language, most universities in Asia "have to rely on people of their own nationality," says Sun Kwok, an astronomer who returned to his hometown to become dean of science at HKU after more than 20 years in Canada and Taiwan.

The pervasiveness of English also allows nonlocal scholars to move up the academic ladder. "If you are not a local and happen to be in Korea, Japan, or even China, I don't think you [can] become department head or dean," says HKUST's Ben Letaief, who was trained in the United States and worked in Australia before coming to HKUST in 1993. In contrast, only four of seven department and center heads at HKUST's school of engineering are Chinese.

"Because we are preparing for the future, I encourage faculties to recruit junior people."

—**LAP-CHEE TSUI**, UNIVERSITY OF HONG KONG

The small size of the two cities—Hong Kong has a population of about 7 million, and Singapore's is only 5 million—encourages looking outward. "If we only recruited within Singapore, it [would be] like saying MIT could only recruit from Boston," says Barry Halliwell, NUS deputy president for research and technology, who came to the university on a sabbatical from King's College London in 1998 and decided to stay.

The Internet has eased if not erased the sense of isolation from Old and New World academic centers by providing immediate access to journals. "It doesn't matter where you are," Ben Letaief says. E-mail and the electronic exchange of information also make long-distance collaborations easier, he notes.

Reputations as cosmopolitan cities help, too. "Hong Kong is a really international city; even if you are a Westerner, you can settle in—no problem," says Tony Chan, a Hong Kong native who spent 2 decades at the University of California, Los Angeles, and who headed the largest research directorate at the U.S. National Science Foundation before becoming president of HKUST in 2009. The same could be said about Singapore.

Tan says Asian universities are using their latecomer status to incorporate global best practices into curricula and programs. Toward that end, NUS forged an alliance with Duke University in Durham, North Carolina, to add a modern medical school as part of Singapore's push to become a biomedical hub. Launched in 2005, the Duke-NUS Graduate Medical School has attracted senior academics such as infectious-disease expert Duane Gubler, formerly of the University of Hawaii,

A Life Outside Work

Outstanding job opportunities in Hong Kong and Singapore may be the prime draw for globe-trotting academics. But their families, their interests, and their social lives are also important considerations.

Quantum information scientist Stephanie Wehner and her nine-person group have turned out a string of papers, including one in *Science*, since joining the Centre for Quantum Technologies at the National University of Singapore (NUS) 2 years ago. She also teaches one course a semester. But "I do have a life outside work," she says. She has taken up ocean canoe racing, training several times a week and competing in the annual Around the Island Race in Hong Kong. "It's extremely easy to live here," she adds. It helps that Hong Kong and Singapore are arguably the most cosmopolitan cities in Asia, with diverse expatriate populations and English in common use.

Biologist Paul Matsudaira worried about finding good schools for his two young children when he began thinking about coming to NUS. He had participated in an alliance with Singapore while at the Massachusetts Institute of Technology in Cambridge and began bringing his family along in 2004 for part of the summer. But the year they spent with him during his 2008–09 sabbatical eased his concerns. The difference in the quality of the educational experience at Singapore's American School compared with what they received back home "was like night and day," he says. "Our kids loved school."

After that experience, the local schools became a reason to join NUS, not a roadblock. "Our daughter wants to graduate from the American School," he says. She is now 12 and entering seventh grade.

The Singapore government is also beginning to shed its reputation for being puritanical. The increased openness extends to lifestyles. Lee Kuan Yew, Singapore's über-influential founding prime minister, in recent years has called for acceptance of homosexuality, saying it should not be criminalized and gay people should not be harassed. Seismologist Kerry Sieh, director of the Earth Observatory of Singapore at Nanyang Technological University, believes that attitudes are indeed changing.

"I feel safer here as a gay person than I do in the United States," Sieh says. "I wouldn't have come here" if top officials were not supportive, he says. Still, he says those changes need to spread to the "intellectual ferment" throughout the city. "They've got to become more open to the arts, more open to freedom of thought and expression."

Sun Kwok, an astronomer who gave up a position at the University of Calgary in Canada to become dean of science at the University of Hong Kong (HKU), says he's been pleasantly surprised by the government's decision to limit development and preserve natural areas in the hinterlands of the crowded metropolis. At the same

CREDIT: D. NORMILE/SCIENCE

Published by AAAS

Manoa, to head the school's program on emerging diseases, and cancer researcher David Virshup, who left the University of Utah in Salt Lake City to lead efforts on cancer and stem cell biology.

One factor behind Hong Kong's increasing research capacity was its switch to the international norm of 12 years of primary and secondary schooling, followed by 4 years for a bachelor's degree. The old system of 3-year undergraduate programs, retained from colonial days, "was an elitist approach that is no longer suitable," Kwok says. The transition began in 2009, and the first students from the new system are entering university this fall. "We are trying to educate a larger population and trying to give a better, well-rounded education," Kwok says.

The shift presented an opportunity to overhaul the curriculum, too. Nonscience majors are now required to take integrated science courses that will give them a broad perspective on important scientific advances, Kwok says. Coursework for science students, he adds, will be "more interdisciplinary and will get students involved in research at the undergrad level."

Both schools are increasing faculty by more than 20% to cover the increased teaching load—HKU to 1100 and HKUST to 510—and have spread recruiting over several years. "Hiring everybody at the same time is not a recipe for building excellence," HKUST's Chan says.

And the emphasis is on youth. "Because we are preparing for the future, I encourage faculties to recruit junior people," says HKU President Lap-Chee Tsui, a geneticist who grew up in Hong Kong and worked for years at University of Toronto in Canada before returning in 2002.

Officials at all these schools say their salary and support packages are competitive with Western institutions. "To support new staff, we put in a lot of [seed] money," Tsui says.

Of course, once researchers set up their labs, they must apply for grants just like anywhere else. No country ever has enough money to fund everything that its scientists would like to do. But NUS's Halliwell thinks that "the success rates are reasonable" for government programs. "They don't throw money away, but if you have a good project you'll probably get [funded]," he says.

"Attracting, nurturing, and retaining top talent is the most vital strategy."

—**TAN CHORH CHUAN**, NATIONAL UNIVERSITY OF SINGAPORE

The opportunity to compete is just what HKU earth scientist Kono Lemke was looking for. A German national with an undergraduate degree from the Technical University of Berlin, Lemke earned a master's degree from the University of Bristol in the United Kingdom and a Ph.D. from Stanford University in Palo Alto, California, before taking a postdoc at ETH Zurich in Switzerland.

Searching for career-track jobs, he discovered that European institutions typically wanted replacements for retiring professors. In contrast, he says, "HKU was looking for people who could not just fill a gap but could bring something into the university that wasn't there already."

In Lemke's case, that means blending chemistry and earth science to study the possible origins of life in high-temperature, high-pressure geological environments. At HKU he has gotten support to recreate the geological conditions that might have fostered the evolution of inorganic to organic material. In Europe, "it would be quite hard to find a position that would cater to [someone with] that background," he says.

He's also grateful for the chance to test his ideas. Friends who landed assistant professorships in New Zealand, the United States, and Europe have become computational scientists, he says, because they can't get funding to conduct experiments.

time, he admits that moving from Calgary has put a crimp on his favorite pastime. "I can't go skiing anymore," he laments. Instead, "every weekend I go to the beach."

The common use of English can create unexpected job opportunities for spouses. HKU earth scientist Kono Lemke says his wife, a Chinese-Malaysian, had difficulty finding a job when he worked at ETH Zurich in Switzerland because she didn't speak German. But her English and Chinese skills were an asset when they moved to Hong Kong in 2008. The university also gave them "a reasonably good housing package" that has proven "quite important if you want to start a family," says Lemke, who has a 2-year-old son.

There are also plenty of options for those with an interest in local politics. Barry Halliwell, an NUS chemist who has lived in Singapore since 1998, is a member of several civic organizations wrestling with the challenges facing an aging society. "You can be as big a part of the community as you wish," he says. **–D.N.**

Beyond the lab. Kono Lemke (*left*) says Hong Kong offers more job opportunities for his wife; Barry Halliwell (*right*) participates in many civic activities in Singapore.

CREDITS: (TOP AND BOTTOM RIGHT) NATIONAL UNIVERSITY OF SINGAPORE; (BOTTOM LEFT) D. NORMILE/*SCIENCE*

Published by AAAS

Ageless opportunity

Young scientists aren't the only ones going to the Far East. For Sieh, 61 and one of the world's leading earthquake experts, the Earth Observatory represents a "stunning opportunity" to build an institution tackling challenges that threaten civilization.

Sieh has worked extensively in Indonesia and knew that Singaporean officials and academics were worried about the region's natural-hazards risks. So when Singapore's National Research Foundation announced its Research Centres of Excellence program in 2007, Sieh and Nanyang Technological University proposed an institute to study climate change, sea-level rise, tsunamis, earthquakes, and volcanoes.

"Hong Kong is a really international city; even if you are a Westerner, you can settle in—no problem."

—TONY CHAN, HONG KONG UNIVERSITY OF SCIENCE AND TECHNOLOGY

In some cases, Western scientists have relocated to rediscover a sense of scientific adventure. Biologist Paul Matsudaira joined the Whitehead Institute for Biomedical Research in Cambridge, Massachusetts, in 1985, just 3 years after its founding. "It was like a start-up," Matsudaira says, with enormous possibilities, plentiful resources, and excitement at the mandate "to do the best science we could."

But after 24 years, Matsudaira confesses, "I was getting complacent." He wanted to push biological imaging in new directions, but his idea was one of thousands competing for scarce resources. After working in Singapore under an alliance that links the Massachusetts Institute of Technology, NUS, and Nanyang Technological University, he spent a sabbatical year at NUS and realized that "there's outstanding research that goes on every day at places other than where I was."

The clincher was NUS's support for a biological imaging center. "People ask me, 'Why would you ever want to leave MIT and Whitehead?' " says Matsudaira, now head of biological sciences at NUS. His answer: "It [offers] the possibility that I could build something here that's unique in the world."

Researchers in fields such as earth sciences, environmental studies, and ecology find that a move to Southeast Asia opens up virgin scientific territory. Sieh mentions visiting a little-studied major fault in Myanmar that is the length of California's San Andreas Fault and runs through the capital of Naypyidaw. In contrast, researchers must work ever harder to discover something new about the San Andreas. "The things we don't know about geological processes and geological history in Southeast Asia are just breathtaking," Sieh says.

Leszek Karczmarski says similar opportunities in marine biology lured him to HKU's Swire Institute of Marine Science. Originally from Poland, Karczmarski has studied the ecology and conservation of marine mammals, particularly dolphins, in South Africa, the United States, and Central and South America. But the Pacific Ocean west of Hawaii and between Japan and Australia is "aqua incognita," he says.

In 2010, he left the University of Pretoria in South Africa for a post at Swire, which was created to focus on marine conservation and ecology, and quickly ramped up research efforts. He has 12 postdocs and grad students conducting fieldwork in Southeast Asia, South America, South Africa, mainland China, Taiwan, and Egypt. He's also set up a small field station in a remote corner of Hong Kong for students to study local issues. "Something like this would take a few years in a number of other places," he says. "Here it happened over a few months."

Karczmarski has also begun to assemble a regional cetacean research network to share data, ideas, and strategies for research and conservation. In just 2 years the nascent group has sponsored six training workshops in modern quantitative research techniques that brought together 50 participants from 10 countries. "We have now a framework in place, and the web of interactions is growing strong," he says, pointing to an increasing number of collaborative research initiatives and jointly co-authored publications.

Moving on

The growing capabilities are not going unnoticed. "People are coming after our junior faculty, especially those whose research is beginning to take off," Halliwell says.

One example is Rudiyanto Gunawan, who left NUS for a position at ETH Zurich last year for both professional and personal reasons. The 35-year-old systems biologist is now closer to the European and U.S. labs working in his area, and he felt it would be easier to attract postdocs to ETH than to NUS. He was also able to negotiate for more lab space. Finally, he thought Switzerland would be a better place to raise his daughter than "fast-paced Singapore."

He values his 4-plus years in Singapore, however, and continues collaborating with two NUS groups. And there are no hard feelings. Poaching is a sign of success, Halliwell says, as long as it doesn't go too far. "If nobody wants anybody [on your staff] you're in trouble. [But] if everybody's going, you're in trouble."

There's also a silver lining to losing good faculty members. They make for "very good advertisements for us," Halliwell says. "And they build links."

There is no question that the competition for talent is going to get tougher. China's universities are striving to gain global recognition, HKUST's Chan says, "and they want to do it like us, in less than 20 years."

Foreign faculty members are already common at many Chinese business schools and at joint programs set up by Chinese and Western universities, says Huiyao Wang, director general of the Center for China and Globalization, a think tank in Beijing. "I think the next wave will be foreign faculty coming in" at the established universities, he says. Universities in Korea, Japan, and Taiwan are also stepping up international recruitment.

If those trends continue, the Stephanie Wehners of the future will have more Asian choices when they draw up a list of the most interesting places to work.

–DENNIS NORMILE

CREDIT: D. NORMILE/*SCIENCE*

Published by AAAS

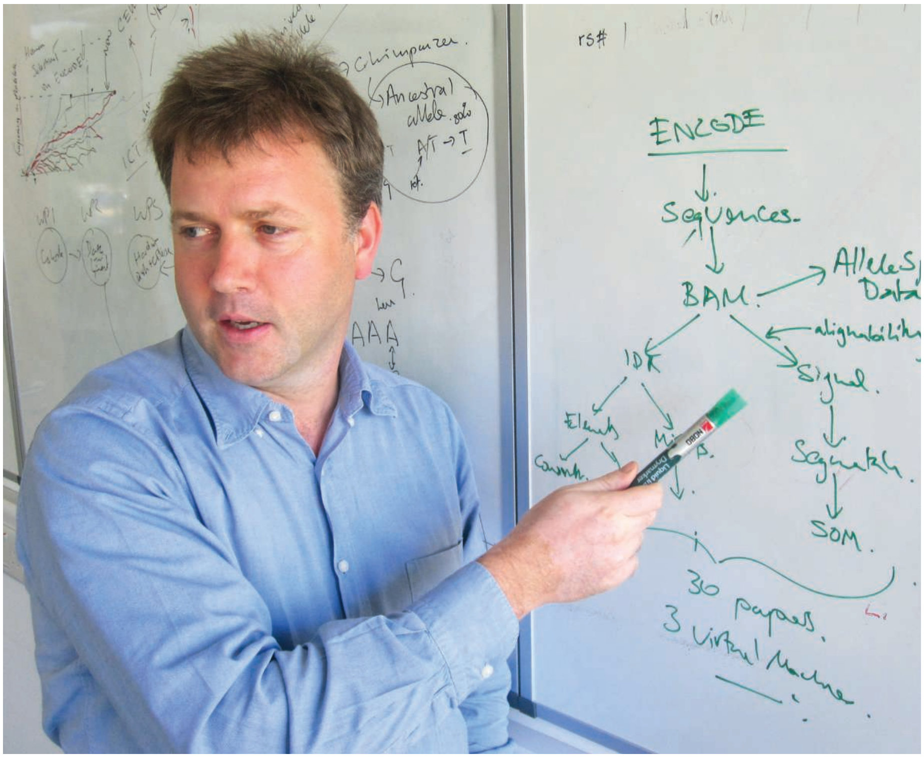

CREDIT: EMBL

PROFILE: EWAN BIRNEY

Genomics' Big Talker

A self-taught programmer turned bioinformatician plays a big role in shaping how researchers perceive and use DNA sequence data

"My ultimate weapon is just talking people into submission," Ewan Birney joked one recent afternoon while describing his role in coordinating one of the most ambitious genomics projects since the human genome was sequenced. A self-taught programmer turned bioinformatician at the European Bioinformatics Institute (EBI) in Hinxton, U.K., Birney has used his gift of gab to pull together 442 researchers to characterize not just the genes but also all the functional elements in the human genome. The Encyclopedia of DNA Elements (ENCODE) project this week published 30 scientific papers that begin to fill in the details of DNA's role in making life possible (see p. 1159). Birney was in charge of data analysis, and, along with his right-hand man, EBI's Ian Dunham, he coordinated the setting of quality standards, the development of consistent protocols, and the planning of the publications as well as developing new ways to look at data. "The ENCODE project would simply not have succeeded without [Birney's] leadership," says Francis Collins, director of the U.S. National Institutes of Health in Bethesda, Maryland.

Some say the secret to Birney's success is youthful exuberance. The 39-year-old will talk about anything to anyone, and he has an opinion about just about everything. Such ebullience serves him well: "It's very difficult for him to say no, and it's very difficult for people to say no to him," says EBI's Paul Flicek. "He has an immense ability to bridge [disciplines]," adds EBI's director, Janet Thornton. "He's very clever and very confident." But that confidence can come off as arrogance. "He does raise antibodies in some people, usually males around the same age," Thornton says.

Some even say Birney is like the kid who can't stop asking questions. At the annual Biology of Genomes meeting at Cold Spring Harbor Laboratory, he raises his hand so often after each talk that the organizers limited the number of questions from any one person. Even during senior management meetings at EBI, each person must raise a hand to speak because Birney, with his unbridled enthusiasm, would otherwise interrupt too much. "He's probably the most extroverted person I know," Thornton says. "I don't think he has an ounce of self-consciousness."

A quiet boy

Birney didn't start out that way. Dyslexic, he initially had trouble at school, where he was sometimes ridiculed for not being able to spell. Yet he wound up a top student at Eton, one of the best and most exclusive private schools in the United Kingdom. As its best science student, he earned a yearlong internship at the Cold Spring Harbor Laboratory in 1991, before heading to the University of Oxford. At Cold Spring Harbor, he lived in James Watson's house and worked for Adrian Krainer, a biochemist, studying RNA-protein interactions. Even then, "one could see he had the potential to play a leadership role," Krainer recalls.

Birney soon became interested in computers, teaching himself programming during the winter at Cold Spring Harbor. Using a computer to align DNA sequences, he surveyed the RNA binding domain in proteins of many organisms, producing a publication that has been cited more than 500 times—and is still cited today, 20 years later.

Yet even then Birney wasn't sure he would become a scientist. One summer in college he worked at an investment bank—which he says was lots of fun—and during his final summer as an undergraduate he worked in the mayor's office in Baltimore, Maryland. (The mayor, Kurt Schmoke, had been a Rhodes scholar at Birney's college and had set up the internship.) "My role was to be posh and British and hopefully charming when big donors came around," Birney recalls. The experience also included spending a week with undercover cops and attending adult literacy classes.

In his senior year at Oxford, he approached Richard Durbin at the newly created Sanger Centre in Hinxton to work with him and the DNA databases being set up there. By the time he left Oxford he had written his own programming language that streamlined the writing of programs for comparing DNA sequences. "It allowed me to write algorithms much faster and to do much more complex algorithms," Birney says. One result was an open-source program called Genewise, which was used by both Celera Genomics—the company run by J. Craig Venter that sequenced the human genome—and a public Web site called Ensembl that Birney helped put together.

Durbin helped Birney get a well-paying fellowship at Sanger that swayed him to pursue a Ph.D. through the University of Cambridge instead of investment banking. "He was already a pretty good researcher and had strong computer skills," recalls Alex Bateman, a biochemist at the Wellcome Trust

Published by AAAS

Sanger Institute. "He also had strong opinions and lots of them."

Birney didn't act like a graduate student. In 1997, for example, he pointed out that the programming approach of the head of Sanger's bioinformatics, Tim Hubbard, was flawed, convincing Hubbard he should try an approach called object-oriented programming instead. "The idea that Ewan [shouldn't] tell somebody 20 years older what to do didn't occur to him," Hubbard says.

During those early years, Birney left his mark on some of molecular biology's most important collections. He rewrote all the code for a database of protein families, Pfam, making it more modular and more robust. A big innovation was to store the data in such a way that one could keep track of revisions.

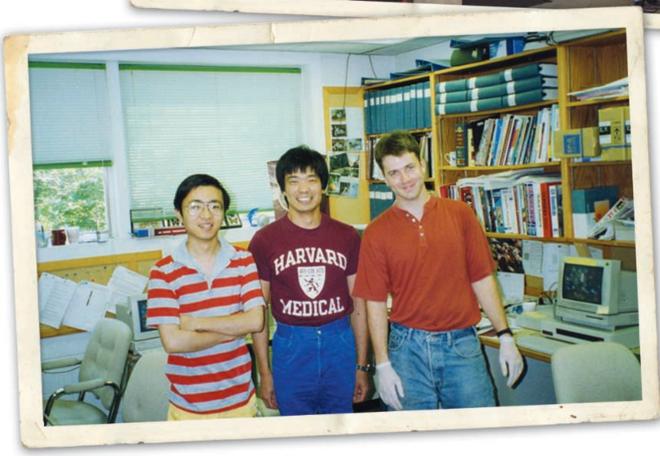

Home away from home. Cold Spring Harbor Laboratory is like a second home to Ewan Birney, who worked there for a year and a summer as a young student (*bottom*; orange shirt), and returns annually to the Biology of Genomes meeting. Captured during a coffee break in 2003 (*middle photo, second from left*) and again in 2010 with Francis Collins (*top*), Birney talks up his new ideas with his colleagues.

Human Genome Project

And that was just a side project, because Birney quickly got swept up in the Sanger scientists' frenzied race to sequence the human genome before Celera did. "I depended heavily on Ewan to carry out a long list of challenging analyses," says Collins, then director of the U.S. National Human Genome Research Institute (NHGRI). Birney and his colleagues quickly realized they needed a computer program that would automatically identify genes in a high-throughput manner. Hubbard wrote what even he calls "horrible" code to do this, and Birney and Sanger postdoc Michele Clamp took over making automated annotation a practical reality. "We had these impossible deadlines," Birney recalls. "People were demanding results in a short-term turnaround for something that had never been done before. It was exhilarating, but it's not the way you should do science."

He moved from Sanger to the building next door, EBI, in 2000, and the genome browser Ensembl was born as a way to make sequence data accessible to the public. The Web site remains one of the key places where researchers go to get and work on genomic data. He also set up a fiercely competitive sweepstakes for predicting the number of genes in the human genome.

It was an exciting time for other reasons as well. Birney and Barley Laycock, now his wife, moved in together in a cramped bachelor flat in London. At that time, Birney, an advocate of open-source software, was given the option to buy in to a company formed to provide services for Linux, the free operating system to which he had contributed code. He couldn't work out how to wire money for the purchase and instead arranged to buy and sell the stock right away. "It turned out to be the genius maneuver," he says, as the stock spiked briefly, netting enough cash that he bought himself a BMW Z3, a two-seater sports car. In 2003, he won the Royal Society's inaugural Francis Crick Lecture, which recognizes promising young investigators.

At EBI, Birney, who was in charge of the nucleotide databases, and Rolf Apweiler, who took care of the protein side of EBI, were a study in contrasts. The two leaders were like "chalk and cheese," Birney admits. Birney's old office was littered with piles of paper and bits of computers, with a big jar of the yeast extract Marmite on his desk for snacks. Apweiler's office was spare and spotless. Birney had a "let's do it and think about how later" attitude. "I have a knack for cajoling people into doing this sort of thing," he says, while Apweiler is much more cautious, working out the details before agreeing to a new course of action. As co–associate directors, they help keep each other balanced. "I'm awful at the finishing process," Birney says, and he sometimes neglects the details.

Enter ENCODE

In 2003, with the human genome completed, Collins approached Birney with a new challenge. NHGRI was funding a pilot ENCODE project that involved many different analyses of 1% of the genome with the eventual goal of extending the project to the entire genome. "It was clear early on that the most significant challenge for ENCODE was not going to be the production of data, but the analysis and synthesis of that data," Collins says. "[Birney] had the right kind of scientific savvy, computational skills, and the people skills to pull this off," says John A. Stamatoyannopoulos, an ENCODE researcher from the University of Washington, Seattle. "He was the glue that held that effort together."

There was no limit to the number of hours Birney was prepared to spend on conference calls or transatlantic flights. In October 2011, when the ENCODE consortium was in the throes of planning its publications, Birney averaged two teleconferences a night, for example. (There were more than 675 over the 4 years.) His task was to move things forward, delicately persuading ENCODE's top scientists to give up a little independence for the joint effort. His job, he says, was "to enable this scientific collaboration to occur and to help get through the tough bits and not get in the way of creativity."

As chief cat-herder, he had to make sure that everyone kept talking to each other and eventually agreed on certain protocols—even the culture conditions for the designated cell types—and data-quality procedures, including statistical analyses, to ensure consistency among the resulting data. And he succeeded:

CREDITS: (PHOTOS, TOP TO BOTTOM) COURTESY OF MEETINGS & COURSES, COLD SPRING HARBOR LABORATORY (2); COURTESY OF ADRIAN KRAINER, COLD SPRING HARBOR LABORATORY; (FRAMES) ISTOCKPHOTO.COM

Published by AAAS

"There was a sense of people really working together and not so much to their own drummer," says Yale University bioinformaticist and ENCODE researcher Mark Gerstein. The pilot ENCODE depended on microarrays that identified relevant sequence using chunks of DNA mounted on an array. But when cheaper sequencing technologies came along, the project quickly shifted to sequencing the regions pinpointed by the assays. Birney helped coordinate the challenging transition.

ENCODE went smoothly in part because the group cut its teeth on the pilot project, published in 2007 (*Science*, 15 June 2007, p. 1556). The pilot initially resulted in five draft papers, but reviewers were quick to pick up on conflicting interpretations. "That was a little bit of a disaster," Birney recalls. After intense discussions, the participants agreed to write just one paper. "Birney has some very clear opinions and very clear biases, but he's open-minded and willing and encouraging to get divergent points of view on the table and try to work out the best alternative," says Thomas Gingeras, a Cold Spring Harbor Laboratory ENCODE investigator. "He's a reasonably good umpire [and] he's tireless."

For the full ENCODE project results published this week, the group planned a more coherent package that includes six papers in *Nature* and 24 in *Genome Research* and *Genome Biology*. To help readers get the most from the papers, the team came up with an iPad and Web application that enables the reader to call up parts of all the papers that are relevant to one of 13 keywords or concepts, such as "enhancer" or "interaction with disease." "It will be interesting to see how people will pick up on this," Birney says. (Related papers appear online in *Science*.)

For those who want to probe the computations, the team is providing a second innovation: a "virtual machine," on the ENCODE Web site that will enable any user to retrace the steps that converted raw data into a finished product. Birney hopes to start a trend. "All papers that do computational work should have virtual machines so we can see precisely how it was done," he says.

The future

This phase of ENCODE is winding down, but Birney's life is no less hectic. He has a wife and two children with whom he'd like to spend more time, and a long commute to Hinxton from the Victorian-era suburb in North London where they live. So he tightly choreographs his days. Each morning he leaves at 7:30 on the dot, combining a walk, short ride on the Tube, a 40-minute journey on a train with a good Internet connection that allows him to catch up on e-mail, and, finally, a bus ride to get to work each day in Hinxton. He reverses the routine each evening to be home by 5:30 to spend time with his 6-year-old son and 3.5-year-old daughter. Then he often has a conference call in the evenings.

Most days his schedule is filled with meetings ranging from a discussion of overhauling EBI's 80 Web sites to a 3-hour session with representatives from the national and international agencies that provide high-speed computer connections among universities and research organizations. He squeezes in a conference call to plan a proposal for a $25 million European Union program aimed at using supercomputers in innovative ways—his group wants to tap them for personalized medicine. Then he meets with several colleagues to discuss their projects and, if there is time, checks in on various research projects.

"Services is my day job and strategy is my thing. But I hope I don't give up scientifically fooling around."

—EWAN BIRNEY

Still into algorithms, he and his colleagues are developing CRAM, a way to further compress raw sequence data for storage. He's working with a cardiologist on making genome data more relevant to physicians, with geneticists about mounting a massive breeding project for the fish medaka, and a phenotype-genotype study of *Drosophila*. "Services is my day job and strategy is my thing," he explains. "But I hope I don't give up scientifically fooling around."

His next big project is a new pan-European bioinformatics effort called ELIXIR, now in the planning stage. Biology has "got potentially more data than physics," Sanger's Hubbard says. EBI alone has seen a 2000-fold increase in the amount of DNA sequence data—just one of several categories—since 2005. To complicate matters, many countries have been developing their own bioinformatics databases. Aiming for more order, EBI hopes to make it possible to access these databases through a single portal, "to allow comprehensive searching of all resources," says EBI Director Thornton. Thirteen European nations have agreed to help set this up. EBI is working out the details over the next year for what could be a 20-year project, although funding has yet to be fully determined.

EBI will become the central hub for ELIXIR. Thornton, Birney, and Apweiler envision other huge computer centers across Europe for storing not just genome and protein data, but also other molecular and phenotypic information on thousands of organisms, including humans. Already, the U.K. government is spending £75 million ($120 million) over the next 10 years on computers and a new EBI building. EBI plans to almost double its staff to 700 in the next 3 years. Birney has traveled to Finland to an old paper mill that—with its large space, easy access to hydroelectric power, and cool temperatures—could be ideal for a big computer center. In February, he goes to Barcelona to see what its computer facilities have to offer, and he's planning a trip to Turkey.

With ELIXIR on his plate, Birney is bowing out of the next ENCODE phase. He, Apweiler, and Thornton talk about EBI becoming the center of gravity for bioinformatics. But Birney is really a force field unto himself. "People who go on to be successful generate their own kind of gravity," Bateman says. "They tend to make themselves the center of things and everything starts to revolve around them."

"Ewan's got a lot of gravity."

–ELIZABETH PENNISI

CREDIT: GENOME RESEARCH LIMITED

LETTERS

edited by Jennifer Sills

Prions: A Piece of the Puzzle?

IN HIS PERSPECTIVE "A UNIFYING ROLE FOR PRIONS IN NEURO-degenerative diseases" (22 June, p. 1511), S. B. Prusiner proposes that Alzheimer's disease (AD) is a prion disorder (*1*). News publications have speculated that AD may be transmitted by blood transfusion (*2*), and caution has been thrown to the wind in Internet outlets. Prusiner's model comes from experiments in which Aβ peptide (the immediate precursor of AD amyloid plaques) induced aggregation in transgenic mice or primates after injection of AD brain extracts (*3*, *4*) or purified and synthetic Aβ peptides (*4*, *5*). However, no plaque appeared in monkeys injected with synthetic Aβ, raising questions about the direct translation of animal results to humans.

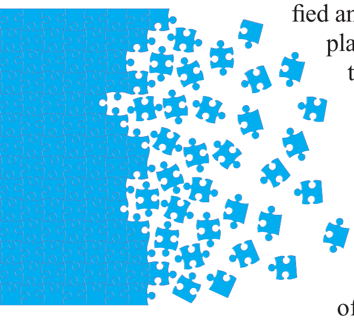

This technical critique ignores fundamental questions of AD etiology. Extracellular Aβ accumulation always accompanies the disease, but is it a cause or a result? How can we explain memory deficits that familial AD model mice exhibit before evidence of plaque deposition (*6*)? Given that direct neuron-to-neuron transmission of nonfibril Aβ exists (*7*), could AD pathogenesis depend on intracellular, nonplaque Aβ?

Multiple environmental risks for AD have been identified; where would they fit into a prion model? In addition to dietary cholesterol, factors such as mid-life exercise, nutrition, education, and early-life exposure to environmental hazards may modify amylodogenesis and AD (*8*). Late-onset neurodegenerative disorders, such as AD, can be explained by the latent early-life associated regulation (LEARn) pathway, in which environmental factors act epigenetically, long before the onset (*8*).

Other evidence suggests that AD has some genetic basis, in seeming contradiction to a prion model. For example, apolipoprotein E is a genetic risk factor. Genetic evidence for the role of the Aβ precursor protein (APP) in age-related cognitive decline and AD suggests that APP protective mutation carriers have lower Aβ peptide levels for their entire lives (*9*).

There is no denying that Aβ subunits play a role in nucleation of Aβ aggregates, but to call them prions, in the sense of the naturally infectious particles that catalyze disease based entirely on their own refolding and aggregation, ignores a great deal of evidence in the field and stirs up public fear prematurely.

DEBOMOY K. LAHIRI

Indiana University School of Medicine, Departments of Psychiatry and of Medical and Molecular Genetics, Institute of Psychiatric Research, Indianapolis, IN 46202, USA. E-mail: dlahiri@iupui.edu

References

1. S. B. Prusiner, *Science* **336**, 1511 (2012).
2. L. K. Wolf, *Chem. Eng. News* **90**, 24 (2012).
3. M. Meyer-Luehmann *et al.*, *Science* **313**, 1781 (2006).
4. R. M. Ridley *et al.*, *J. Neural Transm.* **113**, 1243 (2006).
5. J. Stohr *et al.*, *Proc. Natl. Acad. Sci. U.S.A.* **109**, 11025 (2012).
6. W. Zhang *et al.*, *Free Radic. Biol. Med.* **52**, 1443 (2012).
7. S. Nath *et al.*, *J. Neurosci.* **32**, 8767 (2012).
8. D. K. Lahiri *et al.*, *Mol. Psychiat.* **14**, 992 (2009).
9. T. Jonsson *et al.*, *Nature* **488**, 96 (2012).

Sustaining Metal-Loving Plants in Mining Regions

THE RECENT UNITED NATIONS RIO+20 Conference on Sustainable Development highlighted the rapid increase in industrial mineral exploration and extraction over the past two decades (*1*). Endemic metallophyte plants, which have evolved where metal accumulations extend to the Earth's surface, have inevitably become extinct as a result of these mining activities. Remaining metallophyte refugia are now under acute threat as previously uneconomic deposits of metals, particularly in biodiverse tropical areas, are targeted for extraction (*2*).

Academic awareness of metallophytes has not protected these species, and miners and government regulators appear almost universally ignorant of their presence and/or potential. A revival of mining in the Katanga copper region of the Democratic Republic of the Congo means that hundreds of endemic copper metallophyte species are now some of the most critically endangered plants in the world (*3*). Soaring extinction rates of metallophytes in Brazil have led to calls for authorities to protect metalliferous (metal-containing) ecosystems from mining, but these appear unlikely to succeed given the high cost of compensating mineral rights holders (*4*). Even in Australia's highly regulated mining environment, metallophyte extinction risk remains. The Dugald River

Letters to the Editor

Letters (~300 words) discuss material published in *Science* in the past 3 months or matters of general interest. Letters are not acknowledged upon receipt. Whether published in full or in part, Letters are subject to editing for clarity and space. Letters submitted, published, or posted elsewhere, in print or online, will be disqualified. To submit a Letter, go to www.submit2science.org.

CREDIT: MEHMET ALI CIDA/ISTOCKPHOTO.COM

ore deposit of lead, zinc, and silver was discovered in the 1880s with geobotanical maps describing specific ore-associated metallophyte vegetation (*5*). A recent environmental impact assessment and government vegetation mapping exercises failed to identify any metallophytes (*6*).

To prevent continued biodiversity loss and to benefit from their unique adaptive mechanisms that exclude, tolerate, or even hyperaccumulate toxic metals in mine site rehabilitation, metallophytes must be recognized as vital assets at the development stage of a mining operation (*7*). Where substrate metal concentrations exceed general toxicity thresholds at a site, the presence of metal-tolerant ecotypes should be assumed and addressed appropriately by performing the following steps: (i) Exclude metallic ore deposits with surface mineralization from mining operations; this is unlikely to occur for economic reasons. (ii) Modify mining operations so that areas of surface mineralization are retained intact with metallophyte vegetation. (iii) Move surface mineralization and associated seed banks before mining and reestablish them nearby. (iv) Collect and store metallophyte germplasm, and return it when the mine closes and the site is rehabilitated. (v) Select, breed, and improve metal-tolerant ecotypes and species adapted to a post-mine landscape.

Bioclimatic, geochemical, and physiological matching of metallophyte species to mine waste habitats should become an integral part of a profitable and sustainable global mine site rehabilitation strategy while also protecting highly evolved biodiversity.

P. ERSKINE,* A. VAN DER ENT, A. FLETCHER

Centre for Mined Land Rehabilitation, Sustainable Minerals Institute, The University of Queensland, Brisbane, QLD, 4072, Australia.

*To whom correspondence should be addressed. E-mail: p.erskine@uq.edu.au

References

1. Rio+20, United Nations Conference on Sustainable Development (www.uncsd2012.org).
2. A. L. Jaques, M. B. Huleatt, M. Ratajkoski, R. R. Towner, *Resources Pol.* **30**, 168 (2005).
3. L. Saad *et al.*, *Rest. Ecol.* **20**, 405 (2012).
4. C. M. Jacobi, F. F. do Carmo, I.C. de Campos, *Ambio* **40**, 540 (2011).
5. O. W. Nicolls, D. M. J. Provan, M. M. Cole, J. S. Tooms, *Trans. Inst. Mining Metallurgy* **II**, 695 (1965).
6. Environment and Natural Resource Regulation, Department of Environment and Resource Management, "Environmental impact statement (EIS) report under the Environmental Protection Act 1994: Dugald river project, proposed by MMG" (2011); www.ehp.qld.gov.au/management/impact-assessment/eis-processes/documents/dugald-river-eis-assessment-report.pdf.
7. S. N. Whiting *et al.*, *Rest. Ecol.* **12**, 106 (2004).

LIFE IN SCIENCE

Respect in a Pinch

Early in my career, I didn't know whether facial expressions of emotion were universal (Darwin's claim) or culture-specific (Margaret Mead's claim). In 1967, I traveled to a remote part of New Guinea to find out in an environment virtually untouched by Western culture. Among the secluded Fore people's traditions was cannibalism; the community ate people they respected after they died of natural causes. The Fore were still using stone tools and had never encountered a photograph or camera, and I was unfamiliar with their language and customs. One boy who knew Pidgin (which I had also learned before my trip) served as my translator. With his help, I asked the villagers to look at photographs of people displaying various emotions and invent stories about them. The study progressed slowly; my foreign ways were met with suspicion.

One day, about 2 weeks after my arrival, I was sitting outside eating my lunch of pit-pit (a vegetable similar to asparagus). An elder of the village approached me, and as I stood to greet him, I saw that he was followed by about 100 tribesman—more than half the village. The man stopped directly in front on me, reached down, and began pinching my thigh. To my horror, the villagers behind him began jumping and screaming with emotion. I searched the crowd for weapons and tried to hide my panic.

Suddenly, realization dawned. The people's expressions did not show anger. They were smiling and laughing. As I learned later, the village elder had declared that he planned to eat me when I died. From then on, I was a respected member of the tribe. My research proceeded with full cooperation from the villagers, and showed what I learned that day the hard way: Facial expressions do indeed transcend cultures. I left New Guinea before the elder tribesman could make good on his promise, but I hope at least he found my research palatable.

PAUL EKMAN

Paul Ekman Group LLC, San Francisco, CA 94126–6089, USA. E-mail: honesty@paulekman.com

EDITOR'S NOTE

This is an occasional feature highlighting some of the day-to-day humorous realities that face our readers. Can you top this? Submit your best stories at www.submit2science.org.

CREDIT: PETER AND MARIA HOEY/WWW.PETERHOEY.COM

TECHNICAL COMMENT ABSTRACTS

Comment on "Orthographic Processing in Baboons (Papio papio)"

William Bains

Grainger *et al*. (Reports, 13 April 2012, p. 245) suggest that baboons can discriminate words from nonwords on the basis of two-letter (bigram) frequencies. This ability can also be attributed to baboons being able to recognize specific letters (i.e., shapes) in specific positions in their four-letter words, without reference to letter or bigram frequencies.

Full text at www.sciencemag.org/cgi/content/full/337/6099/1173-b

Response to Comments on "Orthographic Processing in Baboons (Papio papio)"

Jonathan Grainger, Stéphane Dufau, Marie Montant, Johannes C. Ziegler, Joël Fagot

Bains pointed out that some of our nonwords were in fact real words and that an algorithm using only information about single letters and their positions achieves the same level of accuracy as baboons in discriminating words from nonwords. We clarify the operational definition of words and nonwords in our study and point out possible limits of the proposed algorithm.

Full text at www.sciencemag.org/cgi/content/full/337/6099/1173-c

Comment on "Orthographic Processing in Baboons (*Papio papio*)"

William Bains

Grainger *et al*. (Reports, 13 April 2012, p. 245) suggest that baboons can discriminate words from nonwords on the basis of two-letter (bigram) frequencies. This ability can also be attributed to baboons being able to recognize specific letters (i.e., shapes) in specific positions in their four-letter words, without reference to letter or bigram frequencies.

Grainger *et al.* (*1*) present remarkable data on the ability of baboons to learn characteristic patterns in abstract symbols. They and the accompanying commentary by Platt and Adams (*2*) conclude that the animals are learning to discriminate words from nonwords based on the frequency of two-letter combinations (bigrams), which are highly nonrandom in real English text, as opposed to random letter strings. This is proposed as an underlying skill enabling human reading and that this underlying ability is present in baboons.

There are two minor methodological problems with Grainger *et al.*'s study which suggest that, while the learning abilities demonstrated by baboons are impressive, they may be less closely related to the ability of *Homo sapiens* to read than is suggested by Grainger *et al.*

First, a small percentage of the words classified in (*1*) as "nonwords" were actually English words. For example, some words with common usage (like "blog"), recent use but no longer common (like "blub"), archaic but still valid (like "bawd"), or obscure or technical (like "bosc") were included in the "nonwords" list. Overall, the list of 7830 "nonwords" contains between 149 and 279 words (depending on whether obscure words are counted or not). The behavioral data showed that the animals could not distinguish genuine nonwords from actual words that were included in the nonword list (70.0% accuracy in classifying genuine nonwords as nonwords; 69.8% of words in the nonword list classified as nonwords).

Second, and more important, the same learning performance can be obtained without any reference to letter or bigram frequency. Grainger *et al.* state, "Bigram frequency was minimized in the list of nonwords and maximized in the list of words, so that the word versus nonword discrimination could be made implicitly on the basis of statistical dependencies between letters." Discrimination can be made in this way, but there are other ways to discriminate between Grainger *et al.*'s words and nonwords. To illustrate this, I implemented a simple learning algorithm based on letter positions in a tetragram. A scoring function

$$S = \sum l_i w_{li}$$

was calculated, where l_i is the count of the letter l present at position i in a tetragram, and w_{li} is the weight given to letter l at position i in the tetragram. w_{li} could be –1, 0, or +1. Scores of >0 mean that the tetragram is a word, scores of <0 mean that the tetragram is a nonword, and scores of 0 were randomly assigned to word or nonword. At each learning step, 5% of the weights were chose at random and changed to –1, 0, or +1, again randomly. A "fitness score" F was calculated for the new weight set applied to the training set

$$F = \frac{\sum m(S_{\mathrm{words}}) - \sum m(S_{\mathrm{nonwords}})}{300 + C_w}$$

where m(X) is the modulus of X, S_{words} and S_{nonwords} are the scores for words and nonwords as above, and C_w is the number of weights that are not zero. The algorithm iteratively selects new weighting sets that have a higher F than any previous set. Implementing this in Excel resulted in a rapid convergence on an algorithm that could predict whether a word was part of the "word" or "nonword" lists (*3*). Between 40 and 60 letter+position combinations are needed. Figure 1 shows a typical learning curve for the system, and a typical rule.

The appearance of learning bigram frequencies was generated by the system because of the structured nature of English spelling. Following Grainger *et al.*'s supplementary materials, I calculated the sum of the bigram occurences in this data and summed these frequencies for each word. The summed bigram frequencies were averaged based on whether they were for incorrectly or correctly classified words or nonwords. The averages for words and nonwords were highly significantly different (Fig. 2). The words that the system got wrong had bigram frequencies intermediate between words and nonwords.

This could be interpreted as clear evidence that the system was classifying on the basis of bigram frequencies, so it found the words with intermediate bigram frequencies confusing. In fact, as described above, no bigram frequency information was used in the classification algorithm

None of this detracts from the value of Grainger *et al.*'s work in showing that baboons can classify groups of arbitrary abstract characters, which is an important result in these nonverbal

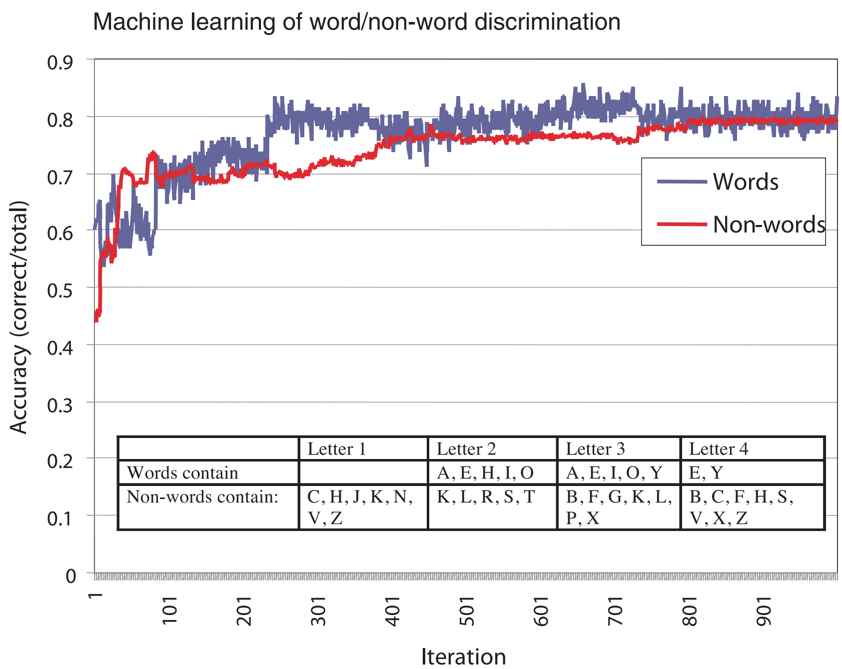

	Letter 1	Letter 2	Letter 3	Letter 4
Words contain		A, E, H, I, O	A, E, I, O, Y	E, Y
Non-words contain:	C, H, J, K, N, V, Z	K, L, R, S, T	B, F, G, K, L, P, X	B, C, F, H, S, V, X, Z

Fig. 1. Typical learning curve for the algorithm discussed. The score on the test set is on the *y* axis, the iteration step on the *x* axis. (**Inset**) A typical algorithm generated by this method, which predicts words to 85% accuracy, nonwords to 71% accuracy.

SENS Laboratory, Chemical Engineering and Biotechnology, Cambridge University, Tennis Court Road, Cambridge CB2 1QT, UK. E-mail: wab35@cam.ac.uk

Fig. 2. Sum of bigram frequencies in each category of word. For each bigram, the number of occurrences of that bigram in the entire tetragram data set was counted. For each word, the bigram frequencies were summed. Shown are the average summed bigram frequencies for words and nonwords that are correctly classified, and words and nonwords that are incorrectly classified. Error bars: 1 SD of average bigram sums from 10 independent runs of the algorithm.

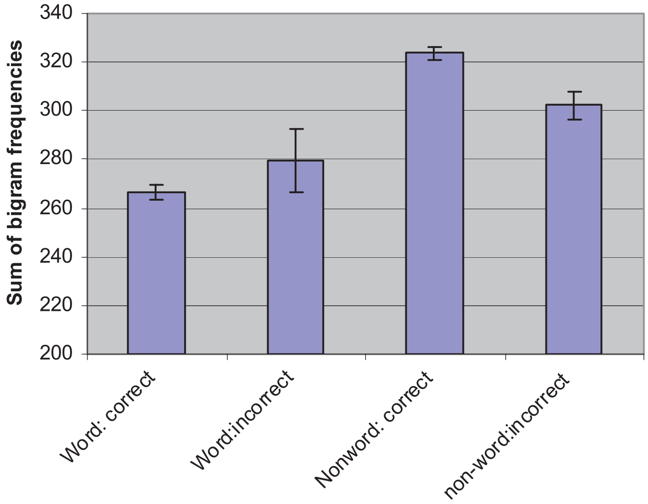

animals. This visually based capacity may well be the same as that underlying elements of human orthographic processing. However, it is not necessarily based on letter frequency or letter pattern recognition, and so may be less closely related to our ability to discriminate likely real words from nonwords than Grainger *et al*. and Platt and Adams imply.

References and Notes

1. J. Grainger, S. Dufau, M. Montant, J. C. Ziegler, J. Fagot, *Science* **336**, 245 (2012).
2. M. L. Platt, G. K. Adams, *Science* **336**, 168 (2012).
3. The spreadsheet, with the algorithm and data discussed here, can be downloaded from the author's Web site at www.williambains.co.uk/baboons/index.html.

9 May 2012; accepted 26 July 2012
10.1126/science.1224508

Response to Comment on "Orthographic Processing in Baboons (*Papio papio*)"

Jonathan Grainger,* Stéphane Dufau, Marie Montant, Johannes C. Ziegler, Joël Fagot

Bains pointed out that some of our nonwords were in fact real words and that an algorithm using only information about single letters and their positions achieves the same level of accuracy as baboons in discriminating words from nonwords. We clarify the operational definition of words and nonwords in our study and point out possible limits of the proposed algorithm.

In his Comment, Bains (*1*) argues that there are two minor methodological problems with the Grainger *et al*. study (*2*), the first being that some of the nonwords were actually rare low-frequency words, such as "blub" and "bosc," and the second that an algorithm based on letters and their positions could learn to discriminate words from nonwords without using higher-level representations such as bigrams.

The first point would appear to reflect a misunderstanding of the goals of Grainger *et al*.'s study and the experimental procedure used to achieve these goals. Although we used real English words, we could have used an entirely artificial lexicon, as is sometimes done in animal learning studies (*3*). What makes a word a word in our study is not its presence in a given dictionary but the fact that, in our experiment, words were repeated whereas nonwords were not (each to-be-learned new word was repeated intermixed with different nonwords and already-learned words until accuracy on the new word reached 80%). To further facilitate word-nonword discrimination, words and nonwords differed in bigram frequency (frequency of co-occurrence of letter pairs in the set of four-letter English words that were used). Nonwords were of low bigram frequency (e.g., "blub" and "bosc"), whereas words were of high bigram frequency. Thus, to a monkey in our experiment, "blub" and "bosc" are nonwords—that is, they are not repeated and have low bigram frequencies. Whether they are real English words outside the monkey experiment is irrelevant, at least to a monkey.

In his second point, Bains makes an interesting theoretical observation. Bains demonstrates that a machine learning algorithm based on letters and their absolute positions, which is also referred to as slot coding (*4*), can discriminate between the words and the nonwords tested in the Grainger *et al*. study. This finding is fully consistent with our main conclusion that monkeys use an orthographic code (i.e., letters and their positions) to discriminate between words and nonwords. However, Bains does not report the results of two critical tests: (i) whether his algorithm would actually generalize to novel words in the same way that monkeys do (significantly more "word" responses on the first presentation of word stimuli compared with nonword stimuli) and (ii) whether it captures the orthographic similarity effects with nonwords (figures 3 and 4 of Grainger *et al*.). In the absence of such key tests, the present simulation results are interesting but incomplete.

CNRS and Aix-Marseille University, Laboratoire de Psychologie Cognitive, Fédération de Recherche 3C, Brain and Language Research Institute, Aix-Marseille University and CNRS, 3 Place Victor Hugo, 13331 Marseille, France.

*To whom correspondence should be addressed. E-mail: jonathan.grainger@univ-amu.fr

References

1. W. Bains, *Science* **337**, 1173 (2012); www.sciencemag.org/cgi/content/full/337/6099/1173-b.
2. J. Grainger, S. Dufau, M. Montant, J. C. Ziegler, J. Fagot, *Science* **336**, 245 (2012).
3. W. T. Herbranson, C. P. Shimp, *Learn. Behav.* **36**, 116 (2008).
4. J. L. McClelland, D. E. Rumelhart, *Psychol. Rev.* **88**, 375 (1981).

11 July 2012; accepted 26 July 2012
10.1126/science.1224939

HUMAN GENOMICS

Making Race Without Racism?

Jonathan Marks

People group themselves in all sorts of ways that, in particular contexts, may mean the difference between life and death: for example, as nations, religions, kin, speech communities, tribes, races, or soccer fans. There are consequently two biocultural fallacies that must be disentangled if one wishes to focus scientifically on the study of race. First, the fallacy of racialism—that the human species is naturally divisible into a reasonably small number of reasonably discrete kinds of people, equivalent to the zoologist's subspecies—a taxonomic fallacy. And second, the judgment of individual worth on the basis of group membership, an essentialist fallacy.

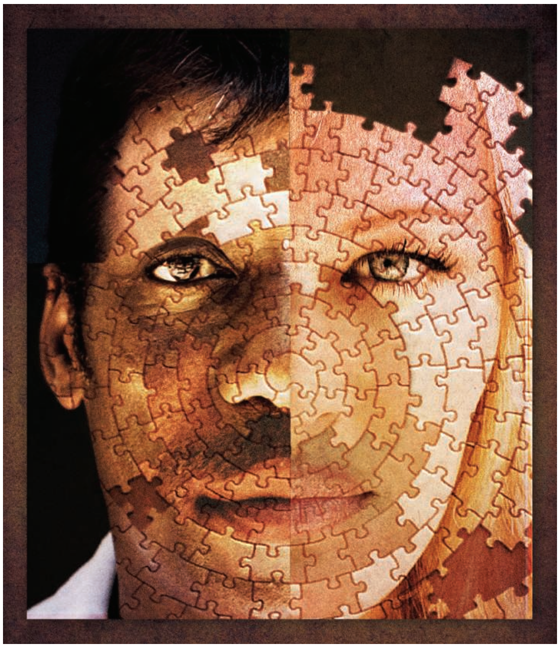

Catherine Bliss's *Race Decoded* begins with a paradox. Announcing the completion of the first human genome sequence in 2000, the leaders of the Human Genome Project declared that they had shown that race has no biological reality. But within a few years, race had become a centerpiece of human genomics. So, how did this "flip-flop" come to pass, and how do researchers in the field navigate this apparent contradiction, now often fundamental to their research?

Bliss (a sociologist of science at Brown University) conducted interviews with prominent researchers in human population genomics and related fields to understand how they conceptualize race and how it affects their science. From those, she has produced a skillful analysis of the production of scientific knowledge and social meaning. Her findings show that genomics researchers are, in the main, interested in doing beneficial things and articulating their views about human diversity in more-or-less introspective and unthreatening ways. But within that description, there exists a considerably wide swath of ideas and views expressed among genomics researchers.

The book's lone shortcoming is that Bliss does not attempt to situate the study of human diversity for the reader and thus reproduces the geneticists' narrative that nothing was known about human diversity until they began studying it in the late 1960s. In fact, anthropologists had already concluded, from intensive empirical research, that the primary patterns differentiating human groups from one another were cultural, cosmopolitan or polymorphic, clinal, and local—at a time when human geneticists were still vainly seeking our species' large natural divisions. In a 1963 paper in *Science*, for example, the prominent geneticist William Boyd authoritatively identified 13 human races, including five from Europe but only one from Africa (*1*)—in hindsight, embedding a lot of cultural information in that conclusion.

Race Decoded
The Genomic Fight for Social Justice
by Catherine Bliss
Stanford University Press, Stanford, CA, 2012. 279 pp. $85. ISBN 9780804774079. Paper, $24.95. ISBN 9780804774086.

The problem is that two centuries of prior science on human diversity had begun with the premise that the human species is indeed divisible into a fairly small number of fairly natural types and that science's job is to find them. It is consequently difficult to think today about human variation outside the framework of race, especially when race has framed so much of our social and political history. The science in *Race Decoded* is undertaken in the shadow of the failure of the Human Genome Diversity Project in the 1990s, the emergence of corporate genomics, and the congressionally imposed guidelines for racial inclusion in health research. These have brought us to the contemporary normative views of human population genomics, which Bliss calls "antiracist racialism"—that is to say, the reification of categories of people without overt value judgments about them.

Now and then, of course, there is the occasional emergence of old-fashioned scientific racism—e.g., papers in *Science* (*2*, *3*) purporting to explain the cranial deficits of Africans genomically or James Watson's public doubts about the innate intelligence of Africans, articulated to the *Sunday Times* of London in 2007. Bliss sees these as contradictions for the field to tackle, but she refrains from asking the harder question of what it might mean for the general credibility of science that some prominent geneticists are still unable to transcend ideologies that other scholarly fields have relegated to their history seminars.

Nevertheless, the primary transformation of human population genomics has been economic. The most spectacular success of human population genomic studies has been the rise of direct-to-consumer genetic testing, in which a major product is "ancestry"—which is commonly transformed into a three-syllable synonym for "race." Bliss navigates the reader through some challenging intellectual waters here: What does it mean when a science as politicized as that of the study of human genetic variation is privatized and corporatized—and its researchers speak not simply for the advancement of knowledge but also for the financial advancement of their sponsors, stockholders, and personal fortunes? That money and truth don't ordinarily mix well has long been recognized: "Ye cannot serve both God and Mammon."

The toe in the water for "racial pharmacogenomics" was BiDil, which recurs in Bliss's narrative several times. As others have documented, despite the lack of solid evidence that it worked differently or better in African-Americans than in anyone else, the drug was approved for use in specifically black heart patients. There are indeed significantly different health risks for blacks and whites in the United States (beginning with a five-year difference in life expectancy) that require social action. But BiDil was not at all a public health measure. Because it was

The reviewer is at the Department of Anthropology, University of North Carolina–Charlotte, Charlotte, NC 28223, USA. E-mail: jmarks@uncc.edu

a mixture of two already-available generic drugs, it could have been sold fairly cheaply, but it wasn't. "BiDil's only benefit beyond taking the generic drugs in combination was its reduction of the pill burden. BiDil would thus lead to African Americans paying more for the same medication."

In sum, Bliss has produced a first-rate analysis of the production and meaning of genomic data that are often being organized according to the naturalistically reified categories of American political life. Anyone perplexed over the mixed messages about race that have been coming out of genomics these past few years will find *Race Decoded* an important book.

References

1. W. C. Boyd, *Science* **140**, 1057 (1963).
2. P. D. Evans *et al.*, *Science* **309**, 1717 (2005).
3. N. Mekel-Bobrov *et al.*, *Science* **309**, 1720 (2005).

10.1126/science.1226880

Updrafting energy. Cumulonimbus over tropical Africa (Senegal and Mali), 5 February 2008.

CLIMATE

A Head in the Clouds Elucidates

Spencer Hill

Misunderstanding of climate abounds, even among those trained in science—many of the most visible climate change skeptics are physicists and engineers. The Princeton Primers in Climate are intended as an antidote. Each short book in the series, written "for students, researchers, and scientifically minded general readers," offers a concise introduction to a particular facet of the interconnected systems that affect climate. In *Atmosphere, Clouds, and Climate*, the series's fourth title, David Randall covers the atmosphere.

The book focuses on the atmosphere's lowest layer (the troposphere) and the physical processes there that are key to understanding Earth's climate. Randall (Colorado State University) has published extensively on clouds, their representation in climate models, and climate dynamics in general. His account here falls into two distinct, although not formal, sections. The early chapters provide a methodical breakdown of large-scale atmospheric circulation; the back half of the book samples nuances of atmosphere and climate.

Atmosphere, Clouds, and Climate
by David Randall
Princeton University Press, Princeton, NJ, 2012. 287 pp. $75, £52. ISBN 9780691143743. Paper, $27.95, £19.95. ISBN 9780691143750. Princeton Primers in Climate.

Randall starts with the must-know basics: climate versus weather, atmospheric composition and vertical structure, radiative transfer, and a superb back-of-the-envelope demonstration of climate change. These aspects combine to yield a simple conceptual picture of the climate system: The Sun preferentially heats the tropics (in contrast with higher latitudes) and the surface (in contrast with higher altitudes), imbalances that drive atmospheric flows to move energy poleward and upward.

Having covered the why of atmospheric circulation, Randall next addresses the how, explaining in depth the processes involved. He spells out how hot, moist air from the tropical surface rises only within narrow, towering cumulus clouds and quantitatively demonstrates how the height of such "cumulus convection" depends on the amount of energy available. The author goes on to show how these narrow cloudy towers set the conditions for the whole tropics. Other highlights include discussion of how Earth's rotation leads to the mid-latitude jet streams and tropical trade winds and of the role of mid-latitude winter storms in moving energy poleward. In four chapters and a mere 139 pages, Randall provides readers with an impressively thorough conceptual understanding of the atmosphere's central role in climate.

Parts of the remainder of the book wander a bit too far. For example, Randall spends a chapter addressing the limits of the atmosphere's long-term predictability, the point being that while weather is chaotic and thus fundamentally unpredictable, climate change (because it is externally driven) can be reliably forecast. For nonspecialists, the multiple pages detailing the underlying mathematics add little intuitive understanding of the system and are therefore expendable.

But overall, *Atmosphere, Clouds, and Climate* paints a lucid, detailed picture of the atmosphere, explaining both how it works now and how that could change due to human influence. Randall illuminates difficult topics with plain-language explanations, colorful analogies, illustrative plots, and even clever jokes. From now on, when thinking about convectively available potential energy, I will picture a hungry dog devouring its food. His passion consistently shines through, as when describing a thunderstorm as an "awe-inspiring thing of beauty." One gets the sense that Randall really enjoyed writing this primer, which makes for a very pleasant read.

One question facing the book and the entire series is simply whether the intended audience will consume the material. By design, the titles split the difference between accounts for lay readers and hardcore textbooks for climate scientists. Is the middle a Goldilocks zone or a no-man's land? Regardless, anyone who peruses *Atmosphere, Clouds, and Climate* will learn from this enjoyable, information-packed book.

10.1126/science.1225615

The reviewer is in the Atmospheric and Oceanic Sciences Program, Princeton University and National Oceanic and Atmospheric Administration Geophysical Fluid Dynamics Laboratory, 201 Forrestal Road, Suite 308B, Princeton, NJ 08540, USA. E-mail: spencerh@princeton.edu

CREDIT: ISS016E027426/NASA

SCIENCE AND SOCIETY

Rebuilding Public Trust in Science for Policy-Making

Ensuring the effectiveness and integrity of science-based policy-making is a high-priority task in Japan.

Tateo Arimoto[1,2] and Yasushi Sato[2*]

Until recently, there was little recognition within Japan's science policy circle of the need to discuss the role of science in government policy-making. A rather innocent notion that the established knowledge and wisdom of scientists would ensure proper decision-making was prevalent.

The great earthquake, tsunami, and nuclear accident that occurred in March 2011 induced a radical alteration of such a simple, optimistic view on science in policy-making. In the nation's bitter struggle for recovery, scientists sometimes created confusion by supplying divergent recommendations on evacuation, food safety, and cleanup. Public confidence in the impartiality of scientists faltered when people suspected that some of them were too easily endorsing government views. Scientific societies did not have access to critical information and failed to be systematically involved in the national effort. Polls have shown that public trust in science in Japan was damaged (see the chart) (*1*).

A more robust system of linking the scientific community to the government is clearly needed. That is not just to prepare for the next national emergencies. In fact, science in a broad range of fields is deeply built into the everyday operation of today's government. Science-based policy-making has grown ever more important in recent years, in parallel with the dramatic increase in the complexity and uncertainty of the ways in which science and technology interact with society and economy at the local, national, and global levels. Installing a proper framework for ensuring its effectiveness and integrity to secure public trust in, and support of, science is becoming an urgent task in Japan.

Antecedents

Looking back, many nations have faced similar situations since the 1990s and have endeavored to straighten out their own systems of incorporating science into the process of policy-making, mainly by establishing principles or guidelines on science-government relations.

In the United Kingdom, controversies surrounding bovine spongiform encephalopathy during 1990s prompted public debate on science and policy-making. In response to mounting criticism that scientific knowledge was not properly reflected in relevant policies, the British government formulated a set of rules for science-based policy-making and then updated them several times, a process that continues to this day (*2*, *3*). In addition, the British government issued a document in 2010, laying down general principles prescribing science-government relations (*4*). It stated that the government should respect the professional expertise of scientific advisers, and, in turn, scientific advisers should respect the decision processes in democracy and appreciate that science is only part of the evidence that government must consider in policy-making.

In the United States, the Obama Administration is strongly promoting scientific integrity in the government. On the basis of his concern that the sciences of climate change, stem cells, etc., were subject to political suppression under the Bush Administration, Obama declared his intention to "restore science to its rightful place." Soon after he took office, he issued a memorandum outlining his administration's basic policy for scientific integrity (*5*). His science adviser, John Holdren, finalized a more detailed guideline in late 2010, in cooperation with relevant departments and agencies, most of which have in turn issued their own guidelines for ensuring scientific integrity by March this year (*6*).

One can find many more ongoing efforts to give order to science-government relations. The European Union has been concerned about the issue since it drew up its own guideline in 2002 (*7*). In Germany, the Berlin-Brandenburg Academy of Sciences and Humanities set up a guideline in 2008, after conducting elaborate studies for several years (*8*). The Netherlands and Canada have also been leaders on this subject. Thus, efforts to ensure the effectiveness and integrity of science-based policy-making have steadily accumulated during the past 15 years.

DIMENSIONS OF SCIENCE COOPERATION

Japan's Effort

In Japan, the fourth 5-year Science and Technology Basic Plan, adopted by the cabinet last August, specifically stated the need to set up basic principles with regard to the relations of science and technology to policy-making (*9*). The Science Council of Japan expressed its resolution to strengthen its own scientific advisory activities (*10*). The Japanese government is now moving toward enhancing the systems for scientific advice, including the appointment of science advisers to the prime minister and other ministers, the enhancement of the think-tank functions, and the strengthening of liaison with the Science Council of Japan.

Recently, the Japan Science and Technology Agency's Center for Research and Development Strategy (JST-CRDS), a semipublic think tank, issued a policy proposal calling for measures to ensure the effectiveness and integrity of science-based policy-making in Japan (*11*). The proposal features a draft of general principles on science-government relations. Formulated by referring to foreign examples and also taking into consideration Japan's particular situations, the draft includes 10 principles:

The role of scientific advice in policy-making. Scientific knowledge is an essential element in the policy-making process, and the government must duly respect it. At the same time, scientific advisers must recognize that scientific knowledge is not the sole basis of government decision-making.

Seeking scientific advice in a timely and pertinent manner. The government shall endeavor to identify policy issues that require scientific knowledge in a timely and pertinent manner and act to acquire the best scientific knowledge available.

Ensuring the independence of scientific advisers. The government must not intervene in the activities of scientific advisers. As a means to ensure objectivity and fairness, scientific advisers shall declare their own conflicts of interest.

Awareness of responsibility as scientific

[1]National Graduate Institute for Policy Studies, 7-22-1, Roppongi, Minato-ku, Tokyo, 106-8677, Japan. [2]Center for Research and Development Strategy, Japan Science and Technology Agency, 7 Gobancho, Chiyoda-ku, Tokyo, 102-0076, Japan.

*Author for correspondence. E-mail: y11sato@jst.go.jp

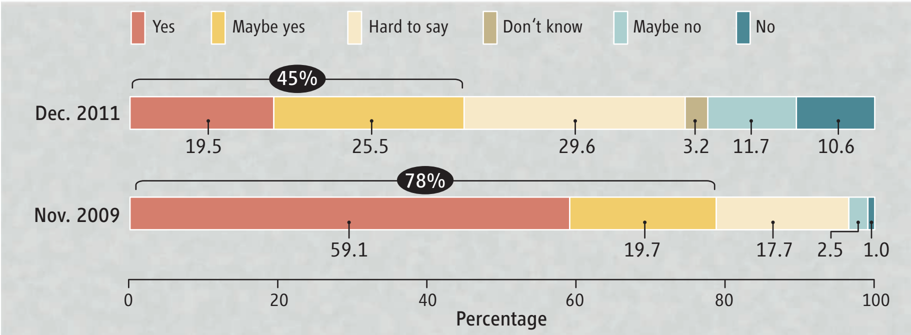

Survey results. Question: Should the direction of research and development be decided by experts who are well-versed in the subject? [Source adapted from (*1*); original data come from surveys conducted by the National Institute of Science and Technology Policy in December 2011 and the Central Research Institute of the Electric Power Industry in November 2009]

advisers. Scientists shall always provide scientific advice for the public welfare and with the awareness of the large influence scientific advice has on the process of public policy formulation.

Achieving broad perspectives and balance. When the government seeks scientific advice, it should strive to secure the participation of scientists with appropriate insight and experience matched to the nature of the issues and to obtain balanced advice based on broad perspectives.

Ensuring the quality of advice and integrating viewpoints. Scientific advisers shall strive for a balanced treatment of observational and experimental results and of cited papers and should seek to improve the quality of scientific advice through peer review. The Science Council of Japan and academic societies shall, where appropriate, endeavor to present high-quality scientific advice by integrating views of the nation's scientific community. The government shall ensure, as needed, that scientific knowledge used in policy-making has gone through independent peer review by qualified experts.

Proper handling of uncertainty and diversity. Scientific advisers shall provide policy-makers with clear explanations of uncertainties and diversity of views associated with scientific knowledge. The government shall respect such uncertainties and diversity of views.

Free disclosure of scientific knowledge. In principle, scientific advisers are free to make their scientific knowledge public. They shall do so responsibly, however, in awareness of the large influence that scientific knowledge can have on policy-making and public opinion, as well as on society as a whole.

Even-handed treatment of scientific advice by the government. The government must treat with fairness the scientific knowledge it acquires. It must not approach scientific advice with any preconception, distort scientific knowledge when making it public, or intentionally add wrong interpretations when using advice in policy-making. The government should explain how scientific advice was considered when drawing up policy. It is especially important for the government to explain the rationales when making policy decisions that are in conflict with the scientific advice obtained.

Ensuring transparency of the scientific advice process. To improve the quality and reliability of policy-making based on scientific advice, the government shall ensure transparency of the scientific advice process.

This draft of principles is intended as a starting point for discussion among a wide range of stakeholders in Japan. It is hoped that, through such discussion, the principles will be finalized, and relevant organizations will draw up and implement their own guidelines, reflecting the characteristics of their respective missions.

Outlook

The efforts for scientific integrity in Japan should not proceed in isolation from those in other nations. The scientific community and the government of Japan, as well as other nations, have the duty to provide their best contributions to solving a broad range of problems that today's society faces, including global problems. At the same time, scientific activities, not only in advanced nations but also in emerging and developing nations, are increasing rapidly. Thus, scientific integrity is a common goal that should be pursued internationally.

Some international efforts are already moving forward. The InterAcademy Council (IAC), which offers scientific advice to international organizations, is leading such efforts. IAC came under the spotlight in 2010, when it conducted a review of the operation of the Intergovernmental Panel on Climate Change (IPCC) and made recommendations to reassure its scientific credibility (*12*). IAC's more recent endeavor is its project to produce educational materials for the global science community on "research integrity and scientific responsibility." Meanwhile, the U.S. National Science Foundation, in May this year, hosted the Global Summit on Merit Review, which stressed the importance of ethics and integrity in review processes. International collaboration at the academic level is also rapidly advancing, as more and more social and natural scientists are taking interest in this issue. They have begun extensive discussion among themselves and with policy-makers (*13*, *14*).

Ensuring the effectiveness and integrity of science in policy-making is a complex problem. In promoting relevant efforts, particularities of diverse policy and scientific fields must be given due consideration. Also, the approach to this problem should vary depending on national differences in political systems and scientific traditions. That is why all stakeholders from all nations should actively participate in this endeavor and advance dialogue. Such a concerted effort will not be easy to organize and manage. But that is exactly what is needed now, as we have entered the age of intense, intricate interaction between science, technology, and the globalized society.

References and Notes

1. Japan Ministry of Education, Culture, Sports, Science and Technology, Summary of a White Paper on science and technology, 2011, July 2012.
2. UK Government Office for Science, The Government Chief Scientific Advisor's Guidelines on the Use of Scientific and Engineering Advice in Policy Making, June 2010.
3. UK Government Office for Science, Code of Practice for Scientific Advisory Committees, November 2011.
4. UK Department for Business, Innovation and Skills, Principles of Scientific Advice to Government, 24 March 2010.
5. The White House, Memorandum for the heads of executive departments and agencies: Scientific integrity, 9 March 2009.
6. J. P. Holdren, Memorandum for the heads of executive departments and agencies, 17 December 2010.
7. Commission of the European Communities, Communication from the Commission on the collection and use of expertise by the Commission: Principles and guidelines, 12 November 2002.
8. Berlin-Brandenburgische Akademie der Wissenschaften, Leitlinien Politikberatung (BBAW, Berlin, 2008).
9. The Government of Japan, The Fourth Science and Technology Basic Plan, 19 August 2011.
10. Statement by the Executive Council of the Science Council of Japan, Recovery from the great east Japan earthquake and the responsibility of the Science Council of Japan, 22 September 2011.
11. JST-CRDS, Toward the Establishment of Principles Regarding the Roles and Responsibilities of Science and Government in Policy Making, March 2012.
12. IAC, Climate change assessments: Review of the processes and procedures of the IPCC, August 2011.
13. J. Lentsch, P. Weingart, Eds., *The Politics of Scientific Advice: Institutional Design for Quality Assurance* (Cambridge Univ. Press, Cambridge, 2011).
14. *Sci. Eng. Ethics* **17** (4) (2011).

10.1126/science.1224004

CELL BIOLOGY

A Scaffold Switch to Insulate

Conformational changes in a protein scaffold can determine signaling specificity.

Roger J. Davis

A fundamental aspect of normal physiology is that cellular signal transduction pathways activated by specific stimuli should lead to appropriate responses. But signaling proteins may function in more than one pathway. How then does specificity arise? How is improper crosstalk avoided? Molecules that can tether signaling proteins in a spatially restricted manner represent one possible mechanism. Such scaffolds may act as insulators that maintain the fidelity of signaling by physically sequestering proteins into distinct pools. On page 1218 of this issue, Zalatan *et al.* (*1*) demonstrate that the insulating function of the prototypical scaffold protein Ste5 is accomplished by a change in its conformation, indicating that the scaffold actively gates the flow of information and is not merely a passive, static structure.

Ste5 is a component of the mitogen-activated protein kinase (MAPK) signaling pathway (*2*, *3*) that is activated by exposure of budding yeast to pheromone and leads to a mating response (*4*). This pathway is formed by the MAP3K isoform Ste11 that activates the MAP2K isoform Ste7 that, in turn, activates the MAPK isoforms Fus3 and Kss1. Unexpectedly, Ste11, Ste7, and Kss1 also participate in the stress response pathway that is activated by starvation and leads to invasive (filamentous) growth. The participation of Ste11 and Ste7 as common components of two different MAPK pathways raises questions about the mechanism of signaling specificity. The Ste5 scaffold solves this problem by imposing signaling specificity that is essential for Fus3 activation (*5*) and repression of the transcriptional response to activated Kss1 (*6*, *7*). Consequently, Kss1 activation mediates the response to starvation, and activation of Fus3 mediates the mating response to pheromone.

The MAPK Fus3 is a poor substrate for the MAP2K Ste7 (*5*). However, phosphorylation of Fus3 by Ste7 is permitted in the presence of the von Willebrand type A (VWA) domain of the Ste5 scaffold (*5*). Earlier structural analysis showed that

Howard Hughes Medical Institute and Program in Molecular Medicine, University of Massachusetts Medical School, Worcester, MA 01605, USA. E-mail: roger.davis@umassmed.edu

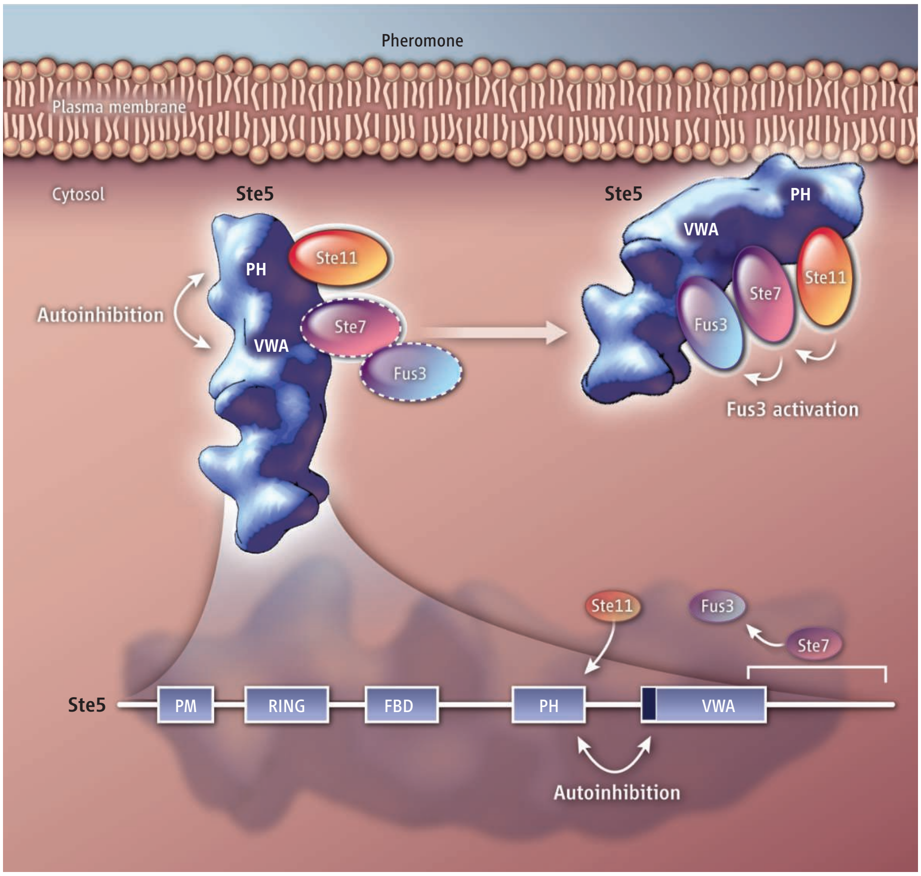

A conformational switch. The domains of the Ste5 scaffold protein and their interactions are shown. Ste5 is inhibited by an intramolecular interaction between the PH domain and a sequence that flanks the VWA domain. In response to pheromone, a signaling pathway is initiated in yeast cells that requires membrane recruitment of Ste5 and a conformational change that disrupts autoinhibition and allows signals to propagate through the signaling cascade.

CREDIT: B. STRAUCH/SCIENCE

two different surfaces on the VWA domain interact with Fus3 and Ste7. The domain works, in part, by presenting Fus3 in a conformationally "unlocked" state that enables phosphorylation by Ste7 (*5*). By contrast, Kss1 phosphorylation by Ste7 is unaffected by the Ste5 scaffold. Although this analysis provided molecular insight into the mechanisms by which Ste5 promotes Fus3 activation, the role of the scaffold in insulating the pheromone MAPK pathway against activation by the starvation MAPK pathway remained unresolved.

Zalatan *et al.* tested whether insulation is mediated by sequestration of shared pathway components (Ste11 and Ste7) within the Ste5 scaffold complex—that is, whether the scaffold segregates a subpopulation of common signaling intermediates. Kinetic analysis in vitro revealed rapid exchange of Ste11 and Ste7 with Ste5. Direct confirmation of this observation in vivo is required. Nevertheless, the rapid exchange kinetics may account for Kss1 activation by the mating pathway in vivo (*6*, *7*). These considerations are inconsistent with insulation by sequestration. The authors instead provide convincing evidence in favor of an alternative hypothesis—that the Ste5 scaffold plays an active role in insulation.

The premise of the alternative hypothesis is based on the observation that starvation can activate Fus3 in yeast cells that express the Ste5 VWA fragment, but starvation does not activate Fus3 in cells expressing full-length Ste5 (*1*). This observation indicates

that although the VWA fragment is sufficient to promote Fus3 activation by Ste7, sequences present in the full-length Ste5 protein are required to insulate the pheromone pathway against activation by the starvation pathway. Combining structural and biochemical analysis, Zalatan *et al.* identify an intramolecular inhibitory interaction between the pleckstrin homology (PH) domain of Ste5 with a sequence that flanks the VWA domain. This finding is consistent with previous genetic and biochemical analysis of activated *Ste5* alleles that promote Fus3 activation (*8*). The intramolecular interaction prevents VWA domain–mediated promotion of Fus3 phosphorylation and accounts for the insulation of the Fus3 pathway against activation by starvation.

The PH domain of Ste5 binds to phosphoinositol 4,5-bisphosphate [PI(4,5)P_2] and is required for recruitment of the scaffold to the plasma membrane in response to pheromone. This membrane localization is required for Fus3 activation (*9–11*). These observations suggest a possible mechanism for regulating Ste5 autoinhibition. Indeed, Zalatan *et al.* demonstrate that the interaction of the PH domain with phospholipid vesicles containing PI(4,5)P_2 can partially disrupt the PH-VWA interaction and thus promote Ste7-mediated Fus3 activation. Complete activation of the Ste5 scaffold may require additional membrane interactions, including the plasma membrane helix domain, which binds phospholipid (*10*), and the RING-H2 domain, which binds to Gβγ, a signaling protein at the plasma membrane (*12*).

In the model of Zalatan *et al.*, pheromone triggers the membrane recruitment of Ste5, engagement of the PH domain, disruption of autoinhibition, and promotion of Fus3 activation. Moreover, pheromone provides two inputs into this signaling pathway—initiating activation of Ste11 by Ste20 and causing a conformational switch in Ste5 to enable Fus3 activation. The Ste5 scaffold is therefore an active participant in MAPK signaling. The determination of atomic structures of Ste5 conformational states that define the switch-like activity of this scaffold protein will be required for understanding Ste5 function and represents an important goal for future studies.

Structural and biochemical studies (*1*, *5*, *13*), together with genetic analysis (*4*) of Ste5, have provided important insights into the function of MAPK scaffold proteins in yeast. The conceptual framework may be relevant to mammalian MAPK scaffold proteins, including c-Jun N-terminal kinase (JNK)–interacting protein (JIP) and kinase suppressor of Ras (KSR) (*14*). Now it's time for detailed studies of these mammalian scaffold proteins to answer to this question.

References

1. J. G. Zalatan, S. M. Coyle, S. Rajan, S. S. Sidhu, W. A. Lim, *Science* **337**, 1218 (2012); 10.1126/science.1220683.
2. K.-Y. Choi, B. Satterberg, D. M. Lyons, E. A. Elion, *Cell* **78**, 499 (1994).
3. S. Marcus, A. Polverino, M. Barr, M. Wigler, *Proc. Natl. Acad. Sci. U.S.A.* **91**, 7762 (1994).
4. R. E. Chen, J. Thorner, *Biochim. Biophys. Acta* **1773**, 1311 (2007).
5. M. Good, G. Tang, J. Singleton, A. Reményi, W. A. Lim, *Cell* **136**, 1085 (2009).
6. M. Z. Bao, M. A. Schwartz, G. T. Cantin, J. R. Yates III, H. D. Madhani, *Cell* **119**, 991 (2004).
7. S. Chou, L. Huang, H. Liu, *Cell* **119**, 981 (2004).
8. C. Sette, C. J. Inouye, S. L. Stroschein, P. J. Iaquinta, J. Thorner, *Mol. Biol. Cell* **11**, 4033 (2000).
9. L. S. Garrenton, S. L. Young, J. Thorner, *Genes Dev.* **20**, 1946 (2006).
10. M. J. Winters, R. E. Lamson, H. Nakanishi, A. M. Neiman, P. M. Pryciak, *Mol. Cell* **20**, 21 (2005).
11. L. S. Garrenton, C. J. Stefan, M. A. McMurray, S. D. Emr, J. Thorner, *Proc. Natl. Acad. Sci. U.S.A.* **107**, 11805 (2010).
12. C. Inouye, N. Dhillon, J. Thorner, *Science* **278**, 103 (1997).
13. R. P. Bhattacharyya *et al.*, *Science* **311**, 822 (2006).
14. D. K. Morrison, R. J. Davis, *Annu. Rev. Cell Dev. Biol.* **19**, 91 (2003).

10.1126/science.1227747

GENETICS

A GPS for Navigating DNA

The integration of DNA variation information with molecular and cellular data may help to elucidate disease mechanisms.

Eric Schadt and Rui Chang

A complete characterization of genetic and epigenetic variations in germline and somatic DNA can provide a blueprint for understanding causal relationships between genes and phenotypes, from hydrogen production in bacteria to glucose homeostasis in humans. Detecting small nucleotide differences, structural variations (such as duplications), and a range of chemical modifications to nucleic acids have pointed to variations that potentially underlie the risk of disease, disease severity, and response to treatments for specific diseases. However, these changes alone are not sufficient to explain how a given variant or constellation of variants increases the risk of disease. What is needed is an integration of many different kinds of genetic and molecular data to elucidate regulatory networks underlying disease (*1*). On page 1190 of this issue, Maurano *et al.* (*2*) contribute such data by characterizing how DNA variants associated with common disease traits are concentrated in noncoding regulatory regions of the human genomes that are marked by hypersensitivity to the enzyme deoxyribonuclease I (DNase I). When appropriately integrated with other molecular, cellular, and physiological data, such information may improve the way we understand normal conditions and diagnose and treat disease.

Genome-wide association studies (GWAS) have shown the difficulty in understanding how common DNA sequence variations disrupt biological processes to predispose to a particular disease (*3*). These studies are limited by the lack of functional context within which to understand such variants. Changes in DNA do not directly lead to changes in disease-related phenotypes, but instead lead to changes in molecular phenotypes; these in turn affect molecular and cellular processes that then lead to changes in physiological states. Understanding how the DNA is read—that is, what DNA is more accessible to proteins that control expression (and under what conditions)—can help to elucidate the functional consequences of DNA variation.

Maurano *et al.* analyzed hundreds of human cell and tissue samples studied under the ENCODE project (*4*), the Roadmap Epigenomics Program (*5*), and the 1000 Genomes Project (*6*) and found that DNase I hypersensitive sites (DHS) in the genome map to regions that associate with human disease such as Crohn's disease and multiple sclerosis. Combined with other recent results demonstrating that DNase I hypersensitive sites are also much more likely to harbor variants associated with gene expression (*7*), the utility of integrating these different

Institute for Genomics and Multiscale Biology, Mount Sinai School of Medicine, New York, NY 10029, USA. E-mail: eric.schadt@mssm.edu

types of data to identify the regulatory networks that underlie disease seems clear. For example, Maurano *et al*. found that 24.4% of DNA sequence variations (called single-nucleotide polymorphisms or SNPs) associated with autoimmune disorders such as type I diabetes, rheumatoid arthritis, Crohn's disease, and lupus fall within DNase I hypersensitive sites that bind to transcription factors that interact with interferon regulatory factor 9, highlighting a portion of a regulatory network important for autoimmune disorders.

Genetic loci associated with gene expression have been used to infer causal relationships among genes and between genes and higher-order phenotypes such as disease (*8*, *9*), but such relationships are statistically inferred, not directly observed, similar to the detection of extrasolar planets by observing the characteristic wobble they induce on the stars they orbit. Statistically inferring the existence of extrasolar planets does not enable the same level of scrutiny afforded by direct observation with advanced, well-positioned telescopes; likewise, statistically inferring causal relationships between genes is not as satisfying as directly observing their physical interactions that give rise to phenotypes of interest. To achieve a more accurate mapping of the flow of information between DNA variation and physiological state, a "global positioning system" is required. Ideally, such a system would clarify the full complement of RNA actively transcribed and translated in the cell, the position of all proteins, the binding of proteins to DNA and the interactions of those proteins with other proteins, and so on, in different cell types and at different stages of development or in response to different environmental stresses. However, until such levels of detail are achieved, the DHS data can serve as a crude global positioning system for identifying disease-associated regulatory networks. An understanding of genomic regions that are actively bound by proteins in a cell or tissue in a condition-specific context could dramatically improve the ability to construct a profile of proteins (biomarkers) that best define a given disease. Through the characterization of more accurate networks, we can achieve a more informed taxonomy of disease based on the processes intrinsic to the onset, progression, and severity of disease (*10*). This could help to pinpoint the combination of targets (genes, RNAs, or proteins) to effectively target a network (*11*, *12*) that are best suited to transform regulatory networks from a disease-oriented state into a more natural, healthy state.

The DHS data of Maurano *et al*. and others not only greatly facilitate the identification of causal variants at a given disease-associated locus, but the regulatory element and corresponding binding protein may be identified as well, providing a far richer context within which to uncover mechanisms of disease. Further, knowing when a given regulatory element is exposed, when it is bound by a protein, in what cell or tissue types, and under what environmental or developmental condition can provide for a rich set of prior information that has the potential to improve the accuracy of predictive network models of disease (see the figure). For example, in RIMBANET (*9*), a probabilistic causal network reconstruction algorithm that can simultaneously consider multiple different types of data, the DHS data could constrain the types of relationships allowed between genes in a condition-specific fashion. This is similar to constraining relationships among genes based on patterns of cis- and trans-acting expression quantitative trait loci or of experimentally determined transcription factor–DNA binding data (*9*, *13*). Although the DHS data may not directly lead to the identification of the actual proteins binding to a region of DNA, the demonstration by Maurano *et al*. that DNase I hypersensitive sites play a critical role in modulating disease risk, progression, and severity strongly motivates integrating DHS data with extensive genome annotation, DNA sequencing, and molecular profiling (transcriptomic, proteomic, and metabolomics), as well as cellular, imaging, and clinical data, to build more predictive models of disease.

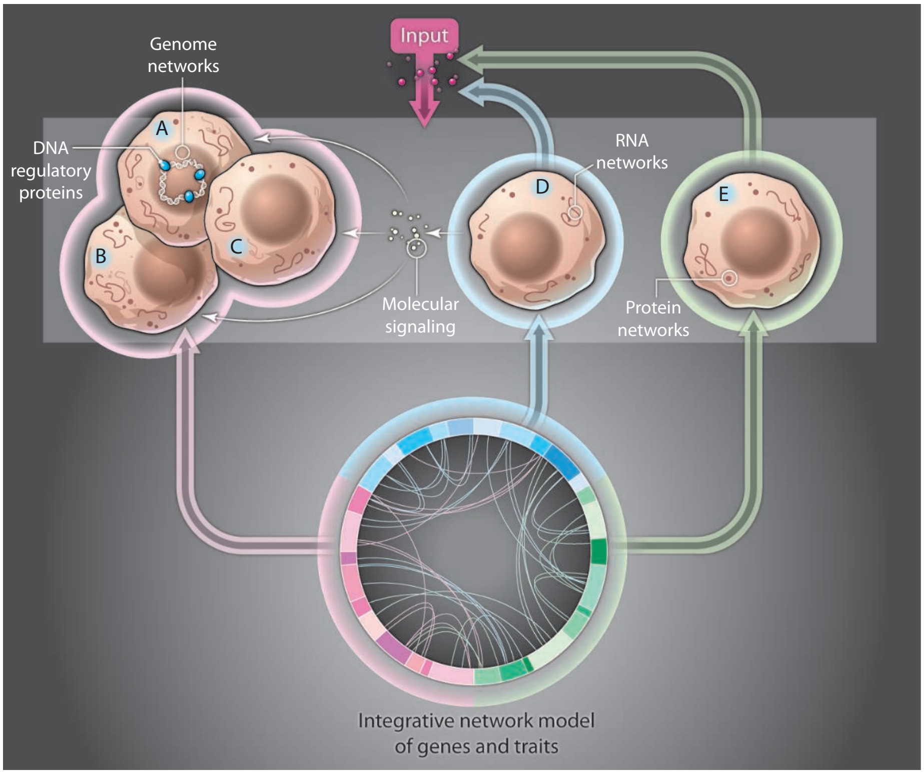

Systems-level predictions. The integration of disease-associated DNA variation information with more dynamic molecular data (such as DHS and RNA abundance information) and cellular data (such as glucose uptake and insulin secretion) across different conditions can lead to the construction of networks for predicting physiological state changes, such as those associated with glucose homeostasis (for which the input would be food intake).

References

1. A. Califano, A. J. Butte, S. Friend, T. Ideker, E. Schadt, *Nat. Genet.* **44**, 841 (2012).
2. M. T. Maurano *et al*., *Science* **337**, 1190 (2012); 10.1126/science.1222794.
3. B. E. Stranger, E. A. Stahl, T. Raj, *Genetics* **187**, 367 (2011).
4. R. E. Thurman *et al*., *Nature* 10.1038/nature11232 (2012).
5. B. E. Bernstein *et al*., *Nat. Biotechnol.* **28**, 1045 (2010).
6. The 1000 Genomes Project Consortium *et al*., *Nature* **467**, 1061 (2010).
7. J. F. Degner *et al*., *Nature* **482**, 390 (2012).
8. E. E. Schadt *et al*., *Nat. Genet.* **37**, 710 (2005).
9. J. Zhu *et al*., *PLoS Biol.* **10**, e1001301 (2012).
10. National Research Council (U.S.), Committee on a Framework for Developing a New Taxonomy of Disease., *Toward Precision Medicine: Building a Knowledge Network for Biomedical Research and a New Taxonomy of Disease* (National Academies Press, Washington, DC, 2011).
11. E. E. Schadt, *Nature* **416**, 218 (2009).
12. E. E. Schadt, S. H. Friend, D. A. Shaywitz, *Nat. Rev. Drug Discov.* **8**, 286 (2009).
13. J. Zhu *et al*., *Nat. Genet.* **40**, 854 (2008).

Published online 5 September 2012;
10.1126/science.1227739

CREDIT: Y. HAMMOND/*SCIENCE*

EVOLUTION

Real Fish Attack Simulated Plankton

An experiment in which predatory fish attack groups of simulated plankton allows evolutionary hypotheses to be tested.

W. L. Romey

Watching a cat chase a laser pointer across the floor makes us wonder how they can so easily be fooled. Yet, cats, humans, and many other animals respond readily to simulations as if they were real. On page 1212 of this issue, Ioannou *et al*. (*1*) report the creation of a virtual world in which real animals interact with simulated groups. In their study, simulated zooplankton (*Daphnia*) interact with each other and are attacked by real fish. The results shed light on fundamental questions in evolutionary biology.

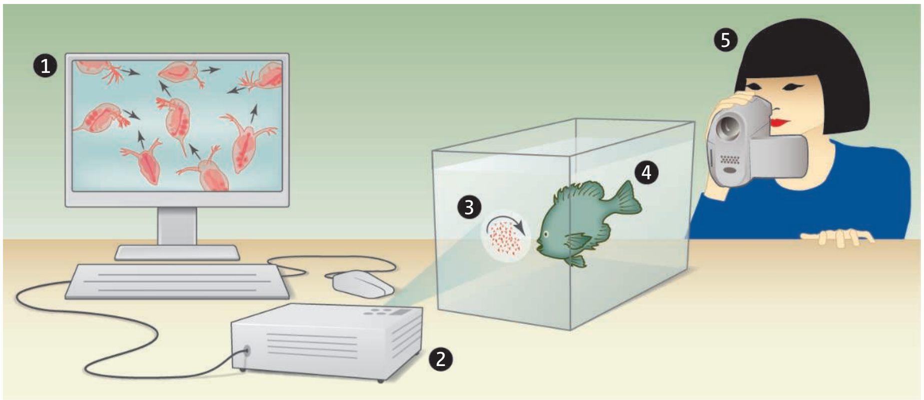

Fish versus simulation. Ioannou *et al*. test hypotheses about evolutionary selection pressure on groups by studying real fish pitted against simulated zooplankton (*Daphnia*). A computer simulation of an interacting *Daphnia* swarm (**1**) is projected (**2**) onto a translucent screen (**3**) inside a fish tank. When a real fish (**4**) attacks the simulated points, a digital video camera (**5**) records the behavior.

One of the hallmarks of modern studies of animal behavior is the use of controlled experiments in which the environment is reduced to its key elements. Almost 60 years ago, Tinbergen presented cardboard models of adult gull heads to chicks to test their innate pecking responses (*2*). More recently, computer animations have been used to investigate the mating behavior of jumping spiders (*3*), robots have been used to understand mate choice in grouse (*4*), and single robotic fish swimming in real fish schools have been studied (*5*). However, the boundaries of what is knowable in animal behavior would be considerably broadened if we could study the behavior of real individuals in response to a simulated group, rather than to individuals only.

In previous work, Ioannou and Krause have presented empirical studies of fish attacking real Daphnia (*6*), and Guttal and Couzin have developed theoretical computer simulation models of grouping (*7*). In the current work (*1*), Ioannou *et al*. combine the two approaches. This allows them to test whether predators choose large groups over small, whether polarization (the degree of parallel orientation between individual prey) influences the rate at which fish attack their prey, and why predators preferentially attack the outsides of groups. Some of these questions have been addressed with experimental studies using real prey (*6*, *8*), but the technique developed by Ioannou *et al*. (*1*) allows biologists to discriminate between alternative hypotheses.

In the first step of their experiments, each simulated prey is given a similar set of rules that move it toward or away from the aggregate group by a unit distance (*9*). The process is iterated over thousands of time steps, like the frames in a movie. The authors then project the simulated prey's movements onto a screen in an aquarium and use a video camera to determine which prey the fish select (see the figure). Ioannou *et al*. measure how the prey group size, the position of the prey relative to the group (inside or outside), and the polarization of the simulated prey influence the fish's attack behavior. This approach allows biologists to see how the behavior of real organisms is influenced by the emergent dynamics of a group; for example, these emergent properties include whether a group of *Daphnia* moves through the water in a straight or curved trajectory.

Ioannou *et al*. confirm earlier studies, which showed that predatory fish preferentially target larger groups, individuals at the edge of a group, and nonpolarized prey. Given that the simulated individuals all follow the same movement rules, the predators must attack prey based on the emergent properties of group position, group size, group speed, and turning, rather than innate differences between individual prey.

There are two main explanations for why a predator would attack the outside of a group or one group over another: First, because the position or size makes it easier to isolate them from the predators point of view, or second, because the ones on the outside are inherently slower or weaker than the others. Ioannou *et al*. conclude that the first explanation is correct. This conclusion is also supported by field studies of predators attacking grouped prey, which have shown that if the position of real prey is randomized so that there are no individual differences (size, sex, or other factors) between positions, predators still attack the outside individuals in a prey group (*8*).

Ioannou *et al*.'s technique also shows that certain movement rules lead to specific emergent properties that may influence predators. Simulation models with greater individual polarization led to groups that moved linearly and were attacked more often by fish. However, the optimum movement rule for a grouping organism is a trade-off between many factors, including avoiding predators and obtaining their own food (*10*).

The pairing of simulated groups and real animals to test behavioral hypotheses, demonstrated in (*1*), has a great deal of promise for helping to understand basic evolutionary principles of grouping and predator-prey dynamics. Other promising advances include the use of multiple robots that interact not only with each other but also with live study organisms (*5*, *11*). Advances in real-time tracking of live individuals and robotics over the next few years will speed up this avenue of research.

Perhaps this line of behavioral research, in which real animals respond to simulated animals, will even lead to development of three-dimensional holograms for behavioral research. For example, scientists may

Department of Biology, State University of New York at Potsdam, Potsdam, NY 13676, USA. E-mail: romeywl@potsdam.edu

be able to control animal migration or conserve grouping animals such as birds, fish, and insects, by having real animals follow projected simulations to survive real-world dangers. Applications of these techniques may also help birds move around buildings or away from airports.

References

1. C. C. Ioannou, V. Guttal, I. D. Couzin, *Science* **337**, 1212 (2012); 10.1126/science.1218919.
2. N. Tinbergen, *The Herring Gull's World* (Collins, London, 1953).
3. D. L. Clark, G. W. Uetz, *Anim. Behav.* **40**, 884 (1990).
4. G. L. Patricelli, A. H. Krakauer, *Behav. Ecol.* **21**, 97 (2010).
5. D. T. Swain *et al.*, *Proc. IEEE* **100**, 150 (2012).
6. C. C. Ioannou, J. Krause, *Anim. Behav.* **75**, 1383 (2008).
7. V. Guttal, I. D. Couzin, *Proc. Natl. Acad. Sci. U.S.A.* **107**, 16172 (2010).
8. W. L. Romey, A. R. Walston, P. J. Watt, *Behav. Ecol.* **19**, 74 (2008).
9. A. Huth, C. Wissel, *J. Theor. Biol.* **156**, 365 (1992).
10. J. K. Parrish, L. Edelstein-Keshet, *Science* **284**, 99 (1999).
11. J. Krause *et al.*, *Trends Ecol. Evol.* **26**, 369 (2011).

10.1126/science.1228217

CELL BIOLOGY

Heart Brakes

Detailing the molecular mechanism of heart muscle contraction provides insight into the cause of a genetic form of heart failure.

Thomas P. Burghardt and Katalin Ajtai

Many of us are keenly aware of muscle diseases because they frequently impact our lives. Heart failure, for example, is a leading cause of death, and its hereditary link has focused research efforts on sequencing the genes encoding muscle proteins (*1*). Several muscle proteins are implicated in heart disease, most notably the abundant motor protein myosin, and the relatively scarce structural protein myosin binding protein C (MyBP-C). Myosin generates the force for heart muscle contraction, but a heart will pump without MyBP-C, and its role in contraction and disease was unknown. In addition, mutations in MyBP-C cause late onset of heart failure, obscuring the link between protein malfunction and disease mechanism (*2*). These challenges have defied a bottom-up approach to characterize isolated MyBP-C's function in vitro, but the heart is too complex for top-down whole-muscle characterization (*3*). New research by Previs *et al*. (*4*) on page 1215 in this issue takes the middle road, using a concise experimental system that preserves relevant tissue structure while allowing the observation of single-particle dynamics to pinpoint MyBP-C's role in muscle contraction.

Cardiac or skeletal muscle consists of parallel fibers that shorten against resistive force. The fibers are built up from micrometer-scale sarcomere units assembled in series. The sarcomere is the unitary contractile element that shortens to produce force while consuming the cellular fuel of adenosine 5′-triphosphate (ATP). It is a structured protein assembly made up predominantly of myosin and its force-producing partner actin. Myosin and actin each form filaments that overlap in a lattice (*5*). Muscle myosin is a linear molecule with a globular head domain at the amino terminus containing the ATP and actin binding sites and a long tail that spontaneously associates with other myosin tails to form the rodlike myosin filament. The head domains project out of the myosin filament toward actin. Actin and myosin filaments slide relative to one another during contraction due to impulsive force provided by myosin while they are tightly bound to each other (*6*, *7*). MyBP-C occupies a portion of the overlap zone called the C-zone where it binds by its carboxyl terminus to the myosin filament (see the figure). The amino terminus of MyBP-C binds the actin filament, creating a secondary actomyosin connection (*8*).

The mouse heart can imitate the human one in its response to human disease mutation. Transgenic mice carrying modified MyBP-C associated with human heart disease develop failing heart characteristics that mimic those in humans (*9*). Previs *et al*. devised a preparation from the transgenic mouse heart, isolating intact myosin filaments from permeabilized tissue strips. The preparation uses the proteolytic enzyme calpain to remove the filaments by cleaving selected proteins holding the sarcomere together, while maintaining the myosin filaments and their complement of MyBP-C. All MyBP-C proteins were present in the excised filaments but with ~80% intact and the remainder cleaved near the amino terminus. Filamentous myosin is a bipolar array where molecules reverse polarity at the midpoint, creating a short "bare zone" where no heads are present and two flanking C-zones where MyBP-C resides, followed by a stretch of myosin heads without MyBP-C. The myosin filaments were adsorbed to a planar glass substrate, with myosin heads on the surface free to move actin filaments. Fluorescence-labeled actin filaments added to the bulk solution above the substrate land on the immobilized myosin. Total internal reflection fluorescence (TIRF) microscopy excites fluorescence within ~100 nm of the glass substrate, enhancing signal-to-noise for this low–light level application (*10*).

Previs *et al*. preselected actin filaments with lengths shorter than the bare zone to avoid actin contacting both flanking C-zones. Thus, actin will slide over similarly oriented myosins and will encounter

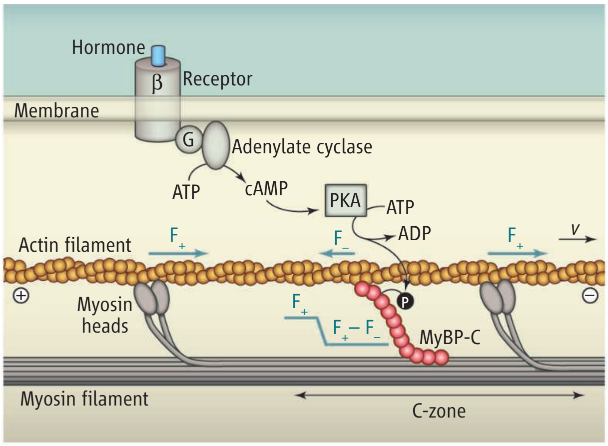

Sliding filaments during heart contraction. Actin and myosin filaments slide relative to one another due to impulsive force (F_+) provided by the myosin power stroke. Net force on actin changes at the C-zone containing MyBP-C due to the braking force (F_-). Actin sliding velocity (v) is measured with TIRF microscopy detection of fluorescence-labeled actin filaments. The β-adrenergic pathway couples MyBP-C phosphorylation with hormone binding to the β receptor through G protein (G) activation, adenylate cyclase–mediated generation of cyclic AMP, and PKA activation.

Biochemistry and Molecular Biology, Mayo Clinic Rochester, Rochester, MN 55905, USA. E-mail: burghardt@mayo.edu

the MyBP-C free zone, the C-zone, or both depending on where the actin filament lands. Measurements of actin displacement versus time showed two constant velocities. Additional experiments on transgenic mouse samples without MyBP-C revealed that the slower velocity describes actin contacting the C-zone, indicating that MyBP-C brakes actin filament sliding. This situation causes a force discontinuity at the edge of the C-zone where a free actin filament might form an inchworm-like arch due to different sliding speeds at the discontinuity.

Skeletal muscle also has MyBP-C, but the heart muscle isoform exclusively contains the so-called M domain near the amino terminus that has several phosphorylatable serines that have been linked with disease (*2*). Manipulation of M-domain phosphorylation, or longer application of calpain to cleave off the amino terminus of MyBP-C, thereby removing the actin binding site and the M domain, clarified the role of phosphorylation in MyBP-C's braking action. The normal mouse heart has ~60% phosphorylation of available sites. Increasing average phosphorylation from normal did not affect sliding velocities; however, decreasing average phosphorylation, similar to what occurs in a human disease-related mutant, enhanced MyBP-C braking of actin movement. Calpain cleavage greatly diminished MyBP-C's effect on actin movement. These data suggest how a disease-related mutant of MyBP-C that lowers its average phosphorylation could result in chronic contraction braking, eventually presenting as a disease and exposing the elusive link between sarcomere protein mutation and disease. Disease relevance may also depend on use of native actin filaments instead of the bare actin used by Previs *et al*. because the former have a calcium regulatory complex affecting motility (*11*) and potentially how MyBP-C interacts with actin.

Demands on the heart change with time, and the heart machine has regulatory mechanisms to rapidly meet changing demand or to compensate for injury or functional deficits (*12*). The β-adrenergic pathway provides hormonal control of protein phosphorylation through heterotrimeric GTP-binding protein (G protein), adenylate cyclase, and protein kinase A (PKA) (see the figure). The findings of Previs *et al*. show how cardiac MyBP-C contributes to regulating contraction velocity by subjecting it to β-adrenergic hormonal control (*13*). More practically, the findings provide insight needed to identify drug targets for MyBP-C–related heart disease. The β-adrenergic pathway is already a drug target in heart disease for up- or down-modulating contractile function. However, that approach may generate unwanted side-effects because it targets an upstream modulator in a complex signaling pathway. A direct intervention targeting MyBP-C would be preferable and is now feasible because these new findings elucidate how MyBP-C brakes a heart.

References

1. I. Olivotto *et al*., *Mayo Clin. Proc.* **83**, 630 (2008).
2. D. Barefield, S. Sadayappan, *J. Mol. Cell. Cardiol.* **48**, 866 (2010).
3. T. P. Burghardt, K. Ajtai, *Biophys. Rev.* **2**, 159 (2010).
4. M. J. Previs *et al*., *Science* **337**, 1215 (2012).
5. H. E. Huxley, *Science* **164**, 1356 (1969).
6. I. Rayment *et al*., *Science* **261**, 50 (1993).
7. R. Dominguez *et al*., *Cell* **94**, 559 (1998).
8. P. K. Luther *et al*., *Proc. Natl. Acad. Sci. U.S.A.* **108**, 11423 (2011).
9. B. K. McConnell *et al*., *J. Clin. Invest.* **104**, 1235 (1999).
10. A. L. Stout, D. Axelrod, *Appl. Opt.* **28**, 5237 (1989).
11. K. Ajtai *et al*., *Biochemistry* **48**, 5263 (2009).
12. F. Sheikh *et al*., *J. Clin. Invest.* **122**, 1209 (2012).
13. S. Sadayappan *et al*., *Circulation* **119**, 1253 (2009).

10.1126/science.1227943

CHEMISTRY

Measuring the Heaviest Atoms

Advanced techniques for trapping ions provide a route to probe the stability of superheavy elements.

Georg Bollen

The existence of superheavy elements, those with many more protons than uranium (proton number 92), was predicted more than 40 years ago. Their increased stability against nuclear fission originates from nuclear shells that are filled with protons and neutrons, similar to the electron orbitals in an atom. For specific combinations of the number of protons and neutrons, so-called magic numbers, a more strongly bound system is formed that also has a longer half-life. The superheavy elements are predicted to populate an "island of stability" located around proton number 120 and neutron number 184. Several groups have sought to pinpoint (*1*–*4*) the location of this island, and along the way (*5*), several superheavy elements have been discovered, the latest being ununoctium with 118 protons. However, concluding whether this is the heaviest element cannot be done, and we are still far from knowing what the heaviest possible element could be. A critical point is understanding the nuclear shell effects that underlie the existence of the heaviest elements. On page 1207 of this issue, Minaya Ramirez *et al*. (*6*) shed light on such shell effects by "weighing" isotopes of the heaviest elements in an ion trap.

Facility for Rare Isotope Beams, Michigan State University, East Lansing, MI 48824, USA. E-mail: bollen@frib.msu.edu

Progress toward characterizing the island of stability is slow because of the low production rates of the superheavy elements, sometimes only one atom per week. The more difficult the synthesis of heavier elements, the more important is the availability of better information on their properties, either through direct measurements or better theoretical predictions. The accurate knowledge of masses is particularly critical. Einstein's mass-energy equivalence relates the mass of an isotope directly to how strongly its nucleons are bound, which determines the element's existence and lifetime before it decays. Systematic mass measurements as a function of neutron number for a given proton number—that is, for different isotopes of a given element, or as a function of proton number for a given neutron number—allow investigation of changes in nuclear binding and the enhancement due to shell effects. Studying shell effects in the region of the heaviest elements is important for testing theories used to predict their existence, structure, and nuclear half-lives, and for providing input on how to best synthesize them.

A variety of new techniques for measuring the mass of unstable isotopes have been developed during the past two decades (*7*). Among those, Penning traps (see the figure) deliver unprecedented accuracy, an applicability to very short-lived isotopes, and a high sensitivity that make them well suited for the study of isotopes that are extremely difficult to produce and only available at low rates. Examples of Penning trap facilities for unstable isotopes are ISOLTRAP at CERN (*8*), the first ion trap facility of that kind, or LEBIT (*9*) at Michigan State University, the only facility to measure masses

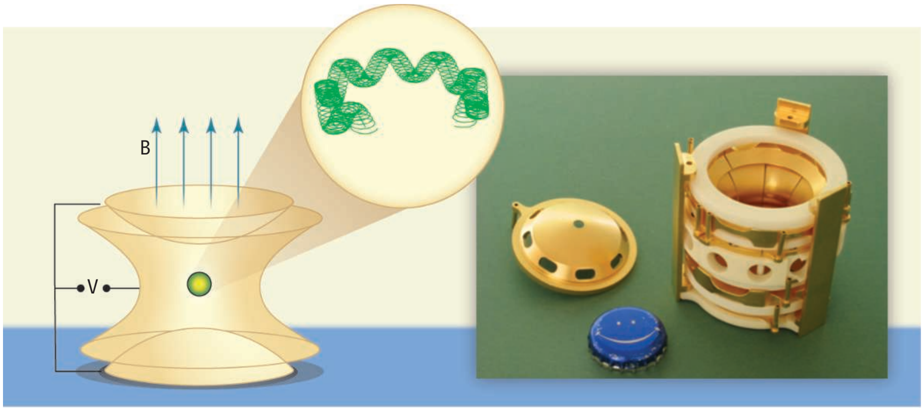

Trap and probe. (**Left**) Concept of a Penning trap and (**right**) example of a Penning trap configuration as used at LEBIT (*9*). With such electrode configurations, an ion can be stored in a strong magnetic field under vacuum for a long time. The frequency of the circular, cyclotron, motion performed by a trapped ion is connected to its charge, mass, and the magnetic-field strength. By determining this frequency, it is possible to obtain the ion's mass. Minaya Ramirez *et al*. have used a similar device in SHIPTRAP (*10*) for their study of nuclear binding of the heaviest elements.

of isotopes produced and delivered at half the speed of light.

SHIPTRAP (*10*) at GSI in Germany is the only ion trap facility specifically designed for the study of the heaviest elements. SHIPTRAP is connected to GSI's velocity filter SHIP, one of the few instruments in the world for the synthesis of superheavy elements. After a first demonstration of mass measurements of the heaviest elements (*11*), the SHIPTRAP team has now studied long series of nobelium and lawrencium isotopes in the vicinity of neutron number 152, where theory predicts a subshell closure (that is, stability).

The experimental results of Minaya Ramirez *et al*. corroborate the existence of this localized region of enhanced binding due to shell effects above the doubly magic lead-208 and confirm 152 to be a magic neutron number. Together with the shell effect strength that is extracted from the differences of the measured masses, this serves as a critical test for theoretical models describing the nuclear properties of the heaviest elements. Determination of this number is decisive for better predicting the location and the strength of the shell closures in heavier and superheavy elements.

Measurements such as those reported by Minaya Ramirez *et al*. are extremely difficult and require extraordinary care and preparation given the very low production rates of these very heavy elements and the need for high accuracy. In addition to providing a very important result, SHIPTRAP has set a new record by demonstrating that direct mass measurements of radioactive isotopes can be performed with detection rates as low as one ion every few hours while reaching an accuracy better than one part per million. The precise measurement of the mass of lawrencium-256 required the detection of about 50 ions and took 93 hours.

Extending such measurements to isotopes of even heavier elements is highly desirable and important but extraordinarily challenging; continued technical and methodological improvements will be needed. A new detection scheme is planned at SHIPTRAP where the mass of a single ion is measured by listening to the electric current it induces in electrodes due to its motion in the trap (*12*). Such single-ion sensitivity would be an important step in paving the way to the superheavy elements, in particular rutherfordium (proton number 104) and dubnium (proton number 105). If SHIPTRAP succeeds in measuring isotope masses of these elements, then it would help to unambiguously identify the new elements with proton numbers 113, 115, and 117 (*3*) by providing reliable mass anchor points for the alpha decay chains originating from these elements.

References

1. S. Hofmann, G. Münzenberg, *Rev. Mod. Phys.* **72**, 733 (2000).
2. K. Morita *et al.*, *J. Phys. Soc. Jpn.* **73**, 2593 (2004).
3. Y. Oganessian, *J. Phys. G* **34**, R165 (2007).
4. L. Stavsetra *et al.*, *Phys. Rev. Lett.* **103**, 132502 (2009).
5. D. Clery, *Science* **333**, 1377 (2011).
6. E. Minaya Ramirez *et al.*, *Science* **337**, 1207 (2012); 10.1126/science.1225636.
7. K. Blaum, *Phys. Rep.* **425**, 1 (2006).
8. M. Mukherjee *et al.*, *Eur. Phys. J. A* **35**, 1 (2008).
9. G. Bollen *et al.*, *Phys. Rev. Lett.* **96**, 152501 (2006).
10. M. Block *et al.*, *Eur. Phys. J. D* **45**, 39 (2007).
11. M. Block *et al.*, *Nature* **463**, 785 (2010).
12. R. Ferrer *et al.*, *Eur. Phys. J. Spec. Top.* **150**, 347 (2007).

10.1126/science.1228467

MICROBIOLOGY

Microbial Cooperative Warfare

Hélène Morlon

Analysis of microbial interactions in the wild shows that microbes cooperate to resist competition.

Cooperation among individuals of the same population directed against competing populations (cooperative warfare) is widespread in animals and plants. What happens in the microbial world is much less understood. Microbes can interact with one another through chemical signals, but little is known about the nature of their interactions, particularly outside the laboratory. On page 1228 of this issue, Cordero *et al.* (*1*) present a detailed analysis of ecological interaction networks, population structures, and genetic relatedness of microbes in the wild. They suggest that cooperative warfare is common in the microbial world.

To defend against invasion or invade established communities, microbes use a myriad of antibiotics. The interactions between producing (P), resistant (R), and sensitive (S) strains are often similar to the children's game "rock-scissors-paper," whereby P dominates S, S outcompetes R, and R outcompetes P (see the figure, panel A) (*2*). These strains cannot coexist in well-mixed populations (panel B). In spatially structured populations, they continuously displace one another, resulting in a dynamic mosaic of nearly clonal populations (panel C). Both theory and experiments suggest that such interactions promote coexistence and biodiversity (*2–4*). However, the extent to which they promote biodiversity in nature remains unclear.

To explore chemical warfare in the wild, Cordero *et al*. analyzed interactions within and between populations of bacteria of the family Vibrionaceae in the coastal ocean. The authors had previously identified ecological populations of *Vibrio* on the basis of

Center for Applied Mathematics, UMR 7641 CNRS, Ecole Polytechnique, Route de Saclay Palaiseau, 91128 France. E-mail: helene.morlon@cmap.polytechnique.fr

a protein-coding gene phylogeny and habitat associations (*5*). In the present study, they systematically analyzed pairwise interactions among 185 *Vibrio* isolates by means of local growth inhibition tests.

They identify a certain degree of genetic difference above which the potential for antagonistic interactions increases sharply. This threshold coincides almost exactly with the average genetic distance separating ecological populations. Hence, antagonism occurs mostly between rather than within natural *Vibrio* populations. Moreover, whole-genome analyses reveal that genomes of the same population share on average only 72% of their genes. Thus, populations are not nearly clonal, contrary to what would be expected under cyclic replacement [(*2*), panel C]. Rather, coexistence is maintained by a cooperative population structure (panel D).

The idea that microorganisms can participate in social behaviors similar to those of macroorganisms is not new (*6*, *7*). Microorganisms cooperate to better exploit resources (*8*), to form microbial mats or fruiting bodies (*6*), and to resist stressful environments (*9*). Cordero *et al*. show that cooperation is also a major force in antibiotic-mediated interference competition between populations. Research on interference competition in microbes has focused on the role of proteins (*10*), but the authors show that most interactions (96%) are in fact mediated by small antibiotic molecules. A single specific antibiotic biosynthesis cluster, apparently subject to frequent horizontal transfer, seems responsible for the antagonistic activity.

Cordero *et al*.'s study suggests that in socially cohesive bacterial populations, superkiller strains release antibiotics that act as "public goods." But how can such social systems evolve? Antibiotic production comes at a fitness cost to the superkillers, and in a Darwinian world of survival of the fittest, why should an individual help others at its own expense? Hamilton's theory of kin selection stipulates that cooperation can be maintained in a population if the cooperative behavior is directed toward relatives carrying the cooperative genes (*11*). Antagonism decreases with genetic relatedness in *Vibrio* populations, which could suggest a form of kin selection. However, the authors found that the nonproducing cells toward which cooperation is directed do not carry genes from the antibiotic biosynthesis cluster.

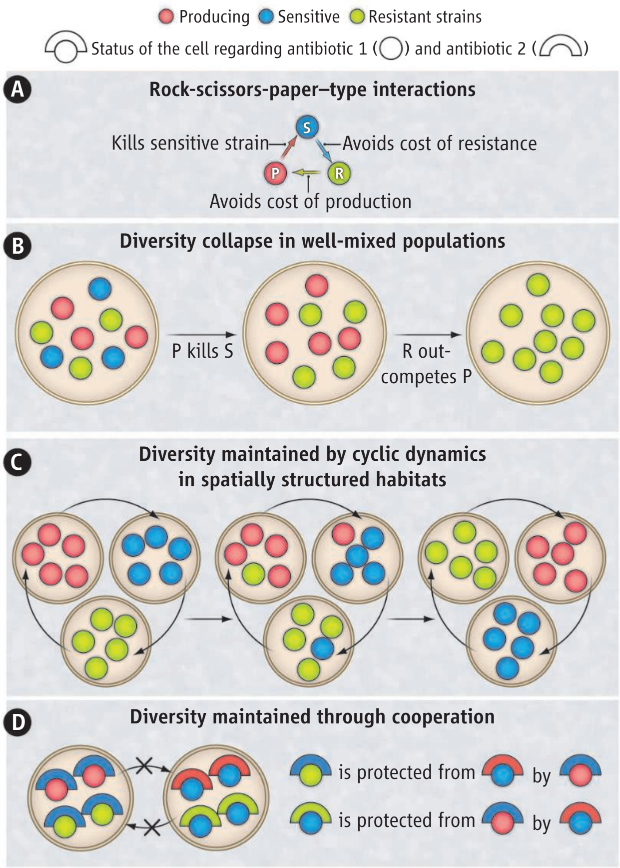

Diverse views of coexistence. **(A)** Antibiotic production often results in rock-scissors-paper–type interactions between bacterial strains. **(B)** In the absence of spatial structure, producing strains kill sensitive strains and resistant strains outcompete producing strains, resulting in diversity collapse. **(C)** In structured habitats, clonal populations are constantly invaded and replaced in a dynamic game, thus maintaining diversity. **(D)** Cordero *et al.*'s results suggest that in nature, cooperation within nonclonal populations prevents invasion and maintains diversity.

This observation raises the intriguing possibility that cooperation can be maintained in microbial populations if it is directed not only toward cells carrying the cooperative genes, but also toward cells that have a greater potential to acquire these genes. Indeed, the cells benefiting from cooperation are already resistant and can thus readily acquire antibiotic-producing genes by horizontal transfer. Nonresistant cells are much less likely to acquire these genes, because producing genes are not genetically linked to their resistance factors. Further empirical and theoretical work aimed at testing this hypothesis will advance our understanding of microbial social structure.

Cordero *et al*. have assembled one of the largest microbial interaction networks to date. A similar network was recently compiled for *Streptomyces* (*4*). Studies of this kind open promising avenues for analyzing ecological networks and will likely bring new insights into the evolutionary ecology of communities. However, the high-throughput growth methods used in these studies have shortcomings. Experiments carried out in a fixed culture medium might not capture what happens in nature, because interactions can vary drastically with environmental conditions (*12*). Likewise, cultivation-dependent techniques presumably miss many strains. It would be insightful to compare these networks to in silico networks constructed from genome-scale models (*12*), or to networks estimated from spatial and temporal associations among microbial taxa identified by molecular techniques (*13*).

Still, a property that seems to emerge across microbial networks is that interactions evolve quickly. This contrasts with the evolutionary conservatism of interactions generally observed in macroorganisms (*14*). Rapid evolutionary changes of ecological interactions imply that we face a daunting task of predicting the future effect of environmental changes or clinical treatments on microbial communities. Further exploration of the evolution of microbial interaction networks may prove crucial to meet major challenges ahead, including evaluating how the ecological services provided by microorganisms will respond to global change and designing effective treatments against resistant bacterial infections.

References and Notes

1. O. X. Cordero *et al.*, *Science* **337**, 1228 (2012).
2. B. Kerr *et al.*, *Nature* **418**, 171 (2002).
3. T. L. Czárán *et al.*, *Proc. Natl. Acad. Sci. U.S.A.* **99**, 786 (2002).
4. K. Vetsigian *et al.*, *PLoS Biol.* **9**, e1001184 (2011).
5. D. E. Hunt *et al.*, *Science* **320**, 1081 (2008).
6. B. J. Crespi, *Trends Ecol. Evol.* **16**, 178 (2001).
7. S. A. West *et al.*, *Nat. Rev. Microbiol.* **4**, 597 (2006).
8. A. S. Griffin *et al.*, *Nature* **430**, 1024 (2004).
9. H. H. Lee *et al.*, *Nature* **467**, 82 (2010).
10. M. A. Riley, J. E. Wertz, *Annu. Rev. Microbiol.* **56**, 117 (2002).
11. W. D. Hamilton, *J. Theor. Biol.* **7**, 1 (1964).
12. S. Freilich *et al.*, *Nat. Commun.* **2**, 589 (2011).
13. J. A. Steele *et al.*, *ISME J.* **5**, 1414 (2011).
14. J. M. Gómez *et al.*, *Nature* **465**, 918 (2010).

Acknowledgments: I thank B. J. M. Bohannan, J. L. Green, S. Kefi, and J. B. Plotkin for comments on a previous draft. Funding was provided by the CNRS and ANR grant ECOEVOBIO-CHEX2011.

10.1126/science.1227512

Systematic Localization of Common Disease-Associated Variation in Regulatory DNA

Matthew T. Maurano,[1*] Richard Humbert,[1*] Eric Rynes,[1*] Robert E. Thurman,[1] Eric Haugen,[1] Hao Wang,[1] Alex P. Reynolds,[1] Richard Sandstrom,[1] Hongzhu Qu,[1,2] Jennifer Brody,[3] Anthony Shafer,[1] Fidencio Neri,[1] Kristen Lee,[1] Tanya Kutyavin,[1] Sandra Stehling-Sun,[1] Audra K. Johnson,[1] Theresa K. Canfield,[1] Erika Giste,[1] Morgan Diegel,[1] Daniel Bates,[1] R. Scott Hansen,[4] Shane Neph,[1] Peter J. Sabo,[1] Shelly Heimfeld,[5] Antony Raubitschek,[6] Steven Ziegler,[6] Chris Cotsapas,[7,8] Nona Sotoodehnia,[3,9] Ian Glass,[10] Shamil R. Sunyaev,[11] Rajinder Kaul,[4] John A. Stamatoyannopoulos[1,12]†

Genome-wide association studies have identified many noncoding variants associated with common diseases and traits. We show that these variants are concentrated in regulatory DNA marked by deoxyribonuclease I (DNase I) hypersensitive sites (DHSs). Eighty-eight percent of such DHSs are active during fetal development and are enriched in variants associated with gestational exposure–related phenotypes. We identified distant gene targets for hundreds of variant-containing DHSs that may explain phenotype associations. Disease-associated variants systematically perturb transcription factor recognition sequences, frequently alter allelic chromatin states, and form regulatory networks. We also demonstrated tissue-selective enrichment of more weakly disease-associated variants within DHSs and the de novo identification of pathogenic cell types for Crohn's disease, multiple sclerosis, and an electrocardiogram trait, without prior knowledge of physiological mechanisms. Our results suggest pervasive involvement of regulatory DNA variation in common human disease and provide pathogenic insights into diverse disorders.

Disease- and trait-associated genetic variants are rapidly being identified with genome-wide association studies (GWAS) and related strategies (*1*). To date, hundreds of GWAS have been conducted, spanning diverse diseases and quantitative phenotypes (*2*) (fig. S1A). However, the majority (~93%) of disease- and trait-associated variants emerging from these studies lie within noncoding sequence (fig. S1B), complicating their functional evaluation. Several lines of evidence suggest the involvement of a proportion of such variants in transcriptional regulatory mechanisms, including modulation of promoter and enhancer elements (*3*–*6*) and enrichment within expression quantitative trait loci (eQTL) (*3*, *7*, *8*).

Human regulatory DNA encompasses a variety of cis-regulatory elements within which the cooperative binding of transcription factors creates focal alterations in chromatin structure. Deoxyribonuclease I (DNase I) hypersensitive sites (DHSs) are sensitive and precise markers of this actuated regulatory DNA, and DNase I mapping has been instrumental in the discovery and census of human cis-regulatory elements (*9*). We performed DNase I mapping genome-wide (*10*) in 349 cell and tissue samples, including 85 cell types studied under the ENCODE Project (*10*) and 264 samples studied under the Roadmap Epigenomics Program (*11*). These encompass several classes of cell types, including cultured primary cells with limited proliferative potential (n = 55); cultured immortalized (n = 6), malignancy-derived (n = 18), or pluripotent (n = 2) cell lines; and primary hematopoietic cells (n = 4) as well as purified differentiated hematopoietic cells (n = 11), and a variety of multipotent progenitor and pluripotent cells (n = 19). We also surveyed regulatory DNA by generating DHS maps from 233 diverse fetal tissue samples across days ~60 to 160 after conception (late-first to late-second trimester of gestation). We used a uniform processing algorithm to identify DHSs and the surrounding boundaries of DNase I accessibility (i.e., the nucleosome-free region harboring regulatory factors) (*12*). We defined an average of 198,180 DHSs per cell type (range 89,526 to 369,920; table S1) spanning on average ~2.1% of the genome. In total, we identified 3,899,693 distinct DHS positions along the genome (collectively spanning 42.2%), each of which was detected in one or more cell or tissue types (median = 5).

Disease- and trait-associated variants are concentrated in regulatory DNA. We examined the distribution of 5654 noncoding genome-wide significant associations [5134 unique single-nucleotide polymorphisms (SNPs); fig. S1 and table S2] for 207 diseases and 447 quantitative traits (*2*) with the deep genome-scale maps of regulatory DNA marked by DHSs. This revealed a collective 40% enrichment of GWAS SNPs in DHSs (fig. S1C, $P < 10^{-55}$, binomial, compared to the distribution of HapMap SNPs). Fully 76.6% of all noncoding GWAS SNPs either lie within a DHS (57.1%, 2931 SNPs) or are in complete linkage disequilibrium (LD) with SNPs in a nearby DHS (19.5%, 999 SNPs) (Fig. 1A) (*12*). To confirm this enrichment, we sampled variants from the 1000 Genomes Project (*13*) with the same genomic feature localization (intronic versus intergenic), distance from the nearest transcriptional start site, and allele frequency in individuals of European ancestry. We confirmed significant enrichment both for SNPs within DHSs ($P < 10^{-59}$, simulation) and also including variants in complete LD ($r^2 = 1$) with SNPs in DHSs ($P < 10^{-37}$, simulation) (fig. S2).

In total, 47.5% of GWAS SNPs fall within gene bodies (fig. S1B); however, only 10.9% of intronic GWAS SNPs within DHSs are in strong LD ($r^2 \geq 0.8$) with a coding SNP, indicating that the vast majority of noncoding genic variants are not simply tagging coding sequence. Analogously, only 16.3% of GWAS variants within coding sequences are in strong LD with variants in DHSs. SNPs on widely used genotyping arrays (e.g., Affymetrix) were modestly enriched within DHSs (fig. S2), possibly due to selection of SNPs with robust experimental performance in genotyping assays. However, we found no evidence for sequence composition bias (table S3).

To further examine the enrichment of GWAS SNPs in regulatory DNA, we systematically classified all noncoding GWAS SNPs by the quality of their experimental replication. This disclosed 2436 unreplicated SNPs; 2374 "internally replicated" SNPs (confirmed in a second population in the initial publication); and 324 "externally replicated" SNPs (confirmed in an independent study) (table S2) (*12*). We observed a monotonic increase in the proportion of disease or trait variants localizing in DHSs with increasing quality of GWAS SNP experimental replication (Fig. 1B), as well as with increasing strength of association and study sample size (fig. S3). For externally replicated noncoding SNPs, 69.8% lie within a DHS (n = 226, $P < 10^{-14}$, simulation, fig. S2). To exclude the influence of population stratification, we compared the fixation index in African and European populations between GWAS SNPs in DHSs and matched SNPs not in DHSs and found them to be nearly identical (F_{ST} = 0.0843 versus 0.0847,

[1]Department of Genome Sciences, University of Washington, Seattle, WA 98195, USA. [2]Laboratory of Disease Genomics and Individualized Medicine, Beijing Institute of Genomics, Chinese Academy of Sciences, Beijing, 100029, China. [3]Cardiovascular Health Research Unit, Department of Medicine, University of Washington, Seattle, WA 98195, USA. [4]Department of Medicine, Division of Medical Genetics, University of Washington, Seattle, WA 98195, USA. [5]Clinical Research Division, Fred Hutchinson Cancer Research Center, Seattle, WA 98109, USA. [6]Immunology Program, Benaroya Research Institute, Seattle, WA 98101, USA. [7]Department of Neurology, Yale University School of Medicine, New Haven, CT 06520, USA. [8]Department of Genetics, Yale University School of Medicine, New Haven, CT 06520, USA. [9]Division of Cardiology, Department of Medicine, University of Washington, Seattle, WA 98195, USA. [10]Division of Genetic Medicine, Department of Pediatrics, University of Washington, Seattle, WA 98195, USA. [11]Division of Genetics, Brigham and Women's Hospital and Harvard Medical School, Boston, MA 02115, USA. [12]Department of Medicine, Division of Oncology, University of Washington, Seattle, WA 98195, USA.

*These authors contributed equally to this work.

†To whom correspondence should be addressed. E-mail: jstam@uw.edu

respectively) (*12*). The monotonic relationship between evidence for association and SNP concentration in DHSs strongly suggests that many variants are functional and that unreplicated or weaker associations may obscure the true degree of enrichment in DHSs.

GWAS variants localize in cell- and developmental stage–selective regulatory DNA. We observed selective localization within physiologically or pathogenically relevant specific cell or tissue types, including affected tissues or known or posited effector cell types (Fig. 1C). For a given disorder, cell-selective localization within physiologically or pathogenically relevant cell types was repeatedly observed for multiple independently associated SNPs distributed widely around the genome (fig. S4). These results suggest a tissue-specific regulatory role for many common variants, as well as the potential for comprehensive regulatory DNA maps to illuminate associations within disease-relevant cell types.

Many common disorders have been linked with early gestational exposures or environmental insults (*14*). Because of the known role of the chromatin accessibility landscape in mediating responses to cellular exposures such as hormones (*15*), we examined if DHSs harboring GWAS variants were active during fetal developmental stages. Of 2931 noncoding disease- and trait-associated SNPs within DHSs globally, 88.1% (2583) lie within DHSs active in fetal cells and tissues. Of DHSs containing disease-associated variation, 57.8% are first detected in fetal cells and tissues and persist in adult cells ("fetal origin" DHSs), whereas 30.3% are fetal stage–specific DHSs (Fig. 1D). GWAS variants in adult stage–specific DHSs localize chiefly in mature hematopoietic cells, connective tissue, endothelial cells, and malignant cells (fig. S6).

We next analyzed the enrichment or depletion of replicated disease-specific GWAS variants in fetal-stage DHSs relative to the proportion of total GWAS SNPs in these DHSs. We found the greatest enrichment in phenotypes for which gestational exposures or growth trajectory have been shown to play major roles, including menarche, cardiovascular disease, and body mass index (Fig. 1E) (*14*, *16*). By contrast, we observed relative depletion in fetal DHSs of aging-related diseases, cancer, and inflammatory disorders with presumed (postnatal) environmental triggers. These findings suggest a recurring connection between an exposure-responsive gestational chromatin landscape, regulatory genotype, and risk for specific classes of adult diseases and traits.

DHSs harboring GWAS variants control distant phenotype-relevant genes. Enhancers may lie at great distances from the gene(s) they control (*17*) and function through long-range regulatory interactions (*4*, *18*), complicating the identification of target genes of regulatory GWAS variants. Most DHSs display quantitative, cell-selective DNase I hypersensitivity patterns, which may be systematically correlated with DNase I sensitivity patterns at cis-linked promoters. DHSs that are strongly correlated ($r > 0.7$) with specific promoters function as enhancers that physically interact with their target promoter as detected by chromosome conformation capture methods, including chromosome conformation capture carbon copy (5C) and chromatin interaction analysis by paired-end tag sequencing (ChIA-PET) (*10*).

To systematically identify the genic targets of DHSs harboring GWAS variants and thereby gain insights into disease mechanisms, we applied the approach described in (*10*) to the much broader

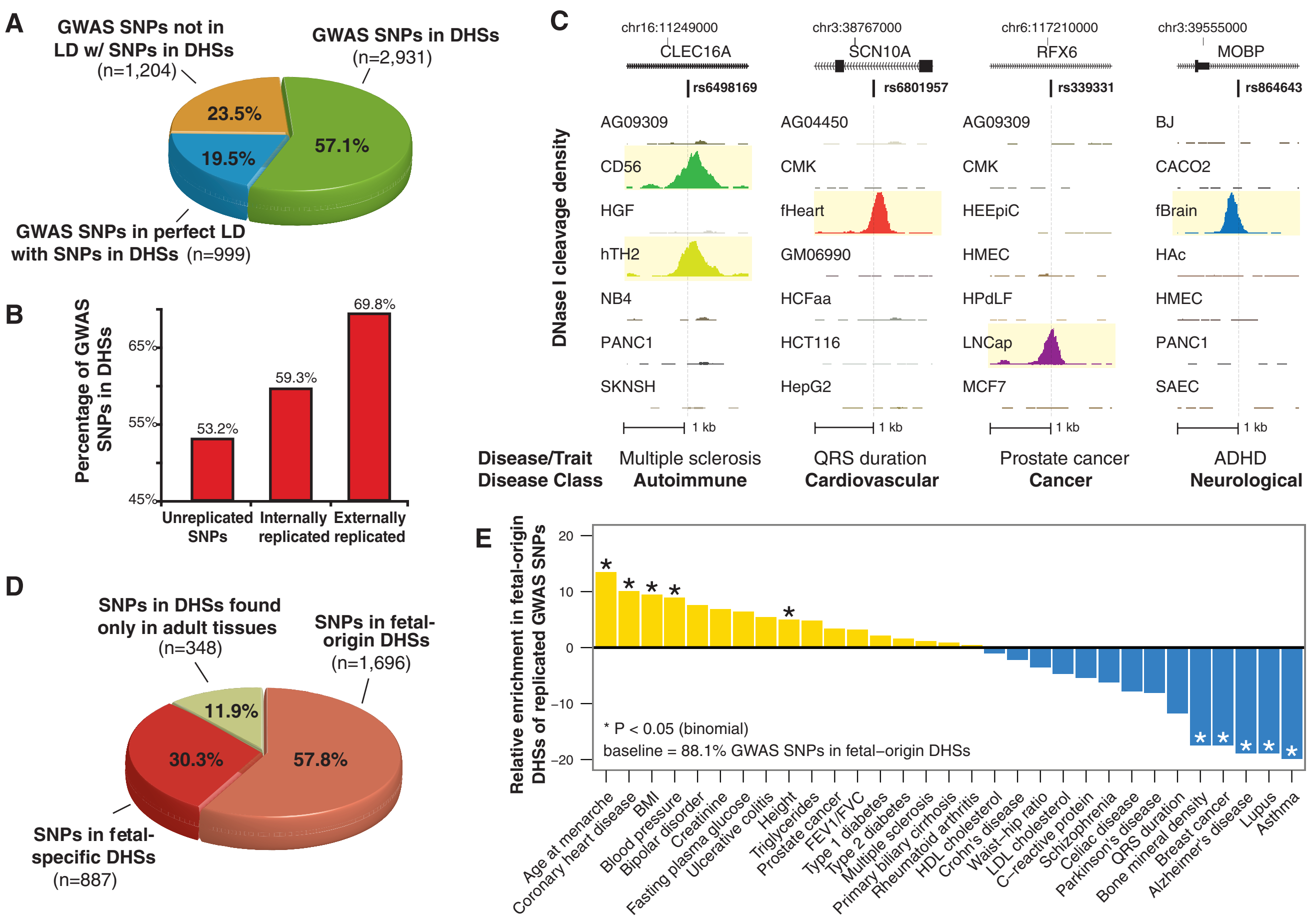

Fig. 1. Disease-associated variation is concentrated in DNase I hypersensitive sites. (**A**) Proportions of noncoding GWAS SNPs localizing within DHSs (green); in complete linkage disequilibrium (LD) ($r^2 = 1$) with a SNP in a DHS (blue); or neither (yellow). Note that 76.5% of GWAS SNPs are either within or in perfect LD with DHSs. (**B**) Proportions of GWAS SNPs overlapping DHSs after partitioning by degree of replication. (**C**) Representative DNase I hypersensitivity (tag density) patterns at diverse disease-associated variants. (**D**) Proportion of GWAS SNPs localizing in DHSs active in fetal tissues that persist in adult cells (salmon); fetal stage-specific DHSs (red); and adult stage DHSs (green). (**E**) GWAS SNPs in DHSs show phenotype-specific enrichment for fetal regulatory elements.

range of cell and tissue types in the present study (*12*) and intersected the result sets with GWAS data. This analysis revealed 419 DHSs harboring GWAS variants that were strongly correlated ($r >$ 0.7) with the promoter of a specific target gene within ±500 kb of the DHS (tables S6 and S7). These include numerous examples of target genes that plausibly explain the disease or trait association (Table 1 and fig. S7). For example, a SNP (rs385893) associated with platelet count (*19*) lies in a DHS tightly correlated (r = 0.97) and physically interacts with the 222-kb distant promoter of JAK2, a cytokine-activated signal transducer linked with platelet production and myeloproliferative disorders (Fig. 2A). Fully 40.8% of correlated DHS-gene pairs span >250 kb (Fig. 2B), and 79% represent pairings with distant promoters versus those of the nearest gene (tables S6 and S7). Notably, these interactions typically extend beyond the range of LD (mean r^2 = 0.06; table S6).

GWAS variants in DHSs frequently alter allelic chromatin state. Next, we examined how GWAS variants in DHSs were distributed with respect to transcription factor recognition sequences, defined with a scan for known motif models at a stringency of $P < 10^{-4}$ (*12*). Of GWAS SNPs in DHSs, 93.2% (2874) overlap a transcription factor recognition sequence. We partitioned GWAS variants into 10 disease or trait classes, and then determined the frequency of GWAS variants associated with a particular disease or trait class that localized within sites for transcription factors independently partitioned into the same classes on the basis of gene ontology annotations (fig. S8) (*12*). This analysis revealed that common variants associated with specific diseases or trait classes were systematically enriched in the recognition sequences of transcription factors governing physiological processes relevant to the same classes.

Table 1. Highest correlated genes of distal DHSs harboring GWAS variants. Examples of distal DHSs-to-promoter connections that highlight candidate genes potentially underlying the association. An asterisk (*) indicates the highest-correlated gene is not the nearest gene. *r*, Pearson's correlation coefficient; ADHD, attention deficit hyperactivity disorder; NMDA, *N*-methyl-D-aspartate.

Disease or trait	*r*	Target gene	Function	Distance (kb)
Amyotrophic lateral sclerosis	1	SYNGAP1*	Axon formation; component of NMDA complex	411
Crohn's disease	1	TRIB1*	NF-κB regulation	95
Time to first primary tooth	0.99	PRDM1*	Craniofacial development	452
C-reactive protein	0.99	NLRP3	Response to bacterial pathogens	20
Multiple sclerosis	0.98	AHI1*	White matter abnormalities	149
QRS duration	0.96	SCN10A*	Sodium channel involved in cardiac conduction	181
Breast cancer	0.96	TACC2*	Tumor suppressor	411
Schizophrenia/brain imaging	0.95	KIF1A*	Neuron-specific kinesin involved in axonal transport	428
Brain structure	0.94	CXCR6*	Chemokine receptor involved in glial migration	357
Rheumatoid arthritis	0.94	CTSB*	Cysteine proteinase linked to articular erosion	359
Ovarian cancer	0.93	HSPG2*	Ovarian tumor suppressor	268
Multiple sclerosis	0.93	ZP1*	Known autoantigen	153
ADHD	0.93	PDLIM5*	Neuronal calcium signaling	328
Breast cancer	0.88	MAP3K1*	Response to growth factors	158
Amyotrophic lateral sclerosis	0.88	CNTN4	Neuronal cell adhesion	306
Schizophrenia	0.81	FXR1*	Cognitive function	120
Type 1 diabetes	0.75	ACAD10*	Mitochondrial oxidation of fatty acids	343
Lupus	0.74	STAT4	Mediates IL-12 immune response and T_H1 differentiation	113

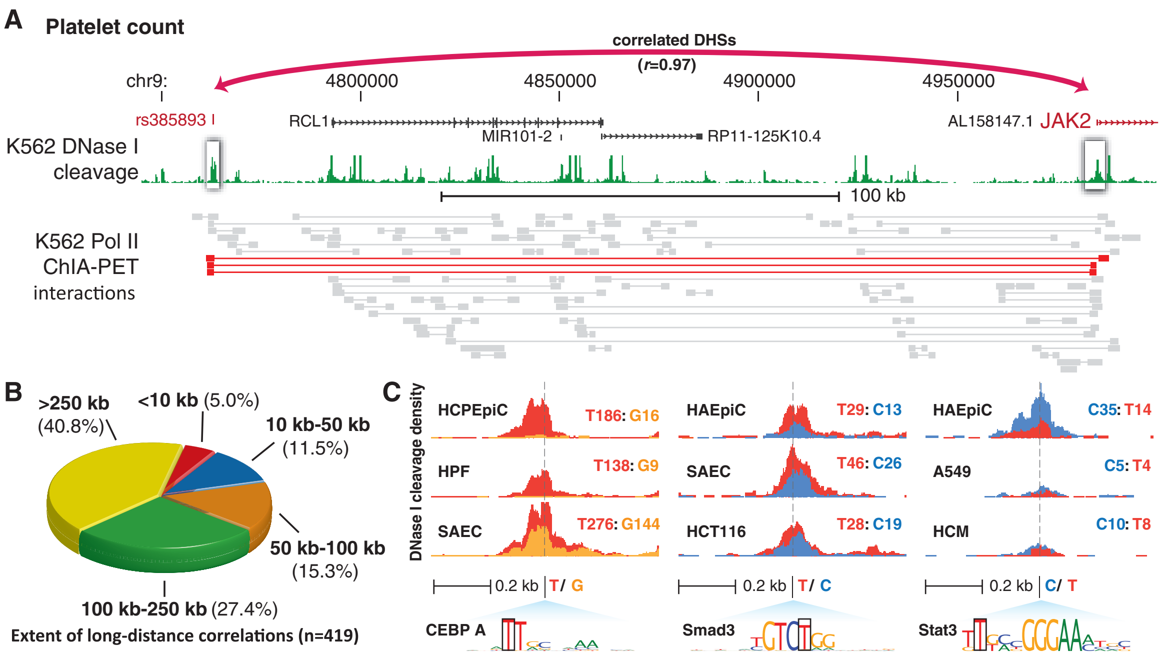

Fig. 2. Candidate regulatory roles for GWAS SNPs. (**A**) GWAS variant associated with platelet count is connected with the JAK2 gene (myeloproliferative disorders) 222 kb away. Below, ChIA-PET tags (*36*) validate direct chromatin interactions; red tags demonstrate an interaction between this DHS and the JAK2 promoter (red). (**B**) Proportion of DHSs harboring GWAS variants that can be linked to target promoters at the indicated distance. (**C**) Examples of allele-specific DNase I sensitivity in cell types derived from heterozygous individuals for GWAS variants that alter transcription factor recognition motifs within DHSs (also see table S9). Each cell type track shows DNase I cleavage density scaled by allelic imbalance at the GWAS variant and colored by variant nucleotide: blue (C), green (A), yellow (G), red (T). Total reads from each allele are also shown.

Functional variants that alter transcription factor recognition sequences frequently affect local chromatin structure. At heterozygous SNPs altering transcription factor recognition sequences, altered nuclease accessibility of the chromatin template manifests as an imbalance in the fraction of reads obtained from each allele (*20*, *21*). As the concentration of sequence reads and highly overlapping read coverage results in an effective resequencing of DHSs, we could both detect cell types heterozygous for common SNPs and quantify the relative proportions of reads from each allele across all cell types (*12*). This imbalance is indicative of the functional effect of a particular allele on local chromatin state. We detected 584 heterozygous GWAS SNPs with sufficient sequencing coverage, of which 120 showed significant allelic imbalance in chromatin state [at a false discovery rate (FDR) of 5%]. We identified sites where regulatory variants were associated with allelic chromatin states, with the predicted higher-affinity allele exhibiting higher accessibility (Fig. 2C). In nearly 50% of cases, the magnitude of imbalance was >2:1 (fig. S9). The GWAS SNPs were the sole local sequence difference between haplotypes, indicating that disease-associated variants are responsible for modulating local chromatin accessibility. Further, at sites with very high sequencing depth (>200×), 38.7% (53/137) show significant allelic imbalance (FDR < 5%). As sensitivity to detect allelic imbalance is governed by sequencing depth, this suggests that nearly 40% of GWAS variants in similarly sequenced DHSs would be expected to show allelic imbalance.

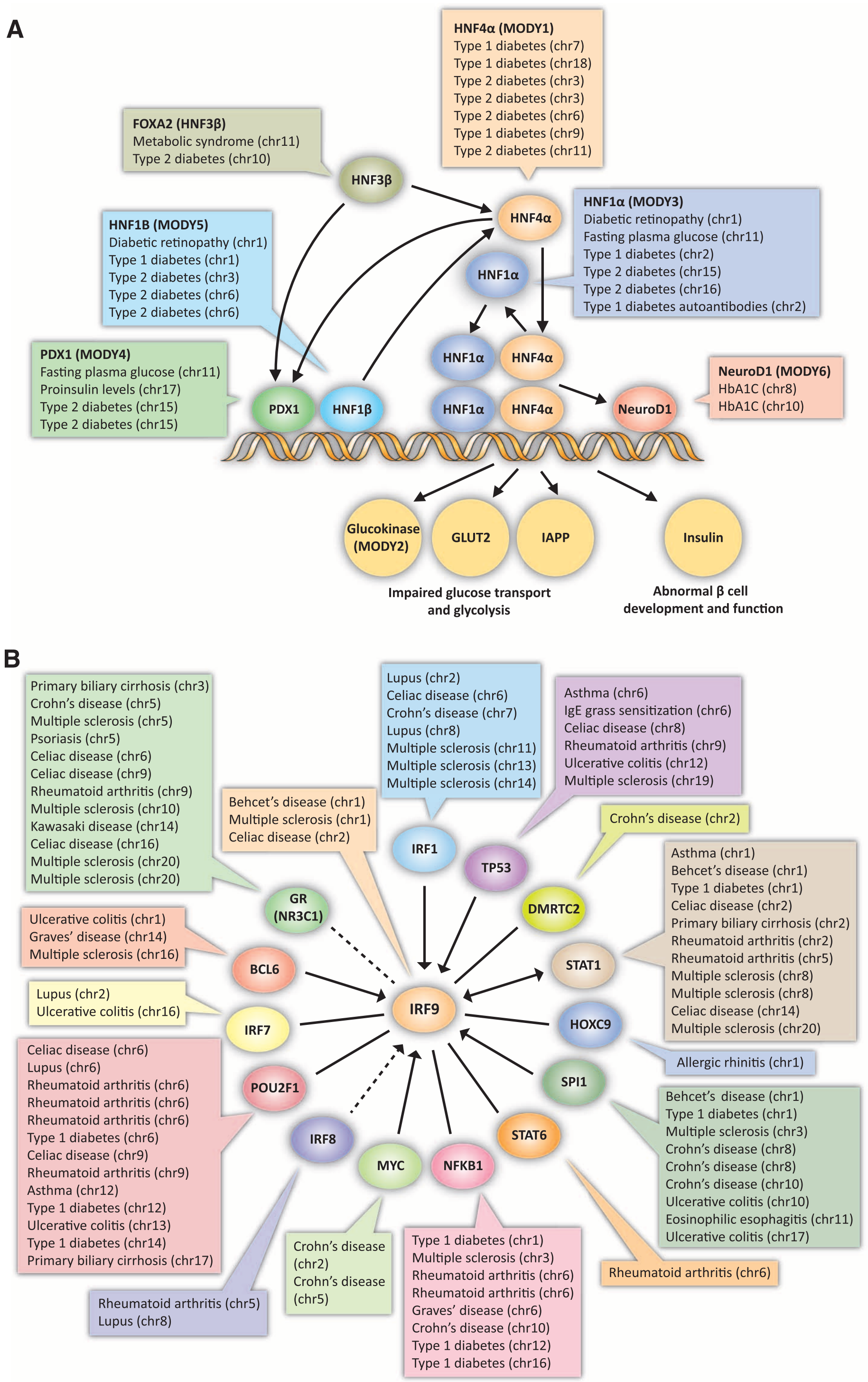

Fig. 3. Common disease-associated variants cluster in regulatory pathways. (**A**) SNPs in DHSs associated with diabetes (type I and type II), diabetic complications, and glucose homeostasis localize in recognition sites of transcriptional regulators (labeled ellipses) controlling glucose transport, glycolysis, and beta cell function that are structurally disrupted in the Mendelian phenotypes of maturity-onset diabetes of the young (MODY). Chromosome of each SNP associated with the indicated phenotype is listed (see table S2). (**B**) Of SNPs associated with autoimmune disorders that fall within DHSs, 24.4% localize in recognition sequences of TFs that interact with IRF9. Arrows indicate directionality of relationship, dotted lines represent indirect interactions (*12*). The complete network is shown in fig. S10.

Disease-associated variants cluster in transcriptional regulatory pathways. Transcriptional control of glucose homeostasis and beta cell genesis and function is mediated by a closely knit transcriptional regulatory pathway defined by specific transcription factors. The Mendelian phenotypes of maturity-onset diabetes of the young (MODY) are caused by separate lesions disrupting the coding sequences of each of these transcription factors (*22*). We observed clustering of common noncoding variants associated with abnormal glucose homeostasis, insulin and glycohemoglobin levels, and diabetic complications within recognition sites for the same six transcription factors ($P < 0.029$, binomial; 48% enrichment over random SNPs; Fig. 3A). This suggests that noncoding variants that predispose to dysregulation of glucose homeostasis perturb peripheral nodes of the same regulatory network responsible for Mendelian forms of type 2 diabetes.

Using known interacting sets of transcription factors, we identified related disease-associated variants in the recognition sequences of a central target factor and its interacting partners (Fig. 3B and figs. S11 and S12) for factors involved in autoimmune disease, cancer, and neurological development. IRF9 is a transcription factor associated with type I interferon induction (*23*) and is a critical component of the JAK/STAT signaling pathway. Of 26 transcription factors in the IRF9-centered interaction network, 15 represent transcription factors with recognition sequences in multiple distinct DHSs that contain GWAS variants associated with a wide variety of autoimmune disorders ($P < 1.6 \times 10^{-13}$, binomial; 2.8-fold enrichment versus random SNPs, Fig. 3B) (*12*).

Notably, 24.4% (64/262) of GWAS SNPs within DHSs of immune cells and associated with autoimmune disease alter one or more of the 15 transcription factor motifs from the IRF9-centered network, suggesting that JAK/STAT-mediated type I interferon responses may have important roles in mediating diverse common inflammatory disorders. This example and those in figs. S11 and S12 illustrate that disease-associated variants from the same or related disorders and traits repeatedly localize within the recognition sequences of transcription factors that form interacting regulatory networks.

Common networks for common diseases. The observation that GWAS variants associated with multiple distinct diseases within the same broader disease class (e.g., inflammation, cancer) repeatedly localize within the recognition sites of interacting transcription factors suggested that cohorts of such transcription factors might form shared regulatory architectures. To explore whether noncoding GWAS SNPs from related diseases perturb different recognition sequences of a common set of transcription factors, we tabulated all transcription factors for which at least eight recognition sequences in DHSs were perturbed by GWAS SNPs associated with autoimmune diseases (Fig. 4A). Among the 22 factors identified were canonical immune signaling regulators, such as signal transducer and activators of transcription 1 (STAT1) and STAT3, nuclear

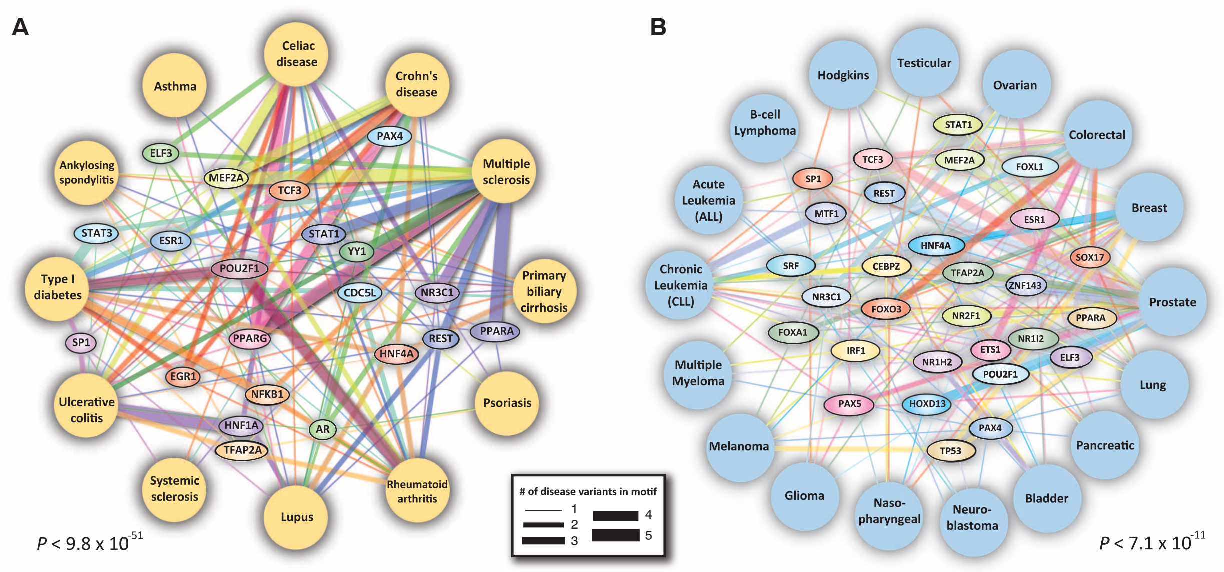

Fig. 4. Common disease networks. GWAS SNPs from related diseases repeatedly perturb recognition sequences of common transcription factors. Shown are factors whose recognition sequences harbor ≥8 or ≥6 GWAS SNPs in inflammatory or autoimmune diseases (**A**) and cancer (**B**), respectively. Edge thickness represents number of associations between transcription factor and disease in DHSs in relevant tissues. Both networks are significantly enriched for overlap with disease-relevant GWAS SNPs and include many well-studied regulators.

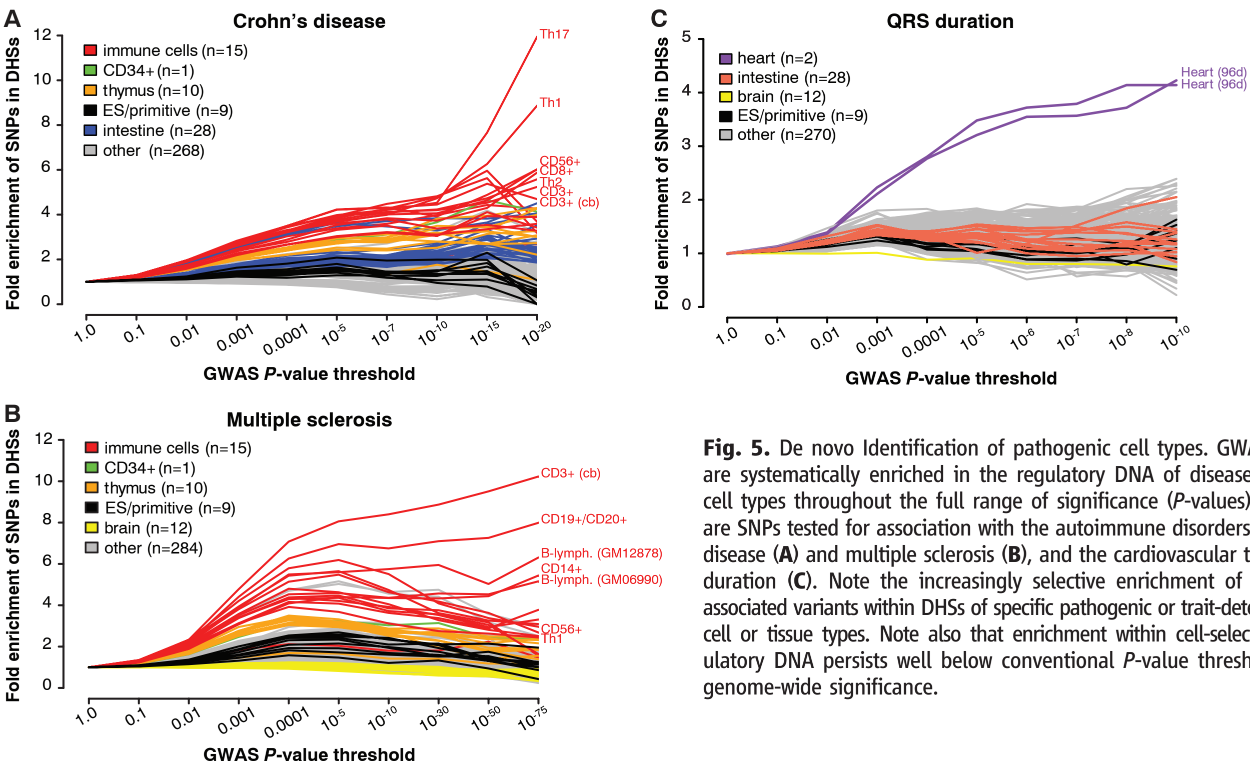

Fig. 5. De novo Identification of pathogenic cell types. GWAS SNPs are systematically enriched in the regulatory DNA of disease-specific cell types throughout the full range of significance (*P*-values). Shown are SNPs tested for association with the autoimmune disorders Crohn's disease (**A**) and multiple sclerosis (**B**), and the cardiovascular trait QRS duration (**C**). Note the increasingly selective enrichment of disease-associated variants within DHSs of specific pathogenic or trait-determining cell or tissue types. Note also that enrichment within cell-selective regulatory DNA persists well below conventional *P*-value thresholds for genome-wide significance.

factor κB (NF-κb), and peroxisome proliferator–activated receptor α (PPAR-α) and PPAR-γ. These 22 transcription factors comprise a highly significant [$P < 9.8 \times 10^{-51}$, simulation versus number of factors for random SNPs (*12*)], shared regulatory architecture that is repeatedly perturbed in a wide range of autoimmune disorders (Fig. 4A).

The same analysis in the context of 17 different malignancies exposed a very different network of transcription factors connecting seemingly disparate cancer types [$P < 7.1 \times 10^{-11}$, simulation (*12*)] including neoplastic regulatory relationships linking FOXA1 and breast cancer, FOXO3 and colorectal cancer, and TP53 and melanoma, breast, and prostate cancer (Fig. 4B). We also analyzed six neuropsychiatric disorders and identified 23 transcription factors whose recognition sequences were perturbed by at least three disease-associated variants (fig. S13). Collectively, these results support the hypothesis that shared genetic liability may underlie many related categories of disease (*24*, *25*).

De novo identification of pathogenic cell types. To provide insights into the cellular structure of disease and potentially highlight pathogenic cell types, we explored the selective localization of GWAS SNPs within the regulatory DNA of individual cell types. We further considered the enrichment of all tested variants, not just those with genome-wide significance, and performed serial determination of the cell- and tissue-selective enrichment patterns of progressively more strongly associated variants to expose collective localization within specific lineages or cell types. We used all SNPs tested in GWAS meta-analyses of two common autoimmune disorders, Crohn's disease (*26*) and multiple sclerosis (MS) (*27*), and a common continuous physiological trait, cardiac conduction measured by the electrocardiogram QRS duration (*28*) (n = 938,703, 2,465,832, and 2,828,796 SNPs, respectively). For SNPs meeting increasingly significant P-value cutoffs, we compared the proportion of SNPs in DHSs of each cell type to the proportion of all SNPs in DHSs of the same cell type (Fig. 5). For all three studies, we observed enrichment of more weakly associated variants in regulatory DNA. This enrichment suggests that a large number of functional variants of small quantitative effect act through modulation of regulatory DNA. Additionally, it suggests that conditioning association analyses on regulatory DNA may ameliorate the stringent statistical correction for multiple testing required for genome-wide testing of unselected SNPs.

Furthermore, with progressively stringent P-value thresholds, we observed increasingly selective enrichment of disease-associated variants within specific cell types (Fig. 5). In the case of Crohn's disease, the T helper 17 (T_H17) (12.0-fold enriched) and T_H1 (8.87-fold enriched) T cell subtypes have a concentration of the most-significant GWAS variants in their DHSs (Fig. 5A). Although Crohn's pathology has classically been associated with T_H1 cytokine responses, an emerging consensus points to a defining role for IL-17–producing T_H17 cells (*29*). Notably, this analysis was accomplished without any prior knowledge about Crohn's disease pathology.

In the case of MS, sequential cell-selective enrichment analysis highlighted two cell types: $CD3^+$ T cells from cord blood and $CD19^+/CD20^+$ B cells (Fig. 5B). Although MS has long been thought to be T cell mediated, a critical role for B cells has only recently been recognized and has major therapeutic implications (*30*). It is notable that cord blood $CD3^+$ cells—essentially a naïve population—garner the most highly selective enrichment, particularly in comparison with total adult $CD3^+$ cells or other T cell subsets, suggesting a role for variants influencing immune education. Also of note, DHSs active in brain tissue were moderately depleted (~10%) for MS-associated variants, suggesting that neural gene expression regulatory elements do not play a substantial role in MS pathogenesis, as proposed (*31*). Analogously, analysis of variants associated with the continuously varying trait of QRS duration revealed similarly specific enrichment within fetal heart DHSs (Fig. 5C). In all three cases, the results were obtained without any prior knowledge of physiological mechanisms. These data suggest a generally applicable approach and highlight the value of extensive maps of regulatory DNA for gaining insights into disease physiology and pathogenesis.

Discussion. Despite a long appreciation of the involvement of regulatory variants in human disease (*32*–*34*), difficulty in delineating regulatory DNA regions, particularly in a cell-specific context, has until now prevented comprehensive assessment of the relationship between gene regulation and common phenotypes. Our results indicating widespread and systematic localization of variants associated with a wide spectrum of common diseases and traits in regulatory DNA marked by DHSs have many implications for interpreting diverse genotype-phenotype association studies. The connection of numerous DHSs harboring GWAS SNPs with promoters of distant genes expands the genomic horizon of disease and trait associations and provides a trove of plausible causal genes to explain those associations. The data also unify seemingly unconnected variants associated with related diseases by virtue of their convergent perturbation of common transcription factor networks. Tissue-selective enrichment of phenotype-associated variants raises the possibility of more focused genetic association studies that prioritize the regulatory DNA of a known or hypothesized target tissue type. Further, selective enrichment of many more weakly associated variants within regulatory DNA of pathogenic cell types points to the quantitative contribution of hundreds of variants of small effect size that modulate transcription factor binding characteristics, in contrast to Mendelian variants in transcription factor genes that may perturb entire networks. The results thus highlight a continuous quantitative spectrum of disordered gene regulation between common disease and Mendelian traits and lend a new perspective on the genetic architecture and heritability of common human diseases and phenotypic traits (*35*).

References and Notes

1. B. E. Stranger, E. A. Stahl, T. Raj, *Genetics* **187**, 367 (2011).
2. L. A. Hindorff *et al.*, A Catalog of Published Genome-Wide Association Studies; available at www.genome.gov/gwastudies.
3. W. Cookson, L. Liang, G. Abecasis, M. Moffatt, M. Lathrop, *Nat. Rev. Genet.* **10**, 184 (2009).
4. M. M. Pomerantz *et al.*, *Nat. Genet.* **41**, 882 (2009).
5. K. Musunuru *et al.*, *Nature* **466**, 714 (2010).
6. O. Harismendy *et al.*, *Nature* **470**, 264 (2011).
7. D. L. Nicolae *et al.*, *PLoS Genet.* **6**, e1000888 (2010).
8. J. F. Degner *et al.*, *Nature* **482**, 390 (2012).
9. D. S. Gross, W. T. Garrard, *Annu. Rev. Biochem.* **57**, 159 (1988).
10. R. E. Thurman *et al.*, *Nature* 10.1038/nature11232 (2012).
11. B. E. Bernstein *et al.*, *Nat. Biotechnol.* **28**, 1045 (2010).
12. Detailed information on methods and analyses can be found in the supplementary materials available on *Science* Online.
13. The 1000 Genomes Project Consortium, *Nature* **467**, 1061 (2010).
14. M. E. Symonds, S. P. Sebert, M. A. Hyatt, H. Budge, *Nat. Rev. Endocrinol.* **5**, 604 (2009).
15. S. John *et al.*, *Nat. Genet.* **43**, 264 (2011).
16. D. J. Barker *et al.*, *Lancet* **341**, 938 (1993).
17. G. A. Maston, S. K. Evans, M. R. Green, *Annu. Rev. Genomics Hum. Genet.* **7**, 29 (2006).
18. L. A. Lettice *et al.*, *Proc. Natl. Acad. Sci. U.S.A.* **99**, 7548 (2002).
19. N. Soranzo *et al.*, *Nat. Genet.* **41**, 1182 (2009).
20. J. C. Knight, B. J. Keating, K. A. Rockett, D. P. Kwiatkowski, *Nat. Genet.* **33**, 469 (2003).
21. M. T. Maurano, H. Wang, T. Kutyavin, J. A. Stamatoyannopoulos, *PLoS Genet.* **8**, e1002599 (2012).
22. S. S. Fajans, G. I. Bell, K. S. Polonsky, *N. Engl. J. Med.* **345**, 971 (2001).
23. T. Tamura, H. Yanai, D. Savitsky, T. Taniguchi, *Annu. Rev. Immunol.* **26**, 535 (2008).
24. International Schizophrenia Consortium *et al.*, *Nature* **460**, 748 (2009).
25. C. Cotsapas *et al.*, *PLoS Genet.* **7**, e1002254 (2011).
26. A. Franke *et al.*, *Nat. Genet.* **42**, 1118 (2010).
27. N. A. Patsopoulos, *Ann. Neurol.* **70**, 897 (2011).
28. N. Sotoodehnia *et al.*, *Nat. Genet.* **42**, 1068 (2010).
29. S. Brand, *Gut* **58**, 1152 (2009).
30. H.-C. von Büdingen, A. Bar-Or, S. S. Zamvil, *Curr. Opin. Immunol.* **23**, 713 (2011).
31. International Multiple Sclerosis Genetics Consortium (IMSGC) *et al.*, *Nat. Genet.* **42**, 469, author reply 470 (2010).
32. M. C. King, A. C. Wilson, *Science* **188**, 107 (1975).
33. F. S. Collins *et al.*, *Nature* **313**, 325 (1985).
34. M. V. Rockman, G. A. Wray, *Mol. Biol. Evol.* **19**, 1991 (2002).
35. G. Gibson, *Nat. Rev. Genet.* **13**, 135 (2012).
36. G. Li *et al.*, *Cell* **148**, 84 (2012).

Acknowledgments: We thank many colleagues for their insightful comments and critical readings of the manuscript. We also thank many colleagues who provided individual cell samples for DNase I analysis. This work was supported by NIH grants U54HG004592 and U01ES01156 (J.A.S.), P30 DK056465 (S.H.), R01HL088456 (N.S.), and R24HD000836-47 (I.G.). We acknowledge the generous sharing of results from the International MS Genetics, International IBD Genetics, and CHARGE QRS Consortia. DNase I data have been deposited in Gene Expression Omnibus (GEO) under accession nos. GSE29692 and GSE18927 and can be viewed and downloaded at genome.ucsc.edu, www.uwencode.org/data, and www.epigenomebrowser.org.

Supplementary Materials

www.sciencemag.org/cgi/content/full/science.1222794/DC1
Materials and Methods
Figs. S1 to S13
Tables S1 to S12
References (*37*–*49*)

3 April 2012; accepted 13 July 2012
Published online 5 September 2012;
10.1126/science.1222794

How Cells Know the Size of Their Organelles

Yee-Hung M. Chan and Wallace F. Marshall

Cells have developed ways to sense and control the size of their organelles. Size-sensing mechanisms range from direct measurements provided by dedicated reporters to indirect functional readouts, and they are used to modify organelle size under both normal and stress conditions. Organelle size can also be controlled in the absence of an identifiable size sensor. Studies on flagella have dissected principles of size sensing and control, and it will be exciting to see how these principles apply to other organelles.

Organelles represent a scale of organization just below that of the cell itself, and their composition is tailored to their functions. Organelles are specialized to perform different biochemical, regulatory, and motile processes, and they display distinct morphologies that range from the unitary nucleus to the reticulated networks of the endoplasmic reticulum (ER) and mitochondria. These morphologies are constructed and maintained by the cell, and the mechanisms by which they are established remain a vital area of research. The fundamental principles of how cells can sense and control the size of their organelles remain unclear.

Why Cells Care About Organelle Size

Why do cells care about the size of their organelles? At a basic level, the cell occupies a finite volume. Cellular reactions and pathways are divided among the individual organelles and cytoplasm, all of which have some size. Thus, at a minimum the cell must in some way ensure that the size of its organelles is greater than zero. In principle, larger organelles can contain larger quantities of metabolic enzymes and thus mediate higher fluxes through their biochemical pathways. Ideally, organelle size should be suited to cellular needs, including functional, distribution, and transport requirements, or other factors (*1*).

Organelle size optimization is evident in cells with specialized roles, such as in secretory cells with greatly expanded ER (Fig. 1A) (*2*) and in rod and cone photoreceptors whose outer segment size correlates to their light sensitivity (Fig. 1B) (*3*). Furthermore, defects in organelle size result in improper cell function. The enlarged vacuole in *fab1* mutants of budding yeast leads to improper karyogamy and fitness defects (*4*). Mitotic spindle-length defects can result in faulty chromosome separation (*5*). Cilia and flagella that are too long or short result in defective motility (*6*, *7*). Thus, maintaining organelle size is critical for cell function.

Department of Biochemistry and Biophysics, UCSF Center for Systems and Synthetic Biology, University of California, San Francisco, San Francisco, CA 94158, USA. E-mail: yhmchan@ucsf.edu (Y.-H.M.C.); wallace.marshall@ucsf.edu (W.F.M.)

A key question is how organelle size is detected or sensed by the cell. This problem is complicated by the stochastic nature of the molecular tools available to the cell. In this Review, we discuss fundamental principles and illustrative examples of the ways in which cells sense organelle size, as well as the reasons why such sensing is performed.

How Do Cells Sense Organelle Size?

Although simple at first, this question is complicated by what it would mean for a cell to sense size. At its simplest, sensing involves a measurement or observation. Although humans can communicate that such an observation has been made, determining whether a cell has made such a measurement is nontrivial. We can infer that a cell meaningfully senses size on the basis of the following criteria: (i) the identification of a readout mechanism that correlates with organelle size and (ii) observing a change in cellular behavior or state as a consequence of that readout.

At an extreme, we might expect that cells have a dedicated reporter molecule whose chemical state gives some readout of organelle size. There are several ways in which a reporter molecule could convey such a measurement within the cell (Fig. 2):

1) Size-dependent accumulation. If reporter molecules bind to the organelle with some affinity or are inserted into the organelle at a fixed density, there will be more the larger the organelle is. Downstream responses would be dependent on the extent of accumulation of the reporter.

2) Concentration gradient. If reporter molecules are synthesized in or delivered to a certain part of the organelle at some rate, then transport or diffusion of the molecule would create a concentration gradient whose properties depend on the size of the structure.

3) Occupancy time. If reporter molecules are synthesized in or delivered to a certain part of the organelle, then residency time within the organelle will depend on the size of the organelle. The kinetics of phosphorylation or some other modification could give a readout of the residency time and thus organelle size.

4) Conformational change. The reporter molecule might change or induce a change in conformation or structure depending on organelle size.

5) Structural scaffold. The size of some organelles is shaped by a molecular scaffold. The scaffold's size is itself dependent on the self-assembly and conformation of the constituent proteins.

The reporter can affect cell processes in several ways, including signaling, transcriptional regulation, or directly (de)activating growth mechanisms. The effects of cellular size measurements include changes in cell state, as in the case of the size checkpoint of budding yeast. More commonly, though, they are used to regulate the size of the structure or organelle being measured.

Multiple mechanisms for size sensing can work in concert. For example, neurite-length sensing has been proposed to have its basis in the anterograde transport and accumulation of the protein shootin1 to the tip balanced by the retrograde diffusion of shootin1 back to the cell body. As a result, the concentration of shootin1 accumulated at the tip depends on the length of the neurite, making it a readout of size. Then, shootin1 participates in a positive-feedback signaling loop to amplify growth in longer neurites. This cycle eventually leads to symmetry breaking and the focused growth of a single axon (*8*).

Telomere-length control depends on the accumulation of Rap1p in budding yeast (*9*) and telomere repeat binding factor 1 (TRF1) and TRF2 in human cells (*10*). These proteins bind to tandem repeat sequences and recruit a number of other factors; longer telomeres have more protein bound. At a certain telomere length, enough protein accumulates to induce a conformational change in the entire protein-DNA complex. At this point, the telomere enters a capped state that is inaccessible to further lengthening by telomerase.

The mitotic spindle provides excellent examples of size-dependent accumulation and concentration-gradient mechanisms. Spindle microtubules elongate with some basal kinetics, but they recruit motors that act to compress the spindle (*11*, *12*) as well as microtubule-depolymerizing [kinesin-8 (*13*)] and -severing [katanin (*14*)] factors that reduce microtubule length (*15*). Longer microtubules are able to recruit more of these shortening factors; thus, larger spindles will grow more slowly until a steady state is reached. Changes in activity of microtubule-severing enzymes between various species is apparently one cause of specific differences in spindle length (*16*). In these cases, the recruited molecules are themselves effectors that change length, so there is no need for an intervening reporter. One molecule that clearly has a role in spindle length is the small guanosine triphosphatase (GTPase) Ran.

How Cells Know…
First in an occasional series

RanGTP is produced at the center of the spindle and diffuses out. The resulting concentration gradient's properties depend on spindle length (*17*), thus providing a length "sensor." It remains to be determined how strongly this gradient influences length in comparison to the other molecules already discussed. Last, there is evidence that the spindle poles may contain a molecular switch that responds to length-dependent changes in mechanical pressure and modulates microtubule depolymerization accordingly (*18*). Such a switch uses mechanical properties as a readout of spindle size.

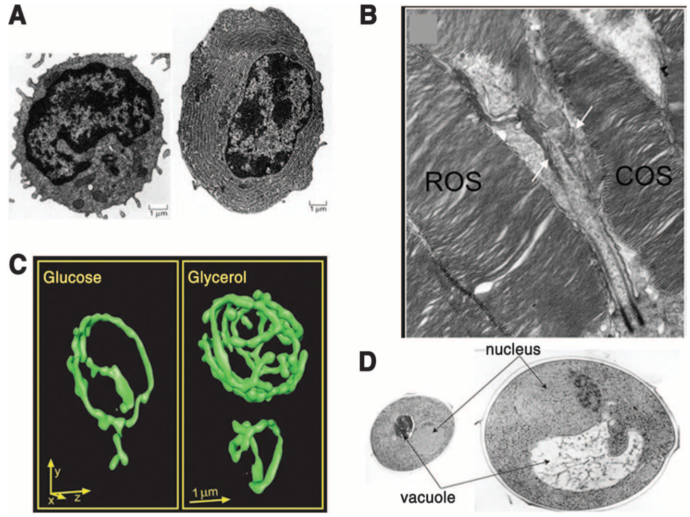

Fig. 1. Examples of organelle size control. (**A**) Cell specialization. The ER expands greatly from an undifferentiated cell (left) to a professional secretory cell (right). [Images from (*43*)] (**B**) Cell specialization. The outer segments in cone (COS) and rod (ROS) cells differ in shape and size, in part because of differences in transport through the connecting cilium (arrows). [Image from (*3*)] (**C**) Functional demand. Mitochondria ramify in a yeast cell grown in respiratory (right) versus fermentative (left) media. [Image from (*24*)] (**D**) Organelle/cell size scaling in yeast. The nucleus in the larger cell (right) is larger than the nucleus in the smaller cell (left). [Image from (*25*)]

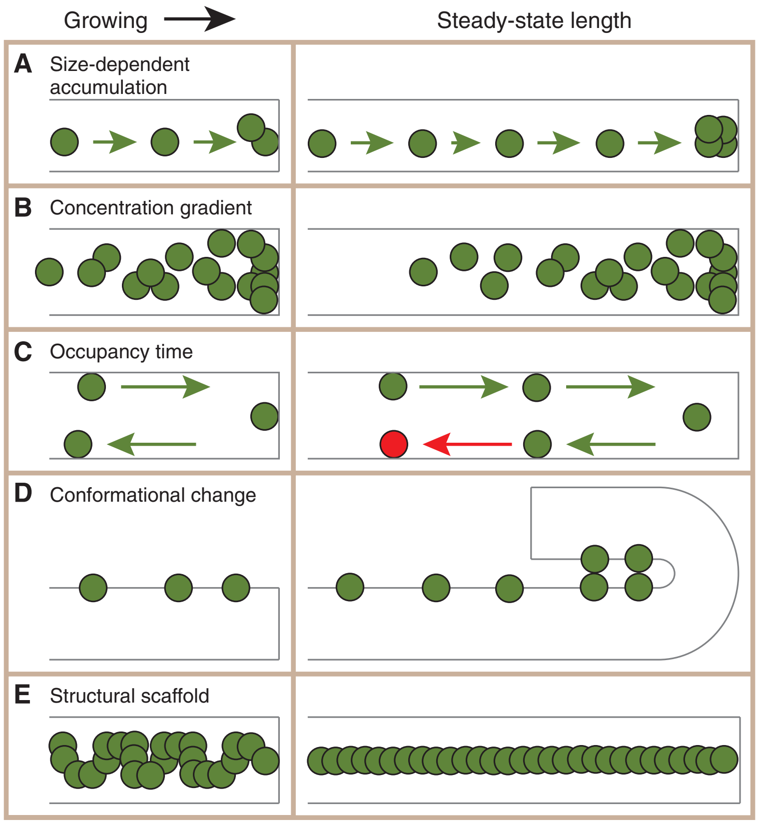

Fig. 2. Cartoons illustrating possible models for size sensing in a one-dimensional organelle, where size-sensing molecules are represented by green and red circles. Examples are shown for when the organelle (black rectangle) is growing (left column) and has reached a steady-state length (right column). The organelle grows until (**A**) enough sensing molecules accumulate on the organelle, (**B**) the concentration gradient of the sensing molecule achieves the right profile, (**C**) the sensing molecule's occupancy time is long enough to induce a state change (green to red circle), (**D**) a conformational change in the organelle is induced by accumulated sensing molecules, or (**E**) its size conforms to a structural scaffold set by the sensing molecule.

A classic example of scaffold-based size control is the clathrin coat, which sterically constrains the size and curvature of endocytic vesicles as it assembles around the lipid membrane. Many infectious bacteria also rely on a structural scaffold to control the length of their injection-needle projections (*19*). In *Yersinia pestis* and *Y. enterocolitica* cells, the ends of the protein YscP are anchored in the proximal and distal ends of the needles. Then, when the needle has reached the length of the YscP "ruler," extension of the YscP protein acts to discontinue the export of the major structural subunit of the needle, stopping growth. Similar proteins have been found to determine the length of T4 and lambda bacteriophage tails (*20*). Remarkably, changing the length of the ruler subunits via protein engineering leads to predictable and systematic decreases in the length of the associated structure.

Indirect Size Sensing

Size may be sensed indirectly, without a molecule whose specific role is to measure size. In the case of organelles, size affects their functional capacity and their distribution around the cell. If an organelle is unable to meet functional demand, that could lead to a build-up of stress agents or other changes in cellular environment, triggering a subsequent response to increase the size of that organelle to relieve that stress. In these cases, there are no specific measures of absolute organelle size. Rather, size sensing is both indirect (the cell infers organelle size on the basis of the accumulation of other molecules) and relative (the organelle is too small to meet the functional demand). However, the end effect is still regulation of organelle size.

An example of such sensing is found in the relation of the ER to the unfolded protein response (UPR). The accumulation of unfolded protein triggers oligomerization of the transmembrane protein Ire1p, leading to phosphorylation of its cytosolic kinase domain and eventually to increased expression of UPR response genes. Among these are lipid biosynthesis genes, and the increase in lipid mass results in growth of the ER, in part to increase ER lumenal capacity to address the unfolded protein stress (*21*, *22*). In another example, exposure of plant and animal cells to oxidative stress induces the expression of Peroxin 1, leading to expansion and proliferation of peroxisomes to deal with increased levels of reactive oxygen species (*23*). Also, mitochondria in budding yeast ramify upon transfer from fermentative to respiratory media (Fig. 1C) (*24*).

Size Control in the Absence of Size Sensing

In many cases, size control occurs without an obvious size sensor. For example, many organelles,

including the nucleus (Fig. 1D) (*25*, *26*), nucleolus (*27*), and vacuoles (*28*, *29*), show a scaling behavior with cell size; that is, larger cells have larger organelles. However, to our knowledge, no specific size sensor of these organelles has been identified. Thus, size control might arise even in the absence of specific size sensors.

One way to achieve size control is to have stereotyped growth, by which both organelle and cell grow according to a preset plan. This seems to be the case with centrosome number control because the organelle's duplication cycle is coupled to the cell cycle. In a simple case of stereotyped growth, both cell and organelle would grow at constant rates. Another way to achieve scaling is allometric growth, in which organelle growth is some constant fraction of cell growth; in this case, the organelle will inherently be some proportion of cell size. This could arise if both organelle and cell growth were dependent on overall metabolism.

The cell can also control size by synthesizing a limited pool of precursor (*30*). Assuming that an organelle grows until the pool is depleted, size would be readily modulated by changing the pool size. Fixed-precursor recruitment has been proposed as a size-control model for the bacterial flagellar hook, in which it is suggested that the C-ring structure of the basal body would act as a "measuring cup" to bind a fixed quantity of hook precursor and then release this fixed precursor set to allow assembly (*31*).

To determine whether these models apply, it is useful to monitor the growth of the organelle along with that of the cell. Stereotyped growth is demonstrated if the growth trajectories fit to standard growth models (i.e., constant or exponential). Otherwise, a consistent pattern of growth among different individuals or in successive cell divisions might also indicate a preexisting plan. In the case of allometric growth, there would be a correlation between instantaneous cell and organelle growth rates. Although these simple models of growth result in inherent organelle-to-cell size scaling, they are sensitive to perturbation because they do not include mechanisms for recovery. To achieve that, growth of either the cell or organelle must be tunable in some way with respect to the relative size of the organelle.

Flagellar Length Control and the Balance-Point Model

The eukaryotic flagellum has been studied in detail as a model system for organelle size control (Fig. 3A). Flagellar length is dependent on competing processes of assembly and disassembly, both of which occur at the distal flagellar tip and rely on the microtubule motor–based transport of structural material, or intraflagellar transport (IFT) (*32*), which carries tubulin to the growing flagellar tip (*33*). When flagella are severed, they regenerate with decelerating kinetics. The rapidity of growth back to the original size argues against a stereotyped growth mechanism for length control, whereas decreased growth rate as the flagella reach their final length is suggestive of feedback control. In the biflagellate green alga *Chlamydomonas*, when one flagellum is severed, during its regeneration the other, intact flagellum shortens until the two flagella reach equal lengths, at which point they resume growth together (*34*). This equalization of lengths seems to indicate that the cell "knows" how long both its flagella are.

As further evidence of flagellar length sensing, the frequency of injection of IFT material into the flagellum from the cytoplasm changes as a function of flagellar length (*35*). The motors and associated proteins that drive IFT associate into linear arrays known as trains, and, as a regenerating flagellum becomes longer, the trains become smaller but more frequent. The net effect is that the total number of individual IFT subunits is roughly independent of length, but this is only achieved by having the frequency and size of the trains vary with length. So how does the IFT system know how long the flagellum is?

As discussed above, one way for the cell to know organelle size is having a dedicated reporter molecule whose state is sensitive to organelle size. The phosphorylation state of an aurora-like kinase depends on flagellar length (*36*), so it could act as a length sensor. On the other hand, depletion of this kinase by RNA interference (RNAi) has no effect on flagellar length (*37*), raising the question of whether the cell uses the information on length encoded by the kinase. A complete feedback loop, in which length regulates the state of a kinase whose function then modulates assembly or disassembly, remains to be found.

One likely output of any length reporter molecule would be regulation of IFT, a critical pathway for maintaining flagellar length. The total quantity of IFT material per flagellum is roughly constant (*32*, *35*). Consequently, the transport rate should be a decreasing function of length, because in longer flagella it takes longer for the motors to reach the tip of the flagellum and deliver their cargo (Fig. 3B). Furthermore, disassembly rate is length-independent (*38*), mediated by microtubule-depolymerizing kinesins (*39*). Combined with the length-dependent assembly rate, this constant disassembly gives a unique steady-state solution for length (Fig. 3C). The maintenance of constant total IFT protein per flagellum is critical for this model, and it appears to be the result of length-dependent changes in the size and

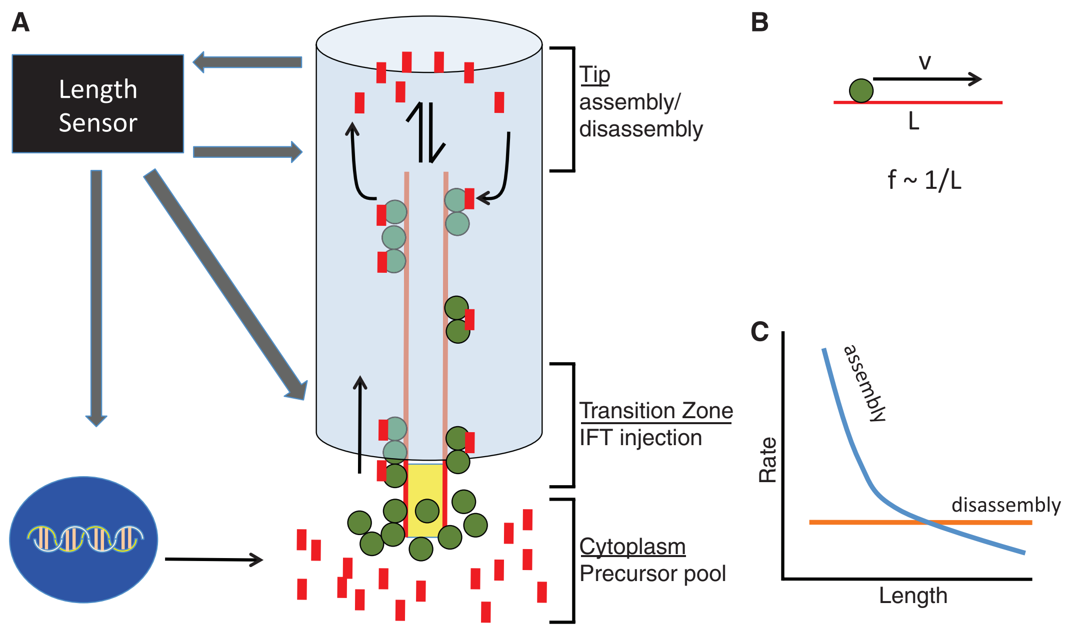

Fig. 3. Illustration of the balance-point model of flagellar length control. (**A**) IFT particles (green) associated with the flagellar basal body bind precursor molecules from cytoplasmic pool (red) and are injected into the flagellum, where they travel to the distal tip to deliver precursor for flagellar assembly. Flagella assembly rate depends on the rate of anterograde IFT, and the disassembly rate is constant. A length sensor may act at the flagellar tip or base or both, and it can affect gene regulation and precursor synthesis, injection of IFT, or assembly or disassembly rates to create feedback loops for length control. (**B**) Assuming a constant IFT speed, *v*, the delivery frequency of IFT particles, *f*, will vary inversely with flagellum length, *L*. (**C**) In the balance-point model, flagellar length reaches a steady state where the assembly rate (blue) and disassembly rate (orange) curves intersect.

frequency of IFT train import into the flagellum. A major goal now is to identify the molecules that mediate these length-dependent processes.

Flagellar length is also regulated, to some degree, by a limiting precusor mechanism. Flagellar assembly is accompanied by massive increase in transcription of virtually all genes encoding flagellar proteins (*40*). In the absence of protein synthesis, flagella can only regenerate to about half of their normal length (*34*). Therefore, control of precursor quantity is a key element of length control and represents a potential target for signaling molecules in a length sensing pathway.

In contrast to eukaryotic flagella, bacterial flagella grow at a constant rate, and it has been proposed that their length is determined by a balance between constant growth and random breakage (*41*).

Distinguishing Mechanisms of Size Control

An ongoing challenge in studying organelle size control is that it can be difficult to make measurements on morphologically complex subcellular structures. Organelles typically use their lumen and their membrane for distinct functions, raising the question of how the cell controls the size of both for a single organelle. Measurements of organelle volume and surface area require three-dimensional analysis. Recent advances in imaging (*24*), tomography (*28*), and analysis methodology (*29*) will be crucial to understanding mechanisms of organelle size control.

The systems that contain dedicated size-sensing pathways tend to be ones for which size plays an obvious part in function. Flagellar length is important for cells to create the appropriate waveform to allow movement. Consequently, length control mutations in *Chlamydomonas* often show severe motility defects, and homologs to these genes are implicated in several ciliopathies (*40*). Mitotic spindle defects can result in improper chromosome segregation, and telomere length is implicated in aging. Bacterial injection needles with altered lengths can show less virulence during infection (*42*).

However, the effect of size in the case of other organelles is less clear. Although the nucleus shows a size scaling to cytoplasmic volume, it does not seem to be related to the amount of genomic DNA, as might be expected from a functional perspective (*25*, *26*). Changes to organelle size under stress conditions can be readily explained, but absent such stress organelle size may be less tightly regulated. To test for this possibility, it is useful to refer to deflagellation and recovery experiments, which illustrate that direct manipulation of the size of organelles can be a powerful tool to establish the principles of size sensing and control. Although deflagellation can be induced by various methods, less is known about how to change other organelles' sizes. Laser ablation can remove centrosomes and sever mitotic spindles. Reversible drug treatment or other manipulations may also be effective.

Monitoring the response after perturbing organelle size will reveal whether there is recovery to the proper size scaling. If the organelle is too small, recovery may involve up-regulation of assembly pathways, synthesis of precursor components, or both. On the other hand, an organelle that is too large could restore scaling by undergoing disassembly or autophagy or by reducing or eliminating its own growth and allowing the cell to grow larger. An absence of recovery would indicate a lack of size sensing and regulation. This could indicate that the organelle size falls within an acceptable range or that there is a passive growth mechanism without size sensing.

Concluding Thoughts

As we have shown, there are several ways in which cells can sense and control the size of their organelles. But a common follow-up issue arises: How is the size sensor calibrated, or how is the size set point determined? For example, how does a bacterial cell ensure that its molecular ruler is the appropriate length? Or how have the rates in *Chlamydomonas* flagellar assembly and disassembly been determined so that the flagella are the correct lengths? Ultimately, the answers to these questions are likely to involve evolutionary tuning of these mechanisms so that organelle size is optimized to some function. As experiments on organelle size sensing and control continue, it will also be necessary to study the functional implications of organelle size.

References and Notes

1. Y.-H. M. Chan, W. F. Marshall, *Organogenesis* **6**, 88 (2010).
2. C. M. Federovitch, D. Ron, R. Y. Hampton, *Curr. Opin. Cell Biol.* **17**, 409 (2005).
3. P. Avasthi *et al.*, *J. Neurosci.* **29**, 14287 (2009).
4. A. Yamamoto *et al.*, *Mol. Biol. Cell* **6**, 525 (1995).
5. G. Goshima, S. Saitoh, M. Yanagida, *Genes Dev.* **13**, 1664 (1999).
6. M. R. Kuchka, J. W. Jarvik, *Genetics* **115**, 685 (1987).
7. S. E. Barsel, D. E. Wexler, P. A. Lefebvre, *Genetics* **118**, 637 (1988).
8. M. Toriyama *et al.*, *J. Cell Biol.* **175**, 147 (2006).
9. S. Marcand, E. Gilson, D. Shore, *Science* **275**, 986 (1997).
10. A. Smogorzewska *et al.*, *Mol. Cell. Biol.* **20**, 1659 (2000).
11. T. J. Mitchison *et al.*, *Mol. Biol. Cell* **16**, 3064 (2005).
12. I. Brust-Mascher, P. Sommi, D. K. Cheerambathur, J. M. Scholey, *Mol. Biol. Cell* **20**, 1749 (2009).
13. V. Varga *et al.*, *Nat. Cell Biol.* **8**, 957 (2006).
14. K. McNally, A. Audhya, K. Oegema, F. J. McNally, *J. Cell Biol.* **175**, 881 (2006).
15. L. N. Weaver *et al.*, *Curr. Biol.* **21**, 1500 (2011).
16. R. Loughlin, J. D. Wilbur, F. J. McNally, F. J. Nédélec, R. Heald, *Cell* **147**, 1397 (2011).
17. P. Bastiaens, M. Caudron, P. Niethammer, E. Karsenti, *Trends Cell Biol.* **16**, 125 (2006).
18. S. Dumont, T. J. Mitchison, *Curr. Biol.* **19**, 1086 (2009).
19. L. Journet, C. Agrain, P. Broz, G. R. Cornelis, *Science* **302**, 1757 (2003).
20. I. Katsura, *Nature* **327**, 73 (1987).
21. A. A. Welihinda, W. Tirasophon, R. J. Kaufman, *Gene Expr.* **7**, 293 (1999).
22. S. Schuck, W. A. Prinz, K. S. Thorn, C. Voss, P. Walter, *J. Cell Biol.* **187**, 525 (2009).
23. E. Lopez-Huertas, W. L. Charlton, B. Johnson, I. A. Graham, A. Baker, *EMBO J.* **19**, 6770 (2000).
24. A. Egner, S. Jakobs, S. W. Hell, *Proc. Natl. Acad. Sci. U.S.A.* **99**, 3370 (2002).
25. P. Jorgensen *et al.*, *Mol. Biol. Cell* **18**, 3523 (2007).
26. F. R. Neumann, P. Nurse, *J. Cell Biol.* **179**, 593 (2007).
27. M. T. Berciano *et al.*, *J. Struct. Biol.* **158**, 410 (2007).
28. M. Uchida *et al.*, *Yeast* **28**, 227 (2011).
29. Y.-H. M. Chan, W. F. Marshall, *Proc. SPIE* **8225**, 822529 (2012).
30. N. W. Goehring, A. A. Hyman, *Curr. Biol.* **22**, R330 (2012).
31. S. Makishima, K. Komoriya, S. Yamaguchi, S.-I. Aizawa, *Science* **291**, 2411 (2001); 10.1126/science.1058366.
32. W. F. Marshall, J. L. Rosenbaum, *J. Cell Biol.* **155**, 405 (2001).
33. L. Hao *et al.*, *Nat. Cell Biol.* **13**, 790 (2011).
34. J. L. Rosenbaum, J. E. Moulder, D. L. Ringo, *J. Cell Biol.* **41**, 600 (1969).
35. B. D. Engel, W. B. Ludington, W. F. Marshall, *J. Cell Biol.* **187**, 81 (2009).
36. M. Luo *et al.*, *Curr. Biol.* **21**, 586 (2011).
37. J. Pan, Q. Wang, W. J. Snell, *Dev. Cell* **6**, 445 (2004).
38. W. F. Marshall, H. Qin, M. Rodrigo Brenni, J. L. Rosenbaum, *Mol. Biol. Cell* **16**, 270 (2005).
39. C. Blaineau *et al.*, *Curr. Biol.* **17**, 778 (2007).
40. V. Stolc, M. P. Samanta, W. Tongprasit, W. F. Marshall, *Proc. Natl. Acad. Sci. U.S.A.* **102**, 3703 (2005).
41. L. Turner, A. S. Stern, H. C. Berg, *J. Bacteriol.* **194**, 2437 (2012).
42. L. J. Mota, L. Journet, I. Sorg, C. Agrain, G. R. Cornelis, *Science* **307**, 1278 (2005).
43. D. Zucker-Franklin, *Atlas of Blood Cells: Function and Pathology* (Lea and Febiger, Milan, Italy, ed. 2, 1998).

Acknowledgments: Y.-H.M.C. acknowledges the support of the Herbert Boyer Postdoctoral Fellowship and NIH National Research Service Award no. 1F32GM090442-01A1. W.F.M. acknowledges the support of NIH grants R01GM097017 and P50GM081879.

10.1126/science.1223539

Unconventional Sequence of Fractional Quantum Hall States in Suspended Graphene

Benjamin E. Feldman,[1] Benjamin Krauss,[2] Jurgen H. Smet,[2] Amir Yacoby[1]*

Graphene provides a rich platform to study many-body effects, owing to its massless chiral charge carriers and the fourfold degeneracy arising from their spin and valley degrees of freedom. We use a scanning single-electron transistor to measure the local electronic compressibility of suspended graphene, and we observed an unusual pattern of incompressible fractional quantum Hall states that follows the standard composite fermion sequence between filling factors ν = 0 and 1 but involves only even-numerator fractions between ν = 1 and 2. We further investigated this surprising hierarchy by extracting the corresponding energy gaps as a function of the magnetic field. The sequence and relative strengths of the fractional quantum Hall states provide insight into the interplay between electronic correlations and the inherent symmetries of graphene.

Application of a strong perpendicular magnetic field B to a two-dimensional electron gas (2DEG) gives rise to flat energy bands called Landau levels (LLs), which normally contain a total of eB/h states, where e is the electron charge and h is Planck's constant. In graphene, each of these states has an additional fourfold degeneracy resulting from the spin and valley degrees of freedom, and the LLs possess an approximate SU(4) symmetry (*1*). Incompressible quantum Hall states are formed when the Fermi energy lies between LLs. In graphene, LLs are filled at filling factors $\nu = nh/eB = 4(N + 1/2)$ in the absence of electron-electron interactions (*2*–*4*), where n is the charge-carrier density and N is the orbital index. In this expression, the quantum Hall sequence is shifted by a half-integer, a distinctive signature that reflects the sublattice pseudospin of graphene.

When disorder is low and at high magnetic fields, Coulomb forces between electrons become important, and many-body effects emerge. One example is the fractional quantum Hall effect (FQHE), in which correlations between electrons generate excitations with fractional charge at certain rational filling fractions (*5*–*8*). Recently, the FQHE of Dirac fermions has attracted considerable attention (*9*–*22*). In graphene, the low dielectric constant and unusual band structure lead to FQH states with energy gaps that are larger than in GaAs at the same field, particularly in the $N = 1$ LL (*10*, *15*, *16*). Moreover, the SU(4) symmetry of charge carriers in graphene could yield FQH states without analogs in GaAs (*11*, *12*, *19*). The FQHE was recently observed (*23*–*25*) in suspended graphene samples at ν = 1/3 and 2/3, and transconductance fluctuations also showed evidence of a state at ν = 2/5 (*26*). Measurements of graphene on hexagonal boron nitride substrates (*27*) revealed further FQH states at all multiples of ν = 1/3 up to 13/3, except at ν = 5/3. The absence of a FQH state at ν = 5/3 might result from low-lying excitations associated with SU(2) or SU(4) symmetry, but alternate scenarios associated with disorder could not be ruled out in earlier studies (*27*).

Here, we report local electronic compressibility measurements of a suspended graphene flake performed with a scanning single-electron transistor (SET) (Fig. 1A) (*28*, *29*). By modulating the carrier density and monitoring the resulting change in SET current, we measure both the local chemical potential μ and the local inverse electronic compressibility of the graphene flake (inverse compressibility $\kappa^{-1} = n^2 d\mu/dn$, but hereafter we drop the prefactor and use the term to mean $d\mu/dn$). Therefore, our local technique provides a direct thermodynamic measurement of bulk sample properties and is sensitive to weak effects that may be obscured by disorder in global transport studies.

The inverse compressibility as a function of carrier density and magnetic field is shown in Fig. 1B. At zero magnetic field, we observe an incompressible peak that arises from the vanishing density of states at the charge neutrality point in graphene. For $B > 0$, strong incompressible behavior occurs at $\nu = 4(N + 1/2)$, confirming the monolayer nature of our sample. In addition to the expected single-particle quantum Hall features, we observe incompressible states at intermediate integer filling factors ν = 0, 1, 3, 4, 5, 7, 8, and 9. These integer broken-symmetry states arise from interactions among electrons (*25*, *27*, *30*, *31*) and are visible at fields well below 1 T, indicating the high quality of our sample. Most intriguing, however, is the appearance of incompressible peaks at fractional filling factors, the strongest of which emerge around $B = 1$ T. It is straightforward to distinguish FQH states from oscillations in compressibility caused by localized states. Localized states occur at a constant density offset from their parent quantum Hall state and are therefore parallel to lines of constant filling factor in the nB plane (*4*). When inverse compressibility is plotted as a function of filling factor (Fig. 1C), localized states curve as the magnetic field is changed, whereas any incompressible behavior caused by an integer or FQH state appears as a vertical feature (*32*).

Figure 2A shows a finer measurement of the inverse compressibility as a function of filling factor and magnetic field for ν < 1. Incompressible peaks occur at ν = 1/3, 2/3, 2/5, 3/5, 3/7, 4/7, and 4/9, reproducing the standard composite fermion sequence observed in GaAs. We resolve the strongest incompressible states, ν = 1/3 and 2/3, down to $B \approx 1$ T, although ν = 2/3 weakens considerably below 4 T. As the filling factor denominator increases, the field at which the corresponding state emerges also increases, with ν = 4/9 only apparent above $B \approx 9$ T.

Between ν = 1 and 2, we observe a different pattern of incompressible behavior (Fig. 2B). Surprisingly, no FQH states with odd numerators occur in this regime. Instead, the system condenses into incompressible states only at ν = 4/3, 8/5, 10/7, and 14/9. The incompressible peaks at ν = 4/3 and 8/5 are the most robust, persisting down to ~1 and ~1.5 T, respectively. In graphene, ν = 2 corresponds to a filled LL ($N = 0$), so it is natural to label FQH states with the filling fraction $\nu^* = 2 - \nu$. Doing so reveals a clear pattern of incompressible peaks at $\nu^* = 2p/(4p \pm 1)$ for $p \leq 2$, which is similar to the composite fermion sequence, except that only filling fractions with even numerators lead to incompressible states.

The absence of odd-numerator fractions indicates that a robust underlying symmetry enables low-lying excitations, preventing the formation of incompressible states. One possible explanation is that the Zeeman effect lifts spin degeneracy, but valley symmetry remains intact, allowing large valley skyrmions to form with a minimal energy penalty at odd-numerator filling factors. The behavior we observe between ν = 1 and 2 is reminiscent of results from strained Si and AlAs 2DEGs, which also have a valley degree of freedom and exhibit weakened odd-numerator states (*33*–*36*). However, the analogy is not perfect. The large effective mass and g-factor in these semiconducting materials lead to fully spin-polarized LLs due to single-particle effects; in contrast, the Zeeman energy is substantially smaller than the LL separation in graphene. In valley-symmetric AlAs, the energy gap at ν = 1/3 is large compared with that at ν = 5/3 (*35*), opposite from the behavior we observe at $\nu^* = 1/3$ and 5/3 when we account for the half-integer shift of LLs in graphene. This suggests that the total electron density, and not just the filling fraction, may play an important role in electronic interactions in the lowest LL, a

[1]Department of Physics, Harvard University, Cambridge, MA 02138, USA. [2]Max-Planck-Institut für Festkörperforschung, Heisenbergstrasse 1, D-70569 Stuttgart, Germany.

*To whom correspondence should be addressed. E-mail: yacoby@physics.harvard.edu

topic that has only recently been explored (*37*). Moreover, whereas the incompressible behavior we observe between ν = 1 and 2 is consistent with SU(2) symmetry, it is evident that this symmetry does not persist between ν = 0 and 1, where the full composite fermion sequence is present. The differing behavior above and below ν = 1 suggests an intriguing interplay between the inherent symmetries of graphene and electronic correlations in the lowest LL. This is different from strained Si, in which odd-numerator states are weakened both above and below ν = 1 (*33*). In the valley-symmetric AlAs data from (*35*), both ν = 7/5 and 3/5 states are absent, whereas ν = 8/5 and 2/5 are visible. At higher magnetic fields, however, the ν = 3/5 state is apparent (*37*), similar to the behavior in graphene.

Averaging over a range of magnetic fields helps to reduce fluctuations from localized states because they do not occur at constant filling factor as the magnetic field is varied. Figure 2C shows the inverse compressibility between ν = 0 and 1, averaged over 9 to 11.9 T (blue), and between ν = 1 and 2, averaged over 4.9 to 6.4 T (red). These curves reveal clear incompressible peaks centered at the filling fractions discussed above, as well as negative contributions to the inverse compressibility immediately surrounding each FQH state, which can be ascribed to interactions among the quasi-particles and quasi-holes involved in the FQHE (*38*). A slight incompressible peak occurring at ν = 1.65 (Fig. 2C) may indicate the emergence of a FQH state at ν = 5/3; however, it is much weaker than all other multiples of ν = 1/3 and is therefore consistent with the conclusion that all odd-numerator FQH states are suppressed for ν > 1.

Integrating the inverse compressibility with respect to carrier density allows us to extract the step in chemical potential $\Delta\mu_\nu$ associated with each FQH state and thereby determine the corresponding energy gap Δ_ν. Figure 3A displays the chemical potential as a function of carrier density at B = 11.9 T. We define $\Delta\mu_\nu$ as the difference between the local maximum and minimum in the chemical potential, and the values for each FQH state as a function of magnetic field are plotted in Fig. 3, B and C. We define the zero of $d\mu/dn$ based on its value at ν = 1/2 to accurately determine $\Delta\mu_\nu$ at each field (fig. S8) (*32*). Because the chemical potential is defined with respect to electrons, the step in chemical potential must be multiplied by the ratio of the quasi-particle charge to the electron charge to obtain the energy gap of fractionally charged quasi-particles.

The steps in chemical potential at each multiple of ν = 1/3 have comparable magnitudes (Fig. 3B), and they scale approximately linearly with the field. The linear dependence of the FQH energy gaps on the magnetic field is surprising because states driven by electronic interactions are expected to scale as $B^{1/2}$; the origin of this behavior is unclear. The steps in chemical potential at ν = 2/5, 3/5, and 8/5 are smaller and also depend approximately linearly on the magnetic field, although we cannot rule out a $B^{1/2}$ scaling. The steps in chemical potential at ν = 3/7, 4/7, 10/7,

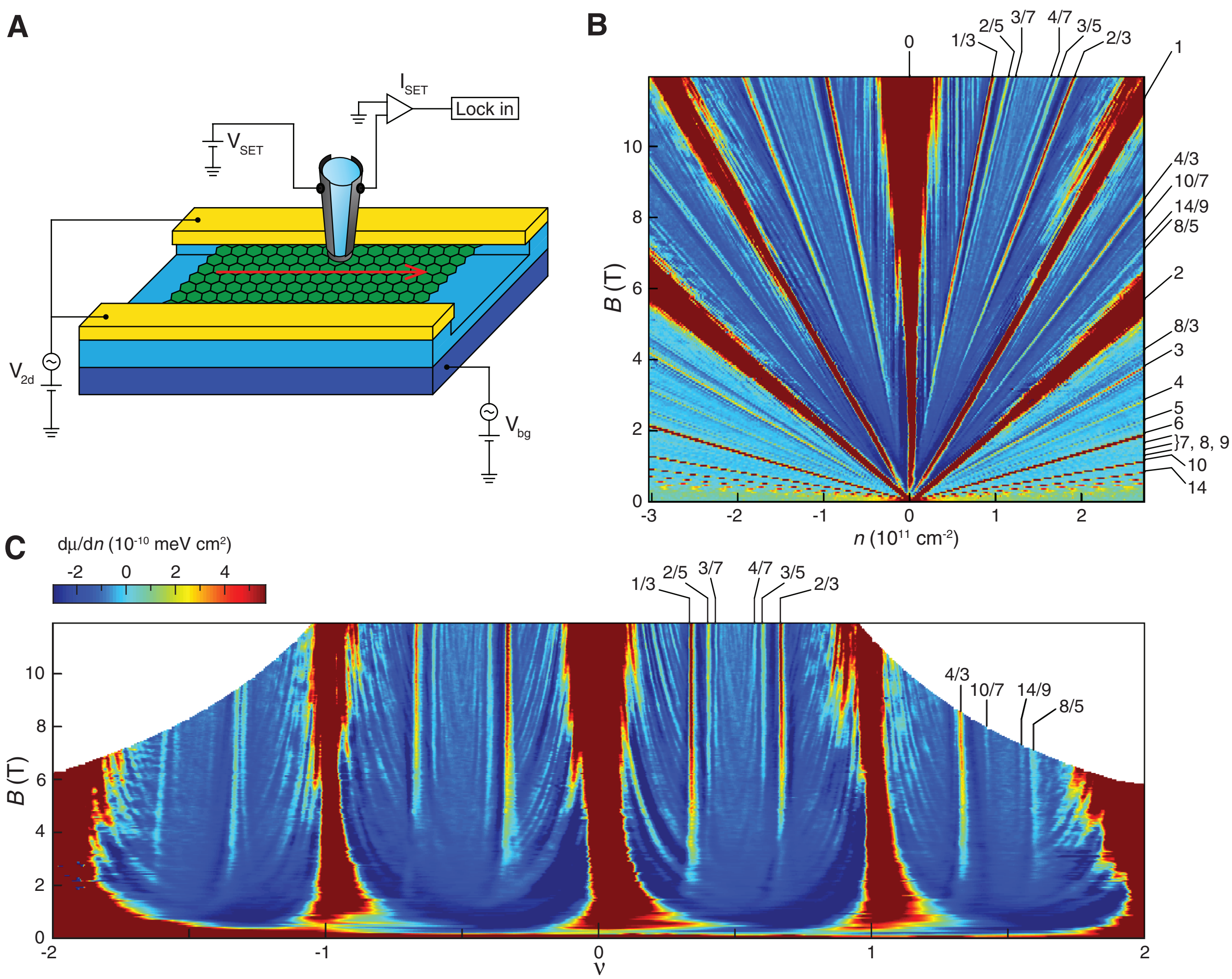

Fig. 1. Measurement setup and Landau fan. (**A**) The SET is ~100 nm in size and is held 50 to 150 nm above the graphene flake. The red arrow indicates the path of the spatial scans in Fig. 4. V, voltage; I, current. (**B**) Inverse compressibility $d\mu/dn$ as a function of carrier density n and magnetic field B. (**C**) Data from (B) plotted as a function of filling factor ν. Vertical features correspond to quantum Hall states, whereas localized states curve as the magnetic field is changed. Principal integer and FQH states are labeled in (B) and (C). These panels share the same color scale.

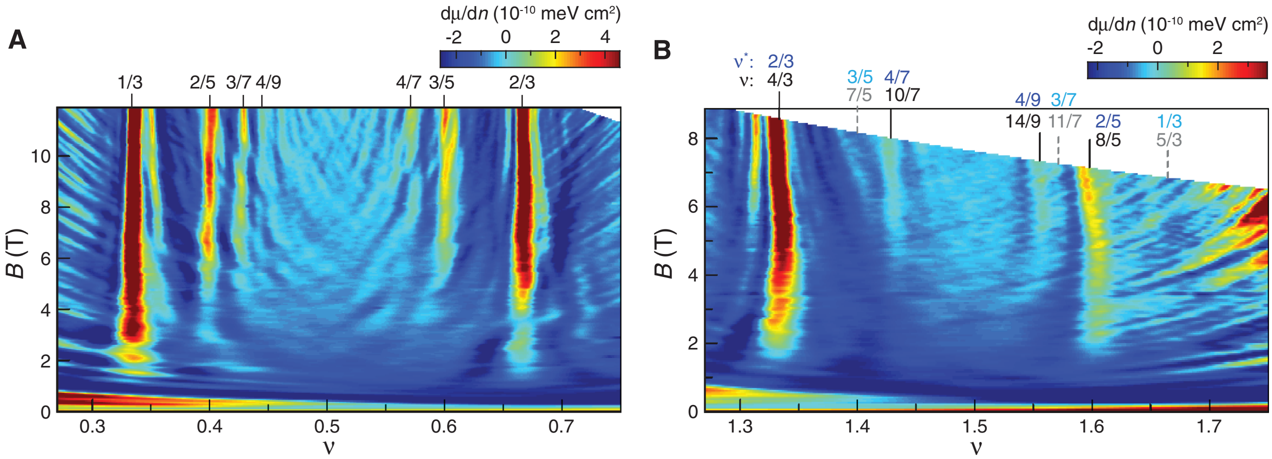

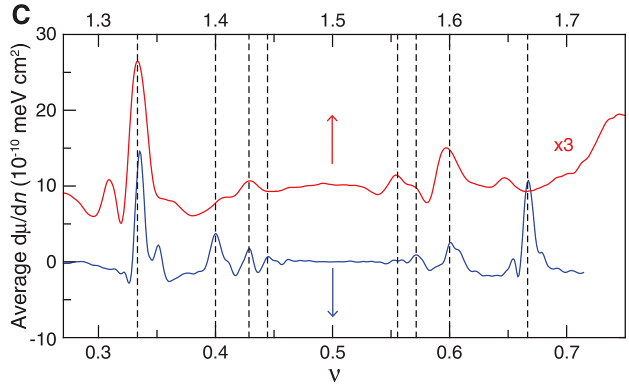

Fig. 2. Incompressible FQH states in the lowest LL. (**A**) Finer measurement of $d\mu/dn$ as a function of filling factor and magnetic field. Incompressible states follow the standard composite fermion sequence between $\nu = 0$ and 1. (**B**) Finer measurement of $d\mu/dn$ between $\nu = 1$ and 2. Incompressible states occur only at filling fractions with even numerators. (**C**) $d\mu/dn$ between $\nu = 0$ and 1, averaged over 9 to 11.9 T (blue), and between $\nu = 1$ and 2, averaged over 4.9 to 6.4 T (red). Curves are offset for clarity. Averaging over magnetic field reduces the influence of localized states and shows clear incompressible peaks centered at ν = 1/3, 2/3, 4/3, 2/5, 3/5, 8/5, 3/7, 4/7, 10/7, 4/9, and 14/9.

4/9, and 14/9 are even smaller (Fig. 3C), and their extracted magnitudes fluctuate substantially as a function of the magnetic field, presumably because of localized states at the measurement point.

The energy gaps obtained from compressibility, which yield the cost of adding charged quasi-particle excitations to the system, have a slightly different physical meaning from those obtained in activation measurements, which probe the energy separation between the ground state and lowest excited state at a given filling factor. Nonetheless, the energy gaps that we extract (Fig. 3) are comparable to results from activation studies (*23*, *27*), which yielded $\Delta_{1/3} \approx$ 1.4 to 1.8 meV at 12 T and $\Delta_{4/3} \approx$ 1.4 meV at 35 T. A comparison to $\Delta_{4/3}$ at 35 T is difficult because of the discrepancy in field strength; however, extrapolating the linear slope we measure in $\Delta_{4/3}$ yields a value of ~2.8 meV at 35 T. At the highest available magnetic fields, our measured energy gaps are only slightly smaller than theoretical predictions at $\nu = 1/3$ but are 3 to 10 times smaller than those theoretically predicted at ν = 2/3, 4/3, 2/5, and 8/5 (table S1) (*9*, *10*, *12*, *15*, *16*, *21*, *32*). This discrepancy probably results in part from sample disorder, which smears out the cusps in $\mu(n)$ and, therefore, decreases the apparent step in chemical potential. The effects of disorder can be partially mitigated by linear extrapolation of the negative slope in $\mu(n)$ surrounding each fractional quantum Hall state (fig. S9) (*32*, *39*). The widths δn of the most

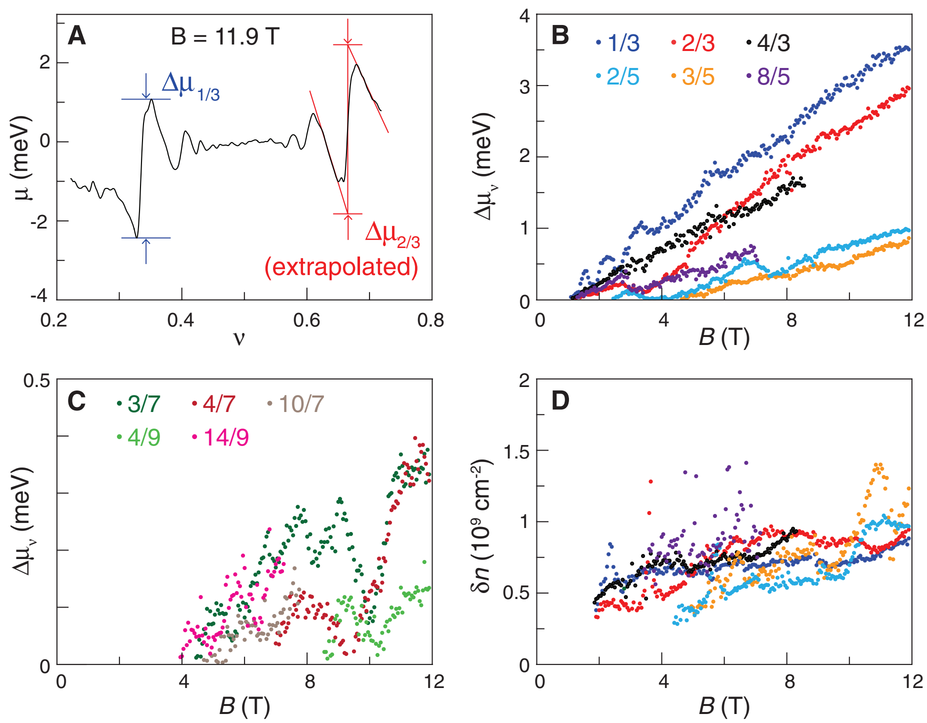

Fig. 3. Steps in chemical potential and incompressible peak widths. (**A**) Chemical potential relative to its value at $\nu = 1/2$ as a function of carrier density at 11.9 T. The step in chemical potential of each incompressible state is given by the difference in chemical potential between the local maximum and minimum (blue). Data presented in (B) and (C) were extracted using this method. (**B**) Steps in chemical potential associated with FQH states at measured multiples of $\nu = 1/3$ and 1/5 as a function of magnetic field. (**C**) Steps in chemical potential of FQH states at measured multiples of ν = 1/7 and 1/9 as a function of magnetic field. (**D**) Incompressible peak width of the FQH states as a function of magnetic field. Colors are same as in (B).

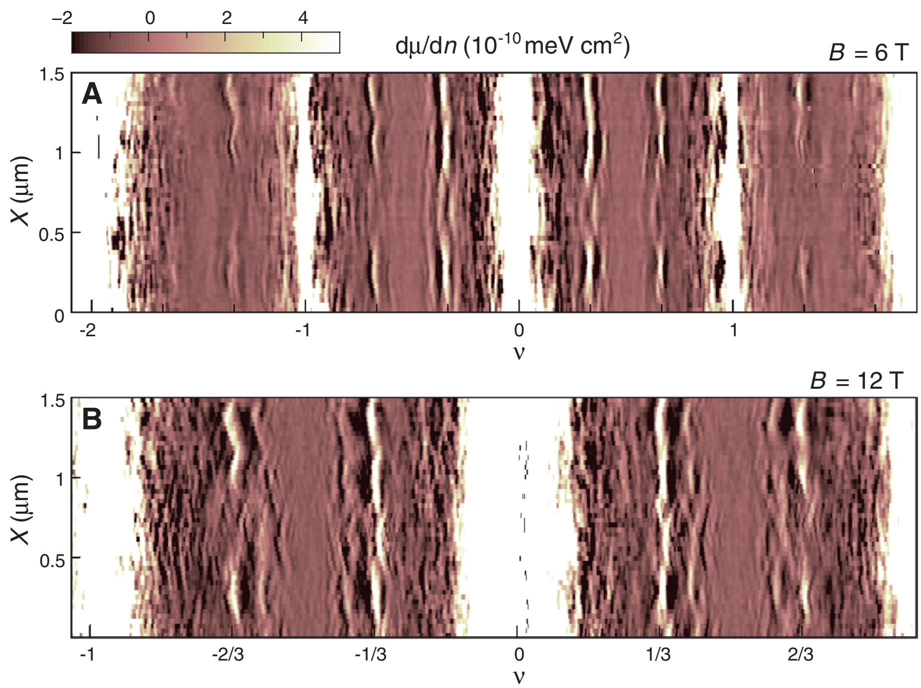

Fig. 4. Spatial dependence of FQH states. (**A**) $d\mu/dn$ as a function of filling factor and position X along the flake (red arrow in Fig. 1) at $B = 6$ T. (**B**) $d\mu/dn$ as a function of carrier density and position at $B = 12$ T. At both fields, we observe density fluctuations and variations in the strength of the FQH states as a function of position. States at $\nu = 2/3$ and $4/3$ appear more susceptible to disorder than does $\nu = 1/3$.

robust FQH states (Fig. 3D) were determined by fitting a Gaussian to the incompressible peak at each filling factor. They are only weakly dependent on magnetic field, suggesting that δn reflects the amount of local disorder in our device (*4*). The exceptionally small peak widths provide another indication that the sample is especially clean.

Together, the unconventional sequence and relative strengths of the FQH states provide insight into the interplay between electronic interactions and symmetry in graphene. Between $\nu = 0$ and 1, the compressibility is approximately symmetric about $\nu = 1/2$, suggesting that the fourfold spin and valley degeneracy is fully lifted. In contrast, the missing odd-numerator states indicate that one symmetry persists between $\nu = 1$ and 2. Nonetheless, the behavior in each regime exhibits some surprising similarities. Notably, the incompressible states that we observe above and below $\nu = 1$ have comparable energy gaps. Further study is necessary to elucidate the exact spin and valley ordering of each state; for example, tilted field measurements decouple Zeeman splitting from orbital effects and could provide insight into spin polarization.

All of the measurements described above were taken at one position. Line scans of the inverse compressibility as a function of filling factor and position at $B = 6$ and 12 T are shown in Fig. 4, A and B, respectively. The gate voltages at which the incompressible peaks occur vary with position, which can be explained by local density fluctuations. The magnitude of these fluctuations is similar to the width of the FQH states and may explain why the FQHE has been so difficult to observe in transport studies: Different regions of the sample form a given FQH state at different back-gate voltages. Figure 4 also shows that incompressible peak magnitude fluctuates substantially as a function of position. Although some incompressible states, such as those at $\nu = 1/3$, persist at virtually all positions, others are more susceptible to disorder. Both $\nu = 2/3$ and $4/3$ fully disappear in some locations, which seem to be correlated with the areas where the integer quantum Hall states are wider, a sign that local disorder is comparatively large. Despite the existence of disordered regions, the ability to perform local measurements reveals a multitude of FQH states in the cleanest areas. The observation of incompressible behavior at multiples of $\nu = 1/9$ indicates a substantial improvement in sample quality; together with the unconventional pattern of FQH states, this shows that graphene provides an especially rich platform in which to investigate correlated electronic states and their interplay with underlying symmetry.

References and Notes

1. K. Nomura, A. H. MacDonald, *Phys. Rev. Lett.* **96**, 256602 (2006).
2. K. S. Novoselov *et al.*, *Nature* **438**, 197 (2005).
3. Y. B. Zhang, Y. W. Tan, H. L. Stormer, P. Kim, *Nature* **438**, 201 (2005).
4. J. Martin *et al.*, *Nat. Phys.* **5**, 669 (2009).
5. D. C. Tsui, H. L. Stormer, A. C. Gossard, *Phys. Rev. Lett.* **48**, 1559 (1982).
6. R. B. Laughlin, *Phys. Rev. Lett.* **50**, 1395 (1983).
7. J. K. Jain, *Phys. Rev. Lett.* **63**, 199 (1989).
8. B. I. Halperin, *Helv. Phys. Acta* **56**, 75 (1983).
9. V. M. Apalkov, T. Chakraborty, *Phys. Rev. Lett.* **97**, 126801 (2006).
10. C. Tőke, P. E. Lammert, V. H. Crespi, J. K. Jain, *Phys. Rev. B* **74**, 235417 (2006).
11. M. O. Goerbig, N. Regnault, *Phys. Rev. B* **75**, 241405 (2007).
12. C. Tőke, J. K. Jain, *Phys. Rev. B* **75**, 245440 (2007).
13. K. Yang, S. Das Sarma, A. H. MacDonald, *Phys. Rev. B* **74**, 075423 (2006).
14. D. V. Khveshchenko, *Phys. Rev. B* **75**, 153405 (2007).
15. N. Shibata, K. Nomura, *Phys. Rev. B* **77**, 235426 (2008).
16. N. Shibata, K. Nomura, *J. Phys. Soc. Jpn.* **78**, 104708 (2009).
17. Z. Papić, M. O. Goerbig, N. Regnault, *Solid State Commun.* **149**, 1056 (2009).
18. Z. Papić, M. O. Goerbig, N. Regnault, *Phys. Rev. Lett.* **105**, 176802 (2010).
19. S. Modak, S. S. Mandal, K. Sengupta, *Phys. Rev. B* **84**, 165118 (2011).
20. Z. Papić, D. A. Abanin, Y. Barlas, R. N. Bhatt, *Phys. Rev. B* **84**, 241306 (2011).
21. C. Tőke, J. K. Jain, *J. Phys. Condens. Matter* **24**, 235601 (2012).
22. M. O. Goerbig, N. Regnault, *Phys. Scr. T* **146**, 014017 (2012).
23. F. Ghahari, Y. Zhao, P. Cadden-Zimansky, K. Bolotin, P. Kim, *Phys. Rev. Lett.* **106**, 046801 (2011).
24. K. I. Bolotin, F. Ghahari, M. D. Shulman, H. L. Stormer, P. Kim, *Nature* **462**, 196 (2009).
25. X. Du, I. Skachko, F. Duerr, A. Luican, E. Y. Andrei, *Nature* **462**, 192 (2009).
26. D. S. Lee, V. Skákalová, R. T. Weitz, K. von Klitzing, J. H. Smet, *Phys. Rev. Lett.* **109**, 056602 (2012).
27. C. R. Dean *et al.*, *Nat. Phys.* **7**, 693 (2011).
28. M. J. Yoo *et al.*, *Science* **276**, 579 (1997).
29. A. Yacoby, H. F. Hess, T. A. Fulton, L. N. Pfeiffer, K. W. West, *Solid State Commun.* **111**, 1 (1999).
30. Y. Zhang *et al.*, *Phys. Rev. Lett.* **96**, 136806 (2006).
31. Z. Jiang, Y. Zhang, H. L. Stormer, P. Kim, *Phys. Rev. Lett.* **99**, 106802 (2007).
32. Supplementary materials are available on *Science* Online.
33. K. Lai *et al.*, *Phys. Rev. Lett.* **93**, 156805 (2004).
34. N. C. Bishop *et al.*, *Phys. Rev. Lett.* **98**, 266404 (2007).
35. M. Padmanabhan, T. Gokmen, M. Shayegan, *Phys. Rev. Lett.* **104**, 016805 (2010).
36. M. Padmanabhan, T. Gokmen, M. Shayegan, *Phys. Rev. B* **80**, 035423 (2009).
37. M. Padmanabhan, T. Gokmen, M. Shayegan, *Phys. Rev. B* **81**, 113301 (2010).
38. J. P. Eisenstein, L. N. Pfeiffer, K. W. West, *Phys. Rev. Lett.* **68**, 674 (1992).
39. V. S. Khrapai *et al.*, *Phys. Rev. Lett.* **100**, 196805 (2008).

Acknowledgments: We thank M. T. Allen for useful discussions and for helping to current anneal the device and B. I. Halperin, D. Abanin, J. K. Jain, S. das Sarma, J. Martin, V. Venkatachalam, S. Hart, and G. Ben-Shach for helpful discussions. This work is supported by the U.S. Department of Energy, Office of Basic Energy Sciences, Division of Materials Sciences and Engineering, under award no. DE-SC0001819. J.H.S. and B.K. acknowledge financial support from the Deutsche Forschungsgemeinschaft graphene priority program, and B.K. acknowledges financial support from the Bayer Science and Education Foundation. This work was performed in part at the Center for Nanoscale Systems (of Harvard Univ.), a member of the National Nanotechnology Infrastructure Network, which is supported by the NSF under award no. ECS-0335765.

Supplementary Materials

www.sciencemag.org/cgi/content/full/337/6099/1196/DC1
Materials and Methods
Supplementary Text
Figs. S1 to S10
Table S1
References (*40–43*)

16 May 2012; accepted 25 July 2012
10.1126/science.1224784

Electron Small Polarons and Their Mobility in Iron (Oxyhydr)oxide Nanoparticles

Jordan E. Katz,[1,2]* Xiaoyi Zhang,[3] Klaus Attenkofer,[3]† Karena W. Chapman,[3] Cathrine Frandsen,[4] Piotr Zarzycki,[5,6] Kevin M. Rosso,[5]‡ Roger W. Falcone,[2] Glenn A. Waychunas,[1] Benjamin Gilbert[1]‡

Electron mobility within iron (oxyhydr)oxides enables charge transfer between widely separated surface sites. There is increasing evidence that this internal conduction influences the rates of interfacial reactions and the outcomes of redox-driven phase transformations of environmental interest. To determine the links between crystal structure and charge-transport efficiency, we used pump-probe spectroscopy to study the dynamics of electrons introduced into iron(III) (oxyhydr)oxide nanoparticles via ultrafast interfacial electron transfer. Using time-resolved x-ray spectroscopy and ab initio calculations, we observed the formation of reduced and structurally distorted metal sites consistent with small polarons. Comparisons between different phases (hematite, maghemite, and ferrihydrite) revealed that short-range structural topology, not long-range order, dominates the electron-hopping rate.

Many important geochemical and biogeochemical redox reactions are linked to the formation or transformation of iron oxide and oxyhydroxide minerals by charge-transfer processes that cycle iron between its two common oxidation states (*1*). Because iron(II) is substantially more soluble than iron(III), reductive transformations of iron(III) (oxyhydr)oxides can dramatically affect the chemistry and mineralogy of soils and surface waters (*2*). However, it remains difficult to predict the outcome of even some common reactions of these minerals. For example, after the exposure of iron(III) (oxyhydr)oxides to reducing agents, interfacial electron transfer (ET) can lead to release of iron(II) (dissolution), formation of alternative iron(III) or mixed-valence phases (transformation), or particle growth (*3*–*5*). Qualitatively, it is known that such diverse behavior is due to the coupling of interfacial redox reactions and interior charge conduction processes (*6*), but it is unclear how this interplay directs these biogeochemical outcomes. Mineral redox reactions are complex, and it is typically unknown whether interfacial charge transfer, interior conduction, or steps such as bond breaking are rate limiting. We sought to measure the mobility of electrons transferred into iron(III) oxides by using time-resolved spectroscopy.

There is an established model describing electrons in materials such as iron oxides that are characterized by short-range metal-ligand bonding (*7*). In this model, conduction band states are highly localized because of strong electron-phonon interactions that stabilize charge carriers in a lattice distortion (*8*, *9*). Specifically, electrons introduced into an iron oxide become localized in unfilled metal three-dimensional states, polarize neighboring atoms, and distort the local structure, forming polarons. Because the coupling with phonons is very strong, the polaron radius is small, on the order of a lattice constant, as depicted in Fig. 1A. These electron small polarons are effectively a localized lower-valence metal site, and conduction occurs through thermally activated electron hopping from one metal site to the next. The small-polaron model is widely used for describing conduction in many semiconductors and insulators, but support for the model is typically indirect, derived from agreement between theory and measurements such as optical spectroscopy (*10*) or temperature-dependent conductivity (*11*, *12*). If Arrhenius analysis reveals the existence of an activation-energy for charge transport, then phenomenological macroscopic transport models furnish an effective elementary hopping rate. For certain material classes, electron localization throughout the material accompanied by Jahn-Teller distortion marks a transition from metallic to a polaronic insulator phase (*13*). However, for most materials in which small-polaron formation is posited, the density of these charge carriers is too low for bulk structural analyses; alternative methods are required to characterize them at a structural level.

We have developed a pump-probe approach to study iron(III) phases with excess electrons and the dynamics of electron transport across multiple time scales (*14*). In the pump step, laser-initiated interfacial ET reduces a fraction of iron atoms at the surface of iron(III) (oxyhydr)oxide nanoparticles sensitized by the dye molecule 2′,7′-dichlorofluorescein (27DCF). In the probe step, time-resolved x-ray absorption spectroscopy (XAS) at the Fe K-edge is used to monitor the oxidation state and coordination geometry (*15*, *16*) of the iron sites affected by interfacial ET. This approach was inspired by research on dye-sensitized semiconductor nanomaterials (*17*) and informed by numerous accomplishments in ultrafast science, including optical-pump–x-ray probe studies of transient electronic and structural configurations in organometallic cluster compounds (*18*–*21*). Here, we report measurements of the mobility of excess electrons introduced into three phases of iron(III) (oxyhydr)oxide. We studied two crystalline phases, maghemite (γ-Fe_2O_3) nanoparticles with average diameter 3.4 nm and 7-nm hematite (α-Fe_2O_3). Additionally, we studied 3-nm 2-line ferrihydrite, an environmentally (*22*) and physiologically (*23*) important nanophase. Synthesis methods were optimized in order to achieve the smallest-size nanoparticles without impurity phases and with particle size distributions below 15%, as confirmed by means of x-ray diffraction and electron microscopy (figs. S1 to S4). Nanoparticle samples were studied in aqueous suspension at pH 4 with or without surface-bound 27DCF.

Continuous illumination of suspensions of all phases of 27DCF-coated nanoparticles caused the generation of dissolved iron(II) (fig. S5). We studied the electron injection process by means

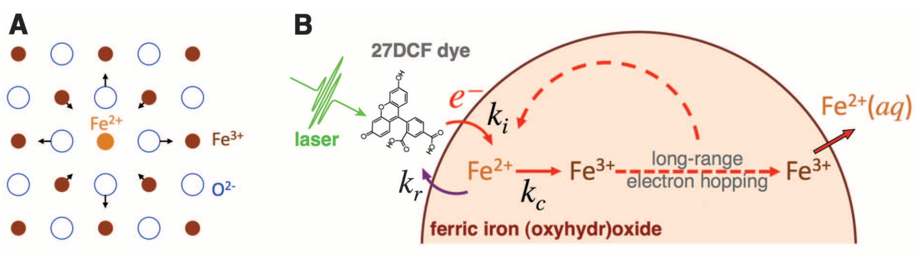

Fig. 1. (**A**) Illustration of a small polaron in iron oxide—the local structural distortion created by the reduction of an iron(III) site. (**B**) Scheme of the ET pathways after light-initiated interfacial ET from a surface-bound dye molecule to a iron(III) oxide or oxyhydroxide nanoparticle in aqueous suspension. The electron-transfer rate constants k_i, k_r, and k_c are associated with interfacial ET, recombination, and internal conduction (by hopping to an adjacent iron neighbor), respectively.

[1]Earth Sciences Division, Lawrence Berkeley National Laboratory, Berkeley, CA 94720, USA. [2]Department of Physics, University of California, Berkeley, Berkeley, CA 94720, USA. [3]X-ray Science Division, Argonne National Laboratory, Argonne, IL 60439, USA. [4]Department of Physics, Technical University of Denmark, Copenhagen 2800 Kongens Lyngby, Denmark. [5]Chemical and Materials Sciences Division, Pacific Northwest National Laboratory (PNNL), Richland, WA 99354, USA. [6]Institute of Physical Chemistry, Polish Academy of Sciences, Warsaw 01-224, Poland.

*Present address: Department of Chemistry and Biochemistry, Denison University, Granville, OH 43023, USA.
†Present address: Brookhaven National Laboratory, Upton, NY 11973, USA.
‡To whom correspondence should be addressed. E-mail: bgilbert@lbl.gov (B.G.); kevin.rosso@pnnl.gov (K.M.R.)

of ultrafast optical transient-absorption (TA) spectroscopy using 520-nm wavelength, 130-fs duration excitation pulses and a broadband visible probe (supplementary materials). The excitation wavelength was chosen for maximum absorption by the bound dye. Unavoidably, a fraction of the excitation intensity was also absorbed by the nanoparticles, generating electron-hole pairs that were characterized separately by studies of bare nanoparticles. All uncoated nanoparticles gave an optical TA response with a lifetime less than 200 ps (fig. S6) interpreted as nonradiative recombination of electron-hole pairs (*24*).

The optical TA data for all 27DCF-coated nanoparticles exhibited significantly longer time-scale dynamics than uncoated nanoparticles, as illustrated for hematite in Fig. 2. The TA data are interpreted as a sum of contributions from different states of the sample after photoexcitation (supplementary materials). The absorption band appearing around 460 nm is attributed to surface-bound 27DCF that has lost one electron through interfacial ET ($27DCF^+$). The suppression of absorption strength from 490 to 550 nm represents bleaching of the dye ground state. The signatures of $27DCF^+$ and the ground-state bleach show a similar decay rate, indicating that some photo-injected electrons recombine with $27DCF^+$ on the nanosecond time scale. (Band gap excitations of the nanoparticles also contributed to the transient response in this wavelength range but could be distinguished by their much faster recombination dynamics.) The rate of interfacial ET cannot be identified at 460 nm through the appearance of the $27DCF^+$ signal because we cannot distinguish it from the neutral photoexcited dye, 27DCF* (*25*). However, the spectral feature in the 490- to 550-nm range additionally exhibits a sub-picosecond decay immediately after photoexcitation. Global fitting analysis shows that the transient spectrum associated with this early time scale is consistent with the fluorescence of 27DCF*, whereas all later transient spectra are dominated by the loss of ground-state absorption (Fig. 2B, inset). The sub-picosecond transient thus represents the decay of stimulated emission (SE) and is strong evidence of electron loss from 27DCF* via interfacial ET. For all 27DCF-coated nanoparticles, SE decay and hence interfacial ET occurred with time constants from 200 to 250 fs, which is close to the rate measured for 27DCF on TiO_2 (*26*). Thus, laser-initiated interfacial ET is much faster than the subsequent spontaneous ET processes described below.

Time-resolved XAS characterized the solid-phase species generated by interfacial ET (supplementary materials). For each sample, ground-state Fe K-edge XA spectra are shown in Fig. 3A, and transient XA spectra acquired 150 ps after ET (Fig. 3B), which is reported as a difference relative to the ground-state spectrum (ΔXA). Although the magnitudes of the ΔXA spectra are small (≤2% of ground-state absorbance), these spectra were observed reproducibly during our studies of dye-sensitized nanoparticles (21 samples analyzed). No ΔXA spectrum above the noise was detectable for any control (fig. S8A). XAS analysis and chemical assays of the samples after reaction showed the gradual accumulation of dissolved aqueous iron(II) (figs. S5 and S13).

All ΔXA are dominated by a positive feature that is at lower energy than the ground-state threshold, which is consistent with a model in which light-initiated ET reduced Fe^{3+} to Fe^{2+} (*16*). The Fe^{3+}/Fe^{2+} K-edge chemical shift for iron that is octahedrally coordinated by oxygen is typically observed to be -1.4 ± 0.1 eV (*27*). Thus, to model iron reduction without associated structural change we simulated ΔXA spectra by mixing the ground-state spectrum in a 99:1 proportion with a duplicate to which this energy shift was applied. The resulting spectra do not match the experimental transient spectra well for any phase, indicating that structural change accompanies reduction. Because the chemical reduction of both maghemite (*28*) and ferrihydrite (*29*) can induce transformation to the mixed-valence inverse spinel magnetite, Fe_3O_4, we tested whether light-initiated ET led to the formation of magnetite domains but again obtained poor matches to the experimental data. Magnetite and maghemite differ in oxygen stoichiometry as well as iron valence, and the poor agreement indicates that atom diffusion to achieve local charge balance and the nucleation of a new mineral phase does not occur within 150 ps (*30*). Thus, interfacial ET causes iron reduction and a structural change that is less extensive than a complete phase change.

We next developed a theoretical approach to test whether the transient spectra observed for hematite and maghemite were consistent with the formation of small polarons in these phases. We used ab initio calculations for periodic systems to predict the distortion in the local structure of an iron(II) site using methods similar to previous work (*9*). Briefly, an extra electron was localized on an iron cation in the ground state, and all atomic coordinates were energy-minimized self-consistently with the wave function until converged. The small-polaron structure was defined relative to the atomic coordinates calculated for a completely iron(III) lattice. The consequences of structural distortion for XAS were investigated by using a full multiple scattering code (*31*) that has been used successfully to interpret metal K-edge spectra (*32*). Simulation parameters were chosen that optimized the agreement between calculated and experimental data for ground-state hematite and maghemite. The XAS

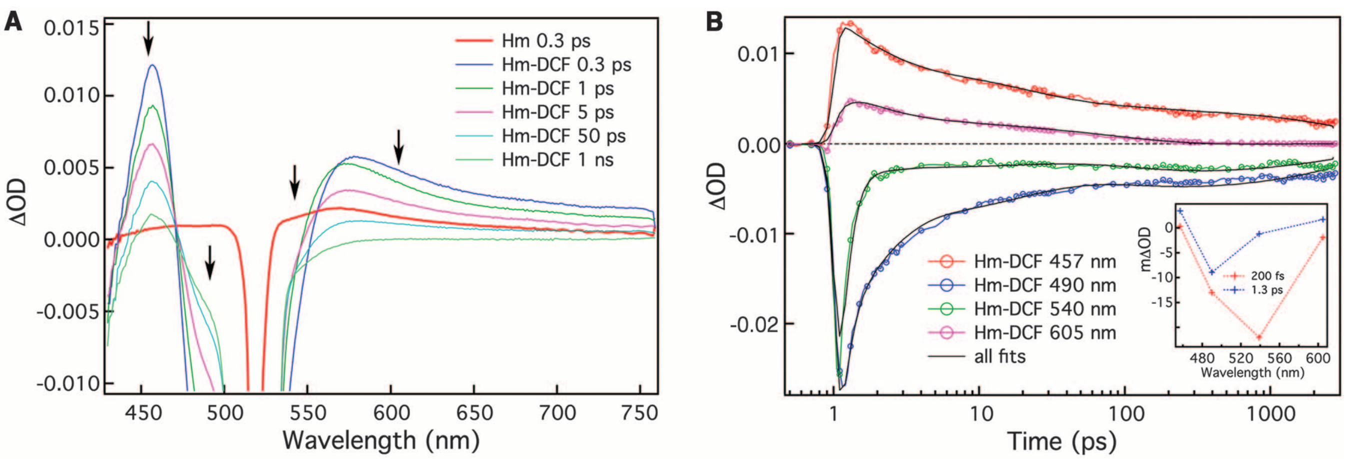

Fig. 2. (**A**) Optical TA spectrum of uncoated hematite (Hm) at 0.3-ps delay after photoexcitation at 520 nm compared with TA spectra of 27DCF-coated hematite nanoparticles (Hm-DCF) at the indicated delays. Arrows indicate the wavelengths at which kinetics curves in (B) were extracted. (**B**) Transient kinetics observed for uncoated and 27DCF-coated hematite nanoparticles at the wavelengths indicated in (A). Also plotted are best-fit transients obtained through global analysis of the Hm-DCF curves with three exponential time constants and one offset. The time axis was shifted 1 ps for plotting on a logarithmic scale. (Inset) Wavelength-dependent amplitudes of the two fastest decay time constants: The transient spectrum that decays in the first 200 fs is consistent with stimulated emission from the excited state of the dye and indicates that interfacial ET occurs on this time scale. The 1.3-ps spectrum is associated with ground-state bleach of the dye and thus represents early interfacial recombination on this time scale. Ground-state absorption and emission spectra are shown in fig. S3.

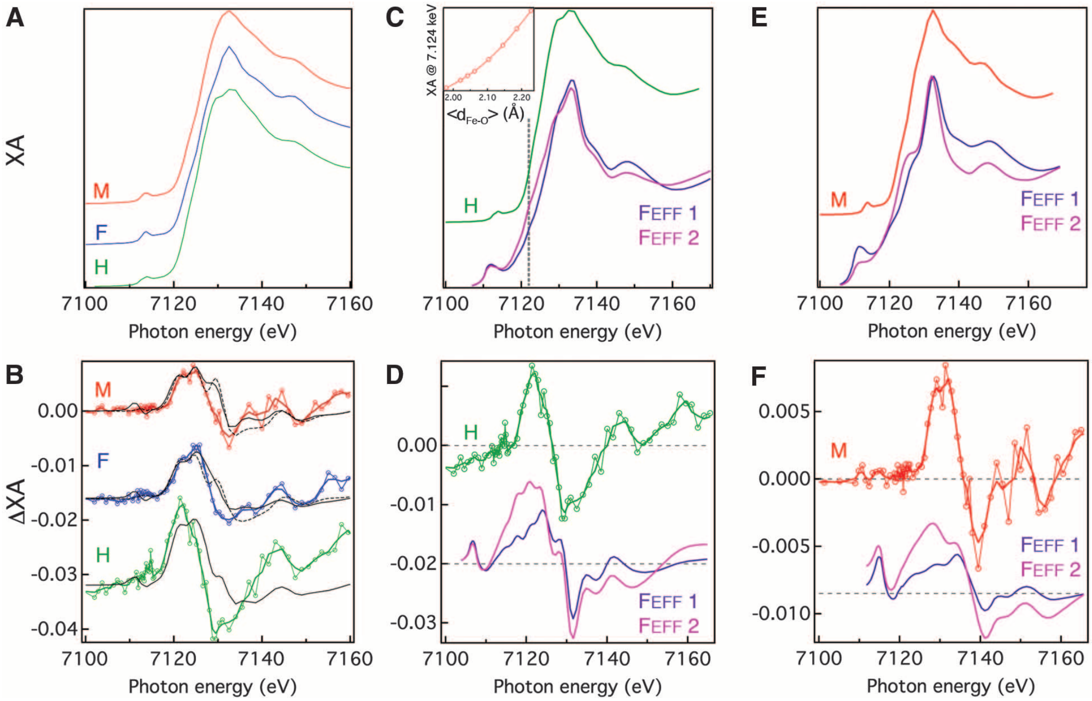

Fig. 3. Iron K-edge XA spectroscopic observation of reduced iron sites in three phases of iron (oxyhydr)oxide nanoparticles: maghemite (M), ferrihydrite (F), and hematite (H). (**A**) Ground state XA spectra of 27DCF-sensitized nanoparticles in suspension. (**B**) Difference (ΔXA) spectra acquired 150 ps after light-initiated ET. The raw (markers) and three-point smoothed (thick lines) data are compared with model spectra obtained by combining the ground-state reference with either a magnetite reference (dashed black lines) or a copy of the ground-state spectrum shifted –1.4 eV to simulate valence change without structural relaxation (solid black lines). (**C**) Comparison of the experimental Fe K-edge XA spectra for hematite with calculated spectra for ground-state hematite (FEFF 1) and for a locally distorted small-polaron site in hematite (FEFF 2) obtained from ab initio structure prediction. (Inset) The calculated on-threshold intensity exhibits high sensitivity to first-shell Fe-O bond length. (**D**) Comparison of the transient hematite ΔXA spectrum with calculated spectra for reduced sites without structural relaxation (FEFF 1) and for reduced and structurally distorted sites (FEFF 2). (**E** and **F**) Comparison of corresponding experimental and simulated spectra for the maghemite phase.

calculations reproduce most features in the ground-state spectra (Fig. 3, C and E, and fig. S15). However, there are evident discrepancies in lineshape broadening and energy position that are greater in magnitude than the transient differences observed in the time-resolved spectra. Consequently, we refined the goal of the simulation study not to reproduce precisely the ΔXA data but to test whether small-polaron formation is a plausible interpretation of the observed lineshapes.

We calculated theoretical ΔXA spectra for reduced Fe sites in hematite and maghemite with or without the structural distortion predicted by simulation (Fig. 3, D and F). For both phases, the calculations predicted that small-polaron formation enhanced the intensity of the key feature of the ΔXA spectra. We sought to understand the structural origin of this feature (fig. S16), finding it to be highly sensitive to the Fe-O bond length (Fig. 3C, inset). As illustrated in Fig. 1A, bond length expansion is the major predicted feature of small-polaron formation, with a ~4% increase in hematite.

The experimental data and simulations provide strong evidence for the small-polaron model by identifying key electronic and structural features of this state after it has formed. Although measurements with sub-picosecond resolution (*15*) will be required to follow small-polaron formation, our measurements of the iron(II) lifetime on the nanosecond and microsecond time scales allowed electron mobility to be quantified. We determined the loss of iron(II) by monitoring the intensity of the transient ΔXA signal at 7.125 keV

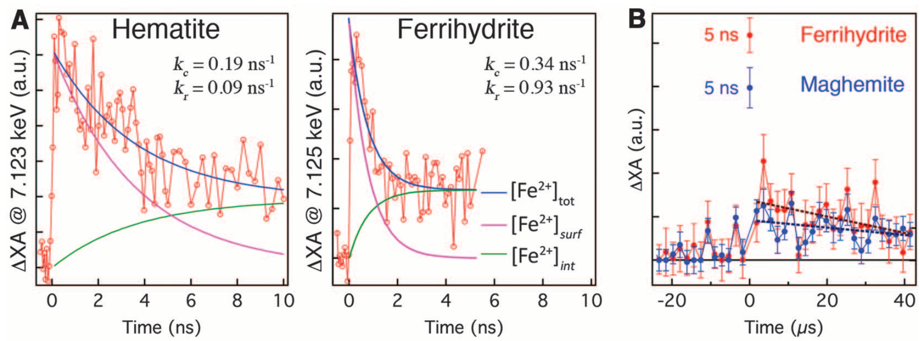

Fig. 4. (**A**) Experimental kinetics curves showing the creation and loss of iron(II) in hematite and ferrihydrite nanoparticles. Maghemite nanosecond kinetics data are given in fig. S8b. Fits to a three-site, two-exponential model are used to obtain k_c and k_r. Errors in the fitted constants are ± 0.05 ns^{-1} or less. (**B**) Experimental kinetic curves showing the presence and continued loss of iron(II) at the microsecond time scale, compared with the iron(II) signals at 5 ns.

(Fig. 4). The iron(II) concentration exhibits a biphasic decay, initially dropping to ~30% of the initial value within ~2 ns [ferrihydrite and maghemite (fig. S8B)] or ~10 ns (hematite). We fitted the nanosecond–time scale kinetics data with a three-site model for the location of an electron transferred to a surface iron site after dye excitation and determined two intrinsic ET rates from fits of the nanosecond kinetics for all phases: k_c, the rate at which electrons at a surface site hop away from the ET site, and k_r, the recombination rate (Fig. 1B). For hematite, $k_c = 0.19 \pm 0.04$ ns^{-1}, a value within the range predicted by ab initio simulations of small-polaron–mediated electron conduction in bulk hematite (*33*). For both ferrihydrite and maghemite, $k_c = 0.34 \pm 0.09$ ns^{-1}. It is surprising that the electron-hopping rates are the same for maghemite, a well-characterized crystal phase, and ferrihydrite, a disordered nanomaterial for which a new structural model (*22*) is debated (*34*, *35*). The finding adds weight to the suggestion that these phases may contain similar structural elements but with alternative long-range organization (*36*). For the maghemite phase, analysis of the site-specific contributions to the ground and transient spectra revealed that both octahedral and tetrahedral iron sites contributed to conductivity at room temperature, in a proportion corroborated by the ab initio calculations (supplementary materials).

The ability to probe electron small polarons is a first step toward experimentally distinguishing the multiple steps that comprise redox transformations of iron (oxyhydr)oxides and measuring their rates. The small-polaron hopping rate is a fundamental mineral phase–dependent limit on the kinetics of many iron redox reactions. As shown in Fig. 4B, we additionally observed iron(II) in the nanoparticles at microsecond time scales, representing itinerant electrons that were trapped within the iron oxides before leaving either by dissolution or recombination. Complementing the present measurements of hopping rates with rates of additional steps, such as bond breaking or the nucleation of new mineral phase, will enable more detailed mechanistic descriptions of the reductive dissolution of iron(III) (oxyhydr)oxides and other important environmental reactions. We anticipate that the combination of transient-absorption spectroscopy, conventional kinetics measurements, and ab initio and kinetic modeling offers a framework for this program.

References and Notes

1. W. Stumm, B. Sulzberger, *Geochim. Cosmochim. Acta* **56**, 3233 (1992).
2. H. D. Pedersen, D. Postma, R. Jakobsen, *Geochim. Cosmochim. Acta* **70**, 4116 (2006).
3. O. Larsen, D. Postma, *Geochim. Cosmochim. Acta* **65**, 1367 (2001).
4. C. M. Hansel, S. G. Benner, S. Fendorf, *Environ. Sci. Technol.* **39**, 7147 (2005).
5. H. D. Pedersen, D. Postma, R. Jakobsen, O. Larsen, *Geochim. Cosmochim. Acta* **69**, 3967 (2005).
6. S. V. Yanina, K. M. Rosso, *Science* **320**, 218 (2008).
7. P. A. Cox, *Transition Metal Oxides: An Introduction to Their Electronic Structure and Properties* (Oxford Univ. Press, New York, 2010).
8. T. Holstein, *Ann. Phys.* **8**, 343 (1959).
9. K. M. Rosso, M. Dupuis, *J. Chem. Phys.* **120**, 7050 (2004).
10. J. Ederth, A. Hoel, G. A. Niklasson, C. G. Granqvist, *J. Appl. Phys.* **96**, 5722 (2004).
11. A. S. Alexandrov, N. F. Mott, *Polarons and Bipolarons* (World Scientific, Singapore, 1996).
12. I. Djerdj *et al.*, *J. Am. Chem. Soc.* **130**, 11364 (2008).
13. N. Mannella *et al.*, *Phys. Rev. Lett.* **92**, 166401 (2004).
14. J. E. Katz *et al.*, *J. Phys. Chem. Lett.* **1**, 1372 (2010).
15. Ch. Bressler *et al.*, *Science* **323**, 489 (2009).
16. G. A. Waychunas, M. J. Apted, G. E. Brown Jr., *Phys. Chem. Miner.* **10**, 1 (1983).
17. M. Grätzel, *Nature* **414**, 338 (2001).
18. C. Bressler, M. Chergui, *Chem. Rev.* **104**, 1781 (2004).
19. L. X. Chen, *Annu. Rev. Phys. Chem.* **56**, 221 (2005).
20. A. Cannizzo *et al.*, *Coord. Chem. Rev.* **254**, 2677 (2010).
21. J. Chen *et al.*, *J. Phys. Chem. A* **111**, 9326 (2007).
22. F. M. Michel *et al.*, *Science* **316**, 1726 (2007).
23. J. M. Cowley, D. E. Janney, R. C. Gerkin, P. R. Buseck, *J. Struct. Biol.* **131**, 210 (2000).
24. N. J. Cherepy, D. B. Liston, J. A. Lovejoy, H. Deng, J. Z. Zhang, *J. Phys. Chem. B* **102**, 770 (1998).
25. G. Benkö, M. Hilgendorff, A. P. Yartsev, V. Sundström, *J. Phys. Chem. B* **105**, 967 (2001).
26. M. Hilgendorff, V. Sundström, *J. Phys. Chem. B* **102**, 10505 (1998).
27. M. Wilke, F. Farges, P.-E. Petit, G. E. Brown Jr., F. Martin, *Am. Mineral.* **86**, 714 (2001).
28. U. Colombo, G. Fagheraz, F. Gazzarrini, G. Lanzavecchia, G. Sironi, *Nature* **219**, 1036 (1967).
29. E. Tronc, P. Belleville, J. P. Jolivet, J. Livage, *Langmuir* **8**, 313 (1992).
30. J. Tang, M. Myers, K. A. Bosnik, L. E. Brus, *J. Phys. Chem. B* **107**, 7501 (2003).
31. A. L. Ankudinov, B. Ravel, J. J. Rehr, S. D. Conradson, *Phys. Rev. B* **58**, 7565 (1998).
32. B. Gilbert *et al.*, *J. Phys. Chem. A* **107**, 2839 (2003).
33. N. Iordanova, M. Dupuis, K. M. Rosso, *J. Chem. Phys.* **122**, 144305 (2005).
34. A. Manceau, *Clay Miner.* **44**, 19 (2009).
35. D. G. Rancourt, J. F. Meunier, *Am. Mineral.* **93**, 1412 (2008).
36. W. Xu *et al.*, *Am. Mineral.* **96**, 513 (2011).

Acknowledgments: Time-resolved x-ray transient spectroscopy was performed at beamline 11-ID-D at the Advanced Photon Source (APS). Laser facilities at 11-ID-D were provided by the Solar Energy Conversion group of Chemical Sciences and Engineering Division of Argonne National Laboratory, which is funded through New Facility and Mid-scale Instrumentation grants to L. X. Chen *et al*. We thank L. X. Chen, G. Jennings, and C. Kurtz. PDF analysis was performed at beamline 11-ID-B at the APS. Transient absorption spectroscopy was performed at the Argonne Center for Nanoscale Materials (CNM), and we thank G. Wiederrecht and D. Gosztola. This work was supported by the Chemical Imaging program of the U.S. Department of Energy, Office of Science, and Office of Basic Energy Sciences (DOE-BES), under contract DE-AC02-05CH11231. K.M.R. and P.Z. gratefully acknowledge support from DOE-BES Geosciences program to PNNL. C.F. acknowledges support from the Danish Council for Independent Research. Use of the APS and the CNM is supported by DOE-BES under contract DE-AC02-06CH11357.

Supplementary Materials
www.sciencemag.org/cgi/content/full/337/6099/1200/DC1
Materials and Methods
Supplementary Text
Figs. S1 to S16
Table S1
References (*37–50*)

20 April 2012; accepted 11 July 2012
10.1126/science.1223598

Photo-Tautomerization of Acetaldehyde to Vinyl Alcohol: A Potential Route to Tropospheric Acids

Duncan U. Andrews,* Brianna R. Heazlewood,*† Alan T. Maccarone,‡ Trent Conroy, Richard J. Payne, Meredith J. T. Jordan,§ Scott H. Kable§

Current atmospheric models underestimate the production of organic acids in the troposphere. We report a detailed kinetic model of the photochemistry of acetaldehyde (ethanal) under tropospheric conditions. The rate constants are benchmarked to collision-free experiments, where extensive photo-isomerization is observed upon irradiation with actinic ultraviolet radiation (310 to 330 nanometers). The model quantitatively reproduces the experiments and shows unequivocally that keto-enol photo-tautomerization, forming vinyl alcohol (ethenol), is the crucial first step. When collisions at atmospheric pressure are included, the model quantitatively reproduces previously reported quantum yields for photodissociation at all pressures and wavelengths. The model also predicts that 21 ± 4% of the initially excited acetaldehyde forms stable vinyl alcohol, a known precursor to organic acid formation, which may help to account for the production of organic acids in the troposphere.

Organic acids are important trace components of the troposphere, with estimates ranging from 60 to 120 megatonnes formed per year (*1*, *2*). However, the mechanism responsible for producing these acids is incomplete (*2–5*); current models underpredict their production by about a factor of two (*1*), implying a missing acid precursor (*2*). Recently, there has been interest in enols as efficient precursors for the formation of organic acids (*4*, *5*). Archibald *et al*. (*4*) modeled the atmospheric fate of enols and concluded that the production of formic acid (HCOOH) was significantly enhanced by their inclusion into the model. However, a viable atmospheric source of enols has not been suggested. We present evidence that photo-induced keto-enol tautomerization occurs under atmospheric conditions and provides such a source.

Carbonyl compounds feature centrally in all atmospheric oxidation pathways (*6*). Their role toward the end of the oxidation pathway is also clear, with measurable concentrations of acetaldehyde and acetone present in smog chambers (*7*). The atmospheric photochemistry of carbonyls seems uncontroversial. In the case of acetaldehyde, there are only two reactions that are important in the troposphere, where photochemistry is limited to wavelengths $\lambda > 295$ nm (*8*).

$$CH_3CHO + h\nu \rightarrow CH_3 + HCO \quad (1)$$

$$\rightarrow CH_4 + CO \quad (2)$$

Under atmospheric conditions, the photolysis quantum yield of acetaldehyde via reactions 1 and 2 is $\phi_{ph} = 14\%$ (vide infra). Atmospheric models assume implicitly that the other 86% of molecules collisionally cool, reverting to thermalized acetaldehyde. We demonstrate experimentally

School of Chemistry, University of Sydney, NSW, 2006, Australia.

*These authors contributed equally to this work.

†Present address: Department of Chemistry, University of Oxford, Oxford, OX1 3QZ, UK.

‡Present address: Department of Chemistry, University of Wollongong, NSW, 2522, Australia.

§To whom correspondence should be addressed. E-mail: scott.kable@sydney.edu.au (S.H.K.); m.jordan@chem.usyd.edu.au (M.J.T.J.)

and theoretically that photo-induced keto-enol tautomerization of acetaldehyde to vinyl alcohol (VA) is significant under collision-free conditions. Under atmospheric conditions, we predict that VA will constitute a significant fraction of the photochemical product yield and propose that photo-tautomerization might be responsible for a significant concentration of organic acids unaccounted for in current models.

A detailed description of the experiments can be found in the supplementary materials. In brief, CH_3CDO, cooled in a supersonic expansion of helium, was photolysed at a variety of wavelengths using a laser. The production of formyl fragments was measured by laser-induced fluorescence. Isotopic labeling allows a more thorough investigation of the reaction mechanism. Specifically, direct photolysis products can be distinguished from indirect products that require isomerization to CH_2DCHO; for example, reaction 1 manifests direct and indirect channels 1a and 1b, respectively.

$$CH_3CDO + h\nu \rightarrow CH_3 + DCO \qquad (1a)$$

$$CH_2DCHO \rightarrow CH_2D + HCO \qquad (1b)$$

Figure 1A shows two action spectra of the $S_1 \leftarrow S_0$ (n,π^*) electronic transition of CH_3CDO that were obtained by monitoring the production of DCO or HCO photoproducts while scanning the photolysis wavelength. The vibrational structure is the same; however, the intensities are clearly different, reflecting the changing quantum yield for direct (ϕ_{1a}) versus indirect (ϕ_{1b}) products as a function of wavelength. The ratio of indirect to total formyl yields, ϕ_{1b}/ϕ_1, derived from these intensities is plotted in Fig. 1B, as explained in the supplementary materials.

At $\lambda > 320$ nm, photolysis can only occur on the ground S_0 state, following internal conversion from S_1, and here ϕ_{1b}/ϕ_1 falls slowly from 20% at 330 nm to 12% at 320 nm. At 320 nm, there is a sudden decrease in ϕ_{1b}, indicated by an exponential function in the figure. This arises because of intersystem crossing from S_1 to T_1. On the triplet surface reaction 1b cannot occur, whereas reaction 1a becomes increasingly dominant at higher energy (*9–11*), with ϕ_{1b}/ϕ_1 falling to ≈0 by 312 nm.

The production of HCO and DCO on S_0 was modeled by calculating transition state theory (TST) or variational TST rate constants for every isomerization and dissociation process. These calculations mirror those that we published (*9*) for another isotopolog of acetaldehyde, CD_3CHO, and so an extensive description of the theoretical methods is left to the supplementary materials. Table S1 lists the critical energies, and table S2 presents a set of rate constants at a typical energy.

A collision-free master equation (ME) analysis was then used to calculate the population of each species as a function of time, with final populations numerically converged to <1%. More details of the ME modeling are provided as supplementary materials. Figure S2 shows the evolution of population with time for photolysis at 320 nm. When the reaction is complete, the main products are $CO + CH_3D$ ($\phi_2 = 15\%$) and formyl + methyl radicals ($\phi_1 = 85\%$) partitioned as direct products ($\phi_{1a} = 70\%$) and indirect products ($\phi_{1b} = 15\%$). Experimentally, at 320 nm, $\phi_1/\phi_2 = 6$ when extrapolated to zero pressure (*12*), in excellent agreement with the 85/15 ratio above. The calculations reveal that the dominant mechanism for reaction 1b, with >90% of the flux, is the isomerization pathway shown in Fig. 2.

The calculated yields ϕ_{1a} and ϕ_{1b} at zero pressure are benchmarked by our experimental data, also under conditions of few collisions. The solid line in Fig. 1B shows the calculated ratio of ϕ_{1b}/ϕ_1 as a function of wavelength. Triplet reaction is not included in the model, so it cannot reproduce the rapid fall-off observed for $\lambda < 320$ nm. The model slightly overestimates ϕ_{1b}; however, the wavelength dependence is reproduced. ϕ_{1b} is very sensitive to the height of the enol-carbene isomerization barrier shown in Fig. 2. If this barrier is raised by only 2 kJ/mol, ϕ_{1b} is reduced, as shown by the dotted curve in Fig. 1B, which provides an excellent fit to the experiments at all energies below the T_1 threshold. A correction of 2 kJ/mol is well within the uncertainty in the calculated barrier height, estimated to be ±5 kJ/mol, based on the level of theory of the calculation. Our model for the collision-free decomposition of CH_3CDO now reproduces quantitatively the relative quantum yield of both chemical channels, ϕ_1 and ϕ_2, and direct versus indirect products, ϕ_{1a} and ϕ_{1b}, validating the critical aspects of the kinetic model.

The pressure dependence of acetaldehyde photolysis was modeled using a one-dimensional ME simulation, as implemented in the MultiWell program package (*13–15*), employing an exponential down collisional energy-transfer model and Lennard-Jones collision frequencies with N_2 at 300 K. The average downward collisional energy transfer is taken to be $\langle \Delta E_{down} \rangle = 150$ cm^{-1}, as described in the supplementary materials and as used previously (*16*). We assume that vibration to rotational/translational (V-R,T) energy transfer dominates because N_2 has a high vibrational frequency. We also assume $\langle \Delta E_{down} \rangle$ is independent of energy; we are only interested in collisional deactivation above the keto-enol tautomerization barrier (>282 kJ/mol) where the density of vibrational states is large. The rate of energy transfer below this barrier only affects how quickly the stable products are thermalized, not the final distribution of products.

The ME model is benchmarked to experiments of Horowitz and Calvert (HC) (*12*) and Moortgat *et al*. (MMW) (*17*). The wavelength dependence of ϕ_{ph} is shown in Fig. 3A, which also shows that the selected $\langle \Delta E_{down} \rangle = 150$ cm^{-1} provides the best fit to experiment. For $\lambda > 300$ nm, the model reproduces the experiments well, but it overestimates ϕ_{ph} at $\lambda < 300$ nm. At higher photolysis energies, quenching on T_1 should be

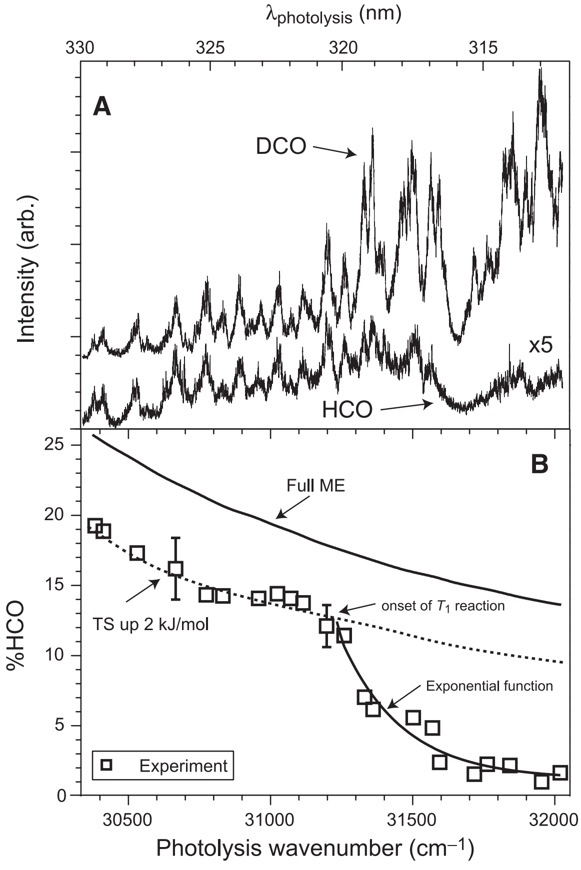

Fig. 1. (**A**) CH_3CDO action spectra monitoring HCO and DCO (displaced vertically). HCO intensity has been increased by a factor of 5 with respect to DCO. (**B**) The percentage of HCO to total formyl radical production measured at each dominant peak in the spectra. Representative error bars are provided. The results of a ME model are shown as a solid line. The effect of raising the rate-limiting transition state (TS) energy by 2 kJ/mol is shown by a dotted line.

included (with a different quenching rate). However, the solar flux at $\lambda < 300$ nm is small, and the discrepancies between our ME model and experimental results will be unimportant for atmospheric chemistry.

HC and MMW also report the dependence of ϕ_{ph} on N_2 or CO_2 pressure at specific wavelengths (*12*, *17*). Figure 3B shows their experimental data as a Stern-Volmer (SV) plot of $1/\phi_{ph}$ versus pressure, *P* (dashed lines). The experimental data at 331.4 nm have considerable uncertainty, and the zero pressure intercept is reported as $1/\phi_{ph} = 18$ ($\phi_{ph} = 0.06$) (*12*). However, at zero pressure, ϕ_{ph} must be ≈ 1 because the radiative quantum yields are very small [< 0.01 at all wavelengths here (*18*)]. We have replotted all the experimental SV plots in Fig. 3B, assuming a zero pressure intercept of 1, and compared them to our ME model results (solid lines). The ME model provides a good representation of the experimental data, with the largest variation occurring at 331.4 nm, where experimental uncertainties are largest. Indeed our ME model predictions sit between the two independent sets of experimental data at $\lambda = 313$ nm.

We now consider the fate of excited acetaldehyde molecules that do not photodissociate and explore the effect of collisional quenching under atmospheric conditions on keto-enol tautomerization. Figure 4A shows the predicted quantum yield of stable enol, ϕ_{enol}, as a function of wavelength, for $\langle \Delta E_{down} \rangle = 150\ cm^{-1}$ and 1 atm pressure. The yield is a maximum at ~315 nm; at shorter wavelengths, the increasing ϕ_{ph} causes a decrease in ϕ_{enol}, whereas at longer wavelengths the molecule cools before keto-enol tautomerization reaches equilibrium. The most sensitive parameter in the model is the height of the keto-enol barrier. Figure 4A also shows the results of the ME model when the barrier is raised and lowered by 5 kJ/mol, an estimate of the theoretical uncertainty. The predicted ϕ_{enol} changes slightly; the maximum quantum yield increases or decreases by about 4%, giving an estimate of the computational uncertainty.

The collision-free ME model has only been strictly validated for $\lambda > 320$ nm (Fig. 1B). However, the collisional ME model appears valid at atmospheric pressure for $\lambda > 300$ nm (Fig. 3A) because quenching on S_1 and T_1 competes with reaction on T_1. As a worst case, we might assume that the sharp decrease in ϕ_{1b}/ϕ_1 in Fig. 1B also applies at $P = 1$ atm. The result of this assumption is shown by the dashed curve in Fig. 4A.

The consequences of keto-enol tautomerization for the atmospheric photochemistry of acetaldehyde can now be evaluated. The rate *k* of a photochemical reaction in the troposphere is the product of the actinic flux $J(\lambda)$, the absorption cross section $\sigma(\lambda)$, and the quantum yield $\phi(\lambda)$ for the specific photochemical process, integrated over wavelength.

$$k = \int J(\lambda)\sigma(\lambda)\phi(\lambda)d\lambda \qquad (3)$$

Figure 4B shows $\sigma(\lambda)$ (*19*) and $J(\lambda)$ under typical conditions (albedo = 0.3 and overhead sun) (*6*) in the spectral region where both are nonzero. Figure 4C shows the right-hand side of Eq. 3, integrated over 1-nm intervals, for absorption of light (i.e., $\phi = 1$) and for photolysis and phototautomerization using ϕ_{ph} from MMW (*17*) in Fig. 3A and ϕ_{enol} from Fig. 4A. The overall photolysis quantum yield is 14%, in agreement with experiments (*12*, *17*). The worst-case scenario for enol production, if the T_1 reaction follows the collision-free quantum yield (Fig. 4A), is 13%, effectively the same as the photolysis yield. Our best estimate of ϕ_{enol} is 21 ± 4%.

Acetaldehyde is the simplest carbonyl compound that can undergo keto-enol tautomerization, and its photochemical properties are typical

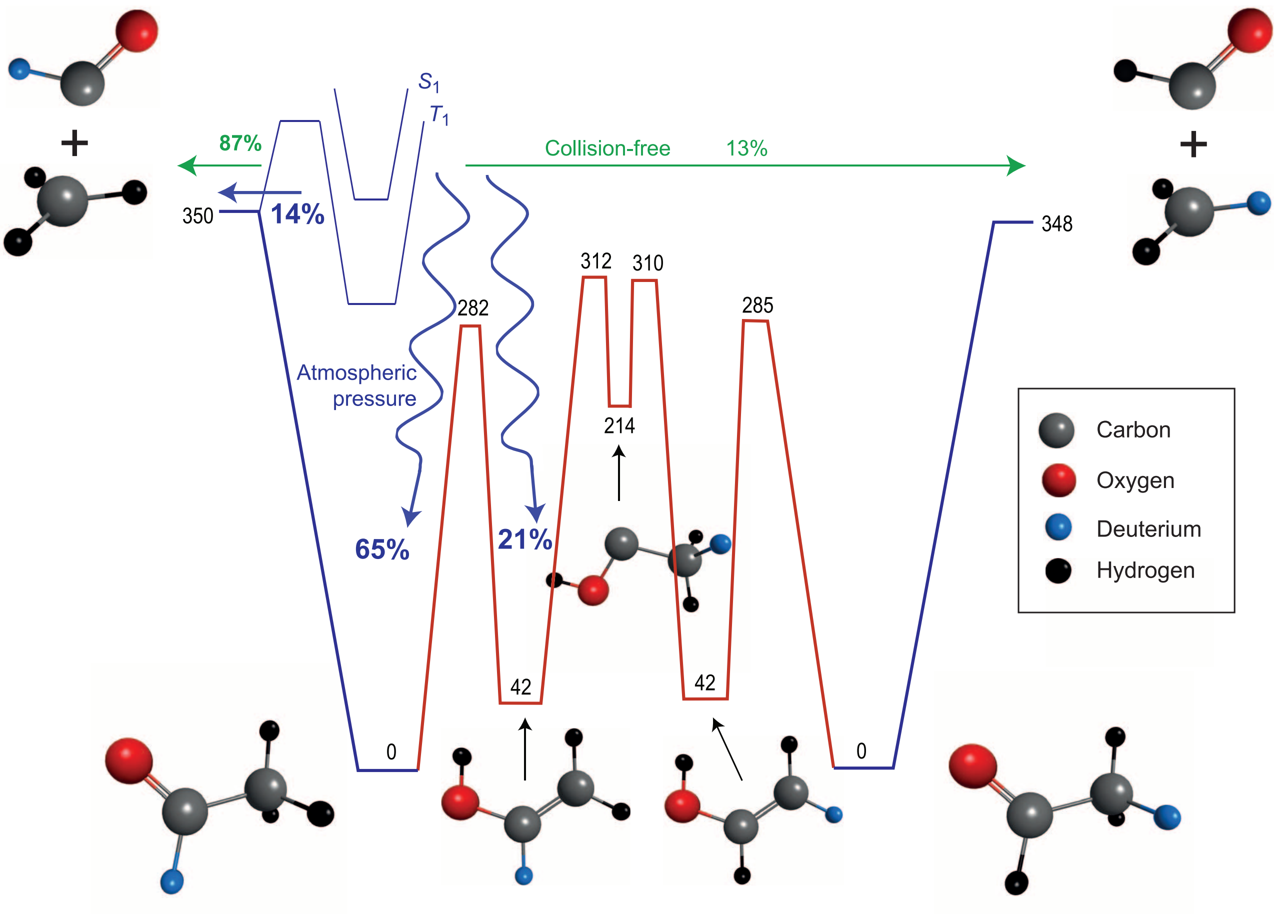

Fig. 2. A schematic showing energies (kJ/mol) and important structures on the CH_3CDO S_0 potential energy surface for the production of DCO and HCO. The green arrows indicate the experimental yields of HCO and DCO at 320 nm under collision-free conditions. Under atmospheric conditions, we predict that excited acetaldehyde collisionally relaxes into both keto and enol forms, as shown by the blue curvy arrows. All energies are from this work, as defined in the supplementary materials.

of smaller carbonyls. The (n,π^*) transition generally lies between 280 and 330 nm, with similar absorption cross sections throughout the family (*8*, *19*). The barrier to tautomerization is also similar (*20*). Therefore, we expect photo-tautomerization of small aldehydes and ketones to be a general characteristic of their fate in the atmosphere.

Enols have a different atmospheric chemistry from carbonyls; indeed, the atmospheric fate of vinyl alcohol is formic acid (*4*, *5*). Despite this, they have not been included in current atmospheric models for two reasons. First, enols have not been observed in the atmosphere. As reactive intermediates, their concentration will be very low. Second, there is no sufficiently large atmospheric source of enols. On the basis of this work, we propose that photo-tautomerization of carbonyls to enols may provide such a source.

It is interesting to speculate about photo-tautomerization for larger carbonyls. For linear aldehydes with ≥4 C atoms, the rate of a Norrish type II mechanism dominates even C-C bond cleavage (*21*), so we expect photo-tautomerization to be less important for these compounds. When chain flexibility is hindered by unsaturation, branching, or cyclization, the Norrish type II mechanism will likely turn off again, whereas tautomerization will always be present. Evaluation of the importance of this new mechanism for enol formation under the complex chemistry of the troposphere requires its inclusion in the relevant atmospheric models. However, good experimental data are first required for a range of prototypical carbonyls under atmospheric conditions.

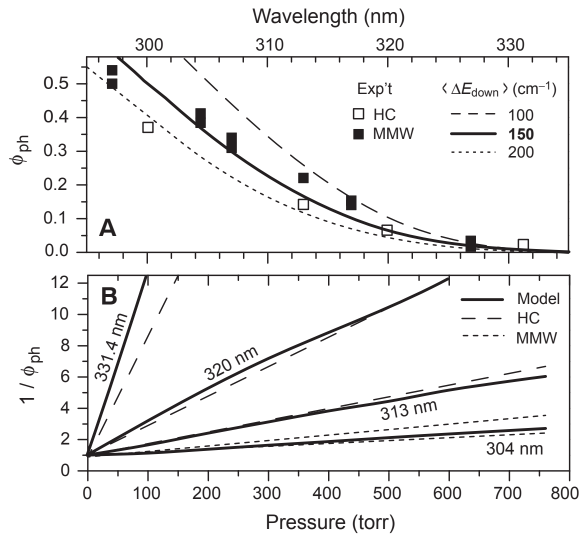

Fig. 3. Comparison of photochemical quantum yields from the ME model and available experiment data. (**A**) ϕ_{ph} as a function of wavelength for P = 1 atm. (**B**) Pressure dependence shown as Stern-Volmer plots. The dashed lines are derived from reported SV fits to experimental data. The ME model used $\langle \Delta E_{down} \rangle$ = 150 cm^{-1}. In both panels: HC (*12*), MMW (*17*).

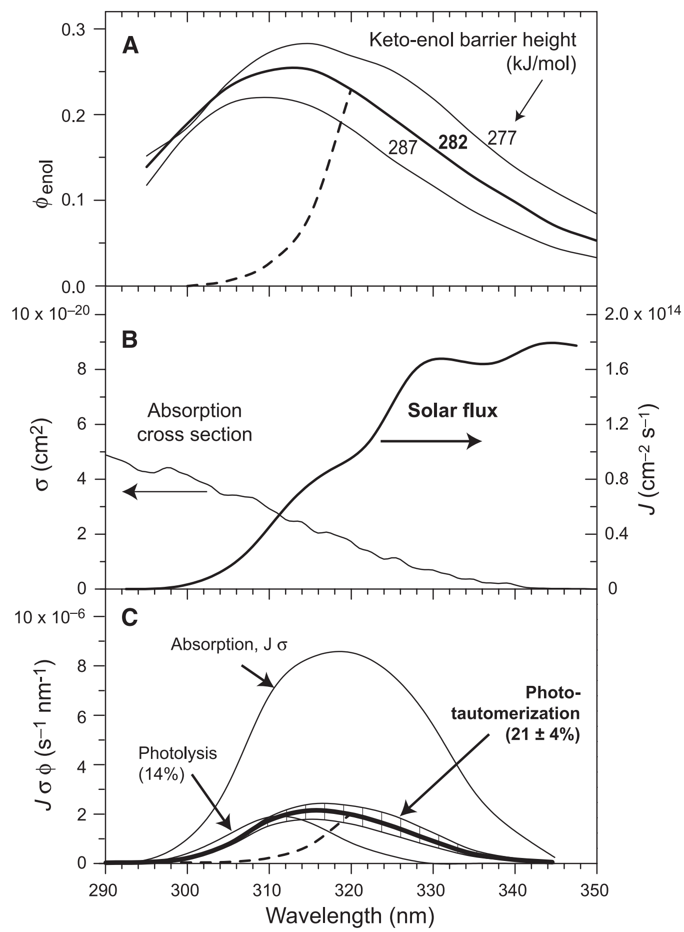

Fig. 4. (**A**) Quantum yield for enol formation according to the ME model for three keto-enol barrier heights. (**B**) Solar flux, *J*, and acetaldehyde absorption cross section, σ. (**C**) Absorption and photochemistry rates. The area surrounding the photo-tautomerization line represents the computational uncertainty. The dashed lines in (A) and (C) represent a worst-case correction for triplet reaction.

References and Notes

1. A. Ito, S. Sillman, J. E. Penner, *J. Geophys. Res.* **112**, D06309 (2007).
2. F. Paulot *et al.*, *Atmos. Chem. Phys.* **11**, 1989 (2011).
3. A. H. Goldstein, I. E. Galbally, *Environ. Sci. Technol.* **41**, 1514 (2007).
4. A. T. Archibald, M. R. McGillen, C. A. Taatjes, C. J. Percival, D. E. Shallcross, *Geophys. Res. Lett.* **34**, L21801 (2007).
5. G. da Silva, *Angew. Chem. Int. Ed.* **49**, 7523 (2010).
6. B. J. Finlayson-Pitts, J. N. Pitts Jr., *Chemistry of the Upper and Lower Atmosphere* (Academic Press, San Diego, CA, 2000).
7. A. Lee *et al.*, *J. Geophys. Res.* **111**, D17305 (2006).
8. R. Atkinson *et al.*; IUPAC Subcommittee, *Atmos. Chem. Phys.* **6**, 3625 (2006).
9. B. R. Heazlewood *et al.*, *Nat. Chem.* **3**, 443 (2011).
10. B. R. Heazlewood, S. J. Rowling, A. T. Maccarone, M. J. T. Jordan, S. H. Kable, *J. Chem. Phys.* **130**, 054310 (2009).
11. A. C. West *et al.*, *J. Phys. Chem. A* **113**, 12663 (2009).
12. A. Horowitz, J. G. Calvert, *J. Phys. Chem.* **86**, 3105 (1982).
13. MultiWell-2012.1 Software, 2012, designed and maintained by J. R. Barker with contributors N. F. Ortiz *et al.*; University of Michigan, Ann Arbor, MI; http://aoss.engin.umich.edu/multiwell.
14. J. R. Barker, *Int. J. Chem. Kinet.* **33**, 232 (2001).
15. J. R. Barker, *Int. J. Chem. Kinet.* **41**, 748 (2009).
16. L. B. Harding, Y. Georgievskii, S. J. Klippenstein, *J. Phys. Chem. A* **114**, 765 (2010).
17. G. K. Moortgat, H. Meyrahn, P. Warneck, *ChemPhysChem* **11**, 3896 (2010).
18. D. A. Hansen, E. K. C. Lee, *J. Chem. Phys.* **63**, 3272 (1975).
19. R. D. Martinez, A. A. Buitrago, N. W. Howell, C. H. Hearn, J. A. Joens, *Atmos. Environ.* **26A**, 785 (1992).
20. P. Pérez, A. Toro-Labbe, *J. Phys. Chem. A* **104**, 1557 (2000).
21. J. Tadic, I. Juranic, G. K. Moortgat, *J. Photochem. Photobiol. A* **143**, 169 (2001).

Acknowledgments: This work was funded by the Australian Research Council (DP1094559) and National Computational Infrastructure Facility. We thank G. Da Silva (University of Melbourne) for discussions about acids in the atmosphere.

Supplementary Materials
www.sciencemag.org/cgi/content/full/science.1220712/DC1
Materials and Methods
Supplementary Text
Figs. S1 to S3
Tables S1 to S3
References (*22*–*35*)

17 February 2012; accepted 1 August 2012
Published online 16 August 2012;
10.1126/science.1220712

Direct Mapping of Nuclear Shell Effects in the Heaviest Elements

E. Minaya Ramirez,[1,2] D. Ackermann,[2] K. Blaum,[3,4] M. Block,[2]* C. Droese,[5] Ch. E. Düllmann,[6,2,1] M. Dworschak,[2] M. Eibach,[4,6] S. Eliseev,[3] E. Haettner,[2,7] F. Herfurth,[2] F. P. Heßberger,[2,1] S. Hofmann,[2] J. Ketelaer,[3] G. Marx,[5] M. Mazzocco,[8] D. Nesterenko,[9] Yu. N. Novikov,[9] W. R. Plaß,[2,7] D. Rodríguez,[10] C. Scheidenberger,[2,7] L. Schweikhard,[5] P. G. Thirolf,[11] C. Weber[11]

Quantum-mechanical shell effects are expected to strongly enhance nuclear binding on an "island of stability" of superheavy elements. The predicted center at proton number Z = 114, 120, or 126 and neutron number N = 184 has been substantiated by the recent synthesis of new elements up to Z = 118. However, the location of the center and the extension of the island of stability remain vague. High-precision mass spectrometry allows the direct measurement of nuclear binding energies and thus the determination of the strength of shell effects. Here, we present such measurements for nobelium and lawrencium isotopes, which also pin down the deformed shell gap at N = 152.

Quantum-mechanical shell effects play a crucial role in determining the structure and the properties of matter. The electronic shell structure defines the architecture of the periodic table. An analogous effect leads to the so-called magic nuclei—closed nucleon shells that result in an enhanced binding of the atomic nucleus—that opposes Coulomb repulsion of protons and governs the landscape of the nuclear chart. The heaviest stable doubly magic nucleus is ^{208}Pb with proton number Z = 82 and neutron number N = 126. The quest for the end of the periodic table and the northeast limit of the nuclear chart (Fig. 1) drives the search for even heavier magic nuclei.

In these superheavy elements (SHEs), nuclear shell effects are decisive for their mere existence. Without them, their nuclei would instantaneously disintegrate by spontaneous fission through Coulomb repulsion. A manifestation of these nuclear shell effects is an increase of the half-life by 15 orders of magnitude compared to liquid-drop-model predictions for nuclei around N = 152 (*1*). Thus, SHEs are a prime testing ground for the understanding of shell effects and the character of the nuclear force.

Already in the late 1960s, about two decades after the introduction of the nuclear shell model (*2*, *3*), an "island of stability" of SHEs far from the known nuclei was predicted. Recent experimental evidence for the existence of isotopes of elements up to Z = 118 (*4*) has confirmed this concept, but the exact location and extension of this island are still unknown (*5*–*7*). The presently known or claimed nuclides in the northeast end of the nuclear chart are shown in Fig. 1. The blue shaded background indicates the gain in binding energy from shell effects. Regions of enhanced binding are predicted for the deformed magic nuclei at N = 152 and 162 around fermium (Z = 100) (*1*) and hassium (Z = 108) (*8*, *9*) and for spherical nuclei at Z = 114, N = 184.

Direct measurement of the strength of shell effects for SHE nuclei has been beyond experimental capabilities until now. It could only be derived either indirectly from a comparison of, e.g., experimental cross sections and half lives with predicted values, or from measured Q_α values, i.e., energy differences, in alpha decays. Here, we report the direct measurement of the neutron shell gap by precision mass measurements on nobelium (Z = 102) and lawrencium (Z = 103) isotopes around N = 152. The results supply valuable information on the nuclear structure of SHEs, which is highly relevant for an improved prediction of the island of stability.

Mass spectrometry is a direct probe of nuclear stability, as the mass includes the total binding energy. Until recently, masses in the region of the heaviest elements could only be inferred via α-decay energies. For nuclides with even numbers of protons and neutrons, where the decay connects ground states, this approach is straightforward as the mass of the mother/daughter nucleus can be derived from the measured decay energy $E = \Delta mc^2$ and the mass of the daughter/mother nucleus, respectively. Although the uncertainties add up along decay chains, the masses of several nuclides between uranium (Z = 92) and copernicium (Z = 112) have been deduced in this way (*10*).

However, in general, the situation is more complex as α decays preferably connect levels with identical configurations, whereas the ground-state configurations of mother and daughter nuclei usually differ for odd-Z and/or odd-N nuclides. These nuclei decay to excited states that in turn generally de-excite to the ground state by emission of photons or conversion electrons. Thus, the total decay energy is shared among the α particle, γ rays, and/or conversion electrons, i.e., the mere knowledge of the α-particle energy is insufficient. Unfortunately, for such nuclides unambiguous decay schemes, which would provide the information needed to obtain the true Q_α values, are rarely available. For many nuclides above fermium (Z = 100), the mass values are only extrapolated with uncertainties of several hundred keV (*10*).

In contrast, direct mass measurements provide absolute mass values and model-independent binding energies E_B with no need for any ancillary

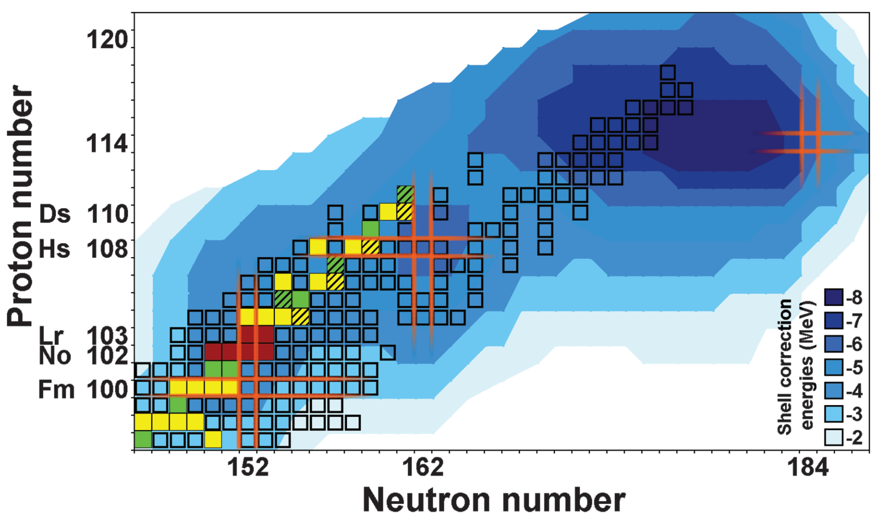

Fig. 1. Chart of nuclides above berkelium (Z = 97). The blue background shows the calculated shell-correction energies (*6*). The orange-shaded lines indicate known and predicted shell closures. The squares represent presently known or claimed nuclides. The nobelium and lawrencium isotopes whose masses are reported here are indicated by red squares. The yellow and green squares represent nuclides whose masses are determined by use of these new mass values, respectively, as anchor points in combination with experimental α-decay energies. Hatched squares show nuclides with unknown or ambiguous excited states. For details, see text.

[1]Helmholtz-Institut Mainz, 55099 Mainz, Germany. [2]GSI Helmholtzzentrum für Schwerionenforschung GmbH, 64291 Darmstadt, Germany. [3]Max-Planck-Institut für Kernphysik, 69117 Heidelberg, Germany. [4]Ruprecht-Karls-Universität, 69120 Heidelberg, Germany. [5]Ernst-Moritz-Arndt-Universität, 17487 Greifswald, Germany. [6]Johannes Gutenberg-Universität, 55099 Mainz, Germany. [7]Justus-Liebig-Universität, 35392 Gießen, Germany. [8]Dipartimento di Fisica and INFN Sezione di Padova, 35131 Padova, Italy. [9]Petersburg Nuclear Physics Institute, Gatchina, 188300 St. Petersburg, Russia. [10]Universidad de Granada, 18071 Granada, Spain. [11]Ludwig-Maximilians-Universität München, 85748 Garching, Germany.

*To whom correspondence should be addressed. E-mail: m.block@gsi.de

information. Thus, by pinning down members of α-decay chains, they can establish anchor points for a larger region in the chart of nuclei. In addition, accurate mass values define differential quantities such as the two-neutron separation energy $S_{2n}(N,Z) = E_B(N,Z) - E_B(N-2, Z)$ that are sensitive to quantum-mechanical shell effects and can uncover underlying nuclear-structure phenomena.

Direct high-precision mass measurements of short-lived nuclides are best performed with Penning traps (*11*, *12*) by determination of the cyclotron frequency $\nu_c = qB/(2\pi m)$ of the ion of interest with charge q and unknown mass m stored in a homogeneous magnetic field B. We have extended earlier $^{252-254}$No ($Z = 102$) measurements (*13*, *14*) to nuclei with an even larger number of protons and neutrons: ^{255,256}Lr (lawrencium, $Z = 103$) and ^{255}No/^{256}Lr ($N = 153$), respectively. The latter are found on the neutron-rich side of the $N = 152$ shell gap (Fig. 1). Combining the new results with our previous measurements, we can now directly determine the strength of the $N = 152$ shell gap at $Z = 102$, the doorway to the SHEs.

SHIPTRAP (*15*) at GSI Darmstadt is a Penning-trap mass spectrometer installed behind the velocity filter SHIP, which is known particularly for the discovery of the elements with $Z = 107$ to 112 (*16*). Nobelium and lawrencium isotopes were produced in fusion reactions of ^{48}Ca projectile ions (accelerated to 218.4 MeV) with ^{206,207,208}Pb and ^{209}Bi targets. The product nuclei were separated from the primary beam by SHIP. Their kinetic energy was reduced from about 40 MeV by Mylar degrader foils and a 2-mg/cm^2 titanium entrance window to the SHIPTRAP gas cell. There, the particles were thermalized in 50-mbar ultrahigh-purity helium. They emerged mainly as doubly charged ions; were cooled, bunched, and accumulated by a radiofrequency-quadrupole ion trap; and then transferred to a 7-T double-Penning-trap system. In the first trap, the ions of interest were selected with a mass-resolving power of up to 10^5. In the second trap, the cyclotron frequency ν_c was determined with the time-of-flight ion–cyclotron-resonance method (*17*) (compare Fig. 2). At least a few tens of ions must be detected to obtain a resonance. Thus, even for modern Penning traps, the extremely low production rates of exotic nuclei pose a major challenge for high-precision mass measurements. In the case of ^{256}Lr, the present measurements required a long measurement time. With a cross section as low as σ = 60 nb (*18*), 93 hours were required for a resonance based on 48 detected ions (Fig. 2).

We determined the mass of the ion of interest by comparing its cyclotron frequency (ν_c) with that of the reference ion $^{133}Cs^+$ ($\nu_{c,ref}$), with well-known mass (*10*) and a mass-to-charge ratio close to that of the doubly charged nobelium and lawrencium ions. The statistical uncertainty depends on the number of detected ions per resonance and the Fourier-limited resolution $\Delta\nu_c \approx 1/t$, which is inversely proportional to the excitation time t that a radiofrequency signal is applied to excite the cyclotron motion of the stored ions. In addition, a systematic uncertainty of 4.5×10^{-8} [based on the residual scattering observed in cross-check measurements with carbon-cluster ions (*19*)] has been taken into account.

The resulting frequency ratios are given in Table 1. In addition to the confirmation for the even-Z nobelium isotopes ^{252}No and ^{254}No (*14*) and a further reduction in their uncertainties, accurate mass values were also determined for the odd-Z element lawrencium. Overall, the decay-energy–based values (*10*) agreed, within their fairly large systematic uncertainties, with our new direct mass measurements of ^{255}No, ^{255}Lr, and ^{256}Lr.

The SHIPTRAP masses provide anchor points of α-decay chains and thus affect the masses of many other nuclides. The mass of ^{255}No determines the masses of its daughters linked by α decay (^{247}Cf) and electron capture (^{247}Bk). Until recently, the nuclear spectroscopy data of the decay chain from ^{270}Ds (darmstadtium, $Z = 110$) to ^{254}No had been incomplete (*20*). However, the recent discovery of an α-decay branch of ^{262}Sg (*21*) now provides the missing link. Thus, the mass excess of ^{270}Ds was experimentally established with an uncertainty of 40 keV. It is the highest-Z anchor point near the deformed doubly magic nucleus ^{270}Hs ($Z = 108$, $N = 162$) (*8*) (compare Fig. 1). Thus, our measurements affect nuclides in a region reaching into the realm of the SHEs.

These high-precision mass values can be used to benchmark nuclear models (*22*) and can be extended to the very heavy nuclides. The center of the island of stability around $N = 184$ is experimentally still out of reach, and reliable theoretical predictions are crucial for directing future experimental efforts. The masses measured at SHIPTRAP provide direct, model-independent values of the total binding energies and precise values

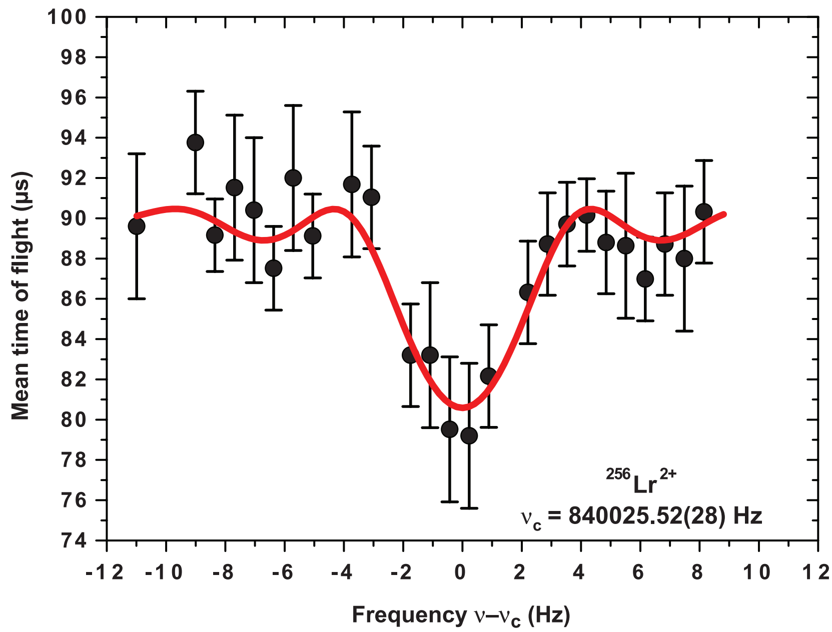

Fig. 2. Time-of-flight ion–cyclotron-resonance of doubly charged $^{256}Lr^{2+}$ (t = 200 ms). The curve is a fit of the expected line shape to the data. Error bars, ±1 SD.

Table 1. Measured frequency ratios and resulting mass-excess [M_{exc} = M(atomic mass) − A(atomic mass number) × u(atomic mass unit)] values for the nuclides investigated in this work, as well as theoretical predictions from several models (*6*, *23*–*25*). The Z and N values of the predicted center of the island of stability by each model are indicated.

Isotope	Frequency ratio	Mass excess (keV)				
	$\nu_{c,ref}/\nu_c$	Experiment SHIPTRAP	FRDM (*2*) Z = 114 N = 184	MPS-03 (*24*) Z = 114 N = 184	TW-99 (*25*) Z = 120 N = 172	SkM* (*23*) Z = 126 N = 184
^{252}No	0.94837684(7)	82870(16)	82200	82950	91566	95308
^{253}No	0.95214494(5)	84356(13)	83840	84190	–	96396
^{254}No	0.95590852(6)	84726(14)	84050	84700	93646	96989
^{255}No	0.95967902(6)	86808(15)	86550	86700	–	98615
^{255}Lr	0.95969174(6)	89958(16)	89300	89920	–	102326
^{256}Lr	0.9634610(3)	91746(83)	91420	91690	–	103727

for derived quantities such as the shell gap parameter (*23*),

$$\delta_{2n}(N,Z) = S_{2n}(N,Z) - S_{2n}(N+2, Z)$$
$$= -2M_{exc}(N,Z) + M_{exc}(N-2, Z) + M_{exc}(N+2, Z),$$

that theoretical predictions can be confronted with or used to calculate other quantities. $\delta_{2n}(N,Z)$ is a sensitive indicator of shell closures and a measure of their strength and is appropriate for examining shell stabilization for $N = 152$. Because the uncertainties of our results are well below the differences among the predictions by the different models, they allow us to test their predictive power. We have selected as representative examples two microscopic-macroscopic models—namely, the global FRDM (*6*) and the approach by Muntian *et al*. (*24*) that is optimized locally for SHEs and served to produce the blue-shaded contour plot underlying Fig. 1—as well as a self-consistent mean-field model using the Skyrme-Hartree-Fock effective interaction SkM* (*23*) and, furthermore, a relativistic mean-field model using the effective interaction TW-99 (only even-even nuclei) (*25*).

Microscopic-macroscopic approaches are based on the liquid-droplet model with modifications by a microscopic shell-correction energy (*26*) crucial for the existence of SHEs. These models describe various nuclear properties across the nuclear chart and predict the island of stability at $Z = 114$ and $N = 184$. Self-consistent mean-field models use energy-density functionals based on effective nucleon-nucleon interactions. Different effective interactions (e.g., Skyrme and Gogny forces) have been developed, which lead to different predictions for the location of the island of stability, e.g., around $Z = 126$, $N = 184$ for the effective interaction SkM*. In recent years, relativistic mean-field models have been applied. In the TW-99 parameterization, the spherical SHE shells are predicted at $Z = 120$, $N = 172$.

Figure 3 shows a comparison between the predicted and experimental $\delta_{2n}(N,Z)$ values around $N = 152$ for nobelium and lawrencium. Compared to the drastic deviation of the predicted mass excess of up to about 10 MeV from the experimental data (compare Table 1), the agreement of $\delta_{2n}(N,Z)$ is significantly better, with deviations below about 500 keV. Not surprisingly, the local model by Muntian *et al.* agrees best with the data. All models, except for the TW-99 parameterization, show a similar trend with increasing neutron number and a peak indicating the deformed $N = 152$ shell. However, the strength of the shell gap differs strongly. From our data, we obtain $\delta_{2n}(152,102)$ = 1242(16) keV. The macroscopic-microscopic models predict a larger neutron shell gap of 1310 keV (Muntian *et al.*) and 1520 keV (FRDM), whereas the self-consistent mean-field model, SkM*, yields a much smaller and more smeared out shell gap (982 keV). For the TW-99 parameterization, for which only data for even-even nuclei are available, a clear shell gap for $Z = 102$ at $N = 154$ of 1375 keV is obtained, also larger than observed experimentally. The difference in values for the size of the shell gap or even a shift from $N = 152$ to $N = 154$ for one of the selected models illustrates the sensitivity of the different predictions on the used parameterization.

The values of $\delta_{2n}(N,Z)$ obtained from our data confirm the existence of a region of enhanced shell stabilization for nuclides above the doubly magic ^{208}Pb. In particular, for $Z = 102$, our data pin down the shell gap at $N = 152$ accurately. The findings are corroborated for $Z = 103$. Thus, our mass measurements have established, with high accuracy, a shell gap at $N = 152$—a major input for theoretical models, which have not yet converged to a common prediction of the location and the strength of the shell closures in SHEs.

In this study, we have measured the masses of ^{255}No and ^{255,256}Lr directly. Mass uncertainties as low as 15 keV have been achieved, and ^{256}Lr is the heaviest nuclide and the one with the smallest production rate ever investigated at an on-line Penning-trap mass spectrometer. The combination of the present results with spectroscopic data fixes the masses of nuclides as heavy as ^{270}Ds ($Z = 110$). Moreover, the accurate experimental binding energies allow mapping of the shell effect at $N = 152$. Thus, our mass measurements on isotopes with production cross sections on the order of only tens of nanobarn pave the way to a better understanding of the superheavy elements.

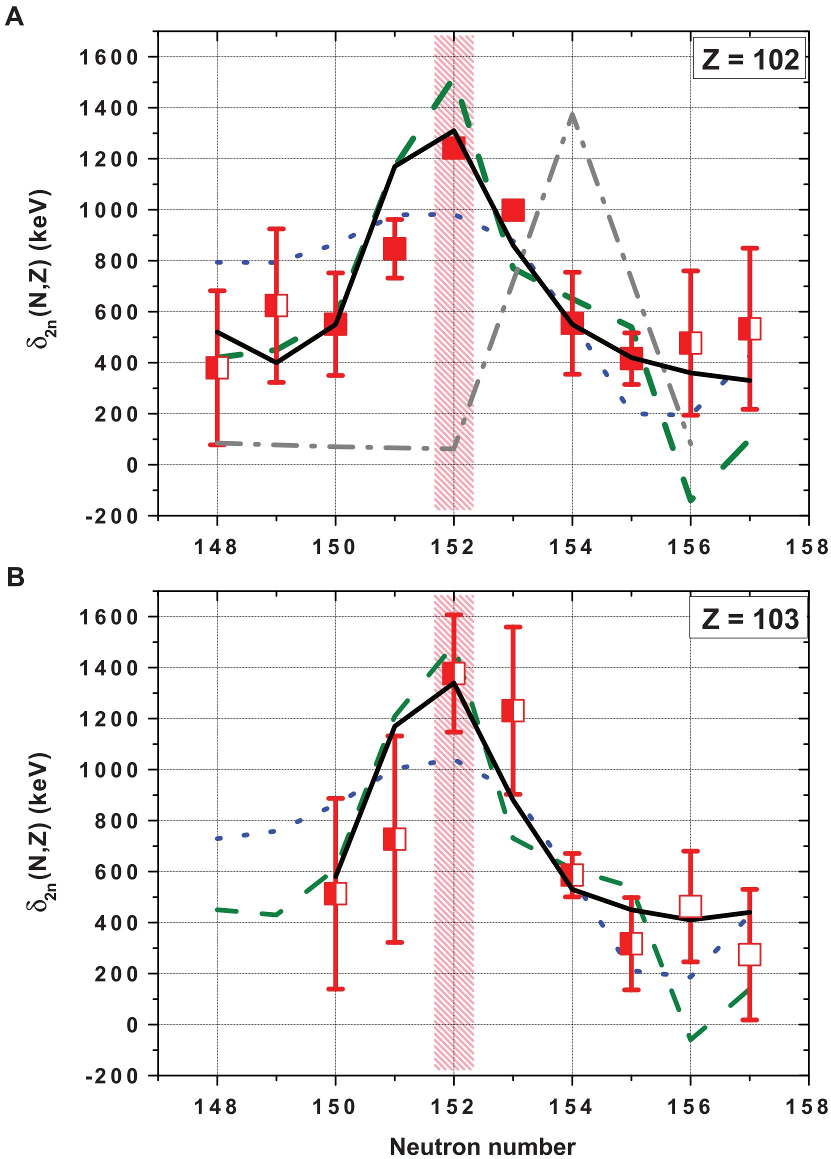

Fig. 3. Experimental shell gap $\delta_{2n}(N,Z)$ (red squares and error bars) and theoretical predictions [dashed green line: Möller (*6*); dotted blue line: SkM* (*23*); black line: Muntian *et al*. (*24*); dash-dotted gray line: TW-99 (*25*), only for (A)] for nobelium (**A**) and lawrencium (**B**). For further details, see text. Experimental values have been calculated using one (semi-filled red squares) or two (filled red squares) masses from this work. Values from the AME 2003 are shown by open red squares. The shaded area at $N = 152$ indicates the position of the deformed neutron shell gap. Error bars, ±1 SD.

References and Notes

1. Z. Patyk, A. Sobiczewski, P. Armbruster, K.-H. Schmidt, *Nucl. Phys. A.* **491**, 267 (1989).
2. M. Göppert-Mayer, *Phys. Rev.* **74**, 235 (1948).
3. M. Göppert-Mayer, J. H. D. Jensen, *Elementary Theory of Nuclear Shell Structure* (Wiley, New York, 1955).
4. Yu. Ts. Oganessian *et al.*, *Radiochim. Acta* **99**, 429 (2011).
5. S. Ćwiok, P. H. Heenen, W. Nazarewicz, *Nature* **433**, 705 (2005).
6. P. Möller, J. R. Nix, W. D. Myers, W. J. Swiatecki, *At. Data Nucl. Data Tables* **59**, 185 (1995).
7. M. Bender, K. Rutz, P.-G. Reinhard, J. Maruhn, W. Greiner, *Phys. Rev. C Nucl. Phys.* **60**, 034304 (1999).
8. J. Dvorak *et al.*, *Phys. Rev. Lett.* **97**, 242501 (2006).
9. A. Sobiczewski, K. Pomorski, *Prog. Part. Nucl. Phys.* **58**, 292 (2007).
10. G. Audi, A. H. Wapstra, C. Thibault, *Nucl. Phys. A.* **729**, 337 (2003).
11. L. Schweikhard, G. Bollen, Eds., special issue of *Int. J. Mass Spectrom.* **251** (2006).
12. K. Blaum, *Phys. Rep.* **425**, 1 (2006).
13. M. Block *et al.*, *Nature* **463**, 785 (2010).
14. M. Dworschak *et al.*, *Phys. Rev. C Nucl. Phys.* **81**, 064312 (2010).
15. M. Block *et al.*, *Eur. Phys. J. D* **45**, 39 (2007).
16. S. Hofmann, G. Münzenberg, *Rev. Mod. Phys.* **72**, 733 (2000).
17. G. Gräff *et al.*, *Z. Phys.* **222**, 201 (1969).
18. F. P. Heßberger *et al.*, *Eur. Phys. J. D* **45**, 33 (2007).
19. A. Chaudhuri *et al.*, *Eur. Phys. J. D* **45**, 47 (2007).
20. S. Hofmann *et al.*, *Eur. Phys. J. A* **10**, 5 (2001).
21. D. Ackermann *et al.*, GSI Ann. Rep. 2010–GSI Rep. 2011-1 (2011), p. 200.
22. D. Lunney, C. Thibault, *Rev. Mod. Phys.* **75**, 1021 (2003).
23. K. Rutz *et al.*, *Phys. Rev. C Nucl. Phys.* **56**, 238 (1997).
24. I. Muntian *et al.*, *Act. Phys. Pol. B* **34**, 2073 (2003).
25. W. Zhang, J. Meng, S. Q. Zhang, L. S. Geng, H. Toki, *Nucl. Phys. A.* **753**, 106 (2005).
26. V. M. Strutinsky, *Nucl. Phys. A.* **95**, 420 (1967).

Acknowledgments: The project was supported in part by the Helmholtz-Institut Mainz, the GSI Helmholtzzentrum für Schwerionenforschung GmbH, the German Federal Ministry of Education and Research (BMBF), the Max-Planck Society, the Russian Minobrnauki, and the ExtreMe Matter Institute (EMMI). Y.N.N. acknowledges support by EMMI.

4 June 2012; accepted 10 July 2012
Published online 9 August 2012;
10.1126/science.1225636

Evidence for NO_x Control over Nighttime SOA Formation

A. W. Rollins,[1]* E. C. Browne,[1] K.-E. Min,[2] S. E. Pusede,[1] P. J. Wooldridge,[1] D. R. Gentner,[3] A. H. Goldstein,[3,4] S. Liu,[5] D. A. Day,[5]† L. M. Russell,[5] R. C. Cohen[1,2]‡

Laboratory studies have established a number of chemical pathways by which nitrogen oxides (NO_x) affect atmospheric organic aerosol (OA) production. However, these effects have not been directly observed in ambient OA. We report measurements of particulate organic nitrates in Bakersfield, California, the nighttime formation of which increases with NO_x and is suppressed by high concentrations of organic molecules that rapidly react with nitrate radical (NO_3)—evidence that multigenerational chemistry is responsible for organic nitrate aerosol production. This class of molecules represents about a third of the nighttime increase in OA, suggesting that most nighttime secondary OA is due to the NO_3 product of anthropogenic NO_x emissions. Consequently, reductions in NO_x emissions should reduce the concentration of organic aerosol in Bakersfield and the surrounding region.

Organic aerosol (OA) constitutes about half of the total submicrometer particulate mass in the troposphere (*1*–*3*). OA is emitted to the atmosphere both directly as particles (primary OA, POA) and produced in the atmosphere through oxidation of volatile molecules (secondary OA, SOA), although evidence suggests that SOA is dominant (*4*). Owing to the complexity of SOA chemistry, major gaps exist in our ability to predict the time evolution of the chemical, physical, and optical properties of aerosols. A key example is our inability to predict the response of SOA to changes in emissions of nitrogen oxides (NO_x). Although laboratory evidence shows that NO_x should substantially affect atmospheric SOA formation, a coherent understanding of the nonlinear SOA/NO_x relationship has not emerged (*5*). This issue is important because NO_x has decreased by 30% or more in the United States and United Kingdom in the last decade, while comparable increases have occurred in China (*6*–*9*). Direct evidence that these changes in NO_x affect aerosol would greatly aid in the understanding of SOA.

SOA is formed through the gas-phase oxidation of volatile organic compounds (VOCs) by reactions with the hydroxyl radical (OH), ozone (O_3), and the nitrate radical (NO_3), producing condensable material (*10*). Most laboratory (*10*, *11*) and field [e.g., (*2*, *12*)] SOA studies have focused on the role of oxidation via O_3 and OH as SOA sources. Reactions of organic compounds with NO_3 are also important for oxidizing unsaturated atmospheric compounds (*13*), and NO_3 is unique in that it is almost exclusively a by-product of anthropogenic NO_x emissions (reaction 1).

$$NO_2 + O_3 \rightarrow NO_3 + O_2 \qquad (1)$$

Due to its photolabile nature and rapid reaction with nitric oxide (NO), NO_3 is present primarily in the nighttime atmosphere. Oxidation products of nitrate radical chemistry have a unique chemical signature due to the high yields, to form organic nitrates ($RONO_2$). Organic nitrates are also formed during the day by OH-initiated chemistry in the presence of NO, but with much lower yields. Laboratory studies of SOA from NO_3 have revealed both large aerosol yields, and the importance of multigenerational chemistry on compounds with multiple C-C double bonds. For example, Ng *et al*. (*14*) and Rollins *et al*. (*15*) studied the aerosol formed during NO_3 oxidation of isoprene. Both studies found large SOA yields (4 to 24%) and showed that the condensable compounds were formed not from the products of the initial NO_3 + isoprene reaction, but mostly from further oxidation of the first-generation products. Similar results were found for NO_3 + limonene (*16*).

We have developed a fast, sensitive, and precise instrument capable of measuring the particulate total alkyl and multifunctional nitrates (pΣANs) (*17*). Using this instrument, we made observations of pΣANs along with key precursors (NO_2, O_3, VOC) and aerosol properties in Bakersfield, California, as part of the CalNex-2010 experiment. Bakersfield is of interest due to its location in California's San Joaquin Valley, with abundant sources of biogenic VOC (BVOC) and NO_x and (for the United States) relatively severe particulate matter (PM) air pollution. We interpret the observations as evidence for a substantial nighttime chemical source of pΣAN.

Air parcels arriving at the site had traveled typically through the agricultural San Joaquin Valley, and then through the Bakersfield urban center for 1 to 2 hours before reaching the site. During the experiment, OA concentrations exceeding 10 μg/m^3 were frequently observed at night. A possible contributor to these high concentrations is the reduction in the boundary layer (BL) depth before sunset in the San Joaquin Valley. At a site near Bakersfield, Bianco *et al*. (*18*) observed that during May and June, the BL on average would decrease from ≈1.7 km at noon to ≈300 m just before sunset. The nighttime increase in OA observed in this study, however, occurred after sunset (Fig. 1), and thus after the BL is thought to have reached its minimum depth. We do not know the extent to which the aerosol that we measured at the surface was well mixed through the nocturnal BL; however, the diurnal

[1]Department of Chemistry, University of California, Berkeley, Berkeley, CA 94720, USA. [2]Department of Earth and Planetary Sciences, University of California, Berkeley, Berkeley, CA 94720, USA. [3]Department of Civil and Environmetal Engineering, University of California, Berkeley, Berkeley, CA 94720, USA. [4]Department of Environmental Science, Policy, and Management, University of California, Berkeley, Berkeley, CA 94720, USA. [5]Scripps Institution of Oceanography, University of California, San Diego, San Diego, CA 92093, USA.

*Present address: NOAA Earth System Research Laboratory and Cooperative Institute for Research in the Environmental Sciences, University of Colorado, Boulder, Boulder, CO 80309, USA.
†Present address: Cooperative Institute for Research in the Environmental Sciences, University of Colorado, Boulder, Boulder, CO 80309, USA.
‡To whom correspondence should be addressed. E-mail: rccohen@berkeley.edu

patterns vary little from day to day, suggesting the observations shown in Fig. 1 are characteristic of a large spatial scale and not dominated by local surface layer plumes. There was no appreciable change in the prevailing wind direction (west-northwest) from 6 p.m. to 11 p.m., and back-trajectories for air arriving at this site in this time interval follow a common path arriving from the west-northwest (fig. S1).

The average diurnal trends in pΣAN, OA, and the ratio of these two are shown in Fig. 1. Additionally, diurnal averages in NO_2, O_3, temperature, and relative humidity are shown in fig. S2. The OA and pΣAN have both a midday maximum and a nighttime/early morning maximum. The average OA maximum at night exceeds that of the midday by 24%, which is an unusual observation compared to studies in other large urban areas that have observed the daily OA maxima midday (*19*–*21*). Although aerosol mass spectrometer (AMS) data did not readily quantify POA and SOA individually at night, size distributions and tracers suggest that POA was at most 10 to 20% of OA (see materials and methods SI).

On average, the pΣAN nitrate groups increased from 2.3% of OA at sunset to 4.7% at 23:30 local time. The rapid increase in the pΣAN fraction begins immediately after sunset, when NO_3 chemistry becomes possible. Although temperature is expected to affect SOA through changes in vapor pressures, it does not appear to have played the dominant role in the trends; temperatures peaked near 15:00 local time and decreased significantly before sunset (fig. S1). The $RONO_2$ contribution to OA is relatively constant in the morning hours between 6:00 and 9:30 before obvious SOA production. After 10:00, when OA concentration is increasing, the observations indicate that as photochemistry generates SOA, pΣAN becomes a smaller fraction of the total OA mass. Factor analysis of AMS measurements are consistent with this interpretation. A unique nighttime factor was identified that becomes less important as the aerosol mass increases during daylight, and daytime SOA factors did not increase until after 9:00.

The observation that pΣAN and pΣAN/OA increase at night suggests not only that NO_3 chemistry is important for SOA production at night, but also that the organic nitrate tracers of this chemistry contribute appreciably to the total OA. Over the 5-hour time period after sunset (18:30 to 23:30), the average total OA increase was 1.54 $\mu g/m^3$. The added mass of $–ONO_2$ functional groups alone accounted for 0.129 $\mu g/m^3$ (8.4%) of this total mass. That this ratio increased continuously for 5 hours after sunset while Bakersfield is only 1 to 2 hours upwind suggests that the effect is somewhat regional. Assuming that the organic molecules with nitrate functional groups have an average molecular weight of 200 to 300 g/mol (*22*), we calculate that 27 to 40% of the OA growth was due to molecules with nitrate functionalities. This fraction of OA molecules that are nitrates is similar to the nitrate yields from a number of NO_3 + BVOC reactions (*23*). Thus, these numbers do not preclude all of the SOA production, including non-nitrates, being a result of NO_3 chemistry. The other potential source of nighttime SOA, O_3 + alkenes, is unlikely to be nearly as important because the rates of these reactions are typically at most one-tenth of the NO_3 rates (materials and methods S1.3).

To examine the role of NO_x emissions for SOA formation, we used observations of $[NO_2]$ and $[O_3]$ to calculate the nitrate radical production rates ($PNO_3 = k_1[NO_2][O_3]$) and compared these to the rate of net increase in pΣAN at night, defined as the difference (ΔpΣAN = ($[$pΣAN$]_{23:30}$ – $[$pΣAN$]_{18:30}$)/5 hours) on each night. Figure 2 compares ΔpΣAN to the average PNO_3. The correlations with PNO_3 are modest (r = 0.44). However, if we exclude those nights when the NO_3 lifetime to gas-phase reactions was short (τ < 65 s), a much stronger correlation between the PNO_3 and ΔpΣAN (r = 0.73) is inferred. A linear fit to this data (ΔpΣAN/PNO_3 = 0.015) suggests that ~1.5% of NO_3 reacts to form particle-bound nitrates, a number that is somewhat lower than expected from chamber studies and could be used to estimate the efficacy of NO_x emission reductions for reducing fine PM at this location.

Generally, NO_3 reactivity at the site is dominated by BVOC from the valley and surrounding mountains (fig. S3). When the NO_3 lifetime is short, we find that a larger fraction of the reactivity is due to primary biogenic VOC than on other nights, suggesting that BVOC can suppress aerosol formation. Previous in situ observations have shown that biogenics react rapidly with NO_3, reducing the NO_3 concentration (*24*). We believe this is the likely mechanism for aerosol suppression. The removal of NO_3 by primary VOC results in production of first-generation gas-phase nitrates with vapor pressures that are too high ($C^* \approx 10^3$ to 10^6 $\mu g/m^3$) for the molecules to be incorporated into aerosol to an

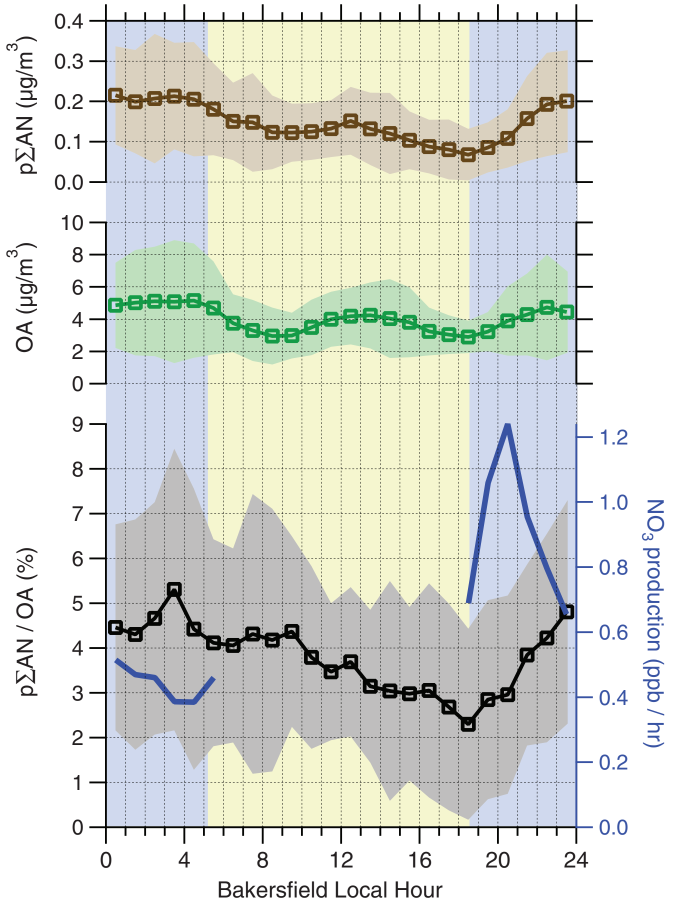

Fig. 1. Diurnal trends (means shown with ±1σ ranges in shading) in pΣAN (brown), OA (green), pΣAN/OA (black), and NO_3 production rate (blue). Blue shading indicates nighttime (solar zenith angle > 85°), and yellow indicates daytime.

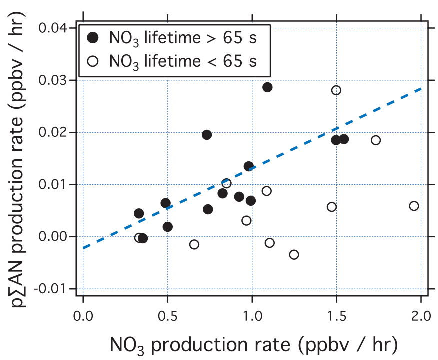

Fig. 2. Observations of trends in nighttime production rate of pΣAN with NO_3 production rate. Data are high NO_3 reactivity (open circles) and lower NO_3 reactivity (solid circles). Dashed blue line is a linear fit to low-reactivity data with a slope of 0.015 and r = 0.73.

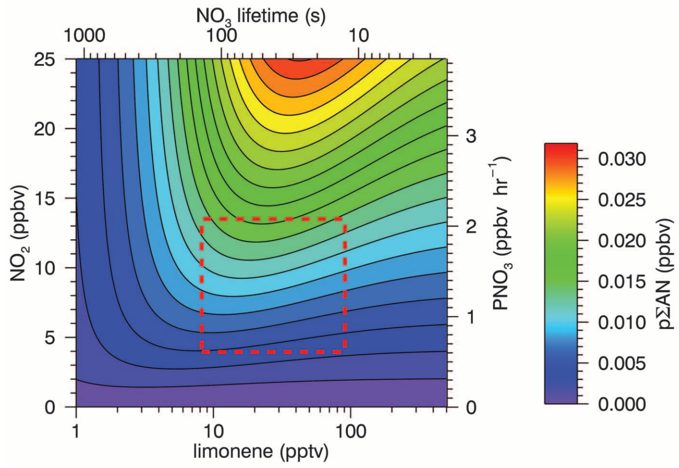

Fig. 3. Simulation of multigenerational SOA formation from the reaction of NO_3 with limonene as a function of NO_2 and limonene at 50 ppb O_3. We assume that Bakersfield (1 to 2 hours upwind) is the major NO_x source and therefore show contours that are ppb of pΣAN after 2-hour model runs. For longer runs (up to 5 hours), the pΣAN scaled approximately linearly with time. The production rates of NO_3 corresponding to the NO_2 concentration are shown on the right axis. Top axis shows the total NO_3 gas-phase lifetime with limonene at 34% of the total NO_3 loss. Red dashed box highlights the NO_2 and limonene concentration range typically observed in Bakersfield, showing that increases in limonene here are expected to lead to less aerosol production. pptv (ppbv), parts per trillion (billion) by volume.

appreciable extent. The condensable nitrates that we observe in the particle phase are likely second- or higher-generation oxidation products, produced by the slower oxidation of the first-generation products (*15*, *16*). Based on the measurements of RH, and aerosol surface area and composition, we estimate that N_2O_5 heterogeneous loss has a small impact on NO_3 concentration (<10%), and thus NO_3 variability is dominated by its source term (reaction 1) and gas-phase reactivity. Figure 2 also shows that the kinetics of aerosol $RONO_2$ formation are approximately linear with PNO_3, indicating that aerosol precursors are abundant and that NO_3 production is rate limiting. Because this SOA is produced by reactions of NO_3, it can be considered anthropogenic. Although the carbon may be of biogenic origin, without high NO_x emissions it would not be produced.

The observation that VOC with high SOA yields may suppress SOA formation is surprising. To demonstrate that this is kinetically possible in the NO_x/VOC regime observed in Bakersfield, we modeled SOA formation from NO_3 oxidation of limonene (Fig. 3). We use limonene as an example VOC because of its relatively high concentrations in Bakersfield and its high SOA yield, and because we have some knowledge of the kinetics of its oxidation products (*16*). Details of the box model used are included in the materials and methods SI. We find that because the second-generation products have SOA yields ~2.5 times as large as those of the first-generation products and that high concentrations of limonene inhibit the formation of these less-volatile products, SOA production slows in the high-limonene regime. At the same time, given sufficient O_3, increases in NO_2 always lead to more SOA owing to the higher NO_3 production rate.

Our findings suggest that SOA formation via nighttime nitrate radical chemistry in Bakersfield is a large PM source, which frequently results in the daily maximum OA concentration during the summer. The high concentrations of NO_2 and O_3 at night resulted in very high NO_3 production rates [frequently greater than 1 part per billion (ppb) hour^{-1}]. Nevertheless, concentrations of reactive BVOCs were frequently high enough that pΣAN formation was inhibited, suggesting that the pΣAN precursors are less reactive than the primary VOCs and have a somewhat reduced volatility. A good correlation between production rates of NO_3 and pΣAN was observed, suggesting that the targeted reductions in NO_x at this location should reduce OA mass. Although attributing sources of daytime SOA as biogenic or anthropogenic remains challenging, our results show that pΣANs are a large fraction of nighttime growth and likely a result of NO_3 chemistry. That this SOA would not be produced in the absence of NO_x makes nighttime pΣANs a clear tracer for anthropogenically controlled SOA, regardless of the carbon source.

References and Notes

1. Q. Zhang *et al.*, *Geophys. Res. Lett.* **34**, L13801 (2007A).
2. J. L. Jimenez *et al.*, *Science* **326**, 1525 (2009).
3. C. L. Heald, D. A. Ridley, S. M. Kreidenweis, E. E. Drury, *Geophys. Res. Lett.* **37**, L24808 (2010).
4. J. de Gouw, J. L. Jimenez, *Environ. Sci. Technol.* **43**, 7614 (2009).
5. C. R. Hoyle *et al.*, *Atmos. Chem. Phys.* **11**, 321 (2011).
6. Q. Zhang *et al.*, *J. Geophys. Res.* **112**, D22306 (2007).
7. U.S. Environmental Protection Agency, Our Nation's Air—Status and Trends through 2008 (Washington, DC, 2010).
8. D. C. Carslaw *et al.*, "Trends in NO_x and NO_2 emissions and ambient measurements in the UK." Version: July 2011.
9. B. W. LaFranchi, A. H. Goldstein, R. C. Cohen, *Atmos. Chem. Phys.* **11**, 6945 (2011).
10. M. Hallquist *et al.*, *Atmos. Chem. Phys.* **9**, 5155 (2009).
11. J. H. Kroll, J. H. Seinfeld, *Atmos. Environ.* **42**, 3593 (2008).
12. L. Hildebrandt *et al.*, *Geophys. Res. Lett.* **37**, L23801 (2010).
13. A. M. Winer, R. Atkinson, J. N. Pitts Jr., *Science* **224**, 156 (1984).
14. N. L. Ng *et al.*, *Atmos. Chem. Phys.* **8**, 4117 (2008).
15. A. W. Rollins *et al.*, *Atmos. Chem. Phys.* **9**, 6685 (2009).
16. J. L. Fry *et al.*, *Atmos. Chem. Phys.* **11**, 3879 (2011).
17. A. W. Rollins, J. D. Smith, K. R. Wilson, R. C. Cohen, *Environ. Sci. Technol.* **44**, 5540 (2010).
18. L. Bianco, I. V. Djalalova, C. W. King, J. M. Wilczak, *Boundary-Layer Meteorol.* **140**, 491 (2011).
19. B. J. Williams *et al.*, *Atmos. Chem. Phys.* **10**, 11577 (2010).
20. A. C. Aiken *et al.*, *Atmos. Chem. Phys.* **9**, 6633 (2009).
21. C. J. Hennigan, M. H. Bergin, A. G. Russell, A. Nenes, R. J. Weber, *Atmos. Chem. Phys.* **9**, 3613 (2009).
22. J. D. Surratt *et al.*, *J. Phys. Chem. A* **112**, 8345 (2008).
23. M. Hallquist, I. Wängberg, E. Ljungström, I. Barnes, K.-H. Becker, *Environ. Sci. Technol.* **33**, 553 (1999).
24. S. S. Brown *et al.*, *Atmos. Chem. Phys.* **9**, 3027 (2009).

Acknowledgments: This work is supported by the California Air Resources Board under grants CARB 08-316 and 09-328. E.C.B. was supported by NASA ESSF fellowship.

Supplementary Materials

www.sciencemag.org/cgi/content/full/337/6099/1210/DC1
Materials and Methods
Figs. S1 to S4
Table S1
References

6 March 2012; accepted 24 July 2012
10.1126/science.1221520

Predatory Fish Select for Coordinated Collective Motion in Virtual Prey

C. C. Ioannou,[1,2]* V. Guttal,[1,3] I. D. Couzin[1]*

Movement in animal groups is highly varied and ranges from seemingly disordered motion in swarms to coordinated aligned motion in flocks and schools. These social interactions are often thought to reduce risk from predators, despite a lack of direct evidence. We investigated risk-related selection for collective motion by allowing real predators (bluegill sunfish) to hunt mobile virtual prey. By fusing simulated and real animal behavior, we isolated predator effects while controlling for confounding factors. Prey with a tendency to be attracted toward, and to align direction of travel with, near neighbors tended to form mobile coordinated groups and were rarely attacked. These results demonstrate that collective motion could evolve as a response to predation, without prey being able to detect and respond to predators.

From herding ungulates to shoaling fish, nesting birds, and swarming crickets, animals living in groups are generally less at risk from predators (*1*). Mechanisms include the ability of groups to detect predators sooner and from a greater distance (the "many eyes" effect) and cognitive confusion of the predator, caused by having to choose among many possible targets

(*1*). Studies have focused on the costs and benefits of group size and position within the group (*2*–*4*), but how predation risk varies with the response of individuals to their neighbors is not well understood because of difficulties in its measurement (*5*, *6*) and manipulation (*7*). One such behavioral response that is common in nature is the tendency for individuals to align their direction of travel with that of near neighbors, forming coordinated "polarized" groups. It is often assumed that coordination between prey makes them harder to catch by enhancing information transfer between individuals (*5, 6*) or by increasing the confusion effect, although little experimental work supports this idea (*7*, *8*).

How animals move together has been simulated by agent-based models with generic behavioral tendencies: repulsion when neighbors are too close and otherwise aligning with, and/or being attracted to, neighbors. These models are able to recreate group movement such as swarms, in which attraction dominates alignment tendency, and coordinated polarized flocks or schools, in which alignment tendency becomes relatively strong (*9*–*13*). Although studies link this mechanistic approach back to functional explanations (*14*–*16*), there are few that have explicitly dealt with the relationship between predation and dynamic group behavior. Models can recreate the macroscopic responses of prey when under threat (*17*) and the evolution of swarmlike or highly polarized, coordinated groups as a direct result of simulated predator behavior (*18*). In many cases, however, it is unclear which properties of prey behavior are being selected for and why, and it remains to be established whether any real-life predators select for coordinated motion.

To explore these issues, we investigated how a predatory fish, the bluegill sunfish (*Lepomis macrochirus*), hunts simulated prey. Bluegills are generalist predators whose body plan is specialized for hunting in complex vegetated environments (*19*). Our system allows us to isolate the specific selection pressure of predation risk from the multitude of factors influencing the evolution of any trait, such as the associated costs of the trait and taxonomic constraints (*20*). In nature there is a wide variety of prey responses to predators; some react to predators as they approach (*2*), whereas others only respond once an attack is made (*21*), and these responses are further influenced by factors such as prey group size (*1*, *21*). Because our simulated prey could not respond to the fish, we analyzed only the first attack from each fish, which is analogous to situations where risk is determined primarily by the first attack (*22*). A simulation of animal movement (*23*) consisting of a behaviorally heterogeneous population of 16 prey was projected onto a translucent screen on an inner side of the test tank (Fig. 1 and fig. S1). Individual prey behavior was encoded by three traits: the strength of their behavioral tendencies to be attracted toward (ωa_i), orientate direction of travel with (ωo_i), or ignore (ωp_i) near neighbors [the three traits were normalized so that their sum was 1 (*12*, *24*, *25*) (table S1)]. Depending on these traits, prey exhibited a range of movement behaviors, including solitary random walk, formation and maintenance of aggregations, and coordinated polarized motion (movie S1).

The predators exerted a strong selection pressure on the virtual population, with some prey being attacked often while others were never attacked (Fig. 2A). The risk of being targeted was minimized for individuals with characteristics that balanced both attraction and orientation, resulting in an interaction between these two parameters [generalized linear model (GLM): likelihood ratio test ($LRT_{1,12}$) = 11.43, $P = 0.00072$]. This suggests that to most effectively avoid predation, prey should both move toward and align with their near neighbors, behavior that generates moving groups of coordinated individuals (*12*).

To a large degree, the strength of attraction mediates the group size for the simulated prey; when attraction is zero, prey are most frequently found alone (Fig. 2B). Although increasing the orientation parameter has only a minor effect on group size, it increases the straightness (i.e., decreases the "curvedness" or tortuosity) of the prey's path substantially when that prey is in a group (Fig. 2C). For example, although the prey type with $\omega a_i = 0.2$ and $\omega o_i = 0.6$ is rarely solitary, it tends to exhibit relatively directed, low-tortuosity motion (Fig. 2C), similar to the prey type that has no social tendency ($\omega a_i = 0.0$ and $\omega o_i = 0.0$) and is rarely found in a group. Furthermore, the tortuosity of a prey individual's path typically scales negatively with their group's polarization (the directional coherence among group members), so that nonsolitary individuals with low-tortuosity paths are typically in groups with high polarization (fig. S2).

To explore how these behaviors mediated the effects of both attraction and orientation on risk, we could not simply correlate the mean group size or tortuosity of a prey type with the number of attacks it received, because any choice made by the predator is constrained by the other prey phenotypes present at the time of attack. Instead, we created a null predator that chose a prey randomly at the same time steps as the observed attacks and compared the relationship between the targets' tortuosity and the group size expected from random targeting to that actually observed from the real predatory fish (*23*). Compared to random targeting, the fish disproportionately targeted prey in smaller groups, and this was strongest when prey were also taking less-tortuous paths (figs. S3 and S4). Prey in groups with a coordinated direction of motion (i.e., with high polarization) (*12*) were at less risk than their counterparts in unpolarized swarms (fig. S3).

Bluegill sunfish employ a characteristic "hovering" behavior during foraging (Fig. 1B) (*19*), allowing us to approximate the time taken to make each targeting decision. Consistent with a confusion effect (*26*), this decision time increased with the prey target's group size (GLM: $LRT_{1,67} = 11.32$, $P = 0.00077$). Although this accounts for the targeting of prey in smaller groups, there was no evidence that a prey's tortuosity, either alone or as part of an interaction with group size, had any additional effect [$LRT_{1,67} = 0.029$, $P = 0.86$; and $LRT_{1,66} = 0.22$, $P = 0.64$, respectively; see also (*7*, *8*)].

In response to the confusion effect (*27*), or simply because they are nearer on average (*3*, *4*), predators will often attack prey at the edge of groups. To test whether prey relatively far from the group center were attacked disproportionately, we used the null predator procedure described previously. The analysis indicates that this is indeed the case, but only for prey moving with relatively low tortuosity (fig. S5A). Although a number of the behavioral types often moved on paths with low tortuosity (Fig. 2C), prey with high orientation relative to attraction tended to be found more often at the edges of groups (fig. S5, C and D). This "self-assortment" (*12*) should contribute to selection against such prey types, in addition to their tendency to be solitary (Fig. 2B). However, the edge effect cannot explain why polarized groups were disproportionately less at risk (fig. S3) and why prey types with no tendency

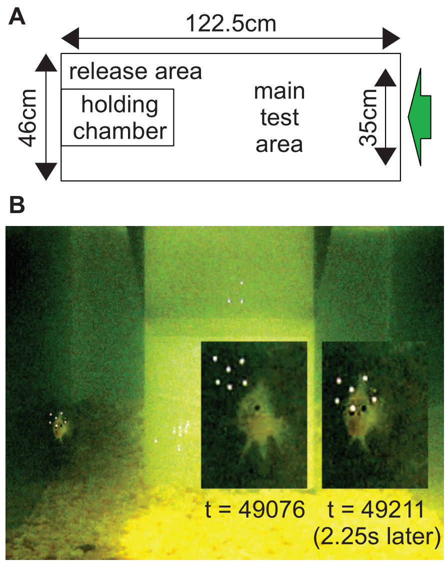

Fig. 1. The experimental system. (**A**) The simulation was projected (green arrow) onto a screen on the opposite side of the test tank to that where the fish was released. (**B**) Each attack was preceded by the fish hovering in front of the prey (white dots) (left inset) before accelerating toward a prey, opening the mouth and gill flaps (right inset). *t*, time step in the simulation.

[1]Department of Ecology and Evolutionary Biology, Princeton University, Princeton, NJ 08544, USA. [2]School of Biological Sciences, University of Bristol, Woodland Road, Bristol BS8 1UG, UK. [3]Centre for Ecological Sciences, Indian Institute of Science, Bangalore 560012, India.

*To whom correspondence should be addressed. E-mail: C.C.Ioannou@bristol.ac.uk (C.C.I.); icouzin@princeton.edu (I.D.C.)

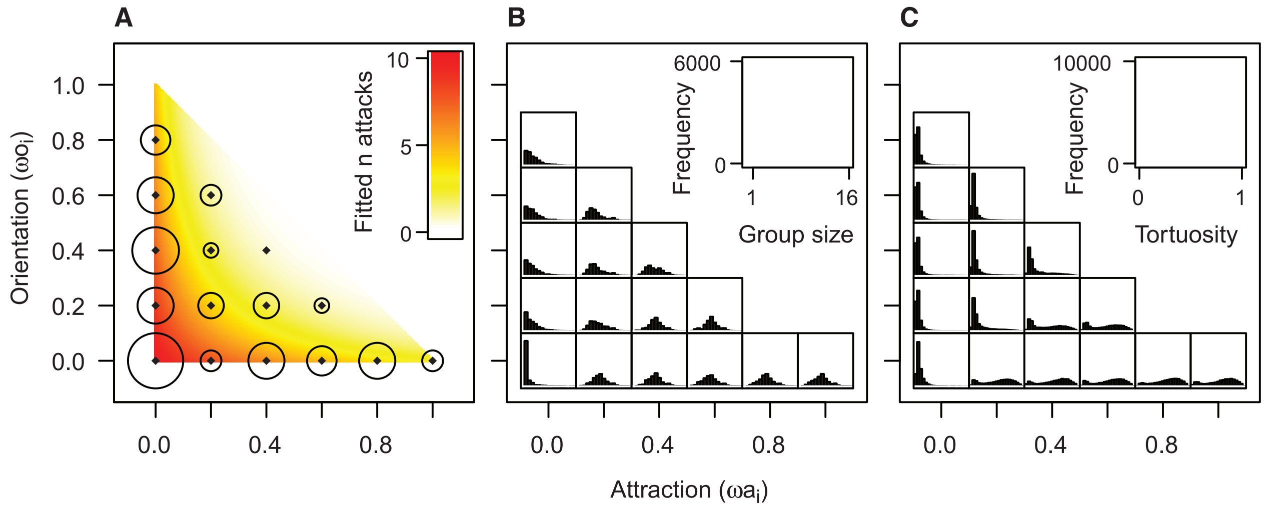

Fig. 2. Risk associated with attraction and orientation traits. (**A**) Based on their particular attraction and orientation tendencies (black diamonds), the number of attacks from a total of 70 that each prey type received (proportional to the area of the open circles; the largest of these is 14 attacks). The colored gradient represents the fitted values of this relationship from the fully factorial model, where red indicates more attacks and white fewer attacks (see color scale, inset). (**B** and **C**) Frequency distributions of each prey type's group size and tortuosity, respectively, pooled from the simulations presented to the fish in experiment 1. The scale of the histograms is shown in empty insets at top right. Group size was determined by the number of interconnected prey (*23*) every 250 time steps, whereas their individual tortuosity was calculated every 100 time steps.

to orient with their neighbors (ωo_i = *0*) were selected against (Fig. 2A).

In complex habitats, such as the littoral zone of lakes where bluegill sunfish are found, both predators and prey often exploit boundaries (*2*). The boundaries of the projection presented to the predators were periodic; i.e., when prey came in contact with a boundary, they would reappear at the opposite boundary with the same velocity. This ensured that the prey types were found with equal probability anywhere in the projected arena and excluded possible spatial artifacts confounding our results, such as swarming prey being found in the corners (*23*). Thus, if there is any tendency for prey with certain characteristics to be attacked in particular locations in the projected area, this must be due to the fish's behavior. We found that targeted prey tended to be in larger groups, and to have more tortuous paths, when they were nearer the top and bottom of the projection (Fig. 3; the vertical axis polynomial effect: GLM: $LRT_{2,65}$ = 13.07, P = 0.0015; and $LRT_{2,65}$ = 14.35, P = 0.00077, respectively). When hunting near the edge, predators experience groups that partly, or completely, cross the boundary (from the localized perception of the predator, this is analogous to prey occlusion by a physical structure in the environment). Individuals in groups with high tortuosity, and thus low net movement, persist for longer in such semi-occluded states and were particularly at risk. In direct contrast, prey in polarized groups were attacked less often, probably because their more directed movement gave less time for targeting to occur when they were within the high-risk area of the boundary. Further analysis of the pattern of risk seen in Fig. 2A demonstrates that although individuals in swarms are vulnerable at the boundaries, further from the boundary this effect weakens (fig. S6).

To ensure that our results were not sensitive to the distribution of prey types employed, and to demonstrate the selection of virtual prey strategies by real predators, we used the risk landscape in Fig. 2A to "evolve" our prey (*23*). We then presented either this evolved population or the original population to the fish in a second experiment (*23*). Although selection changed the frequencies of different prey types, and hence the group sizes and tortuosities in the projected simulation (table S2 and fig. S7), there was no evidence that the pattern observed in Fig. 2A changed between the pre- and postselection populations (population × attraction × orientation GLM: $LRT_{1,18}$ = 0.09, P = 0.76). Selection for orientation and attraction thus generalizes beyond an even distribution of behavioral parameters and appears relatively robust to frequency-dependent effects. Neither was there any evidence that selection had a detrimental effect on the fish's predatory behavior (table S3).

Our results show that predation risk is reduced among prey that exhibit both attraction and orientation under the conditions of our experiment, through an interaction between the confusion effect and the ability of prey to form coherent mobile groups. This is dependent on habitat properties that the predators exploit to facilitate targeting opportunities, without the necessity for prey individuals to react dynamically to the predator's presence, position, and/or attack (*6*, *18*). The degree of control afforded by virtual prey populations, as developed here, could allow a closed feedback loop between predator attack and prey response to explore such properties. This may reveal further dependencies and synergies between anti-predatory adaptations, predator hunting strategies, and habitat variables (*2*, *19*, *27*).

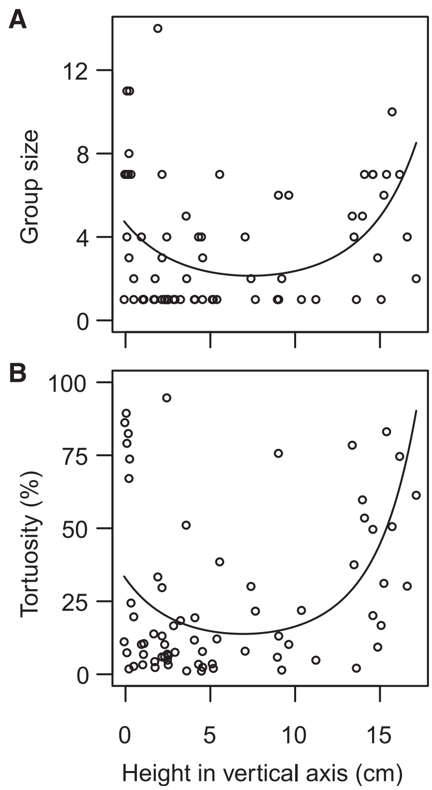

Fig. 3. Preferential targeting of group size (**A**) and tortuosity (**B**) as a function of height in the vertical axis of the projection. The curves show fitted values from models with the (polynomial) vertical axis effect only, because the horizontal axis had no significant effect. Tortuosity is expressed as a percentage of the maximum possible value. The individual tortuosity of the target prey is shown here; a similar trend was found for the tortuosity of the target's group as a whole (GLM: $LRT_{2,65}$ = 14.89, P = 0.00059; group tortuosity = 1 – group polarization).

References and Notes

1. J. Krause, G. D. Ruxton, *Living in Groups* (Oxford Univ. Press, Oxford, 2002).
2. W. Cresswell, J. L. Quinn, *Oikos* **104**, 71 (2004).
3. W. L. Romey, A. R. Walston, P. J. Watt, *Behav. Ecol.* **19**, 74 (2008).
4. W. D. Hamilton, *J. Theor. Biol.* **31**, 295 (1971).
5. M. Ballerini *et al.*, *Proc. Natl. Acad. Sci. U.S.A.* **105**, 1232 (2008).
6. N. O. Handegard *et al.*, *Curr. Biol.* **22**, 1213 (2012).
7. G. D. Ruxton, A. L. Jackson, C. R. Tosh, *Behav. Ecol.* **18**, 590 (2007).
8. K. A. Jones, A. L. Jackson, G. D. Ruxton, *Behav. Ecol.* **22**, 831 (2011).
9. R. Lukeman, Y. X. Li, L. Edelstein-Keshet, *Proc. Natl. Acad. Sci. U.S.A.* **107**, 12576 (2010).
10. Y. Katz, K. Tunstrøm, C. C. Ioannou, C. Huepe, I. D. Couzin, *Proc. Natl. Acad. Sci. U.S.A.* **108**, 18720 (2011).
11. J. Buhl *et al.*, *Science* **312**, 1402 (2006).
12. I. D. Couzin, J. Krause, R. James, G. D. Ruxton, N. R. Franks, *J. Theor. Biol.* **218**, 1 (2002).
13. J. K. Parrish, L. Edelstein-Keshet, *Science* **284**, 99 (1999).
14. S. Bazazi *et al.*, *Curr. Biol.* **18**, 735 (2008).
15. V. Guttal, I. D. Couzin, *Proc. Natl. Acad. Sci. U.S.A.* **107**, 16172 (2010).
16. D. Grünbaum, *Evol. Ecol.* **12**, 503 (1998).
17. R. Vabø, L. Nøttestad, *Fish. Oceanogr.* **6**, 155 (1997).
18. A. J. Wood, G. J. Ackland, *Proc. Biol. Sci.* **274**, 1637 (2007).
19. T. J. Ehlinger, D. S. Wilson, *Proc. Natl. Acad. Sci. U.S.A.* **85**, 1878 (1988).
20. H. Sayama, S. Dionne, C. Laramee, D. S. Wilson, in *IEEE Symposium on Artificial Life* (IEEE Conference Proceedings, Nashville, TN, 2009), pp. 85–91.
21. J. E. Treherne, W. A. Foster, *Anim. Behav.* **30**, 536 (1982).
22. W. Cresswell, *Ibis* **138**, 684 (1996).
23. Materials and methods are available as supplementary materials on *Science* Online.
24. I. D. Couzin, J. Krause, N. R. Franks, S. A. Levin, *Nature* **433**, 513 (2005).
25. I. D. Couzin, J. Krause, *Adv. Stud. Behav.* **32**, 1 (2003).
26. C. C. Ioannou, C. R. Tosh, L. Neville, J. Krause, *Behav. Ecol.* **19**, 126 (2008).
27. C. R. Tosh, *J. Theor. Biol.* **281**, 24 (2011).

Acknowledgments: We thank A. Hundal, M. Jiang, and M. Singh for assistance and A. S. I. Wade, the Couzin lab, and three anonymous reviewers for comments on the manuscript. Funded by Office of Naval Research award N00014-09-1-1074, NSF award PHY-0848755, Searle Scholar award 08-SPP-201, and Army Research Office grant W911NG-11-1-0385 (I.D.C.); Defense Advanced Research Projects Agency grant HR0011-05-1-0057 (Princeton University); Leverhulme Trust Early Career Fellowship (C.C.I.); and a Ramalingaswami Fellowship from the Department of Biotechnology, Government of India (V.G.). All experiments were conducted in accordance with federal and state regulations and were approved by the Princeton University Institutional Animal Care and Use Committee. Data and code are freely available at http://icouzin.princeton.edu.

Supplementary Materials
www.sciencemag.org/cgi/content/full/science.1218919/DC1
Materials and Methods
Figs. S1 to S7
Tables S1 to S3
References (*28–40*)
Movie S1

9 January 2012; accepted 26 July 2012
Published online 16 August 2012;
10.1126/science.1218919

Molecular Mechanics of Cardiac Myosin-Binding Protein C in Native Thick Filaments

M. J. Previs,[1] S. Beck Previs,[1] J. Gulick,[2] J. Robbins,[2] D. M. Warshaw[1]*

The heart's pumping capacity results from highly regulated interactions of actomyosin molecular motors. Mutations in the gene for a potential regulator of these motors, cardiac myosin-binding protein C (cMyBP-C), cause hypertrophic cardiomyopathy. However, cMyBP-C's ability to modulate cardiac contractility is not well understood. Using single-particle fluorescence imaging techniques, transgenic protein expression, proteomics, and modeling, we found that cMyBP-C slowed actomyosin motion generation in native cardiac thick filaments. This mechanical effect was localized to where cMyBP-C resides within the thick filament (i.e., the C-zones) and was modulated by phosphorylation and site-specific proteolytic degradation. These results provide molecular insight into why cMyBP-C should be considered a member of a tripartite complex with actin and myosin that allows fine tuning of cardiac muscle contraction.

Cardiac muscle's pumping capacity is produced by the sarcomere (Fig. 1A), a parallel array of proteins assembled into thick filaments, composed of myosin molecular motors that cyclically interact with actin-containing thin filaments, generating force that propels the thin filaments past the thick filaments. These actomyosin interactions can be modulated on a beat-to-beat basis by cardiac myosin-binding protein C (cMyBP-C) (Fig. 1B), a 140-kD immunoglobulin (Ig) protein superfamily member (Fig. 1C) that is confined to two distinct regions (i.e., C-zones) of the thick filament (*1*, *2*) (Fig. 1A). Mutations in the *MYBPC3* gene are a leading cause of familial hypertrophic cardiomyopathy (FHC) (*1*, *2*). Proposed mechanisms of cMyBP-C's function assume that several Ig-like domains and their linkers (C0–C2) (Fig. 1C) extend away from the thick filament backbone (Fig. 1B) (*3*) and reversibly bind to myosin's motor domains and/or actin filaments (*1*, *2*), with this binding tunable by phosphorylation of four serines (S273, S282, S302, and S307) in the motif linker between domains C1 and C2 (Fig. 1C) (*4*, *5*). Insight into cMyBP-C's function and regulation by phosphorylation has benefited from intact heart and muscle fiber studies, but these complex preparations make molecular-level interpretations difficult. Isolated protein studies, although simpler, lack the sarcomere's spatial relation between the thin and thick filaments. Here, we developed an in vitro sarcomere model system in which single actin filaments could be visualized moving over native cardiac thick filaments with and without cMyBP-C.

Cardiac thick filaments that retained their native length (~1.6 μm), bipolar structure, and central bare zone devoid of myosin heads (Fig. 1D) were isolated from mouse hearts by fine-tissue dissection and limited enzyme-induced protein degradation (0.2 U/μl μ-calpain) (*6*). Quantitative liquid chromatography–mass spectrometry (LC-MS) (*6*) showed that filaments contained the normal complement of cMyBP-C (fig. S1). Because cMyBP-C is a target for calpain-mediated protein degradation (*7*), protein immunoblotting with domain specific antibodies was used to show that 79 ± 4% (SD, $n = 3$) of the cMyBP-C molecules were intact (fig. S2), and in combination with LC-MS analyses, we determined that the remainder of the molecules had 29 kD of their N terminus removed (i.e., C0–C1 plus 17 amino acids of the motif, C0C1f) (Fig. 1C) by cleavage between amino acids R266 and R271 (fig. S3).

To assess cMyBP-C's mechanical impact on actin filament sliding, native cardiac thick filaments were adhered to a microscope cover slip. Fluorescently labeled actin filaments were then introduced onto the cover slip (25 mM KCl, 100 μM ATP, 22ºC), and their sliding along the thick filaments tracked (*6*) with high time (8.3-ms) and spatial (30-nm) resolution (Fig. 2A). The use of short [250 ± 9 nm (SEM)] actin filaments (fig. S4) prevented these filaments from spanning the bare zone (fig. S5), which allowed us to probe one-half of the thick filament where the actomyosin interactions were oriented as in the sarcomere (Fig. 1B). To ensure that a given actin filament traversed regions of the thick filament with and without cMyBP-C, we only analyzed trajectories greater than the C-zone length [i.e., ~350 nm (*8*)], averaging 658 ± 8.7 nm (SEM)

[1]Department of Molecular Physiology and Biophysics, University of Vermont, Burlington, VT 05405, USA. [2]Department of Pediatrics and the Heart Institute, Cincinnati Children's Hospital Medical Center, Cincinnati, OH 45229, USA.

*To whom correspondence should be addressed. E-mail: david.warshaw@uvm.edu

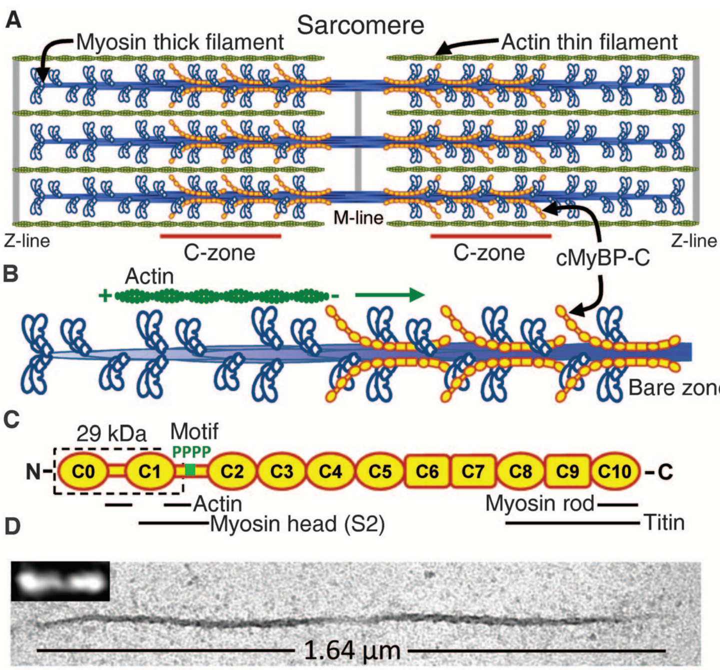

Fig. 1. Native cardiac thick filaments and cMyBP-C. (**A**) Cardiac muscle sarcomere with interdigitating thick and thin filaments with cMyBP-C localized to thick filament C-zones. M-line cross-links thick myosin filaments at the center of a sarcomere; the Z-line forms the boundary of the sarcomere. (**B**) Illustration of one-half of thick filament with an actin filament traveling toward the bare zone, as in experiments. (**C**) Schematic diagram of cMyBPC's Ig-like (oval) and fibronectin (rectangle) domains, with four phosphorylation sites (P) in motif linker, and 29-kD fragment (dashed box). Sarcomeric protein domain interactions are identified. (**D**) Native cardiac thick filament imaged by electron microscopy and total internal reflection fluorescence microscopy (TIRFM) (inset) by effectively labeling the myosin heads with fluorescent adenosine triphosphate (*6*).

before the actin filament diffused away from the thick filament. Displacement versus time traces for these trajectories were characterized by two different modes of travel. The majority (73%) displayed an initial fast velocity followed by a 45% slower velocity (Fig. 2, B and D, and Table 1), whereas the remaining 27% of trajectories (Fig. 2, C and E, and Table 1) had a constant velocity for the entire encounter, no different than the faster velocity observed for actin filaments that displayed two velocity phases. The distance traveled during the slow velocity phase [286 ± 57 nm (SD), $n = 58$] was similar to the C-zone length, which suggested that cMyBP-C had its effect restricted to the C-zone. To confirm this, we isolated thick filaments from cMyBP-C null mice (*9*), which displayed only a single fast velocity (Table 1). Thus, cMyBP-C slowed actomyosin motion generation only within the C-zone, which provided a molecular basis for sudden reductions in unloaded velocity observed in skeletal muscle fibers (*10*).

To explain the various modes of travel on wild-type thick filaments, we implemented an analytical model (*6*) to predict the velocity generated by two spatially distinct populations of myosin molecules (i.e., within the C-zone and outside of it) that mechanically interacted to propel a 250-nm actin filament (Fig. 2F). The predicted trajectories showed a 50% reduction in velocity for 334 ± 50 nm (SD, $n = 20$) (Fig. 2G), nearly equal to that of the C-zone length and that observed experimentally (Fig. 2B). The model also predicted that given our spatial resolution, trajectories would be described by a single velocity once the abundance of intact cMyBP-C within

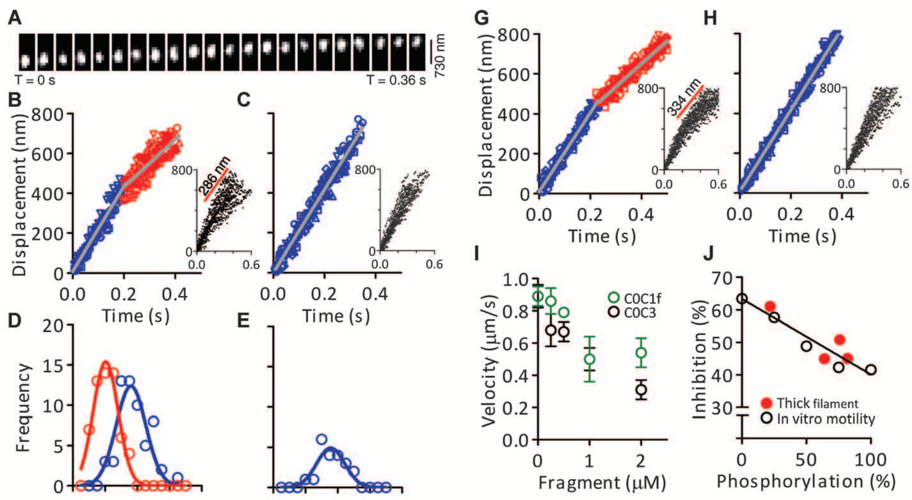

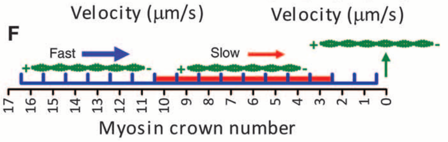

Fig. 2. Effect of cMyBP-C on actin motility. (**A**) TIRFM image series of actin shard moving along a native thick filament. (**B**) Displacement-time plots for five actin filaments on wild-type thick filaments demonstrated two velocity phases (fast, blue; slow, red). (Inset) Displacement-time plots for 20 filaments with distance traveled during slow velocity phase identified by red line. (**C**) As in B except actin filaments exhibited constant velocities. (**D**) Frequency-velocity histograms and Gaussian fits for actin trajectories as in (B) ($n = 58$; fast phase, blue; slow phase, red). (**E**) Frequency-velocity histogram and Gaussian fit for actin trajectories as in C with constant velocities ($n = 21$). (**F**) Spatial relations for an analytic model where actin filaments (green) moved over a thick filament with myosin crowns at the same azimuthal position separated by 43 nm and cMyBP-C localized in the C-zone [red highlighted crowns 3 to 11; (*8*)]. Actin detached upon reaching the bare zone (crown 0). (**G**) Model-generated displacement-time plots for a 250-nm actin filament on a thick filament with 78% intact cMyBP-C, as in (B). Fast phase = 1.98 ± 0.03 µm/s (SEM), slow phase = 1.15 ± 0.02 µm/s (SEM), $n = 5$ (Inset) Displacement-time plots for 20 filaments with slow-phase travel distance identified by red line. (**H**) As in (G) but for a theoretical thick filament with 10% intact cMyBP-C that showed only a constant velocity [2.06 ± 0.01 µm/s (SEM), $n = 5$; inset, 20 runs]. (**I**) Inhibition of actin sliding velocity by C0C1f and C0C3 fragments (mean ± SD) in motility assay. (**J**) Effect of motif phosphorylation on actin filament velocity inhibition by C0C3 in motility assay or by cMyBP-C in native thick filaments. Percent phosphorylation was defined as the average percent phosphorylation at S273, S282, S302, and S307. Percent inhibition of motility assay data was normalized to thick-filament inhibition data, where inhibition is the percent velocity reduction compared with a control without cMyBP-C or fragment.

the thick filament fell between 10 and 20% (Fig. 2H and fig. S6). If one assumes that removal of cMyBP-C's N-terminal 29-kD fragment effectively eliminated cMyBP-C's mechanical impact, then the 27% of actin trajectories over wild-type thick filaments with a single velocity (Fig. 2, C and E) most likely originated from thick filaments with a higher complement of truncated cMyBP-C. If so, then increasing the content of N-terminally cleaved cMyBP-C should increase the percentage of single-velocity trajectories, which was the case.

After increased enzymatic degradation (1.2 U/μl μ-calpain), 70 ± 10% (SD, $n = 3$) of the cMyBP-C had its N terminus removed (fig. S2); correspondingly, 80% of actin trajectories were described by a single velocity (Table 1). For the remaining 20% of actin trajectories that displayed two velocity phases, the faster velocity was unaffected by the increased N-terminal degradation, whereas the reduction in velocity within the C-zone was not as pronounced (i.e., 37%) (Table 1), because at least 50% of the cMyBP-C molecules were cleaved (based on model predictions) (fig. S6). Thus, the 29-kD C0C1f domain probably mediated the slowing of velocity to a large extent. Indeed, bacterially expressed C0C1f was able to inhibit actin filament movement over a surface of monomeric mouse cardiac myosin in an in vitro motility assay (Fig. 2I). Given that C0C1f stereospecifically and reversibly binds actin (*11*, *12*), this portion of the protein may tether the actin filament to the motility surface and act as a viscous load (*6*) to slow myosin's motion generation (*12*). Alternately, C0C1f could slow actin movement by directly binding to myosin, which would alter myosin's kinetics of motion generation (*10*, *13*, *14*).

In response to β-adrenergic stimulation, protein kinase A (PKA) phosphorylation of the motif and its effect on cMyBP-C are believed to be major contributors to enhanced cardiac contractility (*15*–*17*). We used LC-MS to quantify the degree of phosphorylation at each of the motif's phosphorylated serines (*6*), and varied phosphorylation either by treating wild-type thick filaments with kinase or phosphatase or by isolating filaments from transgenic mice (AllP+) (*18*). These AllP+ mice expressed mutant cMyBP-C in which S273, S282, and S302 were replaced by phosphomimetic aspartic acids with S307 phosphorylated endogenously. The high phosphorylation levels observed in the wild-type thick filaments (Table 2) agreed with those found in healthy hearts from mice and humans (*19*, *20*). Despite a modest increase in phosphorylation (<20%) observed when thick filaments were treated with PKA or isolated from AllP+ transgenic mice (Table 2), actin filament trajectories were indistinguishable from nontreated wild-type thick filaments (Table 1). In contrast, substantial dephosphorylation after lambda phosphatase treatment (Table 2) resulted in actin velocities within the C-zone that were 61% slower than the fast phase (Table 1) and suggested that dephosphorylated cMyBP-C was a more potent inhibitor of actomyosin motion generation.

To better define the relation between cMyBP-C phosphorylation and inhibition of actomyosin motility, we bacterially expressed a longer N-terminal cMyBP-C fragment (C0C3) that contained the entire motif with its four phosphorylatable serines and was as inhibitory as C0C1f in the motility assay (Fig. 2I). Mutant C0C3 with the four serines replaced with combinations of alanines and aspartic acids (as phosphomimetics) were expressed, which provided 25, 50, 75, and 100% phosphorylation levels (*6*). Increased levels of phosphomimetic substitution resulted in a proportional reduction in C0C3's inhibitory effect, similar to that observed in the limited thick filament data set (Fig. 2J). A potential mechanism for this effect is that phosphorylation alters the motif's intrinsically disordered structure (*21*) and, as it is directly connected to the 29-kD domain, may limit the C0C1f's spatial freedom to bind actin and/or myosin. Thus, the phosphorylation-dependent increase in velocity within the thick filament C-zone should contribute to both the increased unloaded shortening velocity (*15*) and faster tension recovery after stretch activation (*16*, *17*) observed in mouse myocardial preparations after PKA treatment.

Here, we found a mechanical role for cMyBP-C in modulating cardiac contractility even when restricted to the C-zone. Despite being spatially localized within the sarcomere, cMyBP-C's effective load should be transmitted through the 1-μm-long thin filaments to all attached myosins (Fig. 1A). Normal cardiac structure and function may rely on cMyBP-C's internal load to act as a governor, lowering power output and energy utilization, because sustained power elevation in cMyBP-C null mice leads to cardiac hypertrophy (*22*). Thus, cardiac hypertrophy in FHC patients with cMyBP-C haploinsufficiency (*2*) may be a secondary response to their reduced amount of cMyBP-C, which could lead to a hypercontractile heart. In contrast, excessive dephosphorylation of cMyBP-C, which is associated with cardiac ischemia (*7*, *23*) and failure (*20*), would lead to reduced power output, based on data presented here. Because dephosphorylated cMyBP-C is highly susceptible to proteolytic cleavage (*7*, *23*), the increased presence of the 29-kD fragment in the plasma of patients and animal models with heart failure (*7*) points to N-terminal cleavage, and its effective reduction in the number of functional cMyBP-C as a compensatory mechanism to restore cardiac power to more normal levels. Thus, cMyBP-C provides a measure of contractile tunability to a fully active muscle.

Table 1. Velocities measured on native cardiac thick filaments.

Thick-filament source	Calpain (U/μl)	Runs with slowing: Initial velocity (μm/s ± SE)	Runs with slowing: C-zone velocity (μm/s ± SE)	Runs with slowing: n	Runs without slowing: Velocity (μm/s ± SE)	Runs without slowing: n
Wild type	0.2	1.89 ± 0.06	1.04 ± 0.05	58	1.81 ± 0.09	21
cMyBP-C null	0.2			0	1.72 ± 0.05	55
Wild type	1.2	2.02 ± 0.08	1.27 ± 0.07*	22	1.94 ± 0.05	87
Wild type: PKA-treated	0.2	1.87 ± 0.06	0.92 ± 0.04	65	1.78 ± 0.09	31
AllP+	0.2	1.91 ± 0.07	1.05 ± 0.04	58	1.76 ± 0.07	27
Wild type: λ phosphatase–treated	0.2	1.77 ± 0.05	0.69 ± 0.05*	61	1.80 ± 0.09	20

*Significant difference in C-zone velocity when compared with wild type, $P < 0.01$, Mann-Whitney-Wilcoxon test.

Table 2. Degree of cMyBP-C phosphorylation quantified by LC-MS. Average = (S273 + S282 + S302 + S307)/400 ± error propagation. For values marked with asterisk, the endogenous serine was replaced with aspartic acid to mimic phosphorylation.

Amino acid	Phosphopeptide observed	Percent phosphorylation ± SD: Wild type ($n = 4$)	Wild type: PKA-treated ($n = 4$)	AllP+ ($n = 3$)	Wild type: λ phosphatase–treated ($n = 2$)
S273	^{271}RTS$_p$LAGAGR^{279}	73 ± 8	66 ± 5	100*	3
S282	^{280}RTS$_p$DSHEDAGTLDFSSLLK^{298}	90 ± 3	85 ± 2	100*	5
S302	^{299}KRDS$_p$FR^{304}	37 ± 18	73 ± 16	100*	47
S307	^{305}RDS$_p$KLEAPAEEDVWEILR^{322}	57 ± 6	82 ± 5	29 ± 6	32
Average		64 ± 20	76 ± 16	82 ± 6	22

References and Notes

1. S. Winegrad, *Circ. Res.* **84**, 1117 (1999).
2. S. P. Harris, R. G. Lyons, K. L. Bezold, *Circ. Res.* **108**, 751 (2011).
3. P. K. Luther *et al.*, *Proc. Natl. Acad. Sci. U.S.A.* **108**, 11423 (2011).
4. M. Gautel, O. Zuffardi, A. Freiburg, S. Labeit, *EMBO J.* **14**, 1952 (1995).
5. W. Jia, J. F. Shaffer, S. P. Harris, J. A. Leary, *J. Proteome Res.* **9**, 1843 (2010).
6. Materials and methods are available as supplementary materials on *Science* Online.
7. S. Govindan *et al.*, *J. Mol. Cell. Cardiol.* **52**, 154 (2012).
8. P. K. Luther *et al.*, *J. Mol. Biol.* **384**, 60 (2008).
9. M. E. Zoghbi, J. L. Woodhead, R. L. Moss, R. Craig, *Proc. Natl. Acad. Sci. U.S.A.* **105**, 2386 (2008).
10. P. A. Hofmann, M. L. Greaser, R. L. Moss, *J. Physiol.* **439**, 701 (1991).
11. J. Y. Mun *et al.*, *J. Mol. Biol.* **410**, 214 (2011).
12. A. Weith *et al.*, *J. Mol. Cell. Cardiol.* **52**, 219 (2012).
13. M. V. Razumova *et al.*, *J. Biol. Chem.* **281**, 35846 (2006).
14. J. Ratti, E. Rostkova, M. Gautel, M. Pfuhl, *J. Biol. Chem.* **286**, 12650 (2011).
15. S. Sadayappan *et al.*, *Circulation* **119**, 1253 (2009).
16. J. E. Stelzer, J. R. Patel, R. L. Moss, *Circ. Res.* **99**, 884 (2006).
17. C. W. Tong, J. E. Stelzer, M. L. Greaser, P. A. Powers, R. L. Moss, *Circ. Res.* **103**, 974 (2008).
18. S. Sadayappan *et al.*, *Proc. Natl. Acad. Sci. U.S.A.* **103**, 16918 (2006).
19. S. Sadayappan *et al.*, *Circ. Res.* **97**, 1156 (2005).
20. A. M. Jacques *et al.*, *J. Mol. Cell. Cardiol.* **45**, 209 (2008).
21. A. Karsai, M. S. Kellermayer, S. P. Harris, *Biophys. J.* **101**, 1968 (2011).
22. F. S. Korte, K. S. McDonald, S. P. Harris, R. L. Moss, *Circ. Res.* **93**, 752 (2003).
23. R. S. Decker *et al.*, *Circulation* **111**, 906 (2005).

Acknowledgments: NIH funds supported M.P. (HL007647); J.G., J.R., and D.W. (HL059408); and the Vermont Genetics Network for the LC-MS instrumentation (8P20GM103449). We thank B. Palmer and Y. Wang for mouse colony management; S. Tremble for technical assistance; M. Jennings for LC-MS expertise; M. Von Turkovich and the University of Vermont Microscopy Imaging Center for electron microscopy assistance; and G. Kennedy, from the Instrumentation and Modeling Facility, for imaging expertise. Data described in the paper are presented in the supplementary materials.

Supplementary Materials
www.sciencemag.org/cgi/content/full/science.1223602/DC1
Materials and Methods
Figs. S1 to S6
References (*24–34*)

20 April 2012; accepted 20 July 2012
Published online 23 August 2012;
10.1126/science.1223602

Conformational Control of the Ste5 Scaffold Protein Insulates Against MAP Kinase Misactivation

Jesse G. Zalatan,[1]* Scott M. Coyle,[1,2]* Saravanan Rajan,[4] Sachdev S. Sidhu,[4] Wendell A. Lim[1,3]†

Cells reuse signaling proteins in multiple pathways, raising the potential for improper cross talk. Scaffold proteins are thought to insulate against such miscommunication by sequestering proteins into distinct physical complexes. We show that the scaffold protein Ste5, which organizes the yeast mating mitogen-activated protein kinase (MAPK) pathway, does not use sequestration to prevent misactivation of the mating response. Instead, Ste5 appears to use a conformation mechanism: Under basal conditions, an intramolecular interaction of the pleckstrin homology (PH) domain with the von Willebrand type A (VWA) domain blocks the ability to coactivate the mating-specific MAPK Fus3. Pheromone-induced membrane binding of Ste5 triggers release of this autoinhibition. Thus, in addition to serving as a conduit guiding kinase communication, Ste5 directly receives input information to decide if and when signal can be transmitted to mating output.

Cells use a complex network of signaling proteins to respond to diverse signals and stresses. Execution of proper decisions is complicated by the fact that individual cells contain many closely related signaling proteins (*1*). In fact, the same proteins are often reused in multiple signaling pathways (*2*, *3*). The resulting interlinked networks could lead to inappropriate cross talk between signaling pathways.

Scaffold proteins, which physically assemble components of a signaling pathway (*4*–*6*), provide a possible solution to this problem. By binding and organizing pathway components into complexes, scaffold proteins promote efficient signaling along a particular pathway. Scaffold proteins may also insulate against improper communication by physically sequestering signaling proteins into distinct pools (*7*–*15*). However, to prevent shared proteins from exchanging between pools, a scaffold must bind its partners with dissociation rates that are slow compared to the time scale for signaling. Direct evidence for this prevailing view of scaffold-based insulation is limited.

A prototypical scaffold protein is Ste5, which coordinates the yeast mating mitogen-activated protein kinase (MAPK) response by binding to all three components of the MAPK cascade and

[1]Department of Cellular and Molecular Pharmacology, University of California, San Francisco, 600 16th Street, San Francisco, CA 94158, USA. [2]Program in Biological Sciences, University of California, San Francisco, 600 16th Street, San Francisco, CA 94158, USA. [3]Howard Hughes Medical Institute, University of California, San Francisco, 600 16th Street, San Francisco, CA 94158, USA. [4]Banting and Best Department of Medical Research, Department of Molecular Genetics, and the Terrence Donnelly Centre for Cellular and Biomolecular Research, University of Toronto, 160 College Street, Toronto, Ontario M5S 3E1, Canada.

*These authors contributed equally to this work.
†To whom correspondence should be addressed. E-mail: lim@cmp.ucsf.edu

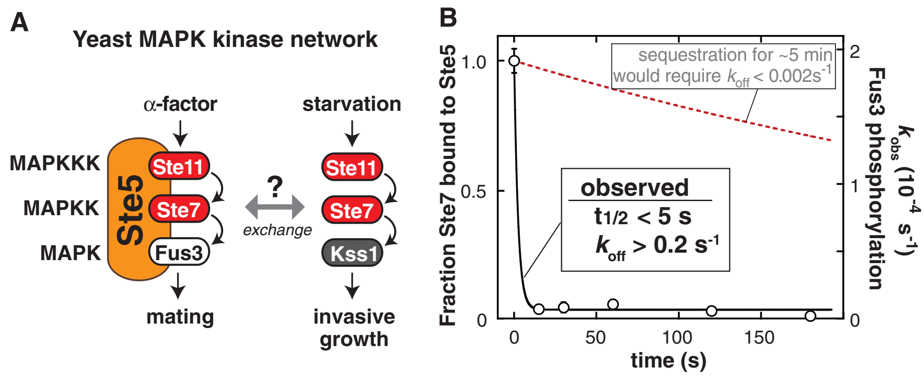

Fig. 1. Exchange of the Ste7 MAPKK from the Ste5 scaffold protein. (**A**) Shared components of the yeast mating and invasive growth pathways yield physiologically distinct input-output responses. (**B**) Dissociation rate of the MAPKK Ste7 from the Ste5 scaffold protein measured with purified recombinant Ste5, the MAPKKK Ste11, the MAPK Fus3, and a constitutively active form of the MAPKK Ste7 [Ste7EE, bearing phosphomimic mutations in the Ste7 activation loop (*16*)]. To a preassembled Ste5-Ste11-Ste7-Fus3 complex, an excess of a Ste7 binding domain [a minimal Ste7 binding domain from Ste5 (residues 759 to 810)] was added to capture Ste7 as it dissociated from Ste5 (fig. S1). At various times, adenosine 5′-triphosphate (ATP) was added, and the initial rate of Fus3 phosphorylation was measured (the amount of Ste5-Ste11-Ste7-Fus3 complex remaining at each timepoint). Error bars, mean ± SD. The observed k_{off} of 0.2 s^{-1} is a lower limit; dissociation occurred on a time scale faster than could be measured with mixing by hand.

serving as a required coactivator of the mating-specific MAPK, Fus3 (*16*, *17*). The Ste5 scaffold is thought to insulate the mating response from other MAPK pathways in yeast, such as the starvation response, which uses the identical MAPK kinase (MAPKK), Ste7, and MAPKK kinase (MAPKKK), Ste11, proteins, but activates a distinct starvation-specific MAPK Kss1 to produce an invasive growth response (Fig. 1A) (*2*, *17*). How the common MAPKK, Ste7, when activated by a specific input, is directed to the correct downstream MAPK is only partially understood. With mating input, both Fus3 and Kss1 are activated (binding to the Ste5 scaffold does not prevent the MAPKK Ste7 from activating Kss1) (*16*, *18*). However, activation of Kss1 by mating input does not lead to cross talk because activated Fus3 overrides the Kss1-induced starvation response by phosphorylating and down-regulating a starvation-specific transcription factor (*19*, *20*). Thus, proper starvation response hinges on preventing Fus3 misactivation by starvation inputs, which would both launch the mating program and directly inhibit the starvation response.

For Ste5 to act as a sequestration-based insulator would require exchange rates for the scaffold-bound shared kinases (Ste11 or Ste7) to be slow relative to the time scale of signaling. Otherwise, shared kinases activated by nonmating inputs would be able to exchange onto the Ste5 scaffold protein and activate the mating response [Fus3 can only be activated when the MAPKK Ste7 is bound to the Ste5 scaffold (*16*)]. We measured the dissociation of purified Ste7 from Ste5 to have a half time ($t_{1/2}$) of <5 s (Fig. 1B), faster by several orders of magnitude than the typical ~5 min time scale of MAPK signaling pathways, and far faster than the time scale of days on which the yeast starvation response operates. Thus, physical sequestration is unlikely to be the primary mechanism that prevents activation of the mating MAPK Fus3 by nonmating inputs.

An alternative model for insulation is that, in the absence of mating input, Ste5 adopts an inactive conformation that blocks its ability to cocatalyze Fus3 phosphorylation (*17*). To investigate this possibility, we measured rates of Fus3

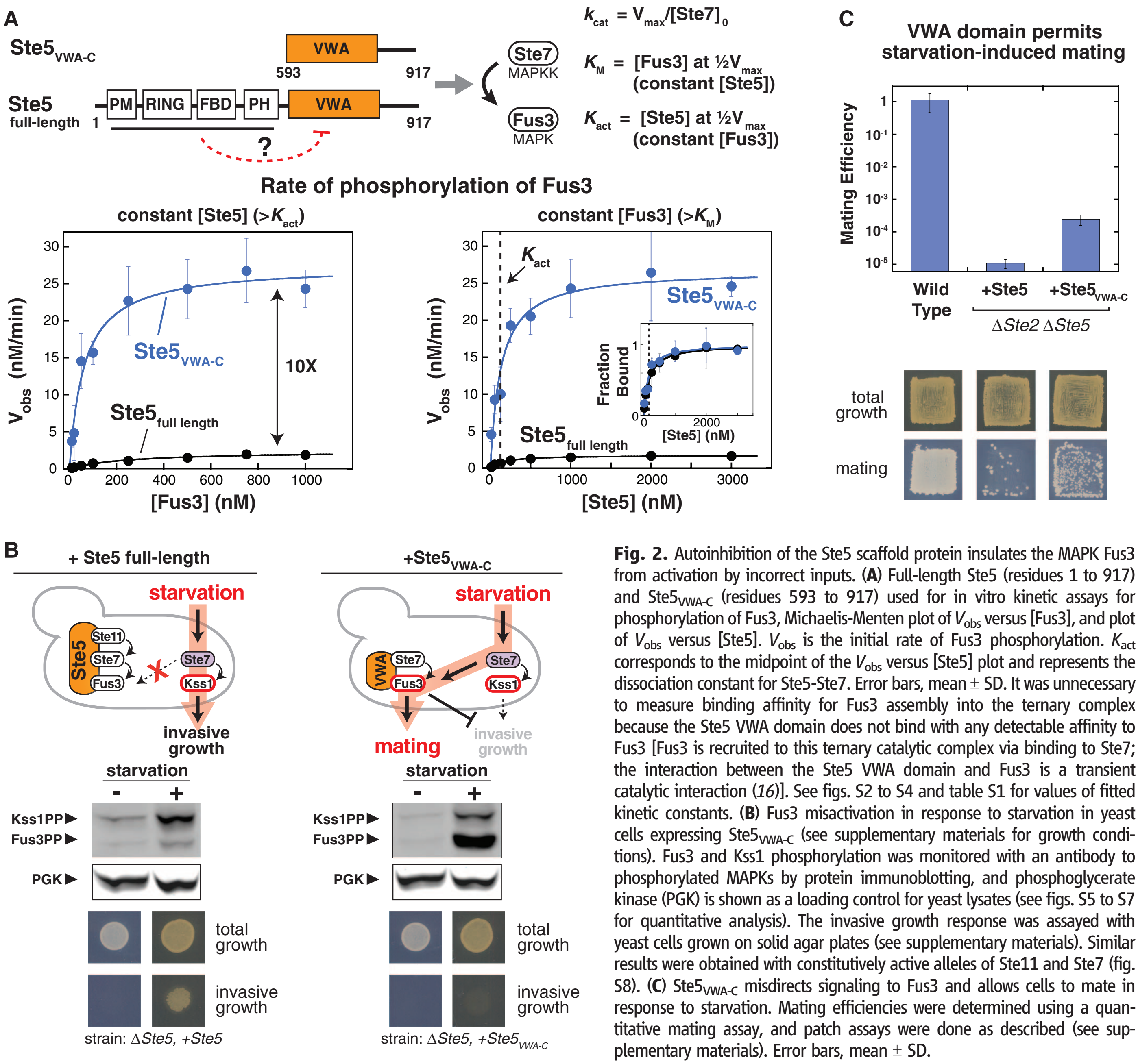

Fig. 2. Autoinhibition of the Ste5 scaffold protein insulates the MAPK Fus3 from activation by incorrect inputs. (**A**) Full-length Ste5 (residues 1 to 917) and $Ste5_{VWA-C}$ (residues 593 to 917) used for in vitro kinetic assays for phosphorylation of Fus3, Michaelis-Menten plot of V_{obs} versus [Fus3], and plot of V_{obs} versus [Ste5]. V_{obs} is the initial rate of Fus3 phosphorylation. K_{act} corresponds to the midpoint of the V_{obs} versus [Ste5] plot and represents the dissociation constant for Ste5-Ste7. Error bars, mean ± SD. It was unnecessary to measure binding affinity for Fus3 assembly into the ternary complex because the Ste5 VWA domain does not bind with any detectable affinity to Fus3 [Fus3 is recruited to this ternary catalytic complex via binding to Ste7; the interaction between the Ste5 VWA domain and Fus3 is a transient catalytic interaction (*16*)]. See figs. S2 to S4 and table S1 for values of fitted kinetic constants. (**B**) Fus3 misactivation in response to starvation in yeast cells expressing $Ste5_{VWA-C}$ (see supplementary materials for growth conditions). Fus3 and Kss1 phosphorylation was monitored with an antibody to phosphorylated MAPKs by protein immunoblotting, and phosphoglycerate kinase (PGK) is shown as a loading control for yeast lysates (see figs. S5 to S7 for quantitative analysis). The invasive growth response was assayed with yeast cells grown on solid agar plates (see supplementary materials). Similar results were obtained with constitutively active alleles of Ste11 and Ste7 (fig. S8). (**C**) $Ste5_{VWA-C}$ misdirects signaling to Fus3 and allows cells to mate in response to starvation. Mating efficiencies were determined using a quantitative mating assay, and patch assays were done as described (see supplementary materials). Error bars, mean ± SD.

phosphorylation by the MAPKK Ste7 with full-length Ste5 and with a minimal Ste5 fragment [Ste5$_{VWA\text{-}C}$, containing a von Willebrand type A (VWA) domain that is required for Fus3 coactivation, together with active MAPKK Ste7 (*16*)]. Under maximal rate (k_{cat}) conditions (saturating concentrations of all components), the rate of Fus3 phosphorylation with full-length Ste5 was one-tenth that in the presence of Ste5$_{VWA\text{-}C}$ (Fig. 2A). Assembly of the Ste5-Ste7-Fus3 complex was similar with either Ste5 construct (Fig. 2A), suggesting that the dominant contribution to the difference in activity is not a binding effect (disruption of kinase complex assembly) but rather a disruption of the catalytic coactivator function of the VWA domain.

To test the possibility that this activity difference contributes to insulation of the mating MAPK Fus3 in vivo, we introduced the fully active Ste5$_{VWA\text{-}C}$ fragment into yeast. In these cells, starvation led to substantial activation of Fus3, whereas cells with full-length Ste5 predominantly activated the starvation MAPK Kss1 (Fig. 2B). Thus, the minimal Ste5$_{VWA\text{-}C}$ fragment promotes Fus3 activation when the MAPKK Ste7 is activated, regardless of whether cells have received the mating signal or not. Because activated Fus3 cross-inhibits the starvation signaling pathway at the transcriptional level (*19*, *20*), this misactivation of Fus3 prevents the normal physiological

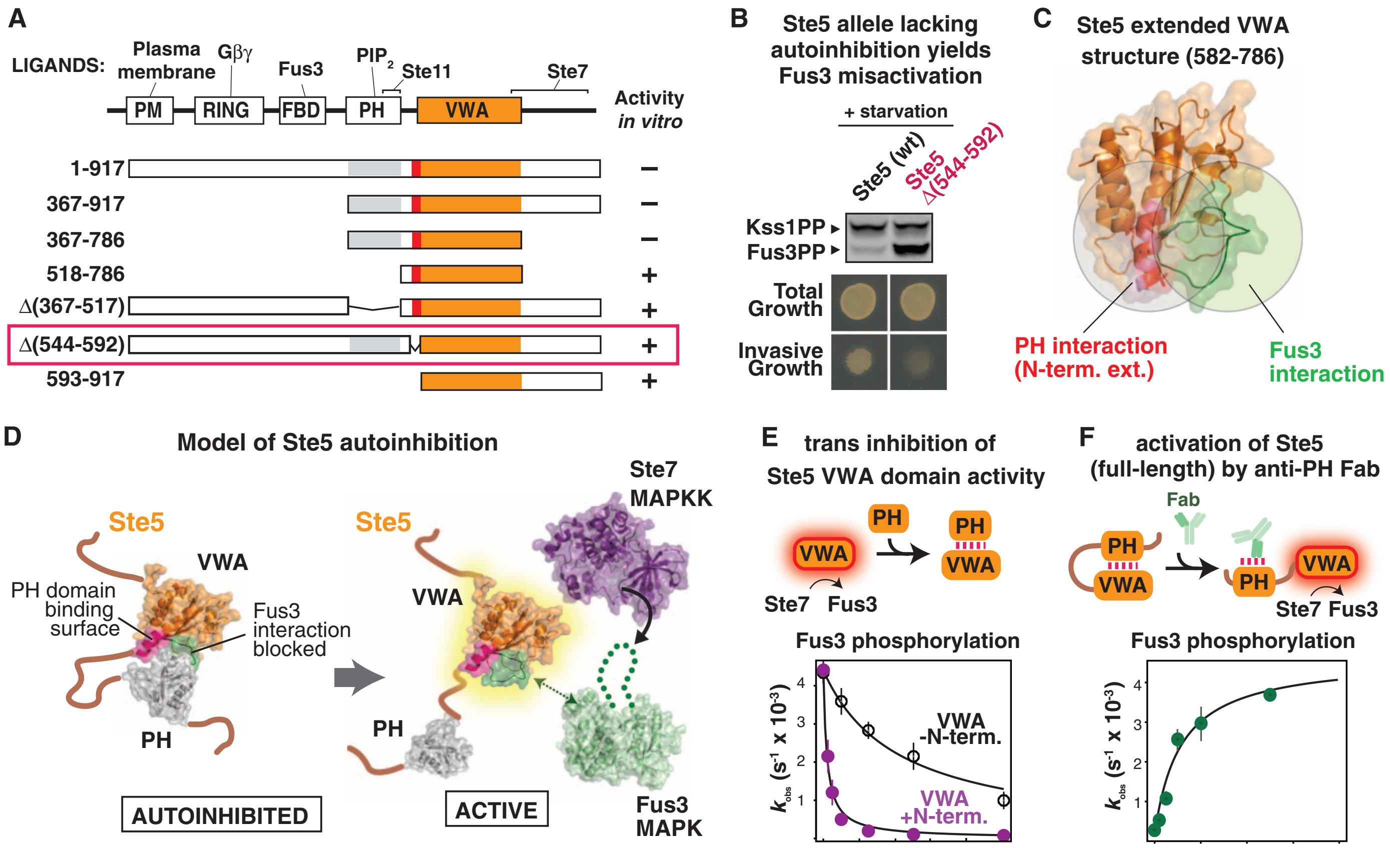

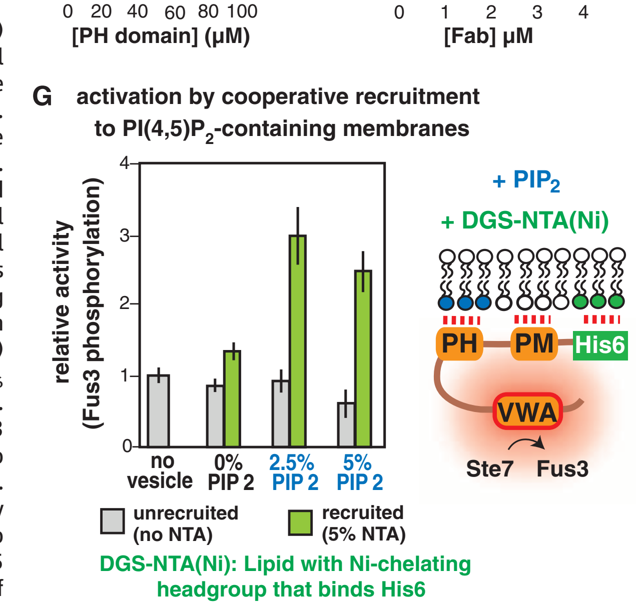

Fig. 3. Mechanism of Ste5 autoinhibition and activation by mating-specific input. (**A**) Diagram of truncation mapping of Ste5 (red is residues 544 to 592). The minimal autoinhibited fragment (367 to 786) contains all elements necessary to assemble the three-tiered MAPK cascade [Fus3 is recruited to the VWA domain by Ste7 (*16*)]. See fig. S9 for additional constructs. (**B**) Effect of deletion of the N-terminal extension of the VWA domain in Ste5 (residues 544 to 592) to disrupt pathway insulation in vivo. Activation of Fus3 measured by protein immunoblotting, and invasive growth assayed on solid agar plates (assays conducted as in Fig. 2B; also see fig. S6). (**C**) Crystal structure of Ste5$_{582\text{-}786}$ (see table S4 for crystallographic statistics). The N-terminal extension (582 to 592) is shown in pink, with surface residues necessary for trans inhibition by the PH domain (fig. S10) shown as sticks in red. The Fus3-coactivating loop of Ste5 (743 to 756) is shown in green. The spatial proximity of the PH-domain interface and the site of Fus3 coactivation is illustrated by overlapping circles. (**D**) Model for Ste5 autoinhibition inferred from truncation mapping data and Ste5$_{582\text{-}786}$ crystal structure, using structural models as described in the supplementary materials. (**E**) Titration of the VWA domain with the PH domain results in inhibition of the Fus3 coactivator activity (k_{obs}) of the VWA construct bearing the N-terminal extension (582 to 786, shown in pink), or lacking the N-terminal extension (593 to 786, shown in black). Error bars, mean ± SD. (**F**) Relief of autoinhibition in full-length Ste5 by a Fab antibody (SR13) that can bind the PH domain. Error bars, mean ± SD. (**G**) Recruitment of Ste5 to membranes with PIP$_2$ stimulates coactivation of Fus3. A minimal, autoinhibited Ste5 fragment bearing a hexahistidine tag can be recruited to small unilamellar vesicles of varying lipid compositions by the DGS-NTA(Ni) lipid (see fig. S13 for exact details of the Ste5 construct used here). Error bars, mean ± SD.

response to starvation (invasive growth) (Fig. 2B). Further, under starvation conditions, $Ste5_{VWA\text{-}C}$ restores a partial mating phenotype in cells that lack the mating receptor, Ste2 (Fig. 2C); full rescue of mating likely requires mating pathway components upstream of the kinase cascade that are not activated by starvation (*21*). Thus, cells expressing the unregulated $Ste5_{VWA\text{-}C}$ fragment misinterpret starvation as a signal to phosphorylate the mating MAPK Fus3, blurring the normally clear insulation between the starvation and mating pathways.

By deletion analysis, we identified two regions of Ste5 essential for autoinhibition of the VWA domain in vitro: the PH domain, which binds to phosphoinositol 4,5-bisphosphate (PIP_2) to facilitate membrane binding (*22*) and binds to the MAPKKK Ste11 (*23*), and an N-terminal extension to the VWA domain (residues 544 to 592), within the linker that connects the PH and VWA domains (Fig. 3A and fig. S9). When Ste5 was replaced by Ste5Δ(544-592) in vivo, activation of Fus3 in response to mating pheromone was normal (fig. S7), but Fus3 was misactivated in response to starvation (Fig. 3B). Because all kinase binding sites are intact in Ste5Δ(544-592), this result supports the idea that physical sequestration of kinases by Ste5 is not sufficient for pathway insulation.

We determined the crystal structure of an extended VWA fragment (residues 582 to 786; we were unable to obtain crystals for a PH-VWA complex) (Fig. 3C). This construct includes the minimal N-terminal extension that binds the PH domain (fig. S10). This extension forms an N-terminal α helix lying directly adjacent to the VWA domain coactivator loop that contains residues essential for Fus3 coactivation (*16*). The spatial proximity of the autoinhibitory PH domain binding site (the N-terminal extension) and the Fus3 coactivator loop indicates that PH domain binding and Fus3 activation might be mutually exclusive, providing a molecular mechanism for Ste5 autoinhibition (Fig. 3D). Indeed, the isolated PH domain of Ste5 inhibited the Fus3 coactivator function of the VWA domain in trans (Fig. 3E). Further, a Fab antibody fragment that binds the PH domain competitively relieved autoinhibition (Fig. 3F and fig. S11). Also, an allele of Ste5 (S770N) that was previously found to constitutively activate the mating pathway (*24*) is not autoinhibited in vitro (fig. S12).

An early step in mating pathway activation is pheromone-induced membrane recruitment of Ste5, which requires a cooperative set of membrane interactions that includes the PH domain binding to PIP_2 lipids (*22*). Thus, binding of Ste5 to PIP_2-containing membranes might disrupt the PH-VWA interaction and relieve autoinhibition. We designed a minimal, membrane-binding Ste5 construct that is autoinhibited, but PIP_2-containing lipid vesicles did not bind or activate this construct in vitro (fig. S13). Because pheromone-induced membrane recruitment of Ste5 is a cooperative process that requires several membrane-binding motifs (*21*), we induced association of the autoinhibited Ste5 construct to the lipid vesicles using other cooperative membrane interactions (Fig. 3G and fig. S13). Under these conditions, PIP_2 caused a 3-fold activation of Ste5 (Fig. 3G), suggesting that membrane recruitment of Ste5 and its interaction with PIP_2 contributes to relief of autoinhibition of Ste5. The inability of such membrane association to completely relieve autoinhibition of Ste5 (a 10-fold effect) (Fig. 2A) could result from incomplete binding to lipid vesicles in vitro (fig. S13) or because complete activation requires additional interactions present in vivo. Ste5 oligomerization has been suggested to contribute to pathway activation (*25*), but we find no evidence that oligomerization plays a direct role in relief of Ste5 autoinhibition (fig. S14).

We propose that, although the shared upstream kinases (MAPKKK Ste11 and MAPKK Ste7) can be activated by other inputs, only mating input activates both the kinase cascade and the Ste5 scaffold protein to permit Fus3 activation (Fig. 4A). Activation of the mating pathway recruits Ste5 to the membrane (*21*), thus activating the MAP kinase cascade by bringing the MAPKKK Ste11 in proximity to its upstream kinase Ste20. Membrane recruitment may also relieve autoinhibition in Ste5 when the PH domain interacts with PIP_2 at the membrane (Fig. 4B).

To further test this model, we decoupled the two functions of Ste5 by deleting the upstream

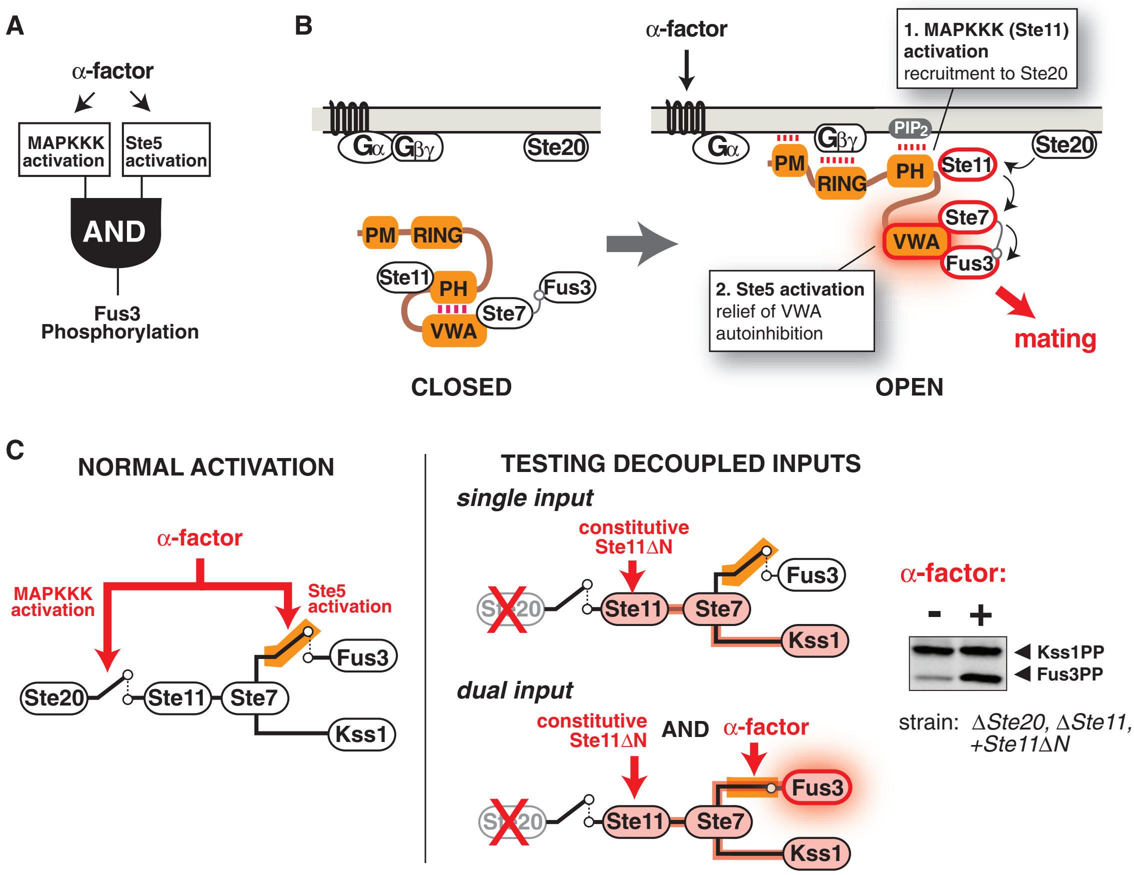

Fig. 4. Mating input–mediated conformational activation of Ste5. (**A**) Simple AND-gate model for specific mating pathway activation. Nonmating inputs that activate the shared MAPKKK do not activate Fus3. (**B**) Revised molecular model for mating pathway activation mediated by the Ste5 scaffold protein. Mating pheromone (α factor) activates a heterotrimeric G protein, leading to release of the Gβγ subunit from Gα and recruitment of Ste5 to free Gβγ at the membrane (*21*). Membrane recruitment triggers activation of the MAPKKK Ste11 and PH domain binding to PIP_2, leading to release of the VWA domain and relief of autoinhibition. (**C**) Fus3 activation in vivo when kinase cascade activation is decoupled from the mating signal (α factor), measured by protein immunoblotting. See fig. S15 for additional Ste11 alleles and controls.

kinase Ste20 (preventing normal activation of the MAPK cascade) and introducing a constitutively active allele of the MAPKKK Ste11, thus rendering activation of the kinase cascade independent of the mating signal. Previous experiments of this type demonstrated that full pathway activation still requires the mating input, suggesting that the input acts on a step downstream of kinase cascade activation (*24*, *26*). Here, we take this approach one step further by using a constitutively active allele, Ste11ΔN (*27*), which lacks the Ste5 binding site (*28*), so that any observed effects of Ste5 activation are likely to arise from promoting the Ste7→Fus3 reaction rather than the Ste11→Ste7 reaction. When wild-type Ste11 was replaced by Ste11ΔN in a yeast strain lacking Ste20, the MAPK Kss1 was preferentially phosphorylated, but when this strain was treated with α factor, activation of Fus3 was observed (Fig. 4C), supporting the idea that pheromone-induced membrane recruitment of Ste5 has two distinct and separable functions: to activate the MAPKKK Ste11 and to relieve autoinhibition in Ste5 to permit Fus3 activation.

Our data do not support the prevailing model that scaffold proteins primarily insulate signaling by sequestration of proteins. Instead, Ste5 appears to function as a conformational switch to gate the flow of information between two distinct signaling outcomes. This mechanism provides a potentially general means to control information flow in complex signaling networks with shared components.

References and Notes

1. S. S. Taylor *et al.*, *Trends Biochem. Sci.* **18**, 84 (1993).
2. M. A. Schwartz, H. D. Madhani, *Annu. Rev. Genet.* **38**, 725 (2004).
3. M. S. Qi, E. A. Elion, *J. Cell Sci.* **118**, 3569 (2005).
4. M. C. Good, J. G. Zalatan, W. A. Lim, *Science* **332**, 680 (2011).
5. D. K. Morrison, R. J. Davis, *Annu. Rev. Cell Dev. Biol.* **19**, 91 (2003).
6. A. S. Shaw, E. L. Filbert, *Nat. Rev. Immunol.* **9**, 47 (2009).
7. H. Saito, *Curr. Opin. Microbiol.* **13**, 677 (2010).
8. D. N. Dhanasekaran, K. Kashef, C. M. Lee, H. Xu, E. P. Reddy, *Oncogene* **26**, 3185 (2007).
9. K. Harris *et al.*, *Curr. Biol.* **11**, 1815 (2001).
10. W. R. Burack, A. S. Shaw, *Curr. Opin. Cell Biol.* **12**, 211 (2000).
11. T. P. Garrington, G. L. Johnson, *Curr. Opin. Cell Biol.* **11**, 211 (1999).
12. A. J. Whitmarsh, R. J. Davis, *Trends Biochem. Sci.* **23**, 481 (1998).
13. T. Pawson, J. D. Scott, *Science* **278**, 2075 (1997).
14. S. Marcus, A. Polverino, M. Barr, M. Wigler, *Proc. Natl. Acad. Sci. U.S.A.* **91**, 7762 (1994).
15. K.-Y. Choi, B. Satterberg, D. M. Lyons, E. A. Elion, *Cell* **78**, 499 (1994).
16. M. Good, G. Tang, J. Singleton, A. Reményi, W. A. Lim, *Cell* **136**, 1085 (2009).
17. L. J. Flatauer, S. F. Zadeh, L. Bardwell, *Mol. Cell. Biol.* **25**, 1793 (2005).
18. E. A. Elion, J. A. Brill, G. R. Fink, *Proc. Natl. Acad. Sci. U.S.A.* **88**, 9392 (1991).
19. M. Z. Bao, M. A. Schwartz, G. T. Cantin, J. R. Yates 3rd, H. D. Madhani, *Cell* **119**, 991 (2004).
20. S. Chou, L. Huang, H. P. Liu, *Cell* **119**, 981 (2004).
21. L. Bardwell, *Peptides* **26**, 339 (2005).
22. L. S. Garrenton, S. L. Young, J. Thorner, *Genes Dev.* **20**, 1946 (2006).
23. C. Inouye, N. Dhillon, T. Durfee, P. C. Zambryski, J. Thorner, *Genetics* **147**, 479 (1997).
24. R. E. Lamson, S. Takahashi, M. J. Winters, P. M. Pryciak, *Curr. Biol.* **16**, 618 (2006).
25. C. Inouye, N. Dhillon, J. Thorner, *Science* **278**, 103 (1997).
26. D. M. Lyons, S. K. Mahanty, K. Y. Choi, M. Manandhar, E. A. Elion, *Mol. Cell. Biol.* **16**, 4095 (1996).
27. B. R. Cairns, S. W. Ramer, R. D. Kornberg, *Genes Dev.* **6**, 1305 (1992).
28. G. Jansen, F. Bühring, C. P. Hollenberg, M. Ramezani Rad, *Mol. Genet. Genomics* **265**, 102 (2001).

Acknowledgments: J.G.Z. is supported by the Damon Runyon Cancer Research Foundation (DRG 2012-09). S.M.C. is supported by a National Science Foundation Graduate Research Fellowship. S.S.S. and S.R. are supported by a grant from the Canadian Institutes for Health Research (MOPS-93725). This work was also supported by NIH grants RO1 GM55040, RO1 GM62583, PN2 EY016546, and P50 GM081879 (W.A.L.) and by the Howard Hughes Medical Institute (W.A.L.). We thank G. Narlikar, H. Madhani, and M. Good for helpful discussions and comments; N. Helman and S. Vidal for plasmids; H. Madhani for providing yeast strains; and C. Waddling for assistance with x-ray data collection. Coordinates have been submitted to the Protein Data Bank (4F2H).

Supplementary Materials

www.sciencemag.org/cgi/content/full/science.1220683/DC1
Materials and Methods
Figs. S1 to S15
Tables S1 to S4
References

16 February 2012; accepted 10 July 2012
Published online 9 August 2012;
10.1126/science.1220683

Rad51 Is an Accessory Factor for Dmc1-Mediated Joint Molecule Formation During Meiosis

Veronica Cloud,[1,2] Yuen-Ling Chan,[2] Jennifer Grubb,[2] Brian Budke,[2] Douglas K. Bishop[1,2,3]*

Meiotic recombination in budding yeast requires two RecA-related proteins, Rad51 and Dmc1, both of which form filaments on DNA capable of directing homology search and catalyzing formation of homologous joint molecules (JMs) and strand exchange. With use of a separation-of-function mutant form of Rad51 that retains filament-forming but not JM-forming activity, we show that the JM activity of Rad51 is fully dispensable for meiotic recombination. The corresponding mutation in Dmc1 causes a profound recombination defect, demonstrating Dmc1's JM activity alone is responsible for meiotic recombination. We further provide biochemical evidence that Rad51 acts with Mei5-Sae3 as a Dmc1 accessory factor. Thus, Rad51 is a multifunctional protein that catalyzes recombination directly in mitosis and indirectly, via Dmc1, during meiosis.

Meiosis reduces chromosome number as required for biparental reproduction. The meiotic program evolved by modification of the mitotic cell cycle, via duplication and specialization of key proteins, including the RecA family members Rad51 and Dmc1 (*1*, *2*). Rad51 and Dmc1 form nucleoprotein filaments on single-stranded DNA (ssDNA) tracts that flank double-strand break (DSB) sites. These filaments search for, and swap strands with, homologous double-stranded DNA (dsDNA) segments on unbroken chromatids to form homologous joint molecules (JMs). Rad51 is the only protein that acts directly in JM formation during mitotic recombination. Dmc1 is a meiosis-specific protein. Normal meiotic recombination depends on both Rad51 and Dmc1. Previous results reveal that both Rad51 and Dmc1 are capable of carrying out homology search and catalyzing the formation of JMs (*3*–*5*), but they do not reveal whether one, the other, or both proteins contribute these activities during wild-type (WT) meiosis.

[1]Committee on Genetics, University of Chicago, Cummings Life Science Center, 920 East 58th Street, Chicago, IL 60637, USA. [2]Department of Radiation and Cellular Oncology, University of Chicago, Cummings Life Science Center, 920 East 58th Street, Chicago, IL 60637, USA. [3]Department of Molecular Genetics and Cell Biology, University of Chicago, Cummings Life Science Center, 920 East 58th Street, Chicago, IL 60637, USA.

*To whom correspondence should be addressed. E-mail: dbishop@uchicago.edu

The *Escherichia coli* RecA protein has two DNA binding sites, a high-affinity site (site I) sufficient for polymerization of proteins on ssDNA tracts and a low-affinity DNA binding site (site II) specifically required for interaction of the ssDNA-protein filament with a second DNA during homology search and JM formation (*6*) (fig. S1A). Site II in RecA includes positively charged residues Arg^{243} (R243) and Lys^{245} (K245) (*7*); a third residue, R227, completes a basic patch on the groove of the helical filament. This patch corresponds to a patch of three residues in Rad51 protein (R188, K361, and K371; fig. S1B). We mutated these three residues in Rad51 to alanine to form Rad51-II3A. This protein was then purified (fig. S2).

To test Rad51-II3A for site I binding activity, we used fluorescence polarization (FP) and electrophoretic mobility shift assays (EMSA). FP detected no difference in apparent binding affinity between the WT protein (Rad51-WT) and Rad51-II3A (Fig. 1A). EMSA analysis showed that both Rad51-WT and Rad51-II3A shift the mobility of both ss- and dsDNA under similar

conditions (Fig. 1B). However, the extent of mobility shift by Rad51-II3A was less than that by Rad51-WT, possibly reflecting a greater tendency of Rad51-II3A to dissociate during electrophoresis and/or a difference in site II binding. In some experiments, Rad51-WT, but not Rad51-II3A, caused a substantial fraction of DNA to be retained in the well. Electron microscopy (EM) analysis showed that Rad51-II3A forms filaments on ssDNA that do not differ from those formed by Rad51-WT with respect to average length, width, or pitch (Fig. 1C and fig. S3). Together these observations indicate that Rad51-II3A retains substantial site I binding activity.

To assay for site II binding, we first saturated site I with unlabeled ssDNA [3 nucleotides (nt) per Rad51 protomer] in the presence of adenylyl-imidodiphosphate (AMP-PNP) to block filament dissociation (*8*). We then added heterologous ^{32}P-labeled dsDNA. EMSA analysis showed that ssDNA-Rad51-WT filaments were able to alter the mobility of up to 25% of input dsDNA (Fig. 1D). The shifted species was not detected with ssDNA-Rad51-II3A filaments under the same conditions, consistent with a site II binding defect.

We then measured the ability of Rad51-II3A to form JMs via a D-loop assay. A ^{32}P-labeled oligonucleotide was preincubated with protein and mixed with homologous supercoiled plasmid DNA (Fig. 2A). Reaction mixtures were incubated for 30 min, at which time D-loop levels plateaued. D-loops were detected by comigration of oligonucleotide and plasmid on gels. The Rad51 mediator Rad52 or the DNA translocase Rad54 was added to enhance Rad51 D-loop activity (*9*). Rad51-II3A had no detectable activity in Rad52-stimulated reactions, whereas 26 ± 8% (SEM) of duplex DNA was converted to D-loops by Rad51-WT (Fig. 2B). Results were similar with Rad54-stimulated assays, although a small amount of activity was detected for Rad51-II3A (0.7 ± 0.3% compared with 11 ± 2% for Rad51-WT; Fig. 2C). These results demonstrate that Rad51-II3A is profoundly defective in the ability to form D-loops despite retaining site I DNA binding activity.

To test for DNA binding activity in vivo, we examined the effect of the *rad51-II3A* mutation on immunostaining Rad51 foci, which are formed by binding at tracts of DSB-dependent ssDNA (*10*). The *rad51-II3A* strain (table S1) formed the same number of Rad51 foci as WT (33 ± 3 in WT and 32 ± 2 in *rad51-II3A*; fig. S4), indicating that the protein retains DNA binding activity in cells. We also stained meiotic nuclei for Dmc1 (fig. S5). The foci formed by Dmc1 in *rad51*Δ are about threefold fainter in average staining intensity than those in WT, implying a role for Rad51 in normal assembly of Dmc1 at DSBs (*11*, *12*). In contrast, *rad51-II3A* formed Dmc1 foci of WT staining intensity. This result suggests that Rad51-II3A retains the ability to enhance assembly of Dmc1 at sites of recombination.

To test for JM activity in vivo, we examined mitotic yeast cells in which Rad51 is the only RecA homolog expressed. Rad51's JM activity promotes recombinational repair of lethal DSBs induced by ionizing radiation. We therefore compared the γ-ray sensitivity of *rad51-II3A* to that of WT and *rad51*Δ. A *rad51*Δ and a *rad51-II3A* mutant showed the same high sensitivity to γ rays; the mean lethal dose (D_0) was about 360 Gy compared to 1410 Gy in WT (Fig. 3A), indicating that *rad51-II3A* cells are severely defective in repair of mitotic DNA breaks.

We next used the *rad51-II3A* mutant to ask whether Rad51's JM activity is required for interhomolog recombination during meiosis. We measured map distance (Fig. 3B), gene conversion frequency (table S2A), and crossover interference (table S2B) by using strains with 12 markers (*13*). No significant differences were detected between WT and *rad51-II3A*, indicating that interhomolog recombination occurs normally in a strain that is severely deficient in Rad51's JM activity.

Previous analysis of the *rad51*Δ mutant using two-dimensional (2D) gels to detect interhomolog (IH) JMs and intersister (IS) JMs in meiosis showed that the null mutant is severely defective in interhomolog bias (Fig. 3C); the 4.8 ± 0.2 to 1 (SEM, $N = 6$) bias toward IH JMs over IS JMs observed in WT is altered to 1 to 3.9 ± 0.3 ($N = 3$) in *rad51*Δ (*3*). In contrast to *rad51*Δ, *rad51-II3A* has the same IH/IS ratio as WT (4.7 ± 0.3 to 1, $N = 6$; Fig. 3D), providing further evidence that Rad51's JM activity does not contribute to its role in meiotic recombination. The only substantial phenotypic differences detected between WT and *rad51-II3A* were a 1-hour delay in formation of JMs and a reduction in spore viability from 99 ± 0.6 to 87 ± 1.9% (Fig. 3E).

As an additional control to ensure that Rad51-II3A lacks recombinogenic activity in meiotic cells, we examined the effect of the mutation in a *hed1*Δ *dmc1*Δ background where Rad51 contributes the only strand-exchange activity. In this background, *RAD51*$^+$ promotes high levels of JM formation, but *rad51-II3A* confers a strong block to Rad51-dependent formation of homologous JMs in meiosis (fig. S6).

Thus, Dmc1's JM-forming activity is sufficient for normal meiotic interhomolog recombination. To confirm that Dmc1's JM activity is necessary for meiotic recombination, we constructed and analyzed a *dmc1-II3A* mutant strain. The *dmc1-II3A* strain showed a uniform meiotic arrest in prophase and a complete block to JM formation identical to that observed in the *dmc1*Δ mutant (fig. S7). This result indicates that, in contrast to Rad51, Dmc1's ability to form nucleoprotein filaments is not sufficient for its role in

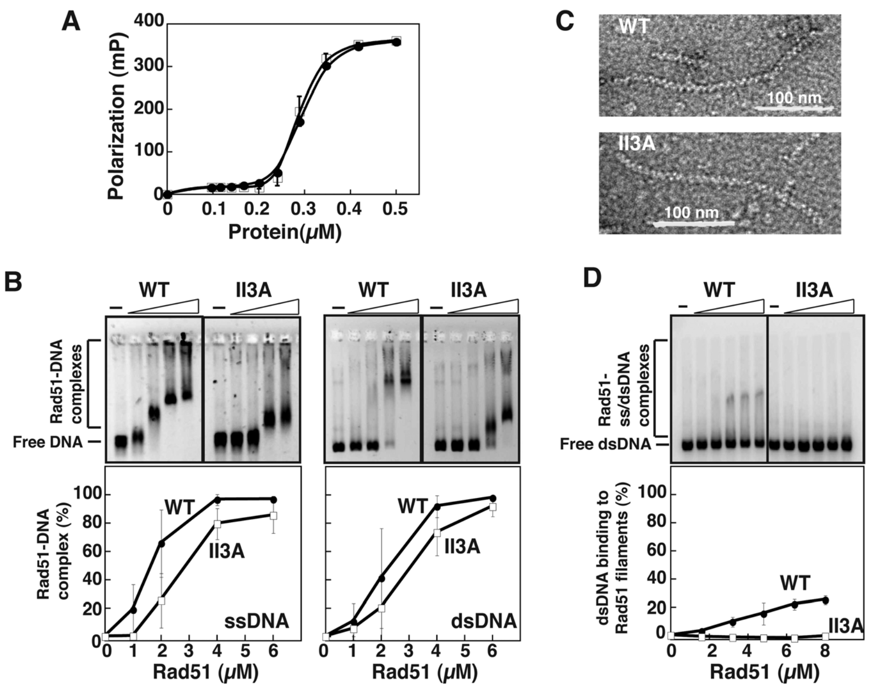

Fig. 1. Rad51-II3A binds DNA to form nucleoprotein filaments. (**A**) Rad51-WT (solid circle) and Rad51-II3A (open square) bind oligo-dT as revealed by fluorescence polarization. mP indicates millipolarization units. Error bars represent SEM, $N = 4$. The apparent affinity of both proteins is about 300 nM. (**B**) EMSA analysis of DNA binding. Protein (at 0, 1, 2, 4, and 6 μM) binds M13mp18 ssDNA (22 μM nucleotides) and linear pBluescript dsDNA (8 μM base pairs). The inverted images of agarose gels are presented. The percentage of DNA in Rad51-DNA complexes is plotted. SEM, $N = 6$ for ssDNA, $N = 3$ for dsDNA. (**C**) Rad51-WT and Rad51-II3A proteins form filaments on a 1000-nucleotide fragment of ØX174 ssDNA. (**D**) ssDNA-Rad51-WT but not ssDNA-Rad51-II3A filaments bind ^{32}P-pBluescript dsDNA (18 μM base pairs). Filament concentrations are 0, 1.5, 2.9, 4.4, 5.8, and 7.3 μM protomer (at 3 nt per protomer). Phosphorimage of radioactive EMSA gel is presented. For plotted data, $N = 3$.

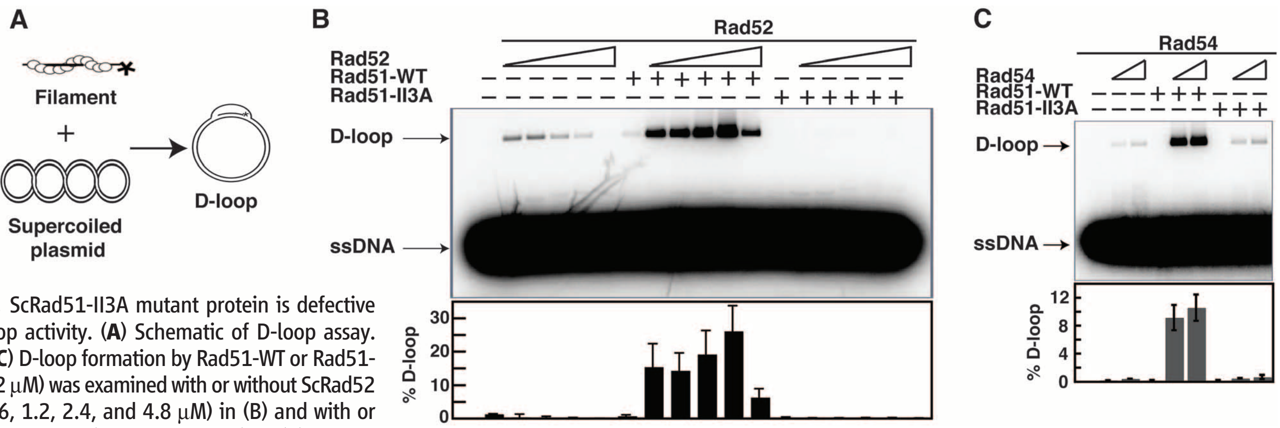

Fig. 2. ScRad51-II3A mutant protein is defective in D-loop activity. (**A**) Schematic of D-loop assay. (**B** and **C**) D-loop formation by Rad51-WT or Rad51-II3A (1.2 μM) was examined with or without ScRad52 (0.3, 0.6, 1.2, 2.4, and 4.8 μM) in (B) and with or without ScRad54 (0.2 and 0.4 μM) in (C). Rad51 was preincubated with either Rad52 or Rad54, followed by incubation with ^{32}P-labeled 90-mer ssDNA (3.6 μM nucleotides) at 37°C. D-loops were generated upon the addition of plasmid (22 μM base pairs) to the mixture. Error bars represent SEM, N = 3.

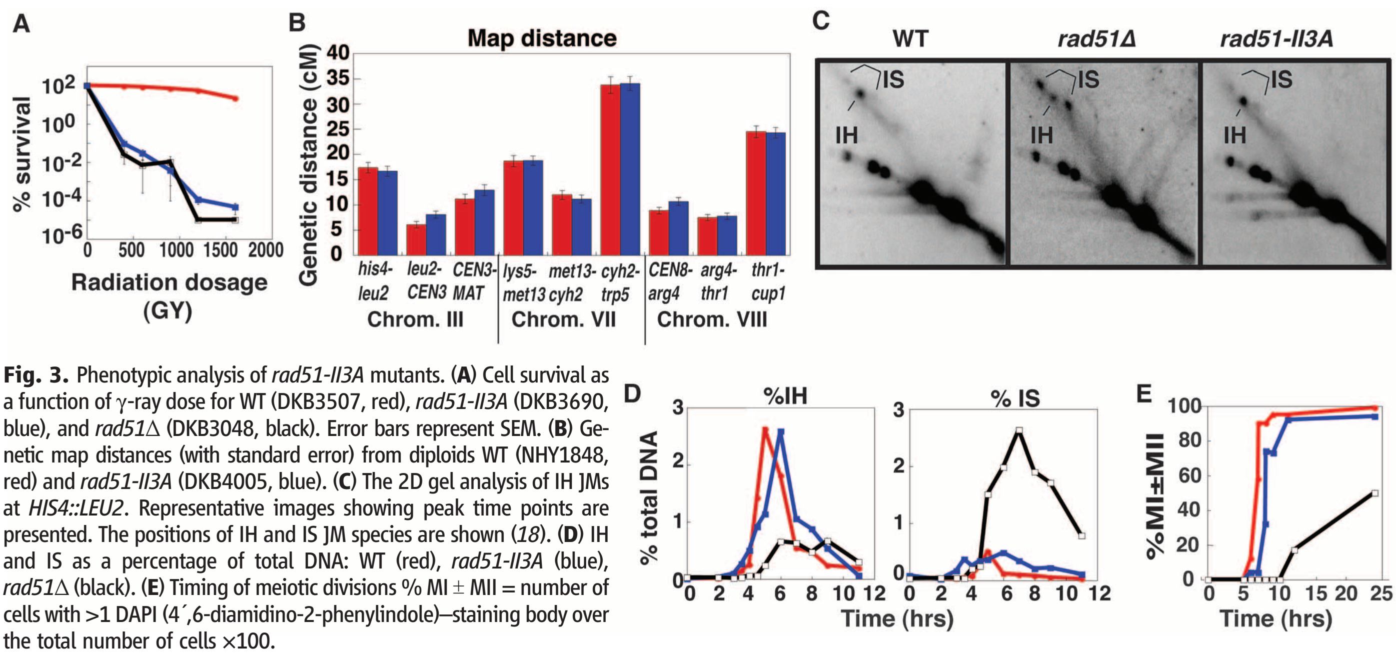

Fig. 3. Phenotypic analysis of *rad51-II3A* mutants. (**A**) Cell survival as a function of γ-ray dose for WT (DKB3507, red), *rad51-II3A* (DKB3690, blue), and *rad51*Δ (DKB3048, black). Error bars represent SEM. (**B**) Genetic map distances (with standard error) from diploids WT (NHY1848, red) and *rad51-II3A* (DKB4005, blue). (**C**) The 2D gel analysis of IH JMs at *HIS4::LEU2*. Representative images showing peak time points are presented. The positions of IH and IS JM species are shown (*18*). (**D**) IH and IS as a percentage of total DNA: WT (red), *rad51-II3A* (blue), *rad51*Δ (black). (**E**) Timing of meiotic divisions % MI ± MII = number of cells with >1 DAPI (4′,6-diamidino-2-phenylindole)–staining body over the total number of cells ×100.

interhomolog recombination. Biochemical experiments showed that, like Rad51-II3A, Dmc1-II3A retains DNA binding but not D-loop activity (fig. S8).

The observation that Rad51 contributes to homolog bias of JM formation independently of its strand-exchange activity, together with the observation that Rad51 promotes formation of Dmc1 foci, implies that Rad51 regulates Dmc1's strand-exchange activity. The heterodimeric mediator Mei5-Sae3 stimulates Dmc1 function in vivo and in vitro (*14*, *15*). We therefore asked whether we could identify conditions under which Rad51 could function with Mei5-Sae3 to promote Dmc1's D-loop activity in a purified system. In the presence of magnesium and adenosine triphosphate, about 1.2 ± 0.5% of duplex plasmid is converted to D-loop in reactions containing 1 μM Dmc1 as the only protein (Fig. 4A, lane 2). Addition of 0.5 μM Mei5-Sae3 reduced the activity of Dmc1 under these conditions such that D-loop yield was 0.5 ± 0.3% (Fig. 4A, lane 8). However, addition of 0.5 μM Rad51-WT protein converted Mei5-Sae3's inhibitory activity to a stimulatory activity, enhancing the level of D-loops to 13 ± 5%, a level 26 ± 17 times higher than adding Mei5-Sae3 alone (Fig. 4A, lane 10). Rad51-II3A protein also stimulated the reaction with Mei5-Sae3 and Dmc1 11 ± 4 times more, indicating that Rad51's D-loop activity is not required for Dmc1 stimulation (Fig. 4B, lanes 10 to 12). The stimulatory activity of Rad51-II3A was less sensitive to dilution than that of the WT protein. Although the reason for this difference remains to be determined, it is possible that removal of three positively charged amino acids from the Rad51 filament groove enhances the direct interaction of Rad51 with Mei5-Sae3 (*16*). Consistent with this idea, modeling studies have suggested that Mei5-Sae3 binds in the filament groove (*17*).

Overall, the results show Rad51 can function with Mei5-Sae3 as a mediator of Dmc1's strand-exchange activity, consistent with the finding that Mei5, Sae3, and Rad51 are required for Dmc1 focus formation during meiosis. It remains to be determined whether and how Rad51's role in Mei5-Sae3–dependent stimulation of Dmc1's D-loop activity is related to its role in homolog bias.

Our results suggest that, after the duplication that created Rad51 and Dmc1, Dmc1 evolved to serve the specialized mechanisms of meiotic recombination. These mechanisms ensure generation of chiasmata connecting every homologous chromosome pair. Rad51 instead has evolved to be an accessory for Dmc1 while retaining its JM-forming activity, as required for mitotic DNA repair. Rad51's JM-forming activity may also be important as a fail-safe for rare occasions when the Dmc1-dependent interhomolog JM mechanism fails. Such a fail-safe function for Rad51 would account for the modest reduction of spore viability observed in *rad51-II3A*. Similar modes of evolution may have formed other functional

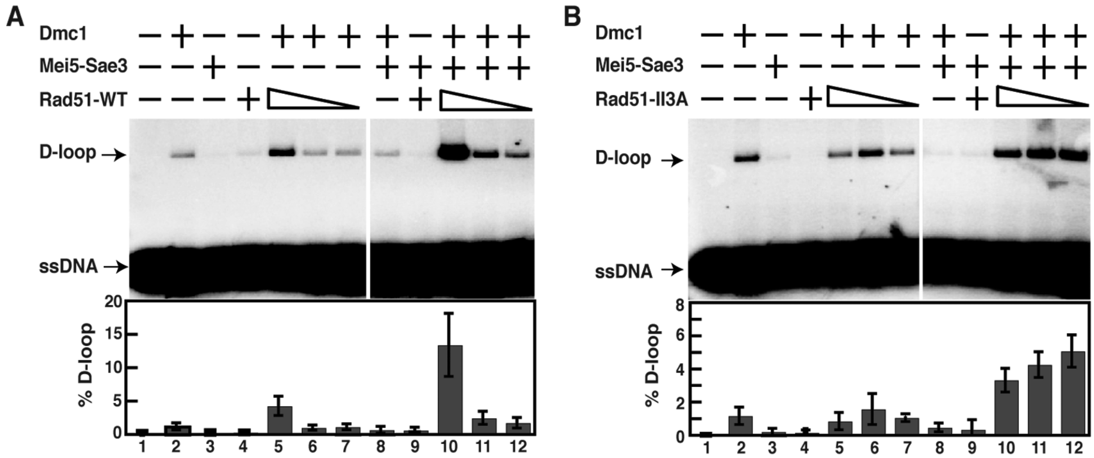

Fig. 4. Rad51 stimulates Dmc1's D-loop activity. Dmc1 (1 μM) was preincubated with or without Rad51-WT (**A**) or Rad51-II3A (**B**) (0.5, 0.1, and 0.02 μM), Mei5-Sae3 (0.5 μM), and ^{32}P-labeled 90-mer ssDNA (3.6 μM nucleotides). Plasmid pRS306 (22 μM base pairs) was then added to initiate D-loop formation. Error bars represent SEM, $N = 4$.

partnerships between meiosis-specific proteins and their mitotically active paralogs.

References and Notes

1. D. K. Bishop, D. Park, L. Xu, N. Kleckner, *Cell* **69**, 439 (1992).
2. A. Shinohara, H. Ogawa, T. Ogawa, *Cell* **69**, 457 (1992).
3. A. Schwacha, N. Kleckner, *Cell* **90**, 1123 (1997).
4. S. Sheridan, D. K. Bishop, *Genes Dev.* **20**, 1685 (2006).
5. H. Tsubouchi, G. S. Roeder, *Genes Dev.* **20**, 1766 (2006).
6. B. Müller, T. Koller, A. Stasiak, *J. Mol. Biol.* **212**, 97 (1990).
7. H. Kurumizaka, S. Ikawa, A. Sarai, T. Shibata, *Arch. Biochem. Biophys.* **365**, 83 (1999).
8. P. Chi, S. Van Komen, M. G. Sehorn, S. Sigurdsson, P. Sung, *DNA Repair (Amsterdam)* **5**, 381 (2006).
9. J. San Filippo, P. Sung, H. Klein, *Annu. Rev. Biochem.* **77**, 229 (2008).
10. S. L. Gasior, A. K. Wong, Y. Kora, A. Shinohara, D. K. Bishop, *Genes Dev.* **12**, 2208 (1998).
11. D. K. Bishop, *Cell* **79**, 1081 (1994).
12. A. Shinohara, S. Gasior, T. Ogawa, N. Kleckner, D. K. Bishop, *Genes Cells* **2**, 615 (1997).
13. S. D. Oh *et al.*, *Cell* **130**, 259 (2007).
14. S. R. Ferrari, J. Grubb, D. K. Bishop, *J. Biol. Chem.* **284**, 11766 (2009).
15. A. Hayase *et al.*, *Cell* **119**, 927 (2004).
16. A. F. Say *et al.*, *DNA Repair (Amsterdam)* **10**, 586 (2011).
17. Y. Kokabu *et al.*, *J. Biol. Chem.* **286**, 43569 (2011).
18. N. Hunter, N. Kleckner, *Cell* **106**, 59 (2001).

Acknowledgments: We are grateful to A. Zhang and P. Rice for structural alignments, N. Hunter for critical reading of the manuscript and strains, P. Sung for plasmid pET11d-ScRad52, and W. Heyer for Rad54 protein. This work was supported by National Institute for General Medical Sciences grant GM50936.

Supplementary Materials
www.sciencemag.org/cgi/content/full/337/6099/1222/DC1
Materials and Methods
Figs. S1 to S8
Tables S1 and S2
References (*19–26*)

19 January 2012; accepted 5 July 2012
10.1126/science.1219379

The Molecular Mechanism of Thermal Noise in Rod Photoreceptors

Samer Gozem,[1] Igor Schapiro,[1] Nicolas Ferré,[2] Massimo Olivucci[1,3]*

Spontaneous electrical signals in the retina's photoreceptors impose a limit on visual sensitivity. Their origin is attributed to a thermal, rather than photochemical, activation of the transduction cascade. Although the mechanism of such a process is under debate, the observation of a relationship between the maximum absorption wavelength (λ_{max}) and the thermal activation kinetic constant (k) of different visual pigments (the Barlow correlation) indicates that the thermal and photochemical activations are related. Here we show that a quantum chemical model of the bovine rod pigment provides a molecular-level understanding of the Barlow correlation. The transition state mediating thermal activation has the same electronic structure as the photoreceptor excited state, thus creating a direct link between λ_{max} and k. Such a link appears to be the manifestation of intrinsic chromophore features associated with the existence of a conical intersection between its ground and excited states.

Rhodopsin (Rh), a heterotrimeric G protein–coupled receptor found in rod cells of the eye, is responsible for vision in dim light. It comprises an opsin apoprotein and the 11-cis retinal protonated Schiff base (PSB11) chromophore covalently linked to the opsin core. Visual pigments of the Rh family mediate vision in all seeing animals (*1*). The activation of visual pigments is normally triggered by the photochemical isomerization of PSB11 to the corresponding all-trans isomer (PSBAT) within the opsin retinal binding pocket (*2*), yielding the ground state (S_0) photocycle intermediate bathoRh. Spectroscopic studies have established that in the prototypical pigment bovine Rh, the isomerization occurs on a femtosecond time scale (*3–5*). The additional observation of S_0 vibrational coherence (*6*) supports a direct transfer of the excited-state (S_1) population to the photoproduct along a downhill path passing through a conical intersection (CI). Such a path has been located along the Rh potential energy surfaces, using multiconfigurational quantum chemical (MCQC) calculations (*7–9*), and has been spectroscopically supported by probing in the infrared (*9*). As outlined in Fig. 1, the resulting photochemical isomerization mechanism is qualitatively different from that of a thermal isomerization, which is expected to be controlled by an energy barrier (E_a^T, thermal activation energy) corresponding to an S_0 transition state (TS) with diradical character (*10*).

In contrast to light activation, the mechanism of thermal activation of visual pigments has not been established. One reason for the ongoing debate is the discrepancy between the measured activation barrier in toad Rh (~22 kcal/mol) (*11*) and the observed energy storage in bovine bathoRh (~32 kcal/mol) (*12*). Because E_a^T for PSB11 in opsin cannot be lower than the product energy, it has been suggested that the thermal mechanism bypasses bathoRh production (*13*). However, there is compelling evidence that the thermal and photochemical activations are mechanistically related. First, the signal triggered by thermal activation is indistinguishable from that caused by light (*11*). Second, as for light activation, the thermal process leads to PSB11 isomerization without substantially changing the secondary structure of the opsin (*14*). The observations above question the validity of the measured activation barrier. Ala-Laurila *et al.* (*15*) and, more recently,

[1]Department of Chemistry, Bowling Green State University, Bowling Green, OH 43403, USA. [2]Institut de Chimie Radicalaire, UMR 7273–Université d'Aix-Marseille, 13397 Marseille Cedex 20, France. [3]Dipartimento di Chimica, Università di Siena, via De Gasperi 2, I-53100 Siena, Italy.

*To whom correspondence should be addressed. E-mail: molivuc@bgsu.edu, olivucci@unisi.it

Luo *et al*. (*16*) have suggested that the barrier value (*11*) is incorrect because it assumes Boltzmann statistics. On the other hand, a computational study by Khrenova *et al*. (*10*) suggests that the barrier is correct but the stored energy is not.

A number of studies have tried to resolve the above discrepancies by proposing more complex mechanisms for the thermal activation, such as an isomerization occurring in an Rh population where the chromophore is deprotonated (*17*), simultaneous hydrolysis and thermal isomerization of PSB11 (*14*), a change in the hydrogen-bonding network near the active site (*18*), fluctuations in the protein structure (*19*), or bioluminescence near the retina (*20*). More recent computations indicate that the S_1 state may be thermally accessed (*21*). However, these mechanistic models do not explicitly address the experimentally observed Barlow correlation (*22*, *23*), which establishes a relationship between the pigment thermal activation kinetic constant (k) and the maximum absorption wavelength (λ_{max}), such that $-\log k$ is directly proportional to $1/\lambda_{max}$. This provides a link between thermal and photochemical activation (*15*, *16*) that any correct mechanism must explain.

The importance of accounting for the Barlow correlation is emphasized by Luo *et al*. (*16*), who have provided quantitative evidence of its validity. Adopting a theory presented by Ala-Laurila *et al*. (*15*), they proposed that the observed thermal activation measurements could be described using a $\log k = \log A(E_a^T, T) - E_a^T/RT$ law (A, pre-exponential factor; T, absolute temperature; R, gas constant) and assumed that $E_a^T = E_a^P$, where E_a^P is an experimentally established function of $1/\lambda_{max}$ called the photochemical energy barrier (*23*). Because the authors associate E_a^P with the minimal photon energy capable of triggering the isomerization, the $E_a^T = E_a^P$ assumption could be interpreted to mean that energy from photons is used to follow the thermal isomerization path. However, this contradicts the established CI-driven S_1 isomerization of Fig. 1, which avoids E_a^T. Furthermore, E_a^P must be a quantity close to the 0-0 excitation energy (i.e., the energy gap between the S_0 and S_1 minima) and far from the S_0 energy barrier (fig. S1). Clearly, the observed proportionality between $-\log k$ and $1/\lambda_{max}$ must reflect a different mechanism. Assuming, consistently with Luo *et al*. (*16*), that chromophore isomerization drives the thermal activation, such a mechanism must explain the relationship between E_a^T and $1/\lambda_{max}$ on the basis of the geometrical and electronic properties of opsin-embedded PSB11.

MCQC calculations allow the computation of E_a^T and $1/\lambda_{max}$ from first principles by locating the pigment equilibrium and TS structures. Computation of these quantities for a set of 12 pigments explains the link between E_a^T and $1/\lambda_{max}$ in terms of the charge distribution of their chromophores. MCQC-based quantum mechanics/molecular mechanics (QM/MM) calculations on bovine Rh show that S_0 PSB11 has a +0.86 e charge residing on the Schiff base moiety (Fig. 1). Vertical excitation to S_1 transfers about 30% of this charge toward the β-ionone moiety. This difference in charge distribution explains the sensitivity of λ_{max} [and corresponding vertical excitation energy $\Delta E(S_1 - S_0)$] to the opsin sequence. Sequences that stabilize the positive charge in the Schiff base region would blueshift the absorption, whereas sequences that stabilize the charge on the β-ionone region would redshift the absorption. Because $-\log k$ is seen to increase linearly as a function of $1/\lambda_{max}$ (*16*), the correct thermal activation mechanism should explain why opsins decreasing E_a^T would also decrease $\Delta E(S_1 - S_0)$, and increasing E_a^T would also increase $\Delta E(S_1 - S_0)$.

As previously reported (*24*), the S_0 potential energy surface of a gas-phase PSB11 model features two TSs [TS_{DIR} and TS_{CT} (DIR, diradical; CT, charge transfer)] controlling the same thermal isomerization (Fig. 2A). In Fig. 2B, we present the TS_{DIR} and TS_{CT} structures computed for bovine Rh using a MCQC/AMBER QM/MM model, in which all the side chains and waters of the chromophore binding pocket are relaxed (figs. S2 to S9) (*25*). The necessarily approximated MCQC levels used to compute the TS geometry (CASSCF/6-31G*) and barriers (CASPT2//CASSCF/6-31G*) have been validated by mapping the S_0 energy surface of a reduced PSB11 model up to the CASPT2/6-31G* and MRCISD+Q/6-31++G** levels, respectively (fig. S8). TS_{DIR} features the structure expected for a homolytically broken double bond with two radical centers delocalized along orthogonal π-systems and corresponds to the TS of Fig. 1. As expected, its charge distribution correlates with that of the S_0 PSB11 reactant, with a +0.98 e charge localized in the Schiff base region. In contrast, TS_{CT} has most of its charge (+0.90 e) located on the β-ionone region and thus more closely resembles the charge distribution of vertically excited S_1 PSB11 (compare the corresponding bubble diagrams in Figs. 2A and 1). We find that TS_{CT} has a computed activation energy of 34 kcal/mol and, unexpectedly, lies 11 kcal/mol in energy below TS_{DIR} (fig. S9). Although this value depends on the MCQC level used in the calculation, an increase in the level of theory invariably leads to a larger stabilization of TS_{CT} (figs. S7 to S9) Therefore, TS_{CT} has full control of the thermal isomerization.

The close electronic characters of TS_{CT} and of the opsin-embedded S_1 PSB11 (i.e., a positive charge preferentially localized on the β-ionone region) provide a direct link between E_a^T and $\Delta E(S_1 - S_0)$ and, in turn, $-\log k$ and $1/\lambda_{max}$. The link is derived from first-principles quantum-mechanical computations and makes the $E_a^T = E_a^P$ assumption (*16*) [and even its more permissive $E_a^T = \alpha E_a^P - \beta$ form, where α and β are constants (*15*, *16*)] unnecessary. Accordingly, any opsin redshifting the absorption would simultaneously decrease E_a^T. The opposite behavior, not consistent with the Barlow correlation, would be observed if the isomerization were controlled by TS_{DIR}. In order to support these conjectures, we display in Fig. 2C the E_a^T versus $1/\lambda_{max}$ correlation computed by modeling a set of pigments. These are five bovine Rh (A1-Rh) mutants and six derivatives featuring the 3,4-dehydro-retinal (A2) chromophore. The QM/MM-derived correlation supports the conclusion that TS_{CT} and S_1 PSB11 have similar charge distributions, displaying a clear positive slope exclusively for the TS_{CT} barriers and closely reproducing the slope of the experimentally derived $E_a^T = 0.84\ hc/\lambda_{max}$ relation (h, Planck's constant; c, speed of light) (*16*) (dashed line in Fig. 2C). The E_a^T values

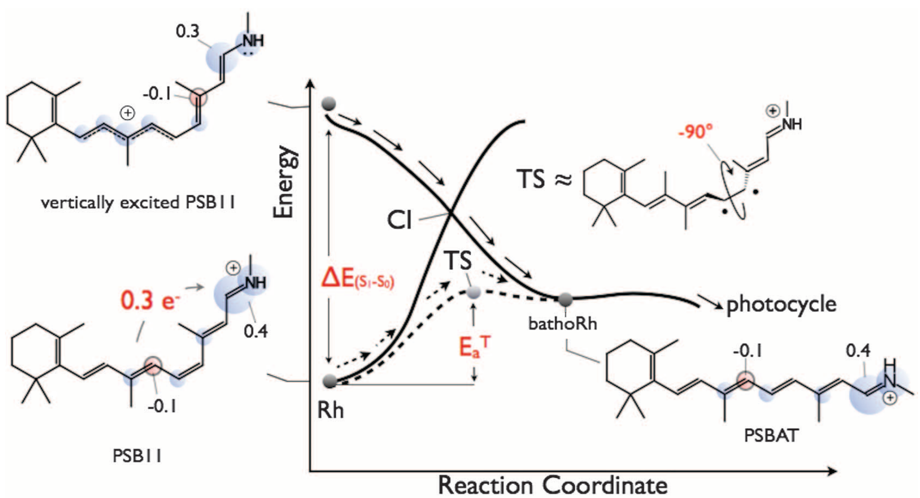

Fig. 1. Schematic representation of the photochemical (solid arrows) and thermal (dashed arrows) isomerization paths. The CI is located energetically above the TS (assumed to have a diradical character), features a different geometrical structure, and drives a far-from-equilibrium process. The CASSCF/6-31G*/AMBER S_0 and S_1 Mulliken charge distributions along the backbone of the bovine Rh chromophore (PSB11) are represented with bubble diagrams on the left of the graph. The labels indicate the maximum and minimum values for the charges. The bond-line formulas represent the dominant electronic configurations of the corresponding states (wavefunctions).

associated with TS_{CT} are therefore proportional to the values derived under the $E_a^T = E_a^P$ assumption.

Although the positive slope characterizing the Barlow correlation is controlled by the changes in E_a^T, the quantitative simulation of the $-\log k$ versus $1/\lambda_{max}$ relationship from first principles requires the computation of the pre-exponential $A(E_a^T, T)$. Although this can be attempted by using TS theory, such a calculation is impractical for molecules the size of visual pigments. Using the computed E_a^T values and assuming the validity of the same Hinshelwood kinetic model originally proposed by Ala-Laurila *et al.* (*15*) and adopted in Luo *et al.* (*16*) to account for the effect of the chromophore vibrational modes, we calculated five A1/A2-Rh rate-constant ratios: 1/8.3 [wild type (WT)], 1/7.3 [$Ala^{269} \rightarrow Thr^{269}$ (A269T)], 1/9.3 (F261Y), 1/9.7 (E113D), and 1/301.2 (T118A) to be compared to the measured ratio between A1 *Bufo* Rh and A2 *Xenopus* Rh of 1/8.9. Using the same Hinshelwood model, a quantitative fit to the observed k versus λ_{max} data for visual pigments was achieved (fig. S10). The computed barriers and rate-constant ratios were obtained via QM/MM models of the pigments and do not contain experimental parameters. The large deviation of T118A from the observed ratio is tentatively assigned to an overestimated barrier for the A1 chromophore.

Thus, the Barlow correlation is explained naturally by considering the quantum-mechanical properties of PSB11. Because the Barlow correlation appears to be generally valid for visual pigments, we conclude that in these systems, TS_{CT}, rather than TS_{DIR}, controls the thermal isomerization. However, the data of Fig. 2C predict that TS_{DIR} will control thermal isomerization for λ_{max} below 470 nm (after accounting for a systematic ~3.2 kcal/mol blueshift in our computed excitation energy), yielding an anti-Barlow correlation, seen as a negative slope in the diagram of Fig. 2C. The same results provide evidence that the rate-determining step controlling the thermal noise must be the canonical PSB11 isomerization, in agreement with the Luo *et al.* (*16*) hypothesis. As discussed in Luo *et al.* (*16*), the observed correlation is not necessarily incompatible with the previously reported 22 kcal/mol apparent activation energy because, in that case, an energy- and temperature-independent pre-exponential factor was assumed (*11*). Also, the computed 34 kcal/mol barrier for TS_{CT} has uncertainty of a few kilocalories per mole because of the MCQC computational error (fig. S8) and the fact that we have used a rather stiff protein model (only the cavity residues are relaxed during the calculations). Our conclusions are also not incompatible with a recently proposed noise model based on protein fluctuations (*19*) or models in which the magnitude of the noise is sensitive to the opsin hydrogen bond network (*18*) (fig. S11), provided that PSB11 isomerization remains the kinetic bottleneck. Finally, the hypothesis that the Barlow correlation is a chromophore property is supported by similar relationships observed for the 13-cis chromophore in solution and in bacterioRh (*26*).

In 1963, Herzberg and Longuet-Higgins showed that the electronic wavefunctions of two states crossing at a CI undergo large changes when moving the molecular structure along a loop encircling a single CI point (*27*). As pictorially illustrated in Fig. 2A, one consequence of their geometric-phase theorem is that such wavefunctions exchange character (*28*) when the molecular structure is displaced from one side to the opposite side of the CI lower cone. This behavior has been computationally demonstrated for PSB11 (*29*) where, near the intersection, S_0 has a covalent/diradical character (ψ_{DIR}), whereas S_1 has a charge-transfer character (ψ_{CT}). Thus,

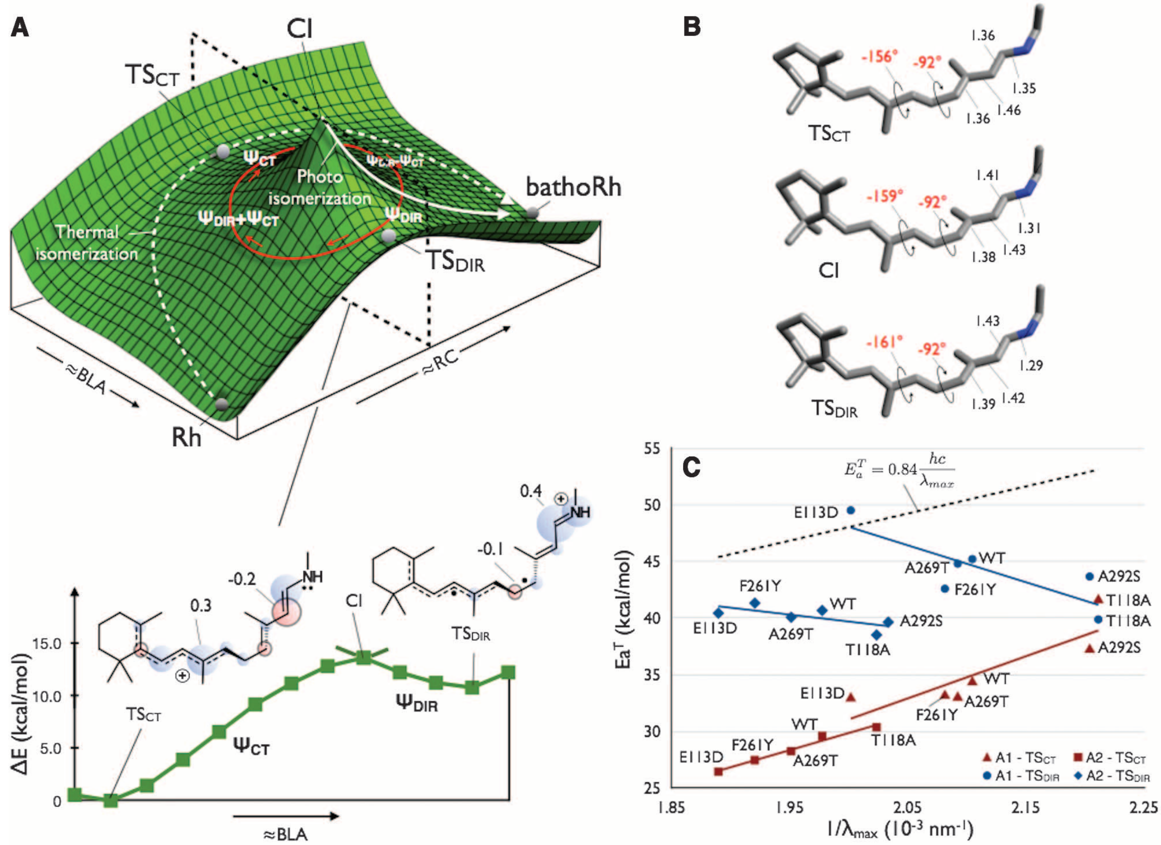

Fig. 2. (**A**) Schematic overview of the S_0 potential energy surface driving the thermal isomerization of bovine Rh, represented by the isomerization coordinate RC. A second coordinate BLA (corresponding to the elongation of double bonds coupled with a shortening of single bonds and connecting TS_{CT}, CI, and TS_{DIR}) is shown in addition to RC. The loop represents the electronic wavefunction changes associated with the presence of a CI. The CASPT2//CASSCF/6-31G*/AMBER relative energy change computed along the BLA coordinate (bottom) shows that TS_{CT} is the lowest energy point separating the reactant from the product energy minima. The S_0 Mulliken charge distributions of TS_{CT} and TS_{DIR} are represented with a bubble diagram, and the bond-line formulas represent the associated dominant electronic configuration (e.g., ψ_{DIR} for TS_{DIR}, S_0 Rh, and bathoRh; and ψ_{CT} for TS_{CT} and S_1 Rh). A region of the S_0 potential energy surface with ψ_{CT} character was also discussed in ref. (*31*). (**B**) CASSCF/6-31G*/AMBER geometrical parameters (in angstroms and degrees) of the TSs driving the thermal isomerization of bovine Rh compared with the corresponding CI values (the CI structure here is the one found along the BLA scan at the bottom of Fig. 2A). (**C**) CASPT2//CASSCF/6-31G*/AMBER-computed E_a^T values versus $1/\lambda_{max}$ for bovine Rh (WT), bovine opsin with the A2 chromophore (WT-A2), and their mutants. The lines indicates linear regression. The dashed line corresponds to the observed ratio described in Luo *et al.* (*16*).

the reported TS_{DIR} and TS_{CT} structures located along the BLA coordinate on opposite sides of the CI appear to be a manifestation of the geometric-phase theorem.

The key to understanding the origin of the thermal noise in rod photoreceptors is the existence of two electronically different TSs, with the lower displaying the same charge-transfer character as the Rh excited state. This is a consequence of the properties of the chromophore electronic wavefunction in the region of the CI (*27*, *28*, *30*). Therefore, the Barlow correlation represents a manifestation of the existence of a CI in Rh and complements the evidence provided by spectroscopic studies (*3*–*5*, *9*). Without this CI, the thermal isomerization would be controlled by the TS_{DIR} barrier and, therefore, high visual sensitivity would be achieved at the red edge of the visible spectrum rather than the blue. Further evidence supporting this theory could be provided by the observation of an "anti-Barlow" correlation (i.e., a decrease of $-\log k$ as a function of $1/\lambda_{max}$) for mutants or pigments containing PSB11 but absorbing radiations shorter than 470 nm.

References and Notes

1. A. Terakita, *Genome Biol.* **6**, 213 (2005).
2. G. Wald, *Nature* **219**, 800 (1968).
3. R. W. Schoenlein, L. A. Peteanu, R. A. Mathies, C. V. Shank, *Science* **254**, 412 (1991).
4. H. Kandori, Y. Shichida, T. Yoshizawa, *Biochemistry (Mosc.)* **66**, 1197 (2001).
5. P. Kukura, D. W. McCamant, S. Yoon, D. B. Wandschneider, R. A. Mathies, *Science* **310**, 1006 (2005).
6. Q. Wang, R. W. Schoenlein, L. A. Peteanu, R. A. Mathies, C. V. Shank, *Science* **266**, 422 (1994).
7. T. Andruniów, N. Ferré, M. Olivucci, *Proc. Natl. Acad. Sci. U.S.A.* **101**, 17908 (2004).
8. L. M. Frutos, T. Andruniów, F. Santoro, N. Ferré, M. Olivucci, *Proc. Natl. Acad. Sci. U.S.A.* **104**, 7764 (2007).
9. D. Polli *et al.*, *Nature* **467**, 440 (2010).
10. M. G. Khrenova, A. V. Bochenkova, A. V. Nemukhin, *Proteins* **78**, 614 (2010).
11. D. A. Baylor, G. Matthews, K. W. Yau, *J. Physiol.* **309**, 591 (1980).
12. G. A. Schick, T. M. Cooper, R. A. Holloway, L. P. Murray, R. R. Birge, *Biochemistry* **26**, 2556 (1987).
13. A. P. Sampath, D. A. Baylor, *Biophys. J.* **83**, 184 (2002).
14. J. Liu *et al.*, *J. Am. Chem. Soc.* **131**, 8750 (2009).
15. P. Ala-Laurila, K. Donner, A. Koskelainen, *Biophys. J.* **86**, 3653 (2004).
16. D. G. Luo, W. W. Yue, P. Ala-Laurila, K. W. Yau, *Science* **332**, 1307 (2011).
17. R. B. Barlow, R. R. Birge, E. Kaplan, J. R. Tallent, *Nature* **366**, 64 (1993).
18. J. Liu *et al.*, *J. Biol. Chem.* **286**, 27622 (2011).
19. V. A. Lórenz-Fonfría, Y. Furutani, T. Ota, K. Ido, H. Kandori, *J. Am. Chem. Soc.* **132**, 5693 (2010).
20. I. Bókkon, R. L. Vimal, *J. Photochem. Photobiol. B* **96**, 255 (2009).
21. V. R. Kaila, R. Send, D. Sundholm, *J. Phys. Chem. B* **116**, 2249 (2012).
22. H. B. Barlow, *Nature* **179**, 255 (1957).
23. P. Ala-Laurila, J. Pahlberg, A. Koskelainen, K. Donner, *Vision Res.* **44**, 2153 (2004).
24. L. De Vico, M. Olivucci, R. Lindh, *J. Chem. Theory Comput.* **1**, 1029 (2005).
25. Materials and methods are available as supplementary materials on *Science* Online.
26. S. J. Milder, *Biophys. J.* **60**, 440 (1991).
27. G. Herzberg, H. C. Longuet-Higgins, *Discuss. Faraday Soc.* **35**, 77 (1963).
28. G. J. Atchity, S. S. Xantheas, K. Ruedenberg, *J. Chem. Phys.* **95**, 1862 (1991).
29. P. B. Coto, A. Sinicropi, L. De Vico, N. Ferre, M. Olivucci, *Mol. Phys.* **104**, 983 (2006).
30. S. Zilberg, Y. Haas, *Photochem. Photobiol. Sci.* **2**, 1256 (2003).
31. A. Warshel, *Proc. Natl. Acad. Sci. U.S.A.* **75**, 2558 (1978).

Acknowledgments: We are grateful to M. A. Robb for a critical reading of the manuscript. This work was supported by the Bowling Green State University. M.O. is grateful to the Center for Photochemical Sciences and the School of Arts and Sciences of Bowling Green State University for startup funds. We are grateful to the Ohio Supercomputer Center for granted computer time.

Supplementary Materials
www.sciencemag.org/cgi/content/full/337/6099/1225/DC1
Materials and Methods
Figs. S1 to S11
Tables S1 to S6
References (*32*–*92*)

13 February 2012; accepted 2 July 2012
10.1126/science.1220461

Ecological Populations of Bacteria Act as Socially Cohesive Units of Antibiotic Production and Resistance

Otto X. Cordero,[1]* Hans Wildschutte,[1]* Benjamin Kirkup,[1]* Sarah Proehl,[1] Lynn Ngo,[1] Fatima Hussain,[1] Frederique Le Roux,[2] Tracy Mincer,[3] Martin F. Polz[1]†

In animals and plants, social structure can reduce conflict within populations and bias aggression toward competing populations; however, for bacteria in the wild it remains unknown whether such population-level organization exists. Here, we show that environmental bacteria are organized into socially cohesive units in which antagonism occurs between rather than within ecologically defined populations. By screening approximately 35,000 possible mutual interactions among Vibrionaceae isolates from the ocean, we show that genotypic clusters known to have cohesive habitat association also act as units in terms of antibiotic production and resistance. Genetic analyses show that within populations, broad-range antibiotics are produced by few genotypes, whereas all others are resistant, suggesting cooperation between conspecifics. Natural antibiotics may thus mediate competition between populations rather than solely increase the success of individuals.

The ratio of intra- versus interspecific competition is a key element regulating populations and determining their success within diverse communities. It is especially important in structured animal and plant populations, in which closely related individuals live in patches and encounter each other often (*1*). In these cases, modulation of intraspecific antagonism or cooperation can mitigate the detrimental effects of niche overlap. However, for bacteria in the wild it has been postulated that populations merely represent loose assemblages of individuals driven by ecological opportunity (*2*, *3*). The reasons given include high dispersal rates and rapid horizontal gene transfer (HGT), which can both rapidly erode population structure by mixing unrelated individuals and introducing novel, potentially advantageous genes to their genomes. This may initiate a dynamic process of rapid but locally and/or temporarily limited expansion of individuals (clones). A classical example of such interactions is interference competition via colicin-type bacteriocins (*4*, *5*), which are almost always encoded by plasmids and are able to kill closely related competitors in a highly specific manner. In these cases, population dynamics are primarily driven by the cyclic invasion of antibiotic production and resistance genes. Similarly, a recent high-throughput screen of mutual interactions among soil isolates indicated changing types of interactions occur over relatively short evolutionary distances. This was interpreted as short-lived dynamics of gene gain and loss, in which antibiotic production selects resistance, which subsequently promotes loss of production and reversion to sensitivity (*6*). In contrast to this gene-centric view of bacterial population dynamics, recent fine-scale environmental mapping of bacterial diversity has suggested that population structure may exist beyond individual clones. Such ecologically defined populations consist of phylogenetic clusters of closely related but nonclonal individuals, which share common ecological associations (*7*, *8*). However, it remains unknown whether individuals within such populations interact sufficiently strongly to allow for

[1]Department of Civil and Environmental Engineering, Massachusetts Institute of Technology, Cambridge, MA 02139, USA. [2]Laboratoire de Génétique et Pathologie BP 133, Insititut Français de Recherche pour l'Exploitation de la Mer, 17390 La Tremblade, France. [3]Department of Marine Chemistry and Geochemistry, Woods Hole Oceanographic Institution, Woods Hole, MA 02543, USA.

*These authors contributed equally to this work.
†To whom correspondence should be addressed. E-mail: mpolz@mit.edu

the development of cohesive population-level social organization akin to structured animal and plant populations.

We asked whether ecologically defined populations show social cohesion beyond association with similar sets of resources. We reasoned that an obvious and important test case would be interference competition mediated by antibiotic production. This required mapping the network of potential antagonistic interactions between bacteria onto their fine-scale genotypic structure in the environment. Thus far, such an exercise has been impeded by the lack of data on genotypically and ecologically delineated natural microbial populations. In recent years, however, we have taken bacteria of the family Vibrionaceae as a model for the ecology and evolution of bacterial populations (*8*–*10*). These populations were originally identified by using an unsupervised machine learning approach that combines genetic similarity and micro-habitat specialization so as to cluster clades with cohesive ecology (*8*) in a way that is agnostic to any preconceived notion of species. The populations thus identified consist of groups of individuals coexisting in micro-habitats and closely related in protein housekeeping gene sequences (genotypic clusters). Many of these clusters cannot be differentiated by the most commonly used marker for phylogenetic classification of microbes, the ribosomal RNA gene, suggesting recent evolutionary age (*8*). Although these genotypic clusters are distinguished by their propensity to occur as free-living or associated with different types of suspended organic particles and zooplankton (*8*, *11*), they co-occur in the guts and on the surfaces of larger marine animals (*11*). Because of their genotypic cohesion and differential environmental distributions, these clusters are hypothesized to represent natural populations and provide a platform to inquire whether factors beyond similarity in environmental association enforce population structure.

We first determined the potential for interference competition among individuals from different populations by measuring antagonistic interactions in an all-against-all framework using 185 *Vibrio* isolates that have been characterized to high genetic resolution by the sequencing of several protein-coding, housekeeping genes (table S2). We used the classic Burkholder plate assay (*12*, *13*), which allows testing for local growth inhibition between bacteria co-plated on nutrient agar (*14*). Testing inhibition in this way provides somewhat realistic conditions for ocean bacteria because interference competition is most likely to occur among individuals coexisting on particle surfaces or in the guts of animals, where local population density can be high (*13*). After screening ~35,000 possible interaction pairs, we obtained a large network containing 830 antagonistic interactions between naturally co-occurring *Vibrio* strains (individual genotypes). Replication of the antagonism assay for a selected number of strains showed this data to be very robust, with more than 97% replicability of interactions (*14*). The data show that nearly half (44%) of the strains were able to inhibit at least one other strain, whereas 86% were inhibited by at least one strain. A few (<5%) "super-killer" strains were able to inhibit more than 25% of all other strains in the collection (Fig. 1A). Using a membrane diffusion method (*14*), we estimate that 96% of the antagonistic interactions are mediated by small molecules and not by proteins such as bacteriocins.

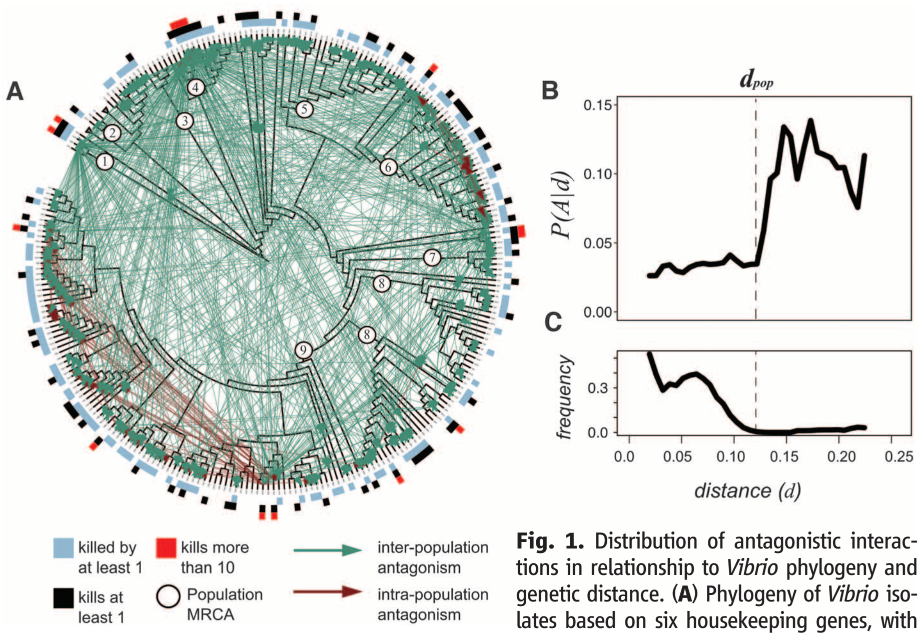

Fig. 1. Distribution of antagonistic interactions in relationship to *Vibrio* phylogeny and genetic distance. (**A**) Phylogeny of *Vibrio* isolates based on six housekeeping genes, with outer, colored rings highlighting antagonists and sensitive strains. Green arrows connect antagonists to sensitive strains. Circles identify the most recent common ancestor (MRCA) of previously identified ecologically cohesive populations: 1, *V. ordalii*; 2, *V. fischeri*; 3, *V. breoganii*; 4, *V. alginolyticus*; 5, *V.* sp. F12; 6, *V. crassostreae*; 7, *V. cyclotrophicus*; 8, V. tasmaniensis; 9, *V. splendidus*. (**B**) The conditional probability of antagonism as a function of genetic distance, *P*(*A*|*d*), shows that antagonistic interactions occur mostly between strains whose genetic distance exceeds a critical threshold. This threshold coincides with the average distance between previously defined populations (dashed line). (**C**) Frequency distribution of within-population genetic distances, showing that the transition point for *P*(*A*|*d*) matched the average boundary of populations.

Mapping the network of antagonistic interactions onto the fine-scale genotypic structure of the tested strains shows that the potential for interference competition is much lower within natural populations than between them. This is expressed by the conditional probability of observing an antagonistic interaction as a function of genetic distance, *P*(*A*|*d*) (Fig. 1B), where distances were computed on the basis of a concatenated alignment of six housekeeping genes. *P*(*A*|*d*) has a sigmoidal shape, with a 75 to 80% reduction in the probability of observing antagonism over relatively short genetic distances. Despite the strong influence that super-killer strains have on these data, this trend holds when considering only narrow-range antagonists with ≤5 inhibited strains (fig. S1), and the bias to long-distance killing is statistically significant ($P = 0.001$) even when controlling for phylogenetic structure and killing activity per strain (*14*). The sharp increase in *P*(*A*|*d*) at a threshold distance indicates that a natural genetic boundary exists for interference competition. This boundary coincides almost exactly with the average value of *d* between strains in different populations, d_{pop}—that is, the average genetic boundary between ecologically cohesive genotypic clusters determined in previous studies (Fig. 1C) (*8*, *10*). This means that antagonism occurs mostly between rather than within natural *Vibrio* populations.

The observed low antagonism within populations is not a result of resistance between near-clonal strains as would be expected from dynamics of clonal expansion followed by gradual gene loss (*6*). Although the *Vibrio* populations consist of isolates with high sequence similarity in the set of shared genes, there is considerable gene content diversity between strains. In 41 sequenced genomes representing 10 *Vibrio* populations (table S4), we find that although populations are clustered by gene content, the average percentage of shared genes between genomes at distances $<d_{pop}$ is only 72% (fig. S2). Moreover, these genomes are highly recombinogenic and show no evidence of a clonal origin (*15*). This implies that the pattern of low intrapopulation antagonism is not likely to be explained by simple vertical inheritance and gene loss; rather, this pattern is generated and maintained in a regime of fast allelic turnover and potential for losing and acquiring new genes.

To further explore whether antibiotic production might have coevolved with populations or was horizontally acquired, we increased the isolate sampling around the most prolific super-killer

in our collection, strain 12B09, belonging to a population of *V. ordalii*. We added a tight cluster of 29 highly related coisolates ($d < 0.01$), which we used to study the population genomics of the super-killer phenotype. Using random transposon mutagenesis, we identified the genetic basis of antibiosis in 12B09 and studied its evolution using whole-genome sequences of both producers and nonproducers. This genomic approach was complemented with chemical screening and identification of active compounds.

By screening a library of 20,000 12B09 transposon mutants against a sensitive indicator strain, we identified 10 mutants with no antagonistic activity, which all had transposon insertions within a hybrid polyketide synthase (PKS)/nonribosomal peptide (NRP) gene cluster (Fig. 2A). A genetic knockout of the central NRP biosynthesis gene shows complete loss of activity, demonstrating a single specific antibiotic biosynthesis cluster is responsible for the antagonistic activity. This is consistent with results obtained from screening a chemical extract from cell-free 12B09 supernatant separated by means of high-performance liquid chromatography, showing that 100% of the activity could be accounted for by a single peak. Accordingly, this peak was absent from the knockout mutant 12B09-HW44, which had no antibiotic activity (figs. S4 and S5). Genes in the PKS-NRP cluster possess sequence similarity to cyclic lipopeptide antibiotic synthases, which typically cause membrane depolarization or pore formation, triggering cell lysis (*16*).

Using the cluster of 29 highly related strains from the expanded *V. ordalii* population, we obtained a high-resolution all-against-all antagonism network comprising 91 strains subdivided roughly equally across three populations of *V. ordalii*, *V. crassostreae*, and *V. tasmaniensis* (table S3). This network revealed that the super-killer phenotype is present in a small fraction (5 out of 29) of the highly related strains within *V. ordalii* (Fig. 2B) and was absent in any of the other populations. Moreover, all *V. ordalii* strains were resistant, confirming our previous result at a much higher genetic resolution level. A polymerase chain reaction (PCR) screen with multiple specific primers diagnostic for the PKS-NRP biosynthetic cluster confirmed that this specific pathway is found in all of the five super-killers identified in the plate assays and not in any of the other *V. ordalii* strains (*14*). This was consistent with data from the 185 strain network (Fig. 1A) showing that individuals resistant to each other did not antagonize the same set of strains (Pearson's $\varphi = 0.04$). Overall, this result shows that the super-killer phenotype in the population is caused by differential presence/absence of genes, not by transcriptional regulation or silencing mutations.

The study of sequenced genomes from two super-killers and three resistant conspecifics confirmed our prediction that recent horizontal gene transfer mediated the acquisition of production and resistance genes in *V. ordalii*. Different lines of evidence supported this. First, a whole-genome phylogeny of the sequenced strains (fig. S3) showed that super-killers share a recent common ancestor, suggesting that the gene cluster is not ancestral to the population but that it was acquired in a single recent event. Second, BLAST (*17*) searches against public databases of fully sequenced genomes identified the antibiotic cluster only in two previously sequenced *Vibrio* isolates from the Pacific Ocean with very low genomic similarity to *V. ordalii*: the shellfish pathogen *V. tubiashii* and the particle-attached SWAT-3 (*14*, *18*). Third, a whole-genome alignment of 12B09 and SWAT-3 revealed a colinear and conserved fragment of 16.3 kb containing only the antimicrobial cluster, which indicated recent acquisition. Moreover, in SWAT-3 the antimicrobial peptide cluster is flanked by a large arrangement of transposases and integrases (Fig. 1B), suggesting that the cluster comprises a mobile element, which was recently acquired in different *Vibrio* populations across distant regions of the ocean. The resistance factors did not appear to be coded within the same mobile cluster because none of the genes in the cluster were present in the resistant but nonproducing *V. ordalii* strains. This suggested that these genes for antimicrobial production are unlinked from their resistance factors and can only invade in populations in which some individuals carry preadaptations that enable them to survive the acquisition of antimicrobial-production genes.

Contrary to the widespread idea that bacterial populations are driven by gene-centric and selfish dynamics, we have shown that ecological

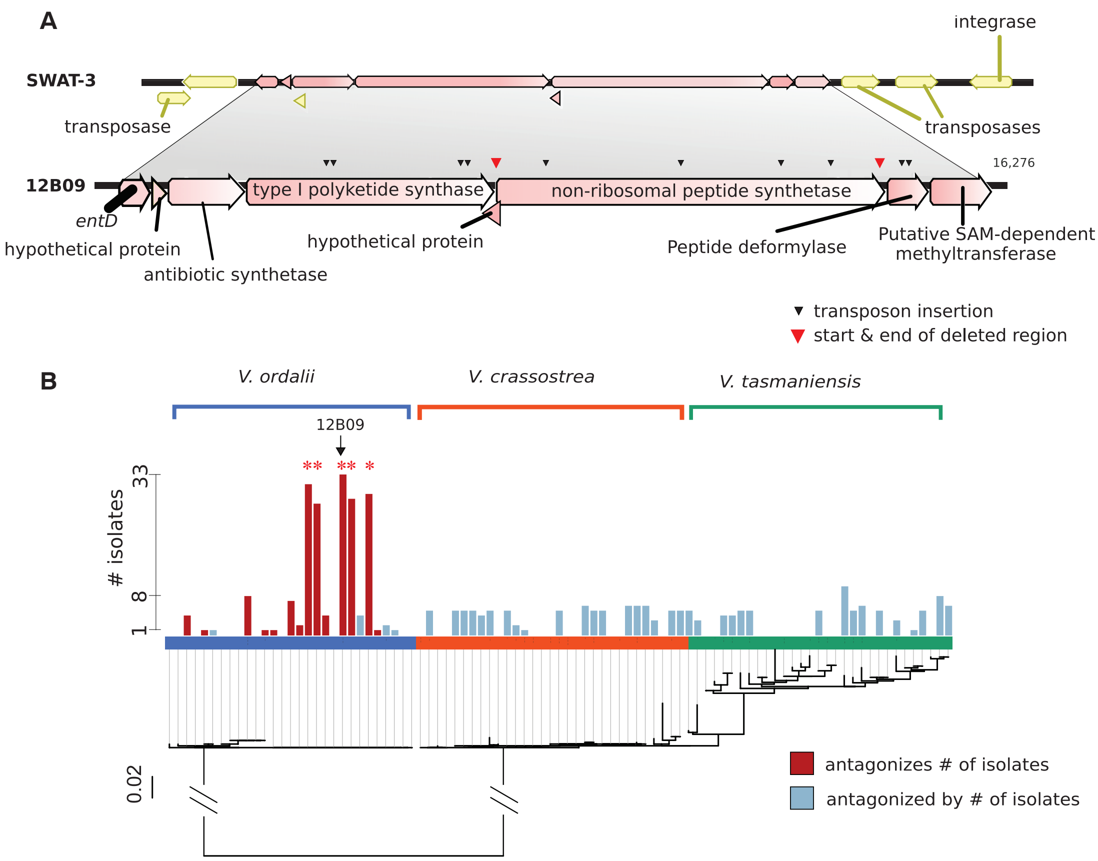

Fig. 2. Antimicrobial peptide cluster and its distribution in the *V. ordalii* population. (**A**) Alignment of NRP cluster from 12B09 showing transposon insertions and knocked-out gene, and homologous cluster from environmental isolate SWAT-3. The figure shows that in SWAT-3, a nearly identical cluster is flanked by transposases and integrases, which is consistent with the idea that the cluster comprises a mobile element. (**B**) Antibiotic activity of *V. ordalii* isolates against *V. ordalii*, *V. crassostreae*, and *V. tasmaniensis* populations. The phylogeny is based on the hsp60 genetic marker, and the bars next to each isolate indicate the number of isolates antagonized (red) and the number of *V. ordalii* isolates that antagonized the isolate (light blue). The red stars mark the five isolates in which the NRP gene cluster was detected by PCR.

populations defined by common microhabitat association also represent socially cohesive units. Although it remains unknown how widespread the observed phenomenon is, low frequency of antagonism within short genetic distances has also recently been observed among *Streptomyces* isolates (*6*). Our results indicate that similar to the case of marine vibrios, this pattern could reflect the ecological and genetic boundaries of structured populations and not a transient gene-centric dynamic (*6*). The fact that each antibiotic is produced by only a small fraction of the population whereas the rest is resistant supports the hypothesis that antibiotics can constitute public goods within populations, benefiting nonproducing but resistant conspecifics. Importantly, such social structure mediates competition between ecological populations rather than benefiting only the carrier of the antibiotic production gene. These results suggest that the ecological population structure of bacteria in the wild is much stronger than previously assumed.

References and Notes

1. C. E. Tarnita, T. Antal, H. Ohtsuki, M. A. Nowak, *Proc. Natl. Acad. Sci. U.S.A.* **106**, 8601 (2009).
2. W. F. Doolittle, *Cold Spring Harb. Symp. Quant. Biol.* **74**, 197 (2009).
3. W. F. Doolittle, O. Zhaxybayeva, *Bioscience* **60**, 102 (2010).
4. E. Cascales *et al.*, *Microbiol. Mol. Biol. Rev.* **71**, 158 (2007).
5. B. Kerr, M. A. Riley, M. W. Feldman, B. J. Bohannan, *Nature* **418**, 171 (2002).
6. K. Vetsigian, R. Jajoo, R. Kishony, *PLoS Biol.* **9**, e1001184 (2011).
7. A. Koeppel *et al.*, *Proc. Natl. Acad. Sci. U.S.A.* **105**, 2504 (2008).
8. D. E. Hunt *et al.*, *Science* **320**, 1081 (2008).
9. J. R. Thompson *et al.*, *Science* **307**, 1311 (2005).
10. S. P. Preheim, S. Timberlake, M. F. Polz, *Appl. Environ. Microbiol.* **77**, 7195 (2011).
11. S. P. Preheim *et al.*, *Environ. Microbiol.* **13**, 265 (2011).
12. P. R. Burkholder, R. M. Pfister, F. H. Leitz, *Appl. Microbiol.* **14**, 649 (1966).
13. R. A. Long, F. Azam, *Appl. Environ. Microbiol.* **67**, 4975 (2001).
14. Materials and methods are available as supplementary materials on *Science* Online.
15. B. J. Shapiro *et al.*, *Science* **336**, 48 (2012).
16. J. M. Raaijmakers, I. De Bruijn, O. Nybroe, M. Ongena, *FEMS Microbiol. Rev.* **34**, 1037 (2010).
17. S. F. Altschul, W. Gish, W. Miller, E. W. Myers, D. J. Lipman, *J. Mol. Biol.* **215**, 403 (1990).
18. R. A. Long *et al.*, *Appl. Environ. Microbiol.* **71**, 8531 (2005).

Acknowledgments: We thank W. Hanage and E. Alm for valuable suggestions. Funding was provided by the Gordon and Betty Moore Foundation, the Broad Institute's Scientific Planning and Allocation of Resources Committee (SPARC) program, NSF grant DEB 0821391, and the NSF-sponsored Woods Hole Center for Oceans and Human Health. Support for O.X.C. was provided by the Netherlands Organisation for Scientific Research. Whole Genome Shotgun projects have been deposited at DDBJ/EMBL/GenBank under the accessions AJWN00000000, AJYD00000000 to AJYZ00000000, and AJZA00000000 to AJZQ00000000 (table S4).

Supplementary Materials

www.sciencemag.org/cgi/content/full/337/6099/1228/DC1
Materials and Methods
Figs. S1 to S5
Tables S1 to S4
References

19 January 2012; accepted 10 July 2012
10.1126/science.1219385

Transforming Fusions of *FGFR* and *TACC* Genes in Human Glioblastoma

Devendra Singh,[1]* Joseph Minhow Chan,[2]* Pietro Zoppoli,[1]* Francesco Niola,[1]*† Ryan Sullivan,[1] Angelica Castano,[1] Eric Minwei Liu,[2] Jonathan Reichel,[2,3] Paola Porrati,[4] Serena Pellegatta,[4] Kunlong Qiu,[5] Zhibo Gao,[5] Michele Ceccarelli,[6] Riccardo Riccardi,[7] Daniel J. Brat,[8] Abhijit Guha,[9] Ken Aldape,[10] John G. Golfinos,[11] David Zagzag,[11,12] Tom Mikkelsen,[13] Gaetano Finocchiaro,[4] Anna Lasorella,[1,14,15]‡ Raul Rabadan,[2]‡ Antonio Iavarone[1,15,16]‡

The brain tumor glioblastoma multiforme (GBM) is among the most lethal forms of human cancer. Here, we report that a small subset of GBMs (3.1%; 3 of 97 tumors examined) harbors oncogenic chromosomal translocations that fuse in-frame the tyrosine kinase coding domains of fibroblast growth factor receptor (FGFR) genes (*FGFR1* or *FGFR3*) to the transforming acidic coiled-coil (TACC) coding domains of *TACC1* or *TACC3*, respectively. The FGFR-TACC fusion protein displays oncogenic activity when introduced into astrocytes or stereotactically transduced in the mouse brain. The fusion protein, which localizes to mitotic spindle poles, has constitutive kinase activity and induces mitotic and chromosomal segregation defects and triggers aneuploidy. Inhibition of FGFR kinase corrects the aneuploidy, and oral administration of an FGFR inhibitor prolongs survival of mice harboring intracranial FGFR3-TACC3–initiated glioma. FGFR-TACC fusions could potentially identify a subset of GBM patients who would benefit from targeted FGFR kinase inhibition.

Chromosomal translocations leading to production of oncogenic fusion proteins are critical events in the pathogenesis of human cancer (*1*–*3*). To examine whether such alterations are present in the tumor glioblastoma multiforme (GBM), we used massively parallel, paired-end sequencing of expressed transcripts (RNA-seq) to detect gene fusions in short-term cultures of glioma stemlike cells (GSCs) freshly isolated from nine patients with primary GBMs. Using TX-Fuse, a methodology that detects split reads and split inserts (see supplementary materials and methods section and fig. S1A), we discovered six rearrangements (all of which were intrachromosomal) that gave rise to in-frame fusion transcripts (table S1). We validated five in-frame fusion predictions by direct sequencing of polymerase chain reaction (PCR) products spanning the fusion breakpoint (Fig. 1 and fig. S1, B to E).

In Fig. 1, A and B, we show the prediction and cDNA sequence validation, respectively, for the fusion with the highest read support involving *fibroblast growth factor receptor 3* (*FGFR3*) fused in-frame with *transforming acidic coiled-coil 3* (*TACC3*) in GSC-1123 and GBM-1123 primary tumor. The cDNA contained an open reading frame coding for a protein of 1048 amino acids resulting from the in-frame fusion of the FGFR3 N terminus (residues 1 to 758) with the TACC3 C terminus (residues 549 to 838) (Fig. 1C and fig. S2A). FGFR3 is a member of the *FGFR* receptor tyrosine kinase (TK) family (*4*), whereas TACC3 belongs to the evolutionarily conserved *TACC* gene family, which also includes TACC1 and TACC2. The distinctive feature of TACC proteins is a coiled-coil domain at the C terminus, known as the TACC domain, which mediates localization to the mitotic spindle (*5*, *6*). TACC proteins are hypothesized to be oncogenic in several human tumors, including GBMs (*7*, *8*).

In the predicted fusion protein, the intracellular TK domain of FGFR3 is fused upstream of the TACC domain of TACC3 (Fig. 1C). Exon-specific gene expression analysis from the RNA-seq coverage in GSC-1123 and quantitative reverse transcription PCR showed that the expression of the fused *FGFR3-TACC3* exons is higher in GSC-1123 than in other GSCs or the normal brain (80- to 130-fold) (fig. S2, B and C). The FGFR3-TACC3 fusion protein was abundantly expressed in GSC-1123 and GBM-1123, and

[1]Institute for Cancer Genetics, Columbia University Medical Center, New York, NY, USA. [2]Department of Biomedical Informatics and Center for Computational Biology and Bioinformatics, Columbia University Medical Center, New York, NY, USA. [3]Tri-Institutional Program in Computational Biology and Medicine, Cornell University and Weill Cornell Medical College, New York, NY, USA. [4]Fondazione Istituto Ricovero e Cura a Carattere Scientifico Istituto Neurologico C. Besta, Milan, Italy. [5]Bioinformatics Center, Beijing Genome Institute, Shenzhen, China. [6]Istituto di Ricerche Genetiche Gaetano Salvatore, Biogem, Ariano Irpino (AV) and Dipartimento di Scienze Biologiche ed Ambientali, Università del Sannio, Benevento, Italy. [7]Department of Pediatric Oncology, Catholic University, Rome, Italy. [8]Departments of Pathology and Laboratory Medicine, Emory University School of Medicine, Atlanta, GA, USA. [9]Division of Neurosurgery, Toronto Western Hospital, University Health Network, University of Toronto, Canada. [10]Department of Pathology, MD Anderson Cancer Center, Houston, TX, USA. [11]Department of Neurosurgery, New York University Langone Medical Center, New York, NY, USA. [12]Department of Neuropathology, New York University Langone Medical Center, New York, NY, USA. [13]Departments of Neurology and Neurosurgery, Henry Ford Health System, Detroit, MI, USA. [14]Department of Pediatrics, Columbia University Medical Center, New York, NY, USA. [15]Department of Pathology, Columbia University Medical Center, New York, NY, USA. [16]Department of Neurology, Columbia University Medical Center, New York, NY, USA.

*These authors contributed equally to this work.
†Present address: Neuroscience and Brain Technologies, Italian Institute of Technology, Genoa, Italy.
‡To whom correspondence should be addressed. E-mail: al2179@columbia.edu (A.L.); rabadan@dbmi.columbia.edu (R.R.); ai2102@columbia.edu (A.I.)

immunoprecipitation followed by mass spectrometry revealed the presence of FGFR3 and TACC3 peptides, consistent with the cDNA translation prediction (fig. S2, D to F). We used PCR to map the genomic breakpoint coordinates to chromosome 4 (1,808,966 for *FGFR3* and 1,737,080 for *TACC3*, genome build GRCh37/hg19), falling within *FGFR3* exon 17 and *TACC3* intron 7, which gives rise to a transcript in which the 5′ *FGFR3* exon 16 is spliced to the 3′ *TACC3* exon 8 (Fig. 1D). The DNA junctions of *FGFR3* and *TACC3* show microhomology within a 10-base region, an observation consistent with results previously reported for other chromosomal rearrangements in human cancer (Fig. 1D) (*9*, *10*).

We next investigated whether *FGFR3-TACC3* fusions are recurrent in GBMs. The analysis of the GBM data set from the Cancer Genome Atlas (TCGA) (*11*) revealed that four tumors display marked co-outlier expression of *FGFR3* and *TACC3* (fig. S3A). The same four tumors harbor microamplification events of the *FGFR3* and *TACC3* genes (fig. S3B). We modified the gene-fusion discovery method as a package called EXome-Fuse to detect split reads and split inserts from exome DNA sequences of the available GBM cases and matched constitutional DNA in TCGA (fig. S3C). From this analysis, *FGFR3-TACC3* emerged as the sole recurrent somatic genomic rearrangement among the six fusions detected in GSCs. We found split reads and split inserts joining *FGFR3* and *TACC3* exons in the four GBM tumor DNAs carrying co-outlier expression and microamplification of the *FGFR3* and *TACC3* genes (fig. S4A and tables S2 and S3). Among the four positive TCGA GBM specimens, two were available for molecular analysis, and we confirmed the predicted fusion transcripts by Sanger sequencing (fig. S4, B and C).

The *FGFR3* and *TACC3* genes are located 48 kb apart on human chromosome 4p16. The other members of the FGFR and TACC families retain the close physical association, with *FGFR1* and *TACC1* paired on chromosome 8p11 and *FGFR2* and *TACC2* paired on chromosome 10q26 (*12*). To determine whether other intrachromosomal *FGFR-TACC* fusion combinations exist in human GBM, we screened cDNA from an independent panel of 88 primary GBMs and discovered two additional cases (one harboring *FGFR1-TACC1* and one *FGFR3-TACC3*), corresponding to 3 of 97 total GBMs (3.1%), including the GBM-1123 case (fig. S4, D and E). None of the tumors harboring *FGFR-TACC* fusions had mutations in *IDH1* or *IDH2* genes (table S4). In all seven GBMs harboring *FGFR-TACC* rearrangements (four from TCGA and three from our tumor collection), the FGFR-TK domain is fused upstream of the TACC domain.

To explore whether *FGFR-TACC* fusions are oncogenic, we transduced Rat1A fibroblasts and *Ink4A;Arf*−/− astrocytes with a lentivirus expressing FGFR3-TACC3, which resulted in the expression of the fusion protein at levels comparable to those present in GSC-1123 (fig. S5, A to D). Rat1A cells expressing FGFR3-TACC3 (or FGFR1-TACC1) but not those expressing a kinase-dead FGFR3-TACC3 protein (FGFR3-TACC3-K508M), FGFR3, TACC3, or the empty lentivirus acquired the ability to grow in anchorage-independent conditions in soft agar (Fig. 2A and table S5). Transduction of the same lentiviruses in primary *Ink4A;Arf*−/− astrocytes followed by subcutaneous injection into immunodeficient mice revealed that only astrocytes expressing FGFR3-TACC3 or FGFR1-TACC1 formed tumors (table S5). The tumors were glioma-like lesions with strong positivity for Ki67, phospho-histone H3, nestin, glial fibrillary acidic protein (GFAP), and Olig2 (fig. S5E). To target a small number of cells with the fusion protein into the brain of immunocompetent animals, we stereotactically transduced the adult mouse hippocampus with purified lentivirus expressing FGFR3-TACC3 and short hairpin RNA (shRNA) against p53 (pTomo-FGFR3-TACC3-shp53) (*13*). Seven of eight mice (87.5%) transduced with FGFR3-TACC3 succumbed from malignant brain tumors within 240 days (Fig. 2B). None of the mice transduced with a lentivirus expressing epidermal growth factor receptor version III (EGFRvIII)/shp53 or the shp53

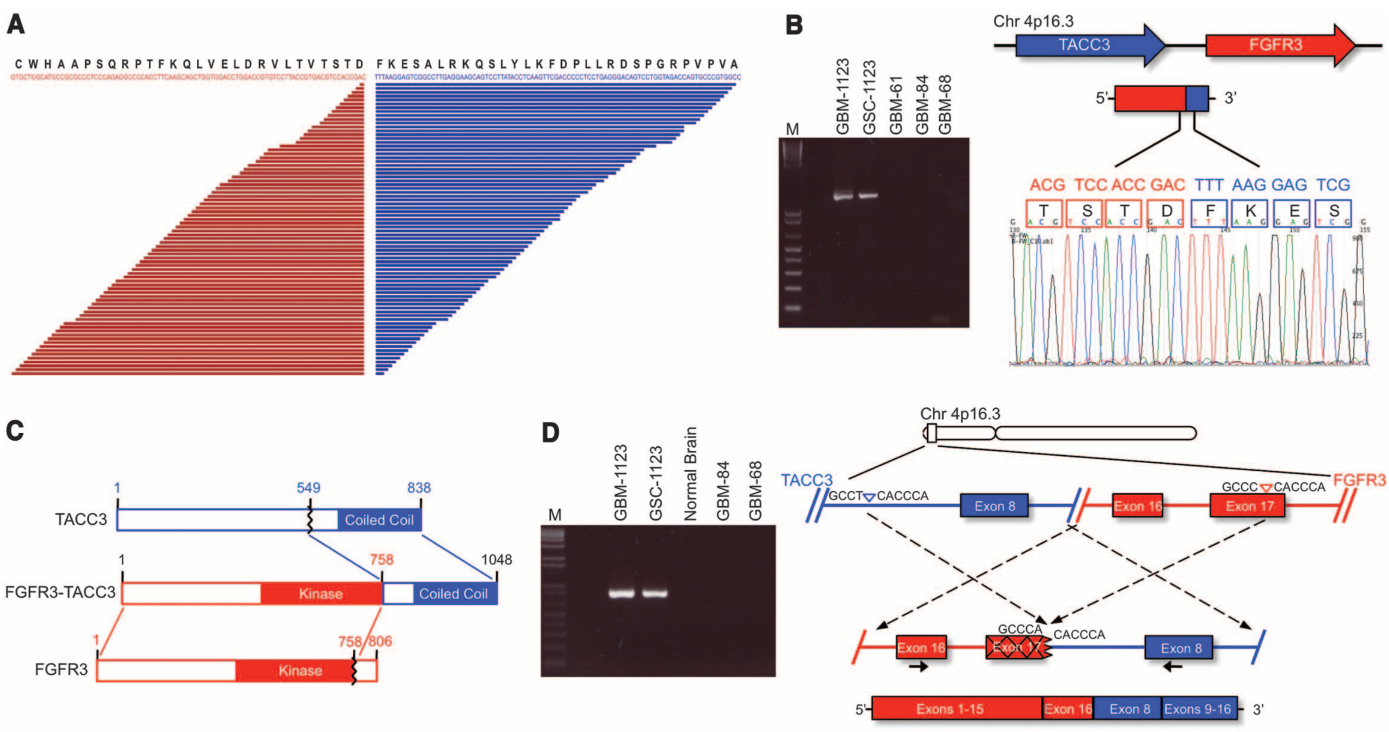

Fig. 1. *FGFR3-TACC3* gene fusion identified by whole-transcriptome sequencing of GSCs. (**A**) Here, 76 split-reads are shown aligning on the breakpoint. The predicted reading frame at the breakpoint is shown at the top with FGFR3 sequences in red and TACC3 in blue. (**B**) (Left) *FGFR3-TACC3*–specific PCR from cDNA derived from GSCs and GBMs. M, 1-kb DNA ladder. (Right) Sanger sequencing chromatogram showing the reading frame at the breakpoint and putative translation of the fusion protein in the positive samples. T, threonine; S, serine; D, aspartic acid; F, phenylalanine; E, glutamic acid. (**C**) Schematics of the FGFR3-TACC3 protein. Regions corresponding to FGFR3 or TACC3 are shown in red or blue, respectively. The fusion protein joins the tyrosine kinase domain of FGFR3 to the TACC domain of TACC3. (**D**) Genomic fusion of *FGFR3* exon 17 with intron 7 of *TACC3*. In the fused mRNA, exon 16 of *FGFR3* is spliced 5′ to exon 8 of *TACC3*. Solid black arrows indicate the position of the fusion-genome primers, which generate fusion-specific PCR products in GSC-1123 and GBM-1123.

control lentivirus developed clinical signs of brain tumors or died. The FGFR3-TACC3 tumors were invasive, rapidly growing high-grade gliomas that stained positive for the glioma stem cell markers nestin and Olig2, the glial marker GFAP, and Ki67 and phospho-histone H3 (Fig. 2C). The FGFR3-TACC3 fusion protein was expressed in the xenograft and intracranial tumor models at levels comparable to those seen in human GSCs and GBMs (fig. S5, C, F, and G).

To investigate the mechanism by which the FGFR-TACC fusion drives oncogenesis, we explored whether it activates downstream FGFR signaling. FGFR3-TACC3 failed to hyperactivate the canonical signaling events downstream of FGFR (pERK and pAKT) in the presence or absence of the ligands FGF-1, FGF-2, or FGF-8 (fig. S6, A to C) (*14*). However, FGFR3-TACC3 displayed constitutive phosphorylation of its TK domain and the adaptor protein FRS2, both of which were abolished by PD173074, a compound that is a specific inhibitor of FGFR-associated TK activity (*15*), or by the $\text{Lys}^{508}\rightarrow\text{Met}^{508}$ (K508M) mutation (fig. S6, D and E). Thus, FGFR3-TACC3 gains constitutive kinase activity that is essential for oncogenic transformation, but the downstream signaling of this aberrant activity is distinct from the canonical signaling events downstream to FGFR. We hypothesized that by driving the localization of the fusion protein, the TACC domain might create TK-dependent functions. Confocal imaging showed that FGFR3-TACC3 painted an arc-shaped structure, bending over and encasing the metaphase spindle poles, frequently displaying asymmetry toward one of the two poles and relocating to the midbody as cells progressed into the late stages of mitosis (telophase and cytokinesis) (Fig. 3A and figs. S7 and S8, A and B). Conversely, the localization of TACC3 was restricted to spindle microtubules; TACC3 did not relocalize to the midbody (fig. S8C). Wild-type FGFR3 lacked discrete localization patterns in mitosis (fig. S8D).

The mitotic localization of FGFR3-TACC3 suggests that the fusion protein might affect the fidelity of mitosis and generate aneuploidy. Time-lapse microscopy revealed that the average time from nuclear envelope breakdown to anaphase onset was increased in cells expressing FGFR3-TACC3 in comparison with control cells. The mitotic delay was exacerbated by delays in the completion of cytokinesis (Fig. 3, B and C). Quantitative analyses of mitoses revealed that cells expressing FGFR3-TACC3 or FGFR1-TACC1 exhibit three to five times more errors in chromosomal segregation compared with control cells. The most frequent mitotic aberrations triggered by the fusion proteins were misaligned chromosomes during metaphase, lagging chromosomes at anaphase, and chromosome bridges that impaired cytokinesis and generated micronuclei in the daughter cells (Fig. 3D, fig. S9A, and table S6). After treatment with the spindle poison colcemid, more than 18% of cells expressing FGFR3-TACC3 displayed prematurely separated sister chromatids, in contrast with less than 3% of control, FGFR3-, or TACC3-expressing cells (figs. S9, B and C). Accordingly, the fusion protein induced resistance to metaphase arrest after nocodazole treatment (fig. S9D). These findings suggest that the FGFR3-TACC3 fusion protein may induce aneuploidy. Karyotype analysis revealed that FGFR3-TACC3 increased the percentage of aneuploidy by more than 2.5-fold and led to the accumulation of cells with broad distribution of chromosome counts when compared with cells transduced with empty vector, FGFR3, or TACC3 (fig. S9E and table S7). Hence, GSC-1123 contained an aneuploid modal number of chromosomes (49) with broad distribution of chromosome counts (table S8).

To explore whether aneuploidy is a direct consequence of FGFR3-TACC3 expression and is induced in diploid neural cells, we analyzed primary human astrocytes 6 days after transduction with the FGFR3-TACC3 lentivirus. The transduced cells exhibited a fivefold increase of the rate of aneuploidy and a wider distribution of chromosome counts than controls (Fig. 3E, fig. S9F, and table S7). Consistent with the notion that aneuploidy is detrimental to cellular fitness, acute expression of FGFR3-TACC3 inhibited the proliferation of human astrocytes. However, continuous culture of FGFR3-TACC3–expressing astrocytes led to progressive gain of proliferative capacity that overrode that of control cells (fig. S10, A and B). Thus, acute expression of FGFR3-TACC3 in normal cells from the central nervous system causes chromosomal instability (CIN) and aneuploidy with an acute fitness cost manifested by slower proliferation.

Next, we determined whether the CIN and aneuploidy caused by FGFR3-TACC3 requires TK activity and can be corrected. Treatment of Rat1A cells with PD173074 corrected FGFR3-

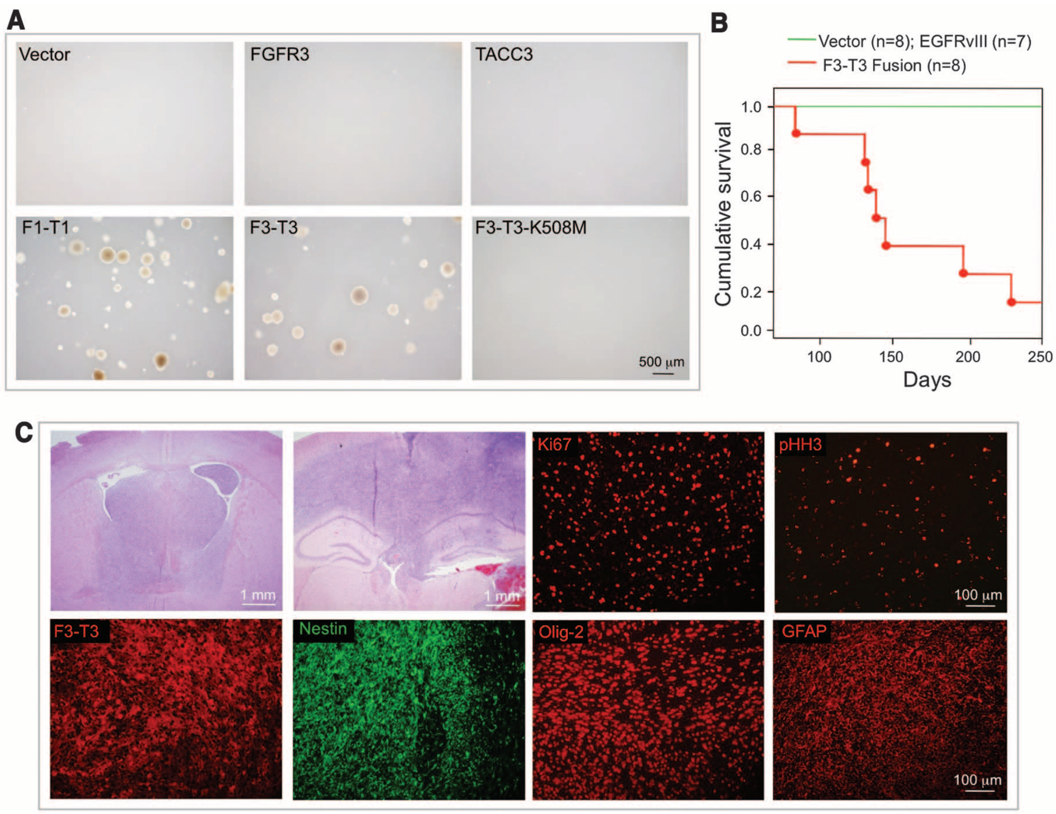

Fig. 2. Transforming activity of FGFR-TACC fusion proteins. (**A**) FGFR1-TACC1 and FGFR3-TACC3 induce anchorage-independent growth in Rat1A fibroblasts. F1-T1, FGFR1-TACC1; F3-T3, FGFR3-TACC3. (**B**) Kaplan-Meier survival curves of mice injected intracranially with pTomo-shp53 (n = 8 animals) or pTomo-EGFRvIII-shp53 (n = 7) (green line) and pTomo-FGFR3-TACC3-shp53 (n = 8) (red line). Points on the curves indicate deaths (log-rank test, P = 0.00001, pTomo-shp53 versus pTomo-FGFR3-TACC3-shp53). (**C**) Representative microphotographs of hematoxylin and eosin staining of advanced FGFR3-TACC3-shp53–generated tumors showing histological features of high-grade glioma. Note the high degree of infiltration of the normal brain by the tumor cells. Immunofluorescence staining shows that glioma and stem cell markers (Nestin, Olig2, and GFAP), proliferation markers (Ki67 and pHH3), and the FGFR3-TACC3 protein are widely expressed in the FGFR3-TACC3-shp53 brain tumors.

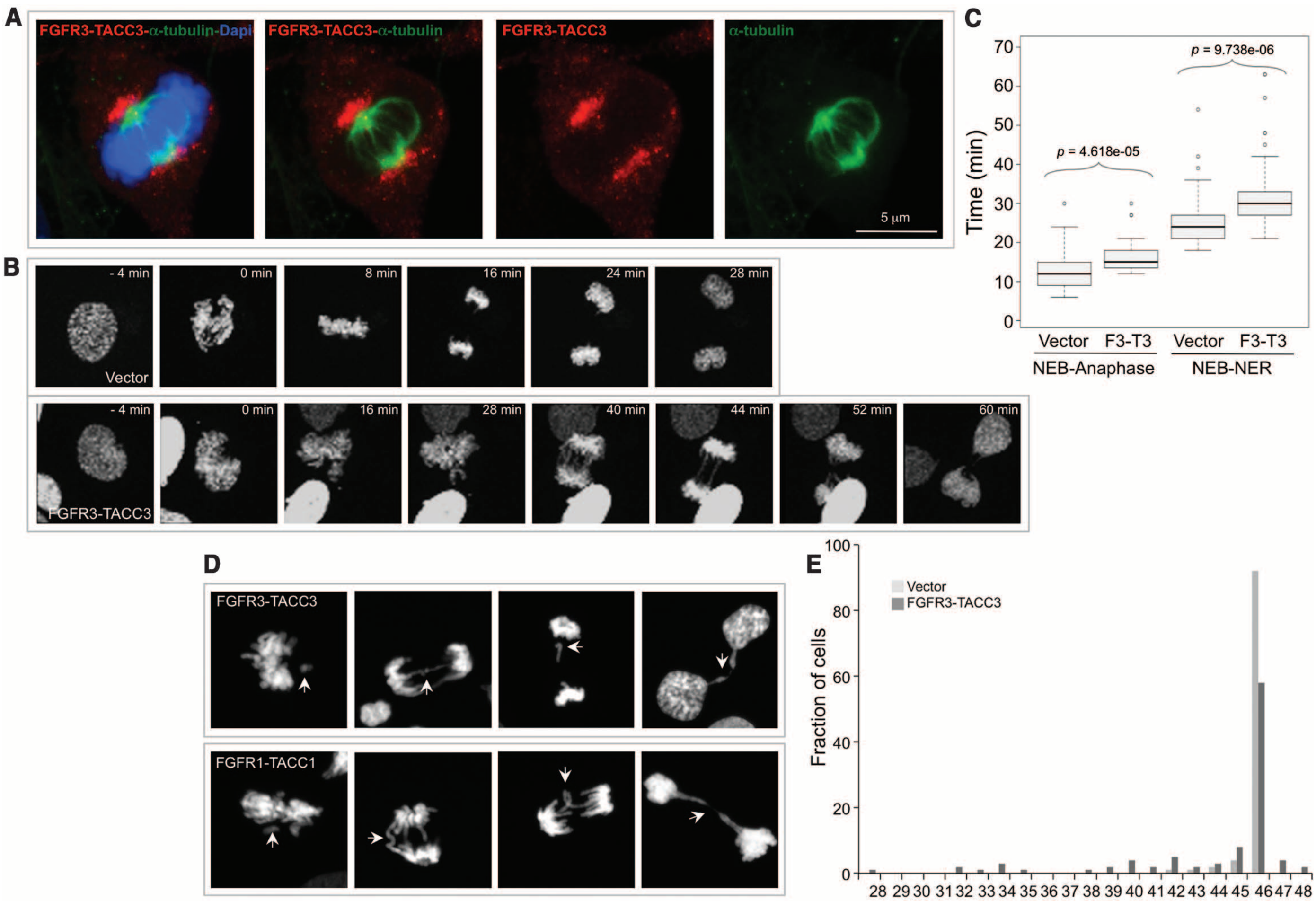

Fig. 3. FGFR3-TACC3 localizes to spindle poles, delays mitotic progression, and induces chromosome segregation defects and aneuploidy. (**A**) Confocal microscopy analysis of FGFR3-TACC3 (red) covering the spindle poles of a representative mitotic cell. α-tubulin, green; DNA [stained with 4′,6-diamidino-2-phenylindole (DAPI)], blue. (**B**) Representative fluorescence video microscopy for cells transduced with vector or FGFR3-TACC3. (**C**) Box-and-whisker plot representing the analysis of the time from nuclear envelope breakdown (NEB) to anaphase onset and from NEB to nuclear envelope reconstitution (NER). The duration of mitosis was measured by following 50 mitoses for each condition by time-lapse microscopy. (**D**) Representative images of cells with chromosome missegregation. Arrows point to chromosome misalignments, lagging chromosomes, and chromosome bridges. (**E**) Distribution of chromosome counts of human astrocytes transduced with control or FGFR3-TACC3–expressing lentivirus. Chromosomes were counted in 100 metaphase cells for each condition to determine the ploidy and diversity of chromosome counts within the cell population.

TACC3–induced aneuploidy by more than 80%, restored the narrow distribution of chromosome counts typical of control cells, and largely corrected the cohesion defect (Fig. 4, A to C, and table S9). To determine whether FGFR-TACC–expressing Rat1A and GSC-1123 cells are dependent on FGFR-TK activity for their growth, we studied the effect of PD173074, AZD4547, or BGJ398. The latter two compounds are highly specific inhibitors of FGFR-TK under clinical investigation (*16*, *17*). Each of the three drugs inhibited the growth of cells expressing FGFR3-TACC3 and FGFR1-TACC1 at concentrations <10 nM, whereas they were ineffective at concentrations as high as 1 μM in cells transduced with vector, FGFR3, TACC3, and the FGFR3-TACC3-K508M mutant (Fig. 4D and fig. S10, C and D). The growth of GSC-1123 was also abolished by nanomolar concentrations of these FGFR-TK inhibitors (Fig. 4E). Targeting of the fusion gene by FGFR3 shRNA inhibited the growth of cells ectopically expressing FGFR3-TACC3 and GSC-1123 in proportion to the silencing efficiency of FGFR3-TACC3 (fig. S10, E and F).

Finally, we studied mice bearing glioma xenografts of FGFR3-TACC3–transformed astrocytes and investigated whether PD173074 affected tumor growth. Twelve days after injection of tumor cells, mice were treated with PD173074 or vehicle (lactate buffer). Only the group treated with PD173074 showed inhibition of tumor growth (fig. S10G). We also tested a more clinically relevant FGFR inhibitor, AZD4547, in mice bearing intracranial luciferase-expressing glioma xenografts. Oral administration of AZD4547 prolonged survival of the mice by 28 days compared with mice treated with the vehicle control (Fig. 4F).

In summary, our functional characterization of the *FGFR-TACC* fusion genes found in a small subset of GBM patients indicates that the constitutively active FGFR-TK and the TACC domain are both essential for oncogenesis. It has long been thought that mutation of the genes that control chromosome segregation during mitosis may explain the high rate of CIN and aneuploidy, which is typical of most solid tumors, including GBMs (*18*). A few examples of mutational inactivation of candidate genes have been reported in human cancer (*19*, *20*). However, gain-of-function mutations causally implicated in the control of mitotic fidelity have not been described. The absence of dominant mutations of CIN genes in human cancer clashes with the classic observation from cell-fusion experiments that the underlying mechanisms that cause CIN behave as dominant traits, indicating that the CIN phenotype results from gain-of-function events rather than gene inactivation (*21*, *22*). The *FGFR-TACC* gene fusion is a mechanism for the initiation of CIN and provides a potential clue to the nature of dominant mutations responsible for aneuploidy in human cancer.

In itself, induction of aneuploidy is detrimental to cellular fitness (*23*). Oncogenic transformation

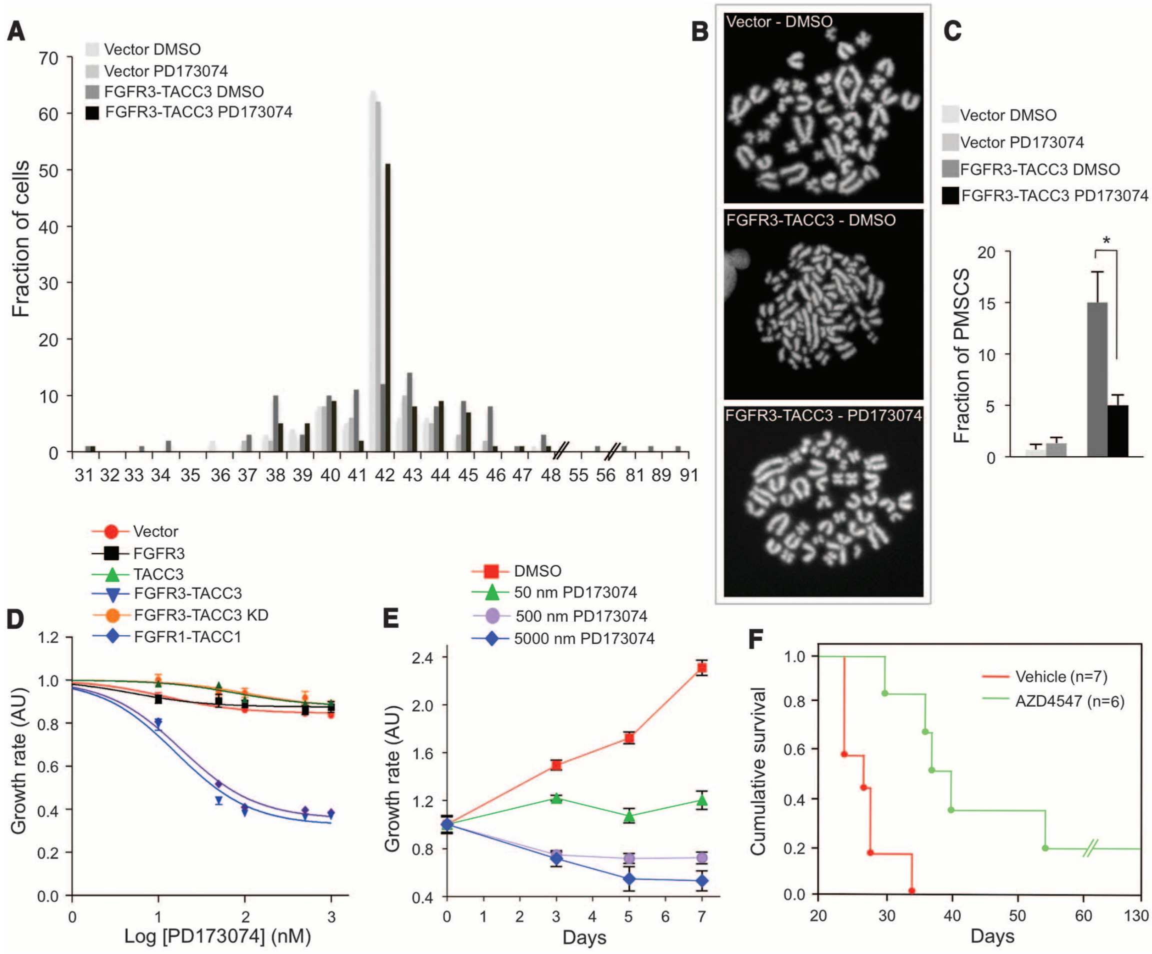

Fig. 4. Inhibition of FGFR-TK activity corrects the aneuploidy and suppresses tumor growth initiated by FGFR3-TACC3. (**A**) Karyotype analysis of Rat1A cells transduced with control or FGFR3-TACC3 lentivirus and treated with vehicle [dimethyl sulfoxide (DMSO)] or PD173470 (100 nM) for 5 days. (**B**) Correction of premature sister chromatid separation (PMSCS) by PD173470 in cells expressing FGFR3-TACC3. Panels show representative metaphase spreads. (**C**) Quantitative analysis of metaphases with loss of sister chromatid cohesion (FGFR3-TACC3 treated with DMSO versus FGFR3-TACC3 treated with PD173470). $P = 0.001$; error bars indicate SD. (**D** and **E**) Growth-inhibition assays of Rat1A cells transduced with the indicated lentivirus (D) and GSC-1123 (E) treated with PD173470 at the indicated concentrations. Cells were treated for 3 days (D) or for the indicated time (E). Cell viability was determined by the MTT assay. Error bars show means ± SE ($n = 4$ culture wells). AU, arbitrary units. (**F**) Survival of glioma-bearing mice was tracked after intracranial implantation of *Ink4A;Arf–/–* astrocytes transduced with FGFR3-TACC3. After tumor engraftment, mice were treated with vehicle or AZD4547 (50 mg/kg) for 20 days (vehicle, $n = 7$ animals; AZD4547, $n = 6$; $P = 0.001$).

requires cooperation between aneuploidy and genetic lesions that confer growth advantage and protect cells against the detrimental effects of aneuploidy (*24*–*26*). The tumor-initiating activity of the FGFR3-TACC3 fusion protein suggests that it has growth-promoting signaling functions that complement the loss of mitotic fidelity and aneuploidy to induce full-blown tumorigenesis (*23*).

There are now several well-known examples in which kinase inhibitors have been developed into effective therapies for patients whose tumors carry functional gene fusions that deregulate kinase activity (*27*, *28*). The antitumor effects in mouse models and the correction of aneuploidy precipitated by FGFR-TK inhibition of glioma cells driven by FGFR-TACC fusions provide a strong rationale for clinical investigation of FGFR inhibitors in GBM patients whose tumors exhibit FGFR-TACC rearrangements.

References and Notes

1. J. Ablain, R. Nasr, A. Bazarbachi, H. de Thé, *Cancer Discov.* **1**, 117 (2011).
2. A. Charest *et al.*, *Genes Chromosomes Cancer* **37**, 58 (2003).
3. F. Mitelman, B. Johansson, F. Mertens, *Nat. Rev. Cancer* **7**, 233 (2007).
4. N. Turner, R. Grose, *Nat. Rev. Cancer* **10**, 116 (2010).
5. F. E. Hood, S. J. Royle, *BioArchitecture* **1**, 105 (2011).
6. I. Peset, I. Vernos, *Trends Cell Biol.* **18**, 379 (2008).
7. C. G. Duncan *et al.*, *Oncotarget* **1**, 265 (2010).
8. R. Yao *et al.*, *Oncogene* **31**, 135 (2012).
9. A. J. Bass *et al.*, *Nat. Genet.* **43**, 964 (2011).
10. P. J. Stephens *et al.*, *Nature* **462**, 1005 (2009).
11. The Cancer Genome Atlas Research Network, *Nature* **455**, 1061 (2008).
12. I. H. Still, P. Vince, J. K. Cowell, *Genomics* **58**, 165 (1999).
13. T. Marumoto *et al.*, *Nat. Med.* **15**, 110 (2009).
14. J. Wesche, K. Haglund, E. M. Haugsten, *Biochem. J.* **437**, 199 (2011).
15. M. Mohammadi *et al.*, *EMBO J.* **17**, 5896 (1998).
16. P. R. Gavine *et al.*, *Cancer Res.* **72**, 2045 (2012).
17. V. Guagnano *et al.*, *J. Med. Chem.* **54**, 7066 (2011).
18. D. J. Gordon, B. Resio, D. Pellman, *Nat. Rev. Genet.* **13**, 189 (2012).
19. D. A. Solomon *et al.*, *Science* **333**, 1039 (2011).
20. S. L. Thompson, S. F. Bakhoum, D. A. Compton, *Curr. Biol.* **20**, R285 (2010).
21. C. Lengauer, K. W. Kinzler, B. Vogelstein, *Nature* **386**, 623 (1997).
22. C. Lengauer, K. W. Kinzler, B. Vogelstein, *Nature* **396**, 643 (1998).
23. J. M. Sheltzer, A. Amon, *Trends Genet.* **27**, 446 (2011).
24. C. H. Coschi, F. A. Dick, *Cell. Mol. Life Sci.* **69**, 2009 (2012).
25. A. J. Holland, D. W. Cleveland, *Nat. Rev. Mol. Cell Biol.* **10**, 478 (2009).
26. B. A. Weaver, D. W. Cleveland, *J. Cell Biol.* **185**, 935 (2009).
27. B. J. Druker, *Nat. Med.* **15**, 1149 (2009).
28. D. E. Gerber, J. D. Minna, *Cancer Cell* **18**, 548 (2010).

Acknowledgments: This work was supported by National Cancer Institute grants R01CA101644 and R01CA131126 (A.L.), R01CA085628 and R01CA127643 (A.I.), U54 CA121852-05 (R.R.), National Library of Medicine grant 1R01LM010140-01 (R.R.), National Institute of Neurological Disorders and Stroke grant R01NS061776 (A.I.), a grant from Partnership for Cure (R.R., 7-78947), and a grant from The Chemotherapy Foundation (A.I.). P.Z. and F.N. are supported by fellowships from the Italian Ministry of Welfare/Provincia di Benevento. G.F. was supported by grants from the Associazione Italiana per la Ricerca sul Cancro and from the Italian Ministry of Health. Three of the authors (A.I., A.L., and R.R.) and Columbia University Medical Center have filed a patent application related to the diagnostic and therapeutic use of *FGFR-TACC* gene fusions. Next-generation RNA-sequencing data have been deposited into the Database of Genotypes and Phenotypes (accession no. phs000505.v1.p1).

Supplementary Materials

www.sciencemag.org/cgi/content/full/science.1220834/DC1
Materials and Methods
Figs. S1 to S10
Tables S1 to S9
References

21 February 2012; accepted 9 July 2012
Published online 26 July 2012;
10.1126/science.1220834

EPITOMICS®
an abcam® company

Now Available
3500 RABBIT MONOCLONALS
Over 7500 Antibodies Total

Antibodies for Epigenetics

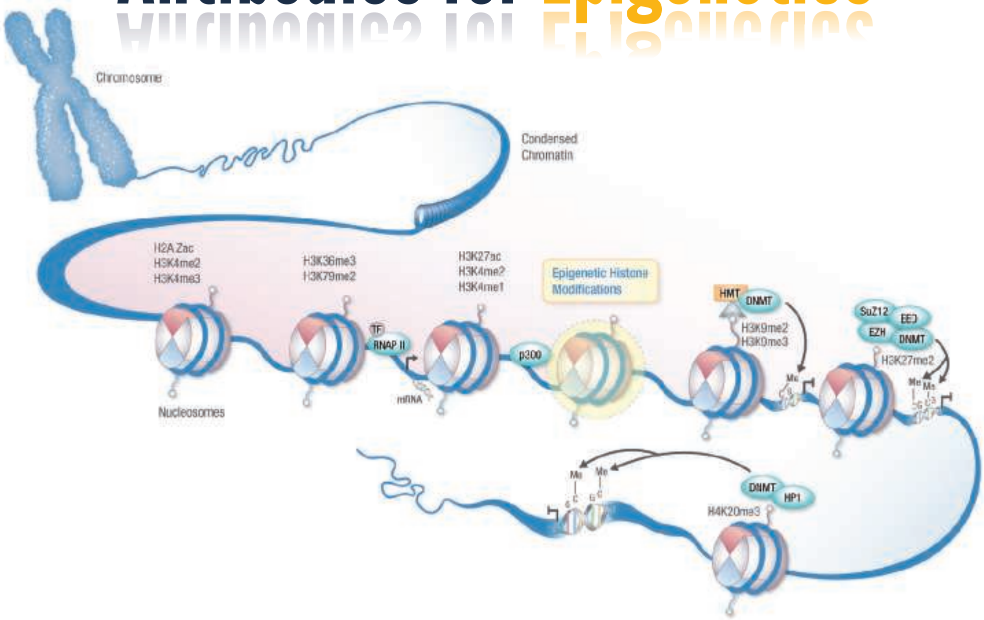

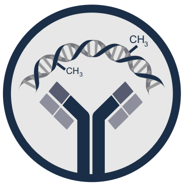

Epigenetics

Our Rabbit Monoclonal Antibodies (RabMAbs®) combine the benefits of the high affinity from the rabbit, with the specificity of a monoclonal, enabling the development of high quality modification-specific antibodies (1, 2). We have now generated more than 500 modification-specific and activation-specific antibodies using our patented technology, including our new 5-Methylcytosine RabMAb (Cat # 3913-1, Clone EP4694) which can be used to identify methylated DNA to study methylation events.

Additionally, we validate every RabMAb in WB, IHC, IF, IP and FACS before release, so you can be assured of which assays the antibody will work in before purchasing.

High Quality Antibodies for Epigenetics

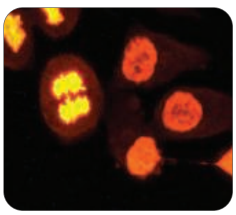

Histone H3 (pS10)
Cat.#: 1173-1

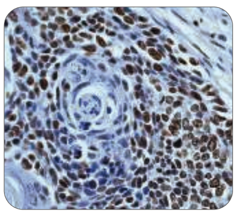

Histone H4 (K8)
Cat.#: 1796-1

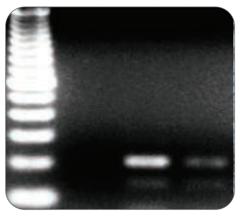

5-Methylcytosine
Cat.#: 3913-1

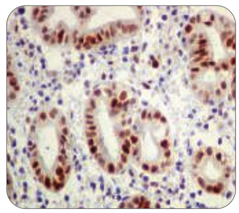

Dnmt1
Cat.#: 3147-1

Learn More @ www.epitomics.com/epigenetics

1. Rabbit monoclonal antibodies: a comparative study between a novel category of immunoreagents and the corresponding mouse monoclonal antibodies, Rossi S. et al., Am J Clin Pathol. 2005 Aug;124(2):295-302
2. Rabbit monoclonal antibody: potential application in cancer therapy, Feng L. et a;. Am J Transl Res. 2011 May 15; 3(3): 269–274


I seek the future.

Days of Molecular Medicine 2012

THE TRANSLATIONAL SCIENCE OF RARE DISEASES: FROM RARE TO CARE

October 8-10, 2012

Palais de Lichtenstein
Vienna, Austria

Join an international roster of academic, industrial and government scientists, headlined by Nobel Laureate Eric Kandel, who will discuss how innovative technologies are shedding light on the causes of rare diseases and strategies for developing new treatments. Topics include:

- A targeted drug for cystic fibrosis
- Exon skipping for muscular dystrophies
- Gene therapy for immunodeficiency and hemophilia
- Tailoring treatments with genomics
- Stem cells for treating blindness

For more information, including a full list of speakers, visit dmm.aaas.org.

BROUGHT TO YOU BY

IMBA Institute of Molecular Biotechnology of the Austrian Academy of Sciences

Days of Molecular Medicine Global Foundation

Science Translational Medicine AAAS

New Products

MICROPLATE READER

The TriStar² microplate reader employs the new optical concept ALL-4-ONE, enabling luminescence, fluorescence, and absorbance measurements. TriStar² is also capable of reading Förster Resonance Energy Transfer (FRET), Bioluminescence Resonance Energy Transfer (BRET), and BRET². The instrument is characterized by a universal detector with extremely low noise for fluorescence and luminescence measurements and is also equipped with a photodiode for absorbance readings. Furthermore, optical filters can be used for luminescence measurements, enabling BRET and multicolored luciferase reporter gene applications. TriStar² can be fitted with up to three reagent injectors and temperature controls for the microplate compartment. A reagent compartment at the front makes reagents easily accessible and allows them to be cooled by the addition of crushed ice when needed. For increased sample throughput, TriStar² can be integrated into lab automation systems. Special reagent mounts provide secure fixation for small reagent vials and ensure complete consumption of reagents by the angle of inclination.

Berthold Technologies

For info: +49-7081-177-0 | www.berthold.com

BULK POWDER HANDLING ENCLOSURE

The PowderSafe Bulk Handling Enclosure fills the need for effective containment during bulk powder manipulation without the expense or space requirements of a traditional walk-in or free-standing enclosure. With a unique drum access port incorporated into the base of the enclosure, the drum can be raised and sealed to the access port, effectively extending the enclosure's containment area into the drum. When drum access is not required, the included access port cover can be used to seal the base, allowing for use as a standard balance enclosure. Designed to provide a turbulence-free airflow environment, PowderSafe Bulk Handling Enclosures move air in a horizontal pattern to maximize containment while minimizing sample loss and balance instability. Proprietary HEPASafe filter change-out technology, incorporated into each PowderSafe Bulk Handling Enclosure, allows the operator to safely and effectively change both the prefilter and primary HEPA filter.

AirClean Systems

For info: 800-849-0472 | www.aircleansystems.com

TRANSILLUMINATOR

The advanced Bi-O-Vision Series transilluminators feature two workstations, producing both 312 nm ultraviolet (UV) and white light. The TD-1000R model offers fixed-intensity control, while the TVD-1000R model offers variable-intensity control of either UV or white light. These units are continuously adjustable from 100% down to 50%. This enables life science researchers to select the exact ultraviolet or white-light illumination needed to photodocument samples with a single piece of equipment. The UVB (312 nm) intensity of the TVD-1000R can be varied. This flexibility in irradiance control helps ensure the longest sample preparation time, while minimizing actual UV damage to the sample. The Bi-O-Vision has two adjacent workstations. The UV side is lit by five 8 W UVB tubes and delivers nanogram sensitivity for detecting ethidium bromide-stained DNA or RNA. The white-light side has three 8 W fluorescent tubes that ensure excellent illumination for viewing Coomassie blue-stained protein gels, methylene blue-stained DNA gels, and autoradiograms.

Spectroline

For info: 800-274-8888 | www.spectroline.com

DENDRITIC CELL GROWTH KITS AND ANTIBODIES

Bovine and ovine Dendritic Cell Growth Kits have been developed to improve dendritic cell (DC) generation by enabling researchers to develop a method for consistent cell generation, and to save time with prevalidated, optimized species-specific reagents. A complementary panel of antibodies for bovine and ovine DC markers has been launched to enable cell surface phenotyping of DCs. The Dendritic Cell Growth Kits are unique to AbD Serotec and were developed in collaboration with the Moredun Research Institute, Edinburgh, and the Institute for Animal Health, Compton, centers recognized worldwide for their research on the infectious diseases of livestock. The kits contain biologically active cytokines in liquid format, premixed at optimal concentrations to facilitate the generation of DCs from peripheral blood mononuclear cells.

AbD Serotec

For info: 800-265-7376 | www.abdserotec.com

MULTIWELL PLATES

A range of multiwell filtration microplates have been optimized for applications including cell harvesting, DNA separations, binding studies, plasmid isolation, general filtration, and sample cleanup. Included within the range are filtration plates that can simultaneously filter 96 or 384 samples of up to 350 µl volume, providing great productivity benefits and high filtered sample integrity. For larger volume applications (up to 5 ml/well), a choice of 48-well filtration plates are available. A broad range of filtration media including glass fiber, nylon, polyvinylidene fluoride (PVDF), and polyethylene allows control of filtration plate flow rates and retention characteristics to best suit many applications. Manufactured to the standard ANSI/SBS footprint, all Porvair filtration plates are fully automation compatible. Each well on the filtration plates has an individual drainage spout ensuring 100% sample transfer and zero crossover contamination. Manufactured from ultrapure grade polypropylene—all filtration plates minimize leachates when used with most common solvents.

Porvair Sciences

For info: +44-(0)-1372-824290 | www.porvair-sciences.com

Electronically submit your new product description or product literature information! Go to www.sciencemag.org/products/newproducts.dtl for more information.

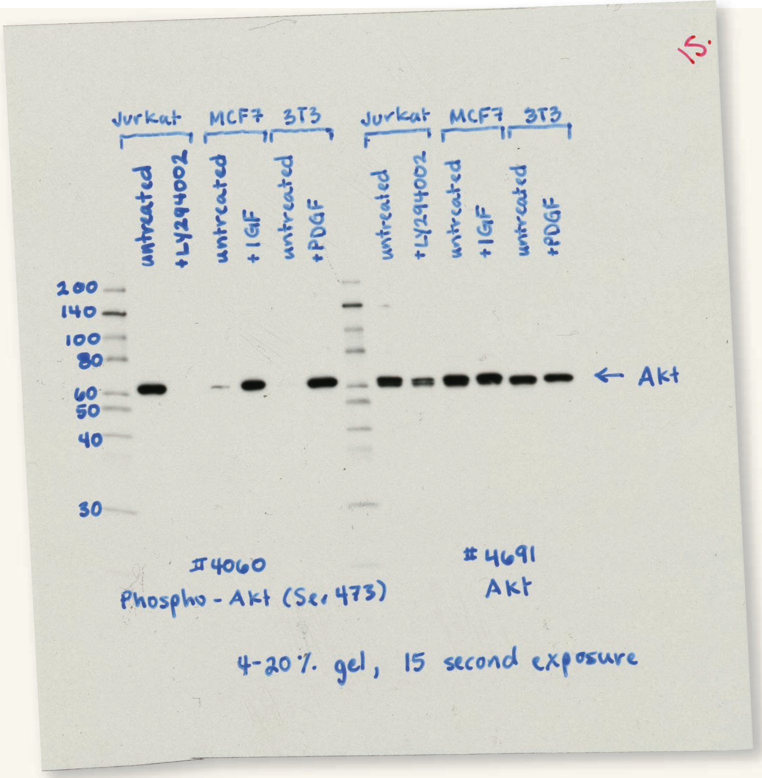

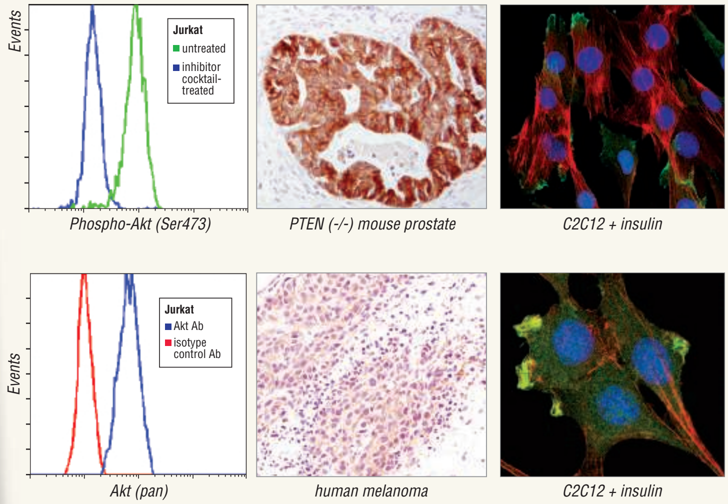

***Phospho-Akt (Ser473) (D9E) XP® Rabbit mAb #4060** (upper)*
*and **Akt (pan) (C67E7) Rabbit mAb #4691** (lower).*
For full validation details see www.cellsignal.com

The Highest Quality
Akt Antibodies
are from Cell Signaling Technology

Over 45 thoroughly validated Akt Antibodies available

Cell Signaling Technology offers the widest range of phospho and total protein Akt antibodies. These reagents are the most thoroughly validated, widely used, and highly cited Akt antibodies available.

:: CST™ phospho and total protein Akt antibodies offer **unsurpassed specificity, sensitivity, and performance**.

:: **Extensive in-house validation** in a wide range of applications means that optimization is not left up to you, the user.

:: **Technical support is provided by scientists** who produce the products and know them best.

Unparalleled product quality, validation, and technical support

for quality products you can trust...

www.cellsignal.com

Cell Signaling TECHNOLOGY®

THE CHINESE UNIVERSITY OF HONG KONG

Applications are invited for:-

Department of Physics
Assistant Professors
(Ref. 1213/004(665)/2)

The Department invites applications for faculty positions at the level of Assistant Professor with prospect for substantiation tenable from the academic year 2013-2014. The Department anticipates that there will be multiple positions.

Applicants should have a relevant PhD degree with postdoctoral research experience. Outstanding candidates in all areas of physics, particularly in the fields of experimental condensed matter physics, atomic, molecular and optical physics, and astrophysics, are welcome to apply. Successful candidates are expected to demonstrate a strong record of research accomplishments, potential for establishing a significant externally funded research programme, and a strong interest in teaching at undergraduate and postgraduate levels. Appointments will normally be made on contract basis for up to three years initially, which, subject to mutual agreement, may lead to longer-term appointment or substantiation later (substantive appointment may be considered during the second three-year contract). Applications will be accepted until the positions are filled.

Salary and Fringe Benefits
Salary will be highly competitive, commensurate with qualifications and experience. The University offers a comprehensive fringe benefit package, including medical care, a contract-end gratuity for appointments of two years or longer, and housing benefits for eligible appointees. Further information about the University and the general terms of service for appointments is available at *http://www.per.cuhk.edu.hk*. The terms mentioned herein are for reference only and are subject to revision by the University.

Application Procedure
Applications (comprising a full curriculum vitae, a detailed publication list with three selected published papers, a research plan, a teaching statement, and three letters of recommendation) should be sent to Professor Ke-Qing Xia, Chairman, Department of Physics, The Chinese University of Hong Kong, Shatin, Hong Kong (email: *physics@cuhk.edu.hk*; fax: (852) 2603 5204). The Personal Information Collection Statement will be provided upon request. Please quote the reference number and mark 'Application - Confidential' on cover.

UNIVERSITY AT ALBANY
State University of New York

Neuroscience Faculty Positions

The University invites applications for **three tenure-track Assistant/Associate Professor positions** in Neuroscience, two in the Biological Sciences and one in Psychology.

Neural Regenerative Biology: the investigation of approaches/processes involved in the repair of the nervous system. This could include cell replacement or axon outgrowth and likely would involve the use of neural stem cells.

To apply: Neural Repair:
http://albany.interviewexchange.com/jobofferdetails.jsp?JOBID=34351

Neural Development/Plasticity: research examining mechanisms of long-term changes in neural structure and function resulting from environmental interactions. This would include, but not limited to, epigenetic mechanisms of experience-dependent synaptic changes or forms of developmental plasticity produced by environmental agents, such as neurotoxins.

To apply: Neural Development:
http://albany.interviewexchange.com/jobofferdetails.jsp?JOBID=34349

The successful candidates are expected to utilize a variety of modern molecular, physiological and/or imaging techniques for the study of nervous systems. They will have their primary appointments in the **Department of Biological Sciences.**

Behavioral Neuroscience: research examining neural mechanisms of behavior and/or behavioral disorders using contemporary cellular, molecular and/or genetic approaches. Candidates should also demonstrate the capacity for high quality undergraduate and graduate teaching in behavioral neuroscience. The primary appointment for this position will be in the **Behavioral Neuroscience Division of the Department of Psychology.**

To apply: Behavioral Neuroscience:
http://albany.interviewexchange.com/jobofferdetails.jsp?JOBID=34155

Successful candidates will join a Neuroscience Program with traditional strengths in Neural Development and Plasticity. Neuroscientists are located in the Life Sciences Research Building, which contains state-of-the-art laboratories and core facilities, and houses Life Science researchers from the Departments of Biology, Chemistry, Physics and Psychology (**http://www.albany.edu/lifesciences**). Successful candidates will be offered a competitive salary and start-up package.

Applications must include a CV with publications cited in detail and any present or past grant funding, statement of research interests, statement of teaching interests, and a minimum of three references with contact information.

Qualifications for Candidates: Ph.D. or M.D. from a college or university accredited by the U.S. Department of Education or an internationally recognized accrediting organization and a strong publication record reflecting significant scientific accomplishments. Applicants must address in their applications their ability to work with and instruct a culturally diverse population. Preferred qualifications include productive post-doctoral training and the potential or demonstrated ability, to obtain independent extramural funding. Applicants at the Associate Professor level must have an established, externally funded research program. Review of applications will begin on November 15, 2012 and continue until the positions are filled.

The University at Albany is an EEO/AA/IRCA/ADA employer.

Memorial Sloan-Kettering Cancer Center

The Best Cancer Care. Anywhere.

FACULTY POSITIONS

Center for Stem Cell Biology & Developmental Biology Program

The Center for Stem Cell Biology (CSCB) and the Developmental Biology Program are seeking innovative individuals who have strong records of research accomplishments in stem cell biology for tenure-track positions at the Assistant Member level (equivalent to Assistant Professor). The CSCB was established to further the interaction of researchers with active stem cell research programs at the Center, to enhance and build novel stem cell related resources and to recruit leading-edge stem cell faculty. The CSCB is interested in research in any aspect of stem cell biology, including the study of stem cells in model organisms, tissue stem cells and the biology and application of human embryonic stem cells or induced pluripotent stem cells. Candidates with a strong interest in applying developmental approaches to studying stem cell biology are particularly encouraged to apply.

Applicants should have a PhD and/or MD degree, a productive postdoctoral experience, dedication to important problems in stem cell biology, and the potential to develop a strong independent program in stem cell research. Successful candidates will be appointed in the Developmental Biology Program and will become a member of the CSCB. Successful candidates are also eligible to hold additional appointments at the Gerstner Sloan-Kettering Graduate School of Biomedical Sciences, the Weill Cornell Graduate School of Medical Sciences, as well as the Tri-Institutional MD/PhD Training Program.

Successful applicants will have access to outstanding resources including expanded state-of-the-art facilities for human pluripotent stem cells, high-throughput chemical and genetic screening, mouse genetics, genomics, flow cytometry, advanced imaging and cancer biology. Memorial Sloan-Kettering offers a unique and exciting multidisciplinary research environment. Faculty in the CSCB participate in the Tri-Institutional stem cell initiative (with Weill Cornell and Rockefeller University) that links stem cell researchers across neighboring institutions.

The deadline for applications is **November 1, 2012**. Interested candidates should visit **facultysearch.ski.edu** to access the on-line faculty application. The site contains important information on the required application materials as well as deadlines for submission of letters of reference.

Inquiries may be sent to **Tiffany Lennon** at **lennont@mskcc.org**; to **Dr. Lorenz Studer, Director CSCB**, at **studerl@mskcc.org**; or to **Dr. Kathryn Anderson, Chair Developmental Biology Program**, at **k-anderson@ski.mskcc.org**.

facultysearch.ski.edu

MSKCC is an equal opportunity and affirmative action employer committed to diversity and inclusion in all aspects of recruiting and employment. All qualified individuals are encouraged to apply.

Director

Ref: 1104

Centre for Cancer Research and Cell Biology

One of the leading universities in the UK and Ireland, Queen's University Belfast is continuing to strengthen its world-class reputation and the international impact of its biomedical research by seeking to recruit a new Director of the internationally renowned Centre for Cancer Research and Cell Biology (CCRCB).

We are seeking an exceptional individual who has the vision, drive and outstanding leadership skills to further develop the CCRCB's world-class research programme that spans basic through to translational to clinical research. The appointee will also ensure that the IPR arising from the CCRCB research programme is exploited commercially and will further develop the entrepreneurial ethos of the Centre which has already produced successful spin-out companies employing staff in both Northern Ireland and in the USA.

The CCRCB is one of four leading Research Centres which, along with the Wellcome Clinical Research Facility, make up the University's Institute of Health Sciences. The CCRCB's mission is to drive discovery, innovation and the development of targeted therapies in order to accelerate the defeat of cancer. It is part of the Experimental Cancer Medicine network and is a CR-UK designated Centre. The CCRCB is a cross-faculty, interdisciplinary research centre, with over 250 clinical and basic researchers from across the world. It has established international partnerships with leading global institutions such as the US National Cancer Institute. Most recently, in recognition of the Centre's leadership of the Northern Ireland Comprehensive Cancer Services (CCS) programme, along with the Northern Ireland Clinical Cancer Centre and the Northern Ireland Cancer Registry, the University was presented with the Diamond Jubilee Queen's Anniversary Prize.

The closing date is 12noon Monday 22 October 2012.

For further information and for details on how to apply, please visit our Academic Recruitment website at **www.qub.ac.uk/jobs** or contact Perrett Laver, our appointed executive search partner, at 020 7340 6200 or at qub@perrettlaver.com.

The University is committed to equality of opportunity and to selection on merit. It therefore welcomes applications from all sections of society and particularly welcomes applications from people with a disability.

Personnel Department
Queen's University Belfast
Belfast, BT7 1NN.
Tel (028) 90973044
Fax (028) 90971040
E-mail on personnel@qub.ac.uk

Perrett Laver

Queen's University Belfast

RUSSELL INTERNATIONAL EXCELLENCE GROUP

Queen's University Belfast is a member of the Russell Group of universities. One of the United Kingdom's top 20 research-intensive universities.

Faculty Positions in School of Life Sciences and Technology, ShanghaiTech University

As a newly established research-oriented university in Zhang-Jiang High-Tech Park of Shanghai, ShanghaiTech University (ShanghaiTech) invites applications for tenure-track faculty positions. Appointments will be in School of Life Sciences and Technology (SLST). The successful candidates should have an exceptional track record of research in life sciences or a closely related discipline within the last five years. Besides maintaining an active research program, the recruited candidates will also be expected to contribute to the educational missions of undergraduate and graduate programs within SLST. Qualified applicants will be invited to attend an interview in Shanghai in the middle of December.

Academic Disciplines:
SLST seeks early career scientists in these five research areas: Protein science and biotechnology; Stem cell research and regenerative medicine; Systems biology and translational medicine; Physical biology and molecular imaging; Chemical biology and innovative pharmacology.

Salaries and Benefits:
ShanghaiTech offers highly competitive salaries and start-up packages.

Contact Us:
Qualified applicants are invited to submit a cover letter with a 2-3 page description of research plans, a CV with up to 3 publications, and the names of three referees to: **slst@shanghaitech.edu.cn**

Mailing Address:
School of Life Science and Technology, ShanghaiTech University
Room105, Building 2, 319 Yueyang Road, Shanghai 200031, China
Tel: +86-21-54201137 Fax: +86-21-54201292

ShanghaiTech University Website: http://www.shanghaitech.edu.cn

Penn Medicine

Assistant Professor (Tenure Track)

The Department of Radiation Oncology, Division of Radiation Research at the Perelman School of Medicine, University of Pennsylvania, invites applications for a tenure-track faculty position at the Assistant Professor level. Candidates with a PhD or an MD/PhD degree, strong publication records in any area of Tumor or Radiation Biology and particularly those with research interest in normal tissue radiobiology, tumor microenvironment or tumor stem cells, are encouraged to apply.

The Division of Radiation Research is comprised of 11 faculty engaged in innovative, translational research with a focus on the study of the tumor micro-environment, radiation response modifiers, photodynamic therapy and proton therapy. Research in the Division is supported by multiple grants from the NIH, DoD, NASA, private foundations and industry. Faculty in the Division can have cross-appointments to other Departments and can belong to different graduate groups such as Cancer Biology and Pharmacology.

The Division has recently moved to a brand new, contiguous laboratory space in the Translational Research Building, in very close proximity to the clinic. State-of-the-art shared instrumentation includes a 3-D conformal irradiator for small animals, live cell microscopy, hypoxia chambers, multiple PDT lasers, etc. The TRC building has its own barrier and non-barrier animal facility and small animal imaging facilities which include optical, MR and CT imaging. A competitive start-up package and laboratory space will be provided.

For more information about the Department of Radiation Oncology, and the Division of Radiation Research please visit: **http://www.xrt.upenn.edu/index.shtml**

Interested candidates should send a curriculum vitae, a one-page summary of their future research goals and the names of three references, preferably in a single PDF, to **Ms. Rebecca Wilson**, at: **Rebecca.Wilson@uphs.upenn.edu**. The deadline for applications is **December 1, 2012**.

We seek candidates who embrace and reflect diversity in the broadest sense. The University of Pennsylvania is an Equal Opportunity, Affirmative Action Employer.

THE UNIVERSITY OF TEXAS
MD Anderson ~~Cancer~~ Center
Making Cancer History®

Assistant/Associate Professor – The Department of Experimental Radiation Oncology

Junjie Chen, Ph.D.
Professor and Chair
Experimental Radiation Oncology
The University of Texas
MD Anderson Cancer Center
1515 Holcombe Blvd., Unit 066
Houston, TX 77030-4009

The Department of Experimental Radiation Oncology at The University of Texas MD Anderson Cancer Center invites applications from researchers for a tenure-track Assistant Professor, Associate Professor or Professor position. Research areas should focus on translational approaches ranging from genetics, cell biology and biochemistry to proteomics and system biology. The department seeks to complement its existing programs in DNA repair, cell cycle control, growth and proliferation, stem cell biology and epigenetics, especially related to translational research in radiation oncology. Female and minority candidates are encouraged to apply. We offer a very attractive recruitment package, active graduate and post-doctoral training programs, and the unmatched scientific environment of the Texas Medical Center, the world's largest biomedical center.

Applicants must have a Ph.D. and/or M.D. degree, and will be expected to develop an internationally recognized, extramurally funded research program. To apply, please send a single pdf file containing: (1) cover letter, (2) curriculum vitae, (3) short research summary (three-page maximum); and (4) contact information for three references by November 31, 2012, to: expradonc@mdanderson.org

MD Anderson Cancer Center is an equal opportunity employer and does not discriminate on the basis of race, color, national origin, gender, sexual orientation, age, religion, disability or veteran status except where such distinction is required by law. All positions at The University of Texas MD Anderson Cancer Center are security sensitive and subject to examination of criminal history record information. Smoke-free and drug-free facility.

DIRECTOR OCEAN, ATMOSPHERE, AND SPACE RESEARCH DIVISION

Office of Naval Research — Science & Technology

The Office of Naval Research (ONR) is seeking an outstanding individual to serve in this Civil Service position in the Senior Executive Service (SES). The Director, Ocean, Atmosphere, and Space Research Division, is responsible for an integrated program across basic research, applied research, and applied technology. The Division Director is responsible for managing and directing extensive activities in fostering innovative concepts, identifying critical program goals and objectives, developing an S&T program to address these objectives, executing this program and setting budget priorities, and transitioning the resulting technology to the Navy and Marine Corps in the fields of science and technology including oceanography, acoustics, remote sensing, and marine meteorology. The Director also serves as expert consultant and advisor in these areas of S&T to the Chief of Naval Research and other top professional and military personnel in the Department of the Navy, the Department of Defense, other government agencies, industry and universities.

For information regarding this vacancy and specific instructions on how to apply, go to **www.usajobs.gov**, log in and enter the following announcement number: **NW2XXXX-00-7182564H414235-S**. Please carefully read the announcement and follow instructions when applying. The announcement closes on 10/04/12. Please contact Jennifer Schiller at **Jennifer.Schiller@navy.mil** for more information.

ONR IS AN EQUAL EMPLOYMENT OPPORTUNITY EMPLOYER AND PROMOTES DIVERSITY IN THE WORKPLACE. WOMEN AND MINORITIES ARE ENCOURAGED TO APPLY.

DEAN School of Arts and Sciences

UNIVERSITY OF PENNSYLVANIA

The University of Pennsylvania seeks an eminent, energetic, strategic, judicious, and collaborative academic leader to serve as the next Dean of the School of Arts and Sciences. The Dean of the School of Arts and Sciences (SAS) is responsible to Penn President, Amy Gutmann, and Provost, Vincent Price, for the conduct, coordination, and quality of SAS's educational programs, research activities, fundraising, finances, outreach, and other operations. The Dean is charged with the responsibility of maintaining the highest standards of teaching and scholarship, and further increasing the eminence and leadership of SAS in the liberal arts and sciences. As a senior member of the Penn leadership team, the Dean works closely and collaboratively with the SAS faculty and the President, the Provost, the Deans of Penn's other eleven schools, and the other senior officers of the University to manage SAS's programs and resources in furtherance of the University's academic and institutional goals, including increasing access, integrating knowledge, and engaging locally and globally, as expressed in the *Penn Compact*.

The successful Dean candidate will present a distinguished record of achievement in research, education, and administration. He or she will demonstrate impeccable academic judgment and an uncompromising commitment to academic excellence, a commitment to diversity in all its forms, an unwavering ethical compass, and a deep commitment to interdisciplinary collaboration. An articulate and enthusiastic communicator, the Dean will be able to develop and implement a strategic vision for the School's future consonant with the *Penn Compact*, establish and pursue clear strategic priorities, and manage resources effectively to steadily advance those priorities.

Penn Arts and Sciences – one of the world's leading liberal arts institutions – is home to nearly 500 distinguished faculty that have been recognized by nearly every major learned society and award committee. Through the College of Arts and Sciences, the School offers some 70 undergraduate majors through 27 academic departments, four interdisciplinary, and three dual-degree programs. The Graduate Division enrolls 1,400 doctoral candidates in more than 30 programs who will take their place as the next generation of leaders in the humanities, social sciences, and natural sciences. The School also offers 12 professional master's degree programs. The School has a FY2013 budget of approximately $460 million, including $89 million in sponsored program support.

The new Dean will join an institution with tremendous momentum and the highest aspirations, led since 2004 by the eminent philosopher and political scientist, Amy Gutmann, whose extraordinarily successful term as President has been extended until at least 2019. One of the world's leading research universities, Penn is home to a distinguished faculty of 2,500 teacher-scholars who cross disciplinary and professional boundaries and who have been recognized by nearly every major learned society and award committee. Penn's 12 schools reside on a single, compact, urban campus; span the arts, sciences, humanities, and professions; and display a special commitment to interdisciplinary scholarship and to energetic local and global engagement.

The anticipated start date is **July 1, 2013**, but the search will remain open until the position is filled. For fullest consideration, nominations and expressions of interest should be received – in the strictest confidence – **no later than September 30, 2012.**

The University has retained Russell Reynolds Associates to assist in this search. All communications should be sent via **email to: upennsas@russellreynolds.com** and may be addressed to:

RUSSELL REYNOLDS ASSOCIATES

Dr. Ilene H. Nagel | ilene.nagel@russellreynolds.com | 805-699-3050

and

Mirah Horowitz | mirah.horowitz@russellreynolds.com | 202-654-7857

Penn
UNIVERSITY *of* PENNSYLVANIA

THE UNIVERSITY OF PENNSYLVANIA IS AN EQUAL OPPORTUNITY AFFIRMATIVE ACTION EMPLOYER AND IS STRONGLY COMMITTED TO DIVERSITY. MINORITIES, FEMALES, VETERANS, AND INDIVIDUALS WITH DISABILITIES ARE STRONGLY ENCOURAGED TO APPLY.

Endowed Professor of Immunology

The Department of Molecular Genetics and Microbiology at Stony Brook Medicine is seeking an immunologist to provide leadership in the research field of immunology. This position will be endowed by a significant philanthropic gift, and it is expected that the successful candidate will become the focus of additional faculty in the field of immunology. With the recent approval of the NYSUNY 2020 Challenge Grant to the University and the announcement of the largest gift ever to public higher education in the State of New York, Stony Brook University School of Medicine is embarking on a transformational expansion of the biomedical and clinical research enterprise. The investment in immunology will include development of multi-departmental immunology programs through additional faculty recruitments in this field.

Applicants for this position should have a demonstrated track record of extramural funding in immunology research. Candidates with research interests in host response to infectious organisms or cancer will complement existing academic strengths.

Required: The successful candidate will have a PhD or MD degree and possess a demonstrated record of scholarship in immunology. For a senior faculty appointment, the candidate must meet the criteria established by the School of Medicine (School of Medicine's Criteria for Appointment, Promotion and Tenure).

For a full position description, application procedures or to apply online visit *www.stonybrook.edu/jobs* (Ref. #: F-7398-12-07). Nominations and applications, to include a State employment application and curriculum vitae, should be submitted to: Dr. Jorge L. Benach, Chair of Search Committee, c/o Ms. Christina Babzien
Life Sciences Building, Room 280A, Stony Brook University, Stony Brook, NY 11794-5222
Electronic applications are preferred.

At Stony Brook Medicine, our highest calling is to put the power of ideas to work in our patients' lives. Stony Brook Medicine integrates and elevates all of Stony Brook University's health-related initiatives: education, research and patient care. It includes Stony Brook University Hospital, Long Island's premier academic medical center. With 597 beds, SBUH is the region's only tertiary care center and Regional Trauma Center. We are home of the Stony Brook Heart Institute, Stony Brook Center for Infectious Diseases, Stony Brook Cancer Center, Stony Brook Long Island Children's Hospital, Stony Brook Neurosciences Institute and Stony Brook Digestive Disorders Institute. Join our team at Stony Brook Medicine – the best ideas in medicine.

Stony Brook Medicine

Stony Brook University/SUNY is an affirmative action, equal opportunity educator and employer.

Department of Health and Human Services
National Institutes of Health

National Institute on Aging

Division of Geriatrics and Clinical Gerontology

http://www.nia.nih.gov/about/offices/division-geriatrics-and-clinical-gerontology-dgcg

Health Scientist Administrator or Medical Officer

The National Institute on Aging's extramural Division of Geriatrics and Clinical Gerontology (DGCG) is seeking an individual to serve as a scientific administrator in its Clinical Gerontology Branch, to oversee and develop a program of grant-supported clinical and translational biomedical aging research.
Developmental aspects of the position include integration of findings from mechanistic, observational and intervention studies to identify research opportunities to advance experimental therapeutics for healthy aging and treatment of age-related conditions, and organizing initiatives to implement such research. Administrative aspects of the position include managing a portfolio of grants and grant applications on clinical and translational research on factors affecting aging over the life span and interventions influencing these factors.

Depending on training and qualifications, appointment to this position may be made either as a Health Scientist Administrator or as a Medical Officer. Candidates should have an M.D., Ph.D., or equivalent doctoral degree, and biomedical research experience. The ideal candidate will have training in a biomedical research field; experience in planning, design, administration, and analysis of clinical research; experience in scientific grant application writing or review; and demonstrated skills in administration and communication. Prior experience in experimental therapeutics and pharmaceutical R&D (e.g., identification of therapeutic targets, drug discovery, and knowledge of regulatory requirements) is highly desirable, but not required. Experience in relevant fields such as clinical physiology, gerontology, and genomics is also particularly valuable.

NIA's Division of Geriatrics and Clinical Gerontology (DGCG) is located in downtown Bethesda, Maryland. NIA is one of the National Institutes of Health (NIH), the premier biomedical research center for the Nation and the world. The 27 NIH Institutes and Centers employ approximately 18,000 persons in a wide array of jobs supporting efforts for improving health.

Salary is commensurate with experience and qualifications. If you have questions about this vacancy, please contact **Caroline McCullough** at **caroline.mccullough @nih.gov** or **410-558-8072**. To apply and to review qualifications, evaluation criteria, application instructions, and salary and benefits information, please visit **www.usajobs.gov** and search for Health Scientist Administrator GS-601-13/14 announcement number NIH-NIA-DE-12-631912 (open to all US citizens) and/or Health Scientist Administrator GS-601-13/14 NIH-NIA-MP-12-631913 (open to current/former federal employees) and/or Health Scientist Administrator GS-601-15 announcement number NIH-NIA-DE-12-631897 (open to all US citizens) and/or Health Scientist Administrator GS-601-15 NIH-NIA-MP-12-631900 (open to current/former federal employees) and/or Medical Officer GS-602-13/14 announcement number NIH-NIA-DH-12-631924 (open to all US citizens) and/or Medical Officer GS-0602-15 announcement number NIH-NIA-DH-12-631925 (open to all US citizens). US citizenship is required. Applications will be accepted from **September 11, 2012 to September 20, 2012**.

DHHS and NIH are Equal Opportunity Employers.

UNIVERSITY OF MARYLAND

Open Rank Faculty Position
University of Maryland College Park
Department of Cell Biology and Molecular Genetics

The Department of Cell Biology and Molecular Genetics at the University of Maryland College Park is seeking to fill a tenure-track faculty position in the broad areas of cell biology and molecular genetics using animal, plant, or microbial systems. The appointment may be made at the Assistant, Associate, or Full Professor level, commensurate with qualifications and experience.

The successful candidate will be expected to maintain a cutting-edge externally funded research program that synergizes with existing core groups in the department including genomics and gene regulation, RNA structure and function, plant biology, microbial pathogenesis and immunology, and virology. The appointed candidate will also participate in undergraduate and graduate teaching. Applicants must have a doctorate degree, an outstanding publication record, and a commitment to excellence in teaching.

The University of Maryland, College Park is the flagship campus of the University System of Maryland. Close proximity to Washington DC, Baltimore, and the Maryland Biotechnology Corridor facilitates interactions with an extraordinary range of major research institutions such as NIH, NIST, FDA, USDA and JCVI, in addition to providing a rich cultural environment.

Applications should be submitted electronically to **https://jobs.umd.edu/applicants/Central?quickFind=57676** position number 118570, and addressed to **Dr. Zhongchi Liu**, chair of the faculty search committee. Applications should consist of a single PDF file containing (1) a cover letter, (2) *curriculum vitae*, (3) summary of research plans (maximum two pages) and teaching philosophy (one page), and (4) contact information for at least three references. Complete applications should be received by **October 15, 2012**, but will be accepted until the position is filled.

The University of Maryland is an Affirmative Action/Equal Opportunity Employer. Women and members of underrepresented groups are especially encouraged to apply.

AgreenSkills
Pathways for inventive researchers

Post-doctoral mobility research projects
Agriculture, environment, food and nutrition, animal health sciences

AgreenSkills is an open programme for international mobility. It supports inventive and talented young researchers from all disciplines and from all over the world, to develop challenging basic or targeted research projects in the fields of **agriculture, environment, food and nutrition, and animal health sciences.**

AgreenSkills offers in-coming and out-going fellowships from and to **Agreenium** member institutions (INRA, Cirad, AgroParisTech, Agrocampus Ouest, Montpellier SupAgro and INPT-ENVT) during a mobility period of between 6 months to 2 years.

AgreenSkills provides **very attractive conditions** in terms of salary, optimal research conditions, training, networking opportunities as well as personalized support for career development plan.

Continuous call for submission over the period 2012-2015
two selection rounds per years.

Information on eligibility criteria and electronic submission of mobility research projects on **www.agreenskills.eu**

AgreenSkills is an international mobility programme co-funded by the European Commission in the frame of the COFUND - FP7 People Programme coordinated by INRA in cooperation with Agreenium.

For inquires: Dr Gilles Aumont, Dr Odile Vilotte
coordinators@agreenskills.eu

Next cut-off date for evaluation of proposals: 15th November 2012

orc.fr

AAAS is here – helping scientists achieve career success.

Every month, over 400,000 students and scientists visit ScienceCareers.org in search of the information, advice, and opportunities they need to take the next step in their careers.

A complete career resource, free to the public, *Science* Careers offers a suite of tools and services developed specifically for scientists. With hundreds of career development articles, webinars and downloadable booklets filled with practical advice, a community forum providing answers to career questions, and thousands of job listings in academia, government, and industry, *Science* Careers has helped countless individuals prepare themselves for successful careers.

As a AAAS member, your dues help AAAS make this service freely available to the scientific community. If you're not a member, join us. Together we can make a difference.

To learn more, visit
aaas.org/plusyou/sciencecareers

AAAS + U = Δ

UNIVERSITY *of* MARYLAND
SCHOOL OF MEDICINE

CANCER BIOLOGISTS

The University of Maryland Marlene and Stewart Greenebaum Cancer Center (UMGCC) is recruiting cancer biologists at the Assistant, Associate, and Full Professor levels for its multidisciplinary research programs in Tumor Immunology and Immunotherapy, Viral Oncology, and Cancer Epidemiology. Candidates should have extensive laboratory or epidemiology research experience with a sustained track record of external peer-reviewed funding and publications. The University of Maryland Schools of Medicine, Dentistry, Nursing, and Pharmacy, adjacent to the Cancer Center, provide excellent facilities and resources, including NMR, Structural Biology, and computer-assisted drug design capabilities. Academic rank, tenure status, and salary will be commensurate with experience. Interested applicants should submit their CV to **Kevin J. Cullen, M.D., Director, University of Maryland Marlene and Stewart Greenebaum Cancer Center, 22 South Greene Street, Baltimore, MD 21201**. Please cite Position **#03-309-xxx**

The University of Maryland Baltimore encourages women and minorities to apply and is an AA/EEO/ADA Employer.

CHILDREN'S MEDICAL CENTER
RESEARCH INSTITUTE
AT UT SOUTHWESTERN

Faculty Position in Cancer Biology

The Children's Research Institute (CRI) at the University of Texas-Southwestern Medical Center in Dallas, TX seeks applications for a **tenure-track faculty position in the area of cancer biology**. Outstanding investigators at any rank will be considered. Candidates must have a Ph.D., M.D. or equivalent degrees and the ability to direct an independently-funded research program exploring any aspect of cancer biology.

The UT-Southwestern Medical Center has a long and distinguished history of excellence in disease-related basic science research. The CRI is a new institute recruiting outstanding individuals dedicated to solving fundamental problems in biology and disease. The CRI is a dynamic, stimulating, and highly collaborative scientific environment. Major areas of focus within the CRI will include stem cell biology, cancer biology, and metabolism.

Please submit a CV, a 2-page summary of past accomplishments and research plans, and ask three references to submit letters by **November 1, 2012** to **CRIApplicants@utsouthwestern.edu**.

UT Southwestern is an Equal Opportunity/Affirmative Action Employer.

Genomic Approaches to the Study of Gene Regulation

The Department of Molecular Biology and Genetics, Cornell University, invites applications for a tenure-track faculty position at the Assistant or Associate Professor level. The ideal candidate will apply both experimental and bioinformatics approaches to study gene regulation. Individuals seeking a creative integration of experimental, computational and comparative approaches will find Cornell a particularly rich environment in which to work (see **http://mbg.cornell.edu/mbg-search.cfm**).

An advanced degree (Ph.D., M.D., or equivalent) is required and postgraduate training is highly desirable.

Candidates should submit a CV, a two to four page research statement, a one page teaching statement, and pdfs of two papers to:

https://academicjobsonline.org/ajo/jobs/1815

Application review begins on November 15, 2012. We encourage women and members of underrepresented minority groups to apply.

Diversity and inclusion have been and continue to be a part of our heritage. Cornell University is a recognized EEO/AA employer and educator.

CHILDREN'S MEDICAL CENTER
RESEARCH INSTITUTE
AT UT SOUTHWESTERN

Faculty Position in Stem Cell Biology

The Children's Research Institute (CRI) at the University of Texas-Southwestern Medical Center in Dallas, TX seeks applications for a **tenure-track faculty position in the area of stem cell biology**. Outstanding investigators at any rank will be considered. Candidates must have a Ph.D., M.D. or equivalent degrees and the ability to direct an independently-funded research program exploring any aspect of stem cell biology.

The UT-Southwestern Medical Center has a long and distinguished history of excellence in disease-related basic science research. The CRI is a new institute recruiting outstanding individuals dedicated to solving fundamental problems in biology and disease. The CRI is a dynamic, stimulating, and highly collaborative scientific environment. Major areas of focus within the CRI will include stem cell biology, cancer biology, and metabolism.

Please submit a CV, a 2-page summary of past accomplishments and research plans, and ask three references to submit letters by **November 1, 2012** to **CRIApplicants@utsouthwestern.edu**.

UT Southwestern is an Equal Opportunity/Affirmative Action Employer.

ILLINOIS
UNIVERSITY OF ILLINOIS AT URBANA-CHAMPAIGN

College of Liberal Arts and Sciences
School of Molecular and Cellular Biology
Department of Microbiology
Assistant Professor

The Department of Microbiology (**http://mcb.illinois.edu/departments/microbiology**) at the University of Illinois at Urbana-Champaign seeks outstanding applicants for one or more tenure track faculty positions at the Assistant Professor level. In accordance with our multi-year plan to enhance the microbial sciences on the UIUC campus, we are interested in applicants working on the physiology, biochemistry, pathogenesis, ecology or evolution of microbes.

Candidates must hold a Ph.D., M.D., or equivalent degree, and have a strong track record of publications within the microbial sciences. The target starting date is August 16, 2013. The successful candidate will be located in the Department of Microbiology and will be expected to conduct independent research, perform academic duties associated with our BS and PhD programs, and have the ability to teach effectively at both the undergraduate and graduate levels. Cross appointment within the Institute for Genomic Biology (**http://igb.illinois.edu**) is possible depending on the research interests of the candidate. Salary is competitive and commensurate with experience. These positions offer excellent laboratory facilities, relocation and start-up funds, and the opportunity to work with outstanding colleagues and graduate students.

The Urbana-Champaign campus offers a wide range of state-of-the-art research support facilities that include the Roy J. Carver Biotechnology Center, the W. M. Keck Center for Comparative and Functional Genomics, as well as facilities for X-ray crystallography, NMR, EPR, proteomics, metabolomics, high-throughput screening, immunology, flow cytometry, microscopy, and transgenic mice. The campus has strong programs in biophysics, bioengineering, biological physics, synthetic biology and chemistry. Superb computational resources are available at the National Center for Supercomputing Applications and the NIH Resource for Macromolecular Modeling and Bioinformatics. The University of Illinois is a partner in the Life Sciences Collaborative Access team (LS-CAT) at nearby Argonne National Labs providing ready access to the synchrotron.

Urbana-Champaign offers the residential advantages of a medium-sized university city, excellent cultural opportunities, and a high quality of life. In 2010, the University of Illinois at Urbana-Champaign received top rankings by Harvard University's Collaborative on Academic Careers in Higher Education for its pre-tenure practices in balancing work and home. (**http://www.insidehighered.com/news/2010/11/15/coache**)

To ensure full consideration, create your candidate profile through **http://go.illinois.edu/MCBAsstProfMicro** and upload your application cover letter, curriculum vitae, a concise summary of past research accomplishments, a statement of future research plans and contact information for three professional references by **November 30, 2012**. Referees will be contacted electronically upon the submission of the application. Although early applications are appreciated and interviews may be conducted before the closing date, no hire will be made until after the closing date. Questions can be addressed to the School of Molecular and Cellular Biology, 217-333-3166.

Illinois is an Affirmative Action /Equal Opportunity Employer and welcomes individuals with diverse backgrounds, experiences, and ideas who embrace and value diversity and inclusivity. (www.inclusiveillinois.illinois.edu).

THE UNIVERSITY of TENNESSEE
HEALTH SCIENCE CENTER

The University of Tennessee-Campbell Clinic, Department of Orthopaedic Surgery and Biomedical Engineering, Open Rank, Tenure-Track Faculty Positions

The faculty appointed to these two positions will work with clinical and basic research scientists at UTHSC for developing translational and interdisciplinary research programs, play a role in the research training of orthopaedic residents and interact with Campbell Clinic Staff and the Joint Program in Biomedical Engineering of the University of Memphis/UTHSC. Collaboration with orthopaedic industry is encouraged, with three major orthopaedic companies located in Memphis. Applications are invited from individuals who will develop internationally recognized, externally funded research programs including stem cell/tissue engineering for orthopaedic applications, orthopaedic biomechanics, cartilage and bone metabolism and pathological conditions, and basic research in the field of orthopaedics.

Requirements: Applicants should have a Ph.D., M.D. or M.D./Ph.D. degree in medicine, engineering, chemistry or biological sciences with a focus in orthopaedic research, a nationally and internationally recognized research program as evidenced by peer reviewed publications and a sustained history of external research funding. Rank will be commensurate with experience.

Letters of application including CVs and names of at least three references should be sent to: **khasty@uthsc.edu**; **Faculty Search Committee, UTHSC Department of Orthopaedic Surgery and Biomedical Engineering/Campbell Clinic 956 Court, Room A302 Memphis, TN 38163**.

For more information go to: **http://www.uthsc.edu/ortho/**

The University of Tennessee Health Science Center is an EEO/AA/Title VI/Title IX/Section 504/ADA/ADEA Employer.

Manager
Cell and Molecular Biology Ph.D. Program
University of Texas at Austin

The University of Texas at Austin seeks an Administrative Manager for its Cell and Molecular Biology (CMB) Ph.D. Program. The CMB Ph.D. Program recruits ~25 students annually and encompasses ~120 training faculty distributed over numerous departments on campus. We are seeking a M.S. or Ph.D. level Manager of the Program. The Manager will be responsible for collecting student and faculty data, and building an on-line repository of these data for use in preparing NIH and NSF training grant applications. The Manager will work with CMB faculty in writing and assembling NIH and NSF training grant applications. The Manager will also provide oversight of daily operations and staff for the CMB graduate program. Applicants should have an advanced degree in Cell and Molecular Biology or a closely related field, excellent communication and organization skills, a broad understanding of biology and knowledge of current standards for graduate training in biomedical sciences at peer institutions.

Austin is located in the Texas hill country and is widely recognized as one of America's most beautiful and livable cities.

Candidates should apply directly for the position (12-07-13-01-9029) through the University of Texas at Austin Human Resources website: **https://utdirect.utexas.edu/apps/hr/jobs**.

To receive full consideration, applicants should submit all materials to the above site by **September 15th, 2012**.

Questions about the position should be directed to **Dr. Jeff Gross**, Chair of the CMB Graduate Studies Committee (**jmgross@austin.utexas.edu**).

Homepages: **http://www.icmb.utexas.edu** and **http://www.icmb.utexas.edu/cmb/**

The University of Texas at Austin is an Equal Opportunity Employer. Qualified women and minorities are encouraged to apply; a background check will be conducted on applicant selected.

TENURE-TRACK ASSISTANT PROFESSORSHIPS IN CHEMISTRY

Harvard University
Faculty of Arts and Sciences
Department of Chemistry and Chemical Biology
Cambridge, MA

Candidates are invited to apply for a tenure-track assistant professorship in inorganic chemistry (**https://academicpositions.harvard.edu/postings/4246**), broadly defined to include reaction chemistry, with potential connections to energy-related research; and, physical chemistry (**https://academicpositions.harvard.edu/postings/4247**). These appointments are expected to begin on July 1, 2013. The tenure-track professors will be responsible for teaching at the undergraduate and graduate levels. We are seeking candidates who have an outstanding research record and a strong commitment to undergraduate and graduate teaching. Ph.D. required by expected start date. Candidates should arrange to have three letters of recommendation sent independently and provide a curriculum vitae, statement of teaching philosophy, list of publications, and outline of their future research plans. All applications and supporting materials must be submitted via the ARIeS portal (see links above) no later than **October 15, 2012**.

Harvard is an Equal Opportunity/Affirmative Action Employer. Applications from women and minorities are strongly encouraged.

Faculty Positions at Shanghai Public Health Clinical Center, Fudan University, Shanghai, China

Shanghai Public Health Clinical Center affiliated with Fudan University was established in 2004 and is dedicated to combat against emerging and re-emerging infectious diseases. The center is constituted of both clinical settings with 500 beds and research settings with state of the art facilities and equipments. The integrity and close collaboration between the clinical and research settings was exemplified during the outbreak of swine-orientated H1N1 in 2009 as the center successfully treated more than 300 swine-originated H1N1 infected patients in clinical settings with the real-time support of diagnostic tools from research settings. In addition, research scientists isolated 17 H1N1 virus isolates from clinical patients. Overall, the facility is optimized for research on infectious diseases (both viruses and bacteria), translational research, pathogens and immunity.

Positions at associate professor or professor level are currently open for scientists <45 years old and specialized on infection immunology in HBV, HIV, TB, respiratory viruses (influenza virus), enteroviruses (EV71), enteric pathogenic bacteria and animal model for infectious diseases (experiences with transgenic animal are preferred). Non-Chinese scientists are encouraged to apply.

A competitive start-up package will be provided for successful applicants. The successful applicants are expected to establish an active, independent, and externally funded research projects. Candidates must have a doctoral degree (PhD, MD, DSc, etc) and postdoctoral experiences demonstrating outstanding potential in his/her research area.

Interested applicants should send a CV with publication list, research proposal, and two letters of references to:

Ying Niu, Director of Human Resource,
Shanghai Public Health Clinical Center, Fudan University
2901 Caolang Road, Jinshan District, Shanghai 201508, China
Email: **niuying@shaphc.org**

Or

Jianqing Xu MD & PhD
Professor and Director of Scientific Research Department, Shanghai Public Health Clinical Center, Fudan University
2901 Caolang Road, Jin Shan District, Shanghai 201508, P.R.China
Phone: 86-21-37990333-7335
Fax: 86-21-57247094
Email: **jianqingxu2008@gmail.com**
Website: **www.shaphc.org**

中国科学院生物和化学交叉研究中心（中国 上海）

Interdisciplinary Research Center of Biology and Chemistry (IRCBC) - Exciting Biomedical Research Career Opportunity in Shanghai, China

The Interdisciplinary Research Center on Biology and Chemistry (IRCBC), the Chinese Academy of Sciences, Shanghai, is an exciting new collaborative research center in China in collaboration with the Shanghai Institute of Materia Medica and the Shanghai Institute of Organic Chemistry. The vision of IRCBC is to bring outstanding biologists and outstanding chemists to work side-by-side at the interface of biology and chemistry using tools of chemistry, cell biology, molecular biology, proteomics, bioinformatics and genomics to address the most interesting and important biological questions that are relevant to neurological and neurodegenerative diseases. The IRCBC offers long-term stable support for research (¥2-3 million per year), highly competitive salary (upto ¥600,000 per year), benefits and generous housing allowance, new laboratory space and state-of-art core facilities. The IRCBC invites applications from outstanding candidates from all stages of career, especially junior investigators who are looking for their first independent research opportunities, to apply for one of the two career tracks: Principle Investigators (PI), who will run independent research laboratories; or Technology Specialists (TS), who will run the platform technology facilities.

The IRCBC is seeking applicants with expertise in following areas:
Cellular and molecular biology; Proteomic and mass spectrometry; Chemical biology; Medicinal chemistry; Bioinformatics; Cellular neurobiology; Electrophysiology; Vertebrate and invertebrate animal models of neurological and neurodegenerative diseases; Behavioral neurobiology; Structural biology; Genomics.

Please submit a curriculum vitae with links to representative publication in the PubMed, one-page description of current research program and accomplishments, two-page description of future plans with relevance to neurological and neurodegenerative diseases and the names of three references by email to"**IRCBC@mail.shcnc.ac.cn**".

Applications will be accepted until the positions are filled. Reviews of applications will begin in **September 2012**.

CHILDREN'S MEDICAL CENTER
RESEARCH INSTITUTE
AT UT SOUTHWESTERN

Faculty Position in Metabolism Research

The Children's Research Institute (CRI) at the University of Texas-Southwestern Medical Center in Dallas, TX seeks applications for a **tenure-track faculty position in the area of metabolism and disease**. Outstanding investigators at any rank will be considered. Candidates must have a Ph.D., M.D. or equivalent degrees and the ability to direct independently-funded research programs. Areas of specific interest include analysis of metabolism at the cellular level, including metabolomics, metabolic flux analysis, metabolic imaging and mitochondrial biology. In addition to analytical equipment dedicated to the investigator's studies, CRI members will also have access to a metabolomics core with triple-quadrupole mass spectrometry and gas chromatography/mass spectrometry. NMR spectroscopy, ^{13}C dynamic nuclear polarization, a human 7-Tesla MRI and a state-of-the-art mouse metabolic phenotyping facility are also available on campus to provide an unparalleled breadth of metabolic analysis.

The UT-Southwestern Medical Center has a long and distinguished history of excellence in disease-related basic science research. The CRI is a new institute recruiting outstanding individuals dedicated to solving fundamental problems in biology and disease. The CRI is a dynamic, stimulating, and highly collaborative scientific environment. Major areas of focus within the CRI will include stem cell biology, cancer biology, and metabolism.

Please submit a CV, a 2-page summary of past accomplishments and research plans, and ask three references to submit letters by **November 1, 2012** to **CRIApplicants@utsouthwestern.edu**.

UT Southwestern is an Equal Opportunity/Affirmative Action Employer.

POSITIONS OPEN

BIOCHEMIST

Williams College the Chemistry Department invites application for a tenure-track position at the **ASSISTANT PROFESSOR** level beginning Fall 2013. A more senior appointment is possible under special circumstances. We are particularly interested in applicants with research interests in experimental biochemistry. Teaching assignments in this position may include courses in biochemistry, biophysical chemistry, upper-level biochemistry courses, introductory chemistry, and courses for non-science majors. A semester teaching assignment normally includes complete responsibility for one course and two laboratory sections, and supervision of student research projects. Candidates should hold a Ph.D. or have completed their dissertation by September 2013 (postdoctoral experience is preferred). The successful candidate must have a strong commitment both to teaching at the undergraduate level and to developing a productive research program. Williams College is a coeducational liberal arts institution located in the Berkshire Hills of western Massachusetts that has built its reputation on outstanding teaching and scholarship and on the academic excellence of its approximately 2,000 students. The Chemistry Department is composed of 12 faculty members and graduates about 30 majors each year; the department has excellent facilities for teaching and research. For more information, see **website: http://chemistry.williams.edu/.** The College is committed to building and supporting the diversity of its science majors and seeks an individual who can help us meet these goals. Mail curriculum vitae, undergraduate and graduate transcripts, descriptions of teaching philosophy and research projects for undergraduates, and three letters of recommendation to: **Professor Thomas E. Smith, Chair, Department of Chemistry, 47 Lab Campus Drive, Williams College, Williamstown, MA 01267, by October 2, 2012.** Electronic applications will not be accepted. All offers of employment are contingent upon completion of a background check. Further information is available at **website: http://dean-faculty.williams.edu/prospective-faculty/background-check-policy/.**

Beyond meeting fully its legal obligations for non-discrimination, Williams College is committed to building a diverse and inclusive community where members from all backgrounds can live, learn, and thrive.

YALE UNIVERSITY
Chemical Biology Institute

The Chemical Biology Institute, a cornerstone of Yale's new West Campus research enterprise, invites applications for tenure-track positions at the **ASSISTANT PROFESSOR** level to commence 1 July 2013. Faculty associated with this Institute will hold primary appointments in any of several life science or physical science departments within the Faculty of Arts and Sciences, the School of Engineering and Applied Science, or the Yale School of Medicine. At this time, we seek candidates whose research interests and accomplishments align best with the Institute and Yale's School of Engineering and Applied Science (**website: http://www.seas.yale.edu**). Successful candidates will be creative teacher-scholars with reputations for outstanding research at the combined interface of engineering, chemistry, biology, and/or medicine and must possess a Ph.D. in a relevant discipline, and must be committed to excellent pedagogy in engineering education. Applicants should create a profile at **website: https://academicjobsonline.org/ajo/jobs/1725** and upload a statement of research plans, curriculum vitae, and up to five reprints of published work(s). Applicants should also arrange for three references to upload their letters of recommendation. For further information, contact: **Jessica Sorensen** at **e-mail: jessica.sorensen@yale.edu** or **P.O. Box 27392, West Haven, CT 06516-7392.** The review of applications will begin on 15 October 2012 and proceed until suitable candidates are identified. *Yale University is an Affirmative Action/Equal Opportunity Employer. Yale values diversity among its faculty, students, and staff and strongly encourages applications from women and underrepresented minorities.*

POSITIONS OPEN

COGNITIVE NEUROSCIENCE

As part of a major research growth initiative, The University of Wisconsin-Milwaukee (UWM) is seeking applicants for a faculty position in Cognitive Neurosciences. This position will build directly on the current strength of our program (**website: http://neuroscience.uwm.edu**). The appointment will be made at the **ASSISTANT PROFESSOR** level.

Successful applicants will participate in the Center for Imaging Research (**website: http://www.mcw.edu/CIR**), which provides multiple research dedicated imaging platforms and technical infrastructure for brain mapping in human subjects and laboratory animals. Area of research specialization is open but outstanding individuals with interests in attention, perception, action, language, or emotion are particularly encouraged to apply. Responsibilities include developing an independent extramurally funded research program and teaching graduate and undergraduate courses in the neurosciences and experimental psychology.

Applicants must have a Ph.D. in neuroscience or a closely related field, research interests in cognitive neuroscience, and significant postdoctoral research experience. Preferred qualifications are strong potential for extramural funding; demonstrated research productivity; interest in fostering graduate and undergraduate research experience; excellence in graduate and undergraduate teaching; and the ability to strengthen or expand existing programs.

Review of applications will begin on November 23, 2012 and continue until the position is filled. To apply online please see **website: http://jobs.uwm.edu/postings/10500.**

A complete application will consist of a cover letter, vita, a concise statement of research interests, and three letters of reference. Candidates may submit a statement of teaching interests. All application materials may be submitted electronically, except applicants should arrange for three letters of reference to be mailed to: **Neuroscience Search Committee, Department of Psychology, UWM, PO Box 413, Milwaukee, WI 53201.** *UWM is an Equal Opportunity Institution committed to diversity.*

FACULTY POSITIONS IN NEUROSCIENCE
University of Maryland School of Medicine

The Department of Pharmacology (**website: http://pharmacology.umaryland.edu**) is expanding by adding multiple tenure-track track faculty positions at the **ASSISTANT, ASSOCIATE,** and **FULL PROFESSOR** levels. Candidates working in all sub- disciplines of neuroscience are welcome to apply. We are particularly interested in building our research relevant to neuroendocrinology, epigenetics, neuroinflammation, neurodevelopment, and the neurobiology of feeding. Successful research programs in these areas will strongly compliment existing strengths within the department and present avenues of collaboration between both basic and translational researchers within the University of Maryland, School of Medicine.

Candidates should hold a Ph.D. and/or M.D. degree and have a strong history of scholarly activity. Preference will be given to those with an independent funded research program and whose presence will catalyze multi-PI initiatives within the department.

We offer an outstanding intellectual and collaborative environment with highly competitive salary and recruitment packages. All department faculty are members of the Graduate Program in Life Sciences which awards the Ph.D. in eight biomedical disciplines (**website: http://lifesciences.umaryland.edu**). Candidates should submit the following as one single PDF file to **e-mail: pharmacology@som.umaryland.edu:** detailed curriculum vitae, a brief statement of research interests and goals, names and contact information for three references. For best consideration, candidates should submit their application by December 1, 2012 (although applications will be accepted until the positions are filled).

Applications should be addressed to the attention of **Dr. Jessica A. Mong,** Department of Pharmacology. *The University of Maryland, Baltimore is an Equal Opportunity/Affirmative Action Employer. Minorities, women, veterans, and individuals with disabilities are encouraged to apply.*

POSITIONS OPEN

ASSISTANT/ASSOCIATE PROFESSOR
Environmental Toxicology

The Department of Biology at the University of North Carolina - Greensboro (UNCG) invites applications for an outstanding individual with research interests in environmental toxicology. We expect to fill the position at the rank of Assistant Professor, although experienced candidates may also be considered for appointment at the Associate rank. This search is part of an initiative to expand our new doctoral program in Environmental Health Science. Our broadly based doctoral program addresses environmental concerns that directly or indirectly affect human health and well-being from the global to the molecular levels. Therefore, we seek individuals whose biological research addresses environmental toxicological issues at one or more levels of biological organization. Successful applicants will be expected to develop a strong, externally funded research program, train undergraduate and graduate students, make significant contributions to our Ph. D. program, and teach courses relevant to their specialty. Synergies with faculty in related disciplines are encouraged. Candidates expected to hold the Ph.D. by August 1, 2013; postdoctoral experience is preferred. Applicants should mail a cover letter, curriculum vitae, brief statements of research goals and teaching philosophies, and arrange for three letters of recommendation (e-mail acceptable with hard copy to follow) to be sent to: **Ms. Kathe Martin** (**e-mail: kamarti3@uncg.edu**), **Biology Department, UNCG, 312 Eberhart Building, 321 McIver St, Greensboro, NC 27412.** Inquiries should be directed to **Dr. Parke Rublee** (**e-mail: parublee@uncg.edu**), Search Committee Chair. The evaluation of applications will begin October 1 and continue until filled. Position starts in August 2013 (pending approval of funding). *UNCG is especially proud of the diversity of its student body, and we seek to attract an equally diverse applicant pool for this position, including women and members of minority groups. UNCG is an Equal Employment Opportunity/Affirmative Action Employer with a strong commitment to increasing faculty diversity*. For information about our Ph.D. program, see **website: http://www.uncg.edu/bio/gradprograms/grad_studies_bio.html.**

FACULTY POSITIONS

The Department of Chemistry at Central Michigan University (CMU) invites applications for two tenure-track faculty positions in the areas of Biochemistry or Chemical Biology. Appointments will be at the Assistant Professor level, beginning August 2013. The successful candidate is expected to develop a vigorous, funded research program that involves undergraduate and graduate students in biochemistry. Teaching responsibilities include introductory/general chemistry as well as undergraduate and graduate biochemistry courses. postdoctoral research experience is expected. Further responsibilities include advising, supervising student research, and department and university service. To view the complete position description and submit application materials, please visit **website: http://www.jobs.cmich.edu.** Review of materials will begin on October 15, 2012, and will continue until the positions are filled. *CMU, an Affirmative Action/Equal Opportunity Institution, strongly and actively strives to increase diversity and provide equal opportunity within its community* (**website: http://www.cmich.edu/aaeo**).

CAREER OPPORTUNITY—Doctor of Optometry (O.D.) degree in 27 months for Ph.D.s in science and M.D.s. Excellent career opportunities for O.D./Ph.D.s and O.D./M.D.s in research, education, industry, and clinical practice. This unique program starts in March of each year, features small classes, and 12 months devoted to clinical care.

Contact the Admissions Office, **telephone: 800-824-5526** at **the New England College of Optometry, 424 Beacon Street, Boston, MA 02115.** Additional information at **website: http://www.neco.edu, e-mail: admissions@neco.edu.**

UNC SCHOOL OF MEDICINE

CHAIR, DEPARTMENT OF CELL BIOLOGY AND PHYSIOLOGY

THE SCHOOL OF MEDICINE AT THE UNIVERSITY OF NORTH CAROLINA AT CHAPEL HILL is searching for an outstanding individual to provide academic and administrative leadership for the research and teaching programs of the newly formed Department of Cell Biology and Physiology. Research interests of current faculty include cardiovascular biology, neurobiology, endocrinology, cell shape motility and adhesion, imaging technology, cytoskeleton, membrane trafficking, cell polarity, protein quality control, and GI, renal and respiratory physiology. The department has outstanding facilities and collaborative relationships with other basic research and clinical departments, research centers, and institutes within the University and maintains strong ties to other academic and industrial institutions in the Research Triangle. The minimum educational requirement for this position includes a Ph.D. and/or M.D. degree in a related field. The successful candidate will have a distinguished record of scientific research and extramural funding and demonstrate outstanding skills in leadership and administration. The Search Committee will begin reviewing candidates immediately and continue until the position is filled.

Interested applicants should submit an online application at **http://unc.peopleadmin.com/postings/7359** to include their detailed curriculum vitae, description of administrative experience, research goals and teaching interests. Questions related to this search may be emailed to the search administrator, Dede Corvinus, **dede_corvinus@med.unc.edu**.

University of North Carolina is an Equal Opportunity Employer. Women and members of under-represented minority groups are especially encouraged to apply.

Our Next Breakthrough **IS YOU.**
Lawrence Postdoctoral Fellowship

The Lawrence Livermore National Laboratory (LLNL) has openings available under its Lawrence Fellowship Program. This is a highly desirable postdoctoral position that provides freedom to conduct independent, cutting-edge research, directed by the candidate, in an area of the candidate's choice. The duration of the Fellowship is up to three years. Typically two to four openings are available each year. Fellowships are awarded only to candidates with exceptional talent, credentials and a track record of research accomplishments.

Successful candidates will propose and subsequently conduct original research in one or more aspects of science relevant to the mission and goals of LLNL. Possible scientific areas include: Physics, Applied Mathematics, Computer Science, Chemistry, Material science, Engineering, Environmental Science, Atmospheric Science, Geology, Energy, Lasers and Biology. Lawrence Fellows may participate in experimental or theoretical work at LLNL and will have access to LLNL's extensive computing facilities and specialized laboratory facilities. a senior scientist will be matched to the Fellow to serve as a collaborator and mentor. the candidates will receive full management and administrative support. the salary is $8, 092/mo.

Please refer to the following web page **http://apptrkr.com/273036** for eligibility requirements and instructions on how to apply. when applying and prompted, please mention where you saw this ad. the deadline for applications is November 1, 2012. LLNL is operated by the Lawrence Livermore National security, LLc for the u.s. department of energy, National Nuclear security administration. we are an equal opportunity employer with a commitment to workforce diversity.

Lawrence Livermore National Laboratory

http://fellowship.llnl.gov

POSITIONS OPEN

TENURE-TRACK ASSISTANT PROFESSOR
Synthetic Organic or Bioorganic Chemistry
Indiana University, Bloomington

The Department of Chemistry at Indiana University invites applications for a tenure-track faculty position at the assistant professor level in organic or bioorganic chemistry beginning August 2013. A Ph.D. in chemistry or a related field is required and postdoctoral experience is preferred. Successful candidates will be expected to develop a visible, externally funded research program and teach at the graduate and undergraduate levels. Candidates with appropriate interests may participate in a new graduate training program in Quantitative and Chemical Biology at Indiana University (**website: http://www.chem.indiana.edu/qcb/**). We seek applicants with interests aligned with current departmental research strengths. Applicants should send a complete curriculum vitae and a summary of future research plans and arrange to have four letters of recommendation forwarded to the department. Applications completed by October 15, 2012 will receive full consideration, but review will continue until the position is filled. Applications and recommendation letters should be addressed to: **Professor Nicola L.B. Pohl, Chair, Faculty Search Committee, Department of Chemistry, Indiana University, 800 E. Kirkwood Avenue, Bloomington, IN 47405** and sent as PDF files to **e-mail: chemchair@indiana.edu.** *Indiana University is an Affirmative Action/Equal Opportunity Employer and especially encourages applications from women and members of minority groups.*

TENURE-TRACK FACULTY APPOINTMENTS
Massachusetts Institute of Technology
Department of Chemistry

The Massachusetts Institute of Technology (MIT) Department of Chemistry invites applications for tenure-track appointments beginning July 2013. Outstanding applicants with research interests in all areas of chemistry are encouraged to apply. MIT Chemistry has particular interest in appointments of faculty whose preference is to teach in the areas of Inorganic, Organic, or Physical Chemistry, broadly defined. Appointments are at the rank of **ASSISTANT PROFESSOR,** but outstanding senior applicants may be considered. A complete application must include curriculum vitae, a one-page summary of research plans, two or more research proposals, a brief statement of teaching interests, and three or more letters of recommendation. Applications are being accepted at Academic Jobs Online (**website: https://academicjobsonline.org/ajo/jobs/1699**.

To receive full consideration completed applications must be received by October 9, 2012. Search Contact: **Ms. Karen Fosher, Personnel Administrator, Department of Chemistry, Room 18-392, Massachusetts Institute of Technology, 77 Massachusetts Avenue, Cambridge MA 02139-4307** (**e-mail: kfosher@mit.edu**). *MIT is an Equal Opportunity/Affirmative Action Employer. Applications from women, minorities, veterans, older workers, and individuals with disabilities are strongly encouraged.*

ASSISTANT PROFESSOR–ALL AREAS
Princeton University
Department of Chemistry

The Department of Chemistry at Princeton University invites applications for a tenure-track Assistant Professor position in all areas of chemistry. Candidates should have a strong commitment to research and to teaching at the undergraduate and graduate levels, and are expected to have completed the Ph.D. in chemistry or a related field at the time of appointment. Applicants should submit a description of research interests, curriculum vitae, a list of publications, and contact information for three references online at **website: http://jobs.princeton.edu/applicants/Central?quickFind=62756**. The search committee will begin review of applications on October 17, 2012 and will continue until the position is filled.

Princeton University is an Equal Opportunity Employer and complies with applicable EEO and Affirmative Action regulations.

POSITIONS OPEN

UNIVERSITY OF HAWAII AT MANOA CANCER CENTER: ASSISTANT RESEARCHER (Cancer Biology Program), **Position #83330,** Tenure-track, Closes October 15, 2012, to begin as early as December 2012. Refer to **website: http://www.pers.hawaii.edu/wuh/** for complete information. *The University of Hawaii is an Equal Opportunity/Affirmative Action Institution. Women and minorities are encouraged to apply.*

UNIVERSITY OF HAWAII AT MANOA CANCER CENTER: ASSISTANT RESEARCHER (Epidemiology Program), **Position #85913,** Tenure-track, Closes October 15, 2012, to begin as early as December 2012. Refer to **website: http://www.pers.hawaii.edu/wuh/** for complete information. *The University of Hawaii is an Equal Opportunity/Affirmative Action Institution. Women and minorities are encouraged to apply.*